REPORT DOCUMENTATION PAGE

Form Approved
OMB NO. 0704-0188

1. AGENCY USE ONLY *(Leave blank)*	2. REPORT DATE	3. REPORT TYPE AND DATES COVERED
	January 1998	Final Report

4. TITLE AND SUBTITLE

XX International Workshop on Condensed Matter Theories

5. FUNDING NUMBERS

DAAH04-96-1-0184

6. AUTHOR(S)

Fazley Malik, principal investigator

7. PERFORMING ORGANIZATION NAMES(S) AND ADDRESS(ES)

Soouthern Illinois University at Carbondale
Carbondale, IL 62901

8. PERFORMING ORGANIZATION REPORT NUMBER

9. SPONSORING / MONITORING AGENCY NAME(S) AND ADDRESS(ES)

U.S. Army Research Office
P.O. Box 12211
Research Triangle Park, NC 27709-2211

10. SPONSORING / MONITORING AGENCY REPORT NUMBER

ARO 35699.1-PH-CF

11. SUPPLEMENTARY NOTES

The views, opinions and/or findings contained in this report are those of the author(s) and should not be construed as an official Department of the Army position, policy or decision, unless so designated by other documentation.

12a. DISTRIBUTION / AVAILABILITY STATEMENT

Approved for public release; distribution unlimited.

12 b. DISTRIBUTION CODE

13. ABSTRACT *(Maximum 200 words)*

No abstract available

14. SUBJECT TERMS

15. NUMBER IF PAGES

16. PRICE CODE

17. SECURITY CLASSIFICATION OR REPORT	18. SECURITY CLASSIFICATION OF THIS PAGE	19. SECURITY CLASSIFICATION OF ABSTRACT	20. LIMITATION OF ABSTRACT
UNCLASSIFIED	UNCLASSIFIED	UNCLASSIFIED	UL

Southern Illinois University at Carbondale
Carbondale, Illinois 62901-4709

Research Development and Administration
Mailcode 4709
618–536–7791
FAX: 618–453–8038

January 6, 1998

Sylvia Hall
US Army Research Office
AMXRO-ICA (Library)
PO Box 12211
Research Triangle Park, NC 27709-2211

RE: Final Report: Grant No. DAAH 04-96-1-0184, XX
International Workshop on Condensed Matter Theories

Dear Ms. Hall:

Pursuant to your request enclosed please find the final scientific report for the grant referenced above in accordance with Part II Conference Grant Special Provision #3.b.

Please call me at (618) 453-4543, if you have any questions.

Sincerely,

Sonjie Schwartz /AB

Sonjie Schwartz
Post Awards Assistant

Encl.

SS/ab

Final Report: Grant No. DAAH 04-96-1-0184
XX. International Workshop on Condensed Matter Theories

The grant enabled 13 scientists from the U.S.A. to participate at the XX International Workshop on Condensed Matter Theories held in Pune, India, in December 1996 and two physicists from the U.S.A. at the follow up XXI International Workshop on Condensed Matter Theories held at Luso, Portugal. Without this grant the U.S. participation at the Workshops would have been very minimal. The grant allowed the U.S. scientists to interact effectively with their international counterparts and develop new collaboration.

The list of the scientists form the U.S.A. who have been supported by this grant is attached in Appendix 1 and the titles of their talks presented at the Workshop are listed in Appendix 2. Participants from the U.S.A. receiving the grant have acknowledged it in their respective articles. Copies of these talks are attached in Appendix 3. All presentations were invited talks and have been accepted for publications in Condensed Matter Theories, Volume 13 and 14. The principal investigator is a co-editor of Volume 14 and a member of the editorial board of the series.

In keeping with the objective of the grant, the primary theme of the workshops was Bose-Einstein condensation. This phenomenon was extensively discussed for atomic gases and in liquid helium. Other topics include the theory of superconducting materials, recent development in density functional theory, quantum phase transitions, plasma waves in solids, and finite size scaling in Heisenberg model.

The Workshop's other key objectives of facilitating interaction among physicists working in diverse areas of condensed matter physics, promoting interaction among physicists of developed and developing nations, cross fertilization of ideas and development of new interest

have been fulfilled.

Thus, the purpose and the objective of the grant have been achieved.

Appendix 1

List of the Participants From the U.S.A. Supported by the ARO Grant No. DAAH 04-96-1-0184

1	Dr.	P. M. Bakshi	Boston College, Chestnut Hill, MA
2	Dr.	C. Campbell	The University of Minnesota, Minneapolis, MN
3	Dr.	D. M. Ceperley	The University of Illinois, Urbana, IL
4	Dr.	R. Chasman	Argonne National Laboratory, Argonne, IL
5	Dr.	S. A. Chin	Texas A&M, College Station, TX
6	Dr.	J. W. Clark	Washington University, St. Louis, MO
7	Dr.	M. de Llano	North Dakota State University, Fargo, ND
8	Dr.	D. Ernst	Vanderbilt University, Nashville, TN
9	Dr.	F. B. Malik	Southern Illinois University, Carbondale, IL
10	Dr.	S. Picozzi	Southern Illinois University, Carbondale, IL
11	Dr.	R. Silver	Los Alamos National Laboratory, Los Alamos, NM
12	Dr.	I. Silvera	Harvard University, Cambridge, MA
13	Dr.	P. Weichman	California Institute of Technology, Pasadena, CA

Appendix 2

Title of the Talks and the Authors of the Articles

No.	Title of Talks	Authors
1	Mathematical Signatures of Plasma Instabilities in Low Dimensional Solid State Systems	P. Bakshi and K. Kempa
2	Bose-Einstein Condensation, Pairing and Odlro: a View From Co-Ordinate Space	C. E. Campbell
3	Conditions of Superfluidity in Molecular Hydrogen	D. M. Ceperly and M. C. Gordillo
4	Pairing Forces in Nuclei	R. R. Chasman
5	Ground State Calculations of Lithium Atoms in a Harmonic Trap	S. A. Chin, H. A. Forbert, and E. Krotscheck
6	Bose-Einstein Condensation in Liquid Helium: A Correlated Density Matrix Theory	J. W. Clark, M. L. Ristig, T. Lindenau and M. Serhan
7	Can BCS and BEC be Synthesized?	V. C. Aguilera-Navarro, M. Casas, S. Fujita, M. G. Lopez, M. De Llano, A. Rigo, O. Rojo, M. A. Solis, and A. A. Valladares
8	Relativistic Kinematics and Unitarity Relations for Proper Self-Energy	D. J. Ernst
9	On the Thermodynamics Phase Transitions Relevant to Superconductivity and Colossal Magneto-Resistivity for a Hubbard Type of Hamiltonian	S. Picozzi, A. N. Proto and F. B. Malik
10	A Model for Colossal Magnetoresistance Based on the Maximum Entropy Principle	S. Picozzi and F. B. Malik
11	Bose Condensation in ^{4}He and Neutron Scattering	R. N. Silver
12	Experiments Designed to Achieve BEC in Spin-Polarized Hydrogen	I. F. Silvera, I. J. Bonaldi, T. M. Brill, K. Penanen, and L. Venkataraman
13	Superfluidity and Criticality in Bose Systems	P. B. Weichman

Appendix 3

Copies of the articles based on materials presented at the XXth and the follow up XX1 st Workshop on Condensed Matter Theories held at Pune, India, in December 1996, and Luso, Portugal, June 1997 by the participants supported by the grant.

Invited Talk at XXth International Workshop on Condensed-Matter Theories (Poone, INDIA, December 9-14, 1996). Shorter version to be published by Nova Science in Condensed-Matter Theories" vol. 12 (1997).

CAN BCS AND BEC BE SYNTHESIZED?

V.C. Aguilera-Navarro[1], M. Casas[2], S. Fujita[3],
M.G. López[4], M. de Llano[4], A. Rigo[2],
O. Rojo[5], M.A. Solís[6] and A.A. Valladares[4]

[1]Instituto de Física Teórica-UNESP, 01405 São Paulo, BRAZIL
and
Departamento de Física, Universidade Estadual de Londrina
Londrina, PR, BRAZIL

[2]Departament de Física, Universitat de les Illes Balears
07071 Palma de Mallorca, SPAIN

[3]Department of Physics, SUNY, Buffalo, NY 14260-1500, USA

[4]Instituto de Investigaciones en Materiales, UNAM
04510 México DF, MÉXICO

[5]PESTIC, Secretaría Académica, IPN, México DF, MÉXICO

[6] Instituto de Física, UNAM, 01000 México DF, MÉXICO

Abstract

Though never proved in detail, the superconducting phase is widely believed to be a kind of Bose condensate. Transition temperatures substantially higher than BCS T_c values for a many-fermion system interacting pairwise via the BCS interaction model ensue from Bose-Einstein condensation (BEC) in either a pure gas of "bosonic" Cooper pairs or in a mixture of the latter plus background fermions when pair-breaking effects are explicitly allowed. Cooper pairs of definite center-of-mass momentum (CMM) but consistent with all relative momentum are "bosonic" since, even if not fulfilling Bose commutation relations, they exhibit indefinite maximum occupation in a given state and thus obey the Bose-Einstein distribution. The transition occurs even in weak coupling, and more significantly even in two dimensions where ordinary BEC is prohibited—due to the crucial ingredient now being the (almost) linear, as opposed to quadratic, dispersion relation of the Cooper pair binding energy as function of its CMM. Nonzero-CMM pairs, neglected in BCS theory, are indeed found to be vanishingly small in number, particularly in small coupling and/or for small Debye-to-Fermi-temperature ratio, but play a crucial role. For example, BEC in the pure "bosonic" gas model is possible for all space dimensions > 1, thus allowing *all* superconductors to be Bose condensates in principle.

1. Introduction

The phenomenon of superconductivity has now been observed in all four broad classes of materials: *metals* (in 1911, by Onnes), *semiconductors* (in 1964 [1]), *polymers* (in 1975 [2]) and *ceramics* (in 1986 [3]). A recent review [4] of some Russian experimental work in certain polymers even suggests the possibility of room-temperature superconductivity.

It seems to be universally believed, though not yet proved, that superconductivity is just another example of Bose-Einstein condensation, as is superfluidity in liquid helium-4 [5] or less directly in liquid helium-3 [6]. The notion of superconductivity as a Bose-Einstein (BE)-like transition of an assembly of bosonic objects is not new, going back at least to Ogg [7] in the forties and to Ginzburg [8] and to Schafroth [9] in the fifties. The idea has resurfaced [10] more recently with the discovery [3] of short-coherence-length cuprate superconductors. Anderson [11] envisages crystalline electrons (or holes) as pair-clusters of excitations that are fermionic, chargeless "spinons"and bosonic, charged "holons"—the latter susceptible [12] to a kind of Bose-Einstein condensation (BEC). Schrieffer and co-workers [13] deal with a bosonic "spin-bag" which is shared by two holes. Friedberg, Lee and Ren [14] achieve fits to the cuprate data of Uemura *et al.* [15] with a BE-like condensation in $2 + \epsilon$ dimensions [16] by assuming an effective bosonic pair mass in the direction perpendicular to the copper-oxide planes approaching the pronounced uniaxial anisotropy of 10^5 reported experimentally [17], e.g., in TlBaCaCuO. Indeed, the value of ϵ itself can be determined analytically in idealized situations [12], and is estimated [18] to be about 0.03 in cuprate superconductors—its small but nonzero value being a measure of the coupling between copper-oxide planes. Alexandrov and Mott [19], as well as Ranninger and co-workers [20], concentrate on a bipolaronic picture and note an amazing similarity between at least two cuprate superconductors (with $T_c \simeq$ 92K and 107K) and liquid ^{4}He ($T_c \simeq 2.2$K) as regards their empirical specific heat singularities across T_c. Fujita and co-workers [21, 22, 23, 24] have generalized the Bardeen-Cooper-Schrieffer (BCS) formalism to include hole-hole (as well as particle-particle) Cooper pairs, stressing in addition that either type of pair (called "pairons") propagate not with a quadratic but with a *linear* dispersion relation, and are bosons which may BE-condense in 2D as well as in 3D according to very specific, unique T_c formulae which differ markedly from the familiar BEC T_c formula associated with quadratic-dispersion-relation bosons. The linear dispersion behavior of Cooper pairs was noted at least as early as 1964 in Schrieffer's monograph [25] on superconductivity.

Indeed, a BE *paradigm* in superconductivity is suggested by the recent T_c *vs* T_F or T_{BE} data extended beyond the cuprates by Uemura *et al.* [26] to virtually *all* exotic superconductors, whether 1D-like, 2D-like or 3D-like, where T_F is the Fermi temperature and the 3D BEC temperature $T_{BE} = 0.218T_F$ if *all* fermions in the original fermion gas are imagined paired. The exotic superconducting samples studied by Uemura *et al.* [26] have T_c values spanning almost three orders of magnitude and reveal an intriguing universal behavior roughly parallel to but shifted *down* from the straight line designating T_{BE} in the "Uemura plot" of T_c *vs* T_F or T_{BE}, thus suggesting a BE mechanism somehow implicit in an appropriately generalized BCS formalism.

Based on earlier work by Eagles [27] and by Leggett [28], Miyake [29] and later Randeria, Duan and Shieh [30] formulated the 2D many-fermion problem at zero absolute temperature ($T = 0$) within a BCS formalism whereby *both* the gap equation and the number equation are solved self-consistently [31] but without explicit reference to the underlying (possibly singular) two-fermion interaction potential which is replaced by a scattering t-matrix. The latter in turn is then related, at low-scattering energies, to the s-wave "scattering length". This self-consistent formulation leads to the usual BCS theory in the limit of weak coupling, and to an ideal gas of tightly-bound, well-separated bosons in the opposite, strong-coupling, limit. The so-called "BCS-Bose crossover" [32] formulation in 2D has been extended to finite T by van der Marel [33], as well as by Drechsler and Zwerger [34] who used an elegant functional integral approach which in lowest-order gives a Ginzburg-Landau theory. Following Ref. [30] a generalized coherence length (or, more precisely, a root-mean-square pair radius) was formulated within the BCS-Bose crossover picture in 1D, 2D and 3D by Casas *et al.*[35], and the 2D case compared with cuprate superconductor data. Their results suggested that these latter materials, among other 3D-like superconductors, might be moderately well described, at least in lowest order, as *weakly-coupled* within the BCS-Bose crossover formalism.

The 3D BCS-Bose crossover problem was incisively analyzed by Nozières and Schmitt-Rink [36]—in fact shortly before the 1986 discovery [3] of high-T_c cuprate superconductivity. Its definitive formulation in two transparent papers [37, 38] by Haussmann stressed the vital importance of *triple* self-consistency (*viz.*, in the gap, number *and* single-particle-energy equations; cf. also Ref. [39]). Haussmann employs the Thouless criterion [40] whereby the divergence of the real part of the temperature-dependent t-matrix evaluated at zero momentum and zero frequency leads to a (mean-field) superfluid transition temperature T_c that increases monotonically and smoothly from the weak-coupling (BCS) to the strong-coupling (Bose) extreme, the resulting T_c exactly reproducing, at the two limits, respectively, the BCS T_c formula (given in terms of the s-wave scattering length) as well as the familiar Bose-Einstein condensation temperature formula. Coherence lengths in 3D at $T = 0$ have also been calculated [41] over the entire range of coupling/density within the BCS-Bose picture.

In this paper we derive explicit T_c-formulae for BEC in d (> 0) dimensions for an ideal gas of identical bosons having a quadratic (Section 2) or a linear dispersion relation (Section 4); Cooper-pair dispersion relations, viz., binding-energy *vs.* center-of-mass-momenta curves are obtained numerically in 2D and in 3D in Section 3 by assuming Coulomb plus electron-phonon interactions mimicked via the familiar BCS interaction model; in Section 5 Cooper pairs are clearly distinguished from familiar elementary excitations such as zero-sound phonons or plasmons; Section 6 elaborates on the Davydov interpretation of the BCS ground state as an ideal mixture of fermion and boson ideal gases; Section 7 sketches a four-fluid statistical model of such a mixture that again leads to substantially higher critical transition temperatures than the BCS theory; and Section 8 gives conclusions.

2. BEC of quadratic-dispersion-relation bosons in any dimension

According to Ref. [16] on an ideal quantum gas of permanent (*i.e.*, number-conserving) bosons in d spatial dimensions, there exists a non-zero absolute temperature T_c below which a macroscopic occupation emerges for a *single* (of an infinitely many) quantum state only if $d > 2$. (The $d = 2$ case, in fact, displays the *same* [42] smooth, singularity-free temperature-dependent specific heat for either bosons or fermions). The Bose-Einstein distribution summed over all states yields the total number of bosons N, each of mass m, of which, say N_0 are in the lowest state $\varepsilon_k = \hbar^2 k^2/2m =$ (0 in the thermodynamic limit). Explicitly

$$N = N_0 + \sum_{\mathbf{k}} \frac{1}{e^{\beta(\varepsilon_k - \mu)} - 1} \ , \tag{1}$$

where $\beta \equiv 1/k_B T$ and $\mu \leq 0$ is the chemical potential. For $T > T_c$, N_0 is negligible compared with N; while for $T < T_c$, N_0 is a sizeable fraction of N. At precisely $T = T_c$, $N_0 \simeq 0$ and $\mu \simeq 0$, while at $T = 0$, $N = N_0$ (*viz.*, absence of any exclusion principle). To find T_c the sum in (1) can be converted to an integral over *positive* $k \equiv |\mathbf{k}|$, where $\mathbf{k}$ is a d-dimensional vector. The volume $V_d(R)$ of a hypersphere of radius R in $d \geq 0$ dimensions is given [43] by

$$V_d(R) = \frac{\pi^{d/2} R^d}{\Gamma(1 + d/2)}. \tag{2}$$

For $d = 3$, this is just $4\pi R^3/3$; for $d = 2$ it is the area πR^2 of a circle of radius R; for $d = 1$ it is just the "diameter" $2R$ of a line of "radius" R; and for $d = 0$ it is unity. Using (2) for $d > 0$ the summation in (1) over our d-dimensional vector $\mathbf{k}$ becomes, in the thermodynamic limit,

$$\sum_{\mathbf{k}} \longrightarrow \left[\frac{2\pi^{d/2}}{\Gamma(d/2)}\right] \left(\frac{L}{2\pi}\right)^d \int dk k^{d-1} \tag{3}$$

with the prefactor in square brackets reducing as it should to 2, 2π and 4π for d = 1, 2 and 3, respectively. Defining the number density in d dimensions through $n \equiv N/L^d$, (1) with $T = T_c$, $N_0 \simeq 0$ and $\mu \simeq 0$ becomes an elementary integral easily evaluated in terms of the so-called Bose integrals [43] (with $z \equiv e^{\mu/k_B T}$ the so-called activity)

$$g_\sigma(z) \equiv \frac{1}{\Gamma(\sigma)} \int_0^\infty dx \frac{x^{\sigma-1}}{z^{-1} e^x - 1} = \sum_{l=1}^{\infty} \frac{z^l}{l^\sigma} \quad \xrightarrow[z \to 1]{} \quad \zeta(\sigma), \tag{4}$$

where $\zeta(\sigma)$ is the Riemann zeta-function of order σ. Solving (1) for T_c then gives

$$T_c = \frac{2\pi\hbar^2}{m k_B} \left[\frac{n}{\zeta(d/2)}\right]^{2/d}. \tag{5}$$

This result is formally valid for all $d > 0$. Note, however, that for $0 < d \leq 2$, $T_c = 0$ since $\zeta(\sigma) = \infty$ for $\sigma \leq 1$, the case $d = 2$ dimensions giving the celebrated harmonic

series $\zeta(1) = 1 + \frac{1}{2} + \frac{1}{3} + \ldots$ which is well-known to diverge. Clearly, for $d = 1$, the series $\zeta(1/2) = 1 + \frac{1}{\sqrt{2}} + \frac{1}{\sqrt{3}} + \ldots$ diverges even more severely, etc. All this is consistent with the well-known fact that BEC does *not* occur for quadratic-dispersion-relation bosons for $d \leq 2$ dimensions. For $d = 3$ dimensions (5) becomes

$$T_c = \frac{2\pi\hbar^2 n^{2/3}}{m k_B [\zeta(3/2)]^{2/3}} \simeq \frac{3.31\hbar^2 n^{2/3}}{m k_B}, \tag{6}$$

since $\zeta(3/2) \simeq 2.612$. This is the familiar T_c-formula for BEC in 3D, a phenomenon finally observed experimentally [44] in ultra-cold alkali-atom gas clouds only recently.

3. Cooper-pair dispersion relations

Let fermions with kinetic energies $\epsilon_k \equiv \hbar^2 k^2/2m^*$ and $\epsilon_{k'} \equiv \hbar^2 k'^2/2m^*$ interact pairwise via the *BCS model interaction*

$$V_{kk'} = \begin{cases} -V & \text{if } E_F - \hbar\omega_D < \epsilon_k,\ \epsilon_{k'} < E_F + \hbar\omega_D \\ 0 & \text{otherwise,} \end{cases} \tag{7}$$

with $V > 0$ and $\hbar\omega_D$ the maximum energy of a vibrating-ionic-lattice phonon, where $V_{kk'}$ is the double Fourier transforms of the interaction, and m^* the fermion effective mass.

The total energy E_T eigenvalue equation for a (Cooper) pair of fermions interacting via the BCS interaction model and immersed in a background of $N - 2$ inert spectator fermions in a spherical Fermi surface (in k-space) of radius k_F is given [45] by

$$1 = V \sum_{\mathbf{k}}{}' [2\epsilon_k - (E_T - \hbar^2 K^2/4m^*)]^{-1} \tag{8}$$

where $\hbar\mathbf{K} = \hbar(\mathbf{k}_1 + \mathbf{k}_2)$ is the center-of-mass momentum of the pair, while $\hbar\mathbf{k} = \hbar(\mathbf{k}_1 - \mathbf{k}_2)/2$ is its relative momentum. The prime on the summation sign denotes the conditions

$$\begin{aligned} k_F < k_1 \equiv |\mathbf{k} + \frac{1}{2}\mathbf{K}| < (k_F^2 + k_D^2)^{1/2}, \\ k_F < k_2 \equiv |\mathbf{k} - \frac{1}{2}\mathbf{K}| < (k_F^2 + k_D^2)^{1/2} \end{aligned} \tag{9}$$

where $\hbar^2 k_D^2/2m^* \equiv \hbar\omega_D$, with $\hbar\omega_D$ the Debye energy. Setting $E_T \equiv 2E_F - \Delta_K$, the pair is bound if $\Delta_K > 0$ and (8) becomes an eigenvalue equation for the pair (positive) binding energy Δ_K. For $K = 0$ (8) then becomes

$$1 = V\sum_{\mathbf{k}}{}' [2\epsilon_k - 2E_F + \Delta_0]^{-1} = V\int_{E_F}^{E_F+\hbar\omega_D} \frac{g(\epsilon)d\epsilon}{2\epsilon - 2E_F + \Delta_0}, \tag{10}$$

from which one immediately obtains for the $K = 0$ pair binding energy, *exact* in 2D [as well as in 1D or 3D provided that $\hbar\omega_D \ll E_F$ so that $g(\epsilon) \simeq g(E_F)$, a constant that can be taken outside the integral], the familiar result

$$\Delta_0 = \frac{2\hbar\omega_D}{e^{2/g(E_F)V} - 1}, \tag{11}$$

where $g(E_F)$ is the density-of (fermionic)-states for one spin, evaluated at the Fermi surface. Finite-temperature BCS theory, on the other hand, gives the T_c formula

$$T_c = 1.13\Theta_D\, e^{-1/\lambda} \tag{12}$$

where $\lambda \equiv g(E_F)V \leq 1/2$. Since $\Theta_D \simeq 300$K, the critical temperature (12) is at most about 46K. This has been dubbed the "phonon barrier". Since actual superconductors are now known to have $T_c \leq 164$K, the BCS "phonon barrier" of 46K has prompted many workers to search for non-phonon mechanisms such as excitons, plasmons, magnons, etc., that can substitute sizably larger values for the temperature scale Θ_D in (12), and thus lead to higher T_c's. Note that since (11) yields only $\Delta_0 \leq 11$K (for $\lambda \leq 1/2$ and $\Theta_D \simeq 300$K) compared with the total rest mass of two electrons which is $\simeq 10^{10}$K, a Cooper pair is very weakly bound indeed when compared, say, with the deuteron for which these two energies are, respectively, about 2 MeV and 2,000 MeV.

For $K \geq 0$ and $d = 2$, eq.(8) reduces to

$$1 = \frac{4\lambda}{\pi}\int_0^{\pi/2} d\phi \int_{[1-\kappa^2(1+\nu)\sin^2\phi]^{1/2}+\kappa(1+\nu)^{1/2}\cos\phi}^{[1+\nu-\kappa^2(1+\nu)\sin^2\phi]^{1/2}-\kappa(1+\nu)^{1/2}\cos\phi} d\xi\, \xi[\tilde{\Delta}_\kappa + 2(1+\nu)\kappa^2 - 2 + 2\xi^2]^{-1} \tag{13}$$

where $\lambda \equiv g(E_F)V$ is a dimensionless coupling constant, $g(E_F) \equiv L^2m^*/2\pi\hbar^2$ the 2D density of states; $\xi \equiv k/k_F$; $\kappa \equiv K/2(k_F^2 + k_D^2)^{1/2}$; $\tilde{\Delta}_\kappa \equiv \Delta_K/E_F$; $\nu \equiv \hbar\omega_D/E_F = k_D^2/k_F^2$. For small K, one obtains from (13)

$$\Delta_K \xrightarrow[K\to 0]{} \Delta_0 - \frac{2}{\pi}\frac{[(1+\nu)^{1/2} + e^{2/\lambda}]}{e^{2/\lambda} - 1}\hbar v_F K + O(K^2). \tag{14}$$

which for weak coupling $\lambda \to 0$ reduces to

$$\Delta_K \xrightarrow[K\to 0]{} \Delta_0 - \frac{2}{\pi}\hbar v_F K + O(K^2). \tag{15}$$

Figure 1 compares the linear approximation (14) to the exact dispersion relation obtained numerically from (13), for the specified values of λ and ν. Indeed, the linear approximation is very good for moderately small λ and ν over the entire range of K values for which $\Delta_K \geq 0$.

For $d = 3$, assuming $\nu << 1$ and the 3D density of states $g(E_F) = (L^3/\pi^2\hbar^3)\sqrt{m^{*3}E_F/2}$ eq. (8) becomes

$$1 = 2\lambda \int_0^{\frac{\pi}{2}} d\phi \sin\phi \int_{[1-\kappa^2(1+\nu)\sin^2\phi]^{\frac{1}{2}}+\kappa(1+\nu)^{\frac{1}{2}}\cos\phi}^{[1+\nu-\kappa^2(1+\nu)\sin^2\phi]^{\frac{1}{2}}-\kappa(1+\nu)^{\frac{1}{2}}\cos\phi} d\xi\, \xi^2[\bar{\Delta}_\kappa + 2(1+\nu)\kappa^2 - 2 + 2\xi^2]^{-1} \tag{16}$$

which for small K, assuming the weak-coupling expressions $\bar{\Delta}_0 \simeq 2\nu e^{-2/\lambda}$, gives

$$\Delta_K \xrightarrow[K\to 0]{} \Delta_0 - e^{4/\lambda} \frac{\sqrt{1-\nu e^{-2/\lambda}}\sqrt{1+\nu}(2e^{-2/\lambda} + \nu e^{-2/\lambda} + 1)}{[e^{2/\lambda}\nu\{\ln A + \ln B\} + \nu\ln(AB) + 2e^{2/\lambda}\sqrt{1-\nu e^{-2/\lambda}}]} \cdot$$

$$\frac{1}{\sqrt{1+\nu}(e^{2/\lambda} + 1 - \sqrt{1+\nu})} \hbar v_F K + O(K^2) \tag{17}$$

where $A \equiv \frac{\sqrt{1+\nu} - \sqrt{1-\nu e^{-2/\lambda}}}{\sqrt{1+\nu} + \sqrt{1-\nu e^{-2/\lambda}}}$, and $B \equiv \frac{1+\sqrt{1-\nu e^{-2/\lambda}}}{1-\sqrt{1-\nu e^{-2/\lambda}}}$. For $\nu << 1$, $\lambda \to 0$ and $K \to 0$ (17) reduces to the result cited without proof in [25], namely

$$\Delta_K \xrightarrow[K\to 0]{} \Delta_0 - \frac{1}{2}\hbar v_F K + O(K^2). \tag{18}$$

Results in 3D are qualitatively similar to those in 2D illustrated in Fig. 1.

4. BEC of linear-dispersion-relation bosons in any dimension

Fujita and co-workers [24] (cf. Ref. [43], p. 211) have shown that BEC *is* possible in 2D for bosons with a linear, instead of the usual quadratic, dispersion relation. Photons and phonons are examples of such bosons but, however, are non-permanent (i.e., non-number-conserving). Cooper pairs do *not* obey the standard Bose commutation relations but can be considered as "bosons" (called "pairons" in [25]) since they obey the Bose-Einstein distribution function for a given center-of-mass momentum but *all* compatible relative momenta. A detailed proof of this is found in [21] chapter 9, but is also clear from the following. If $n_{\mathbf{k}_1}$ is the occupation number, 0 or 1, of a fermion in state $\mathbf{k}_1$, the occupation number for a singlet Cooper pair will be $n_{\mathbf{k}_1\uparrow}n_{\mathbf{k}_2\downarrow}$ and continues to be 0 or 1. Alternately, a given singlet pair can be characterized by $\mathbf{k}$ and $\mathbf{K}$ instead of by $\mathbf{k}_1$ and $\mathbf{k}_2$, in which case the occupation number is say, $\mathcal{N}_{\mathbf{k},\mathbf{K}} = 0$ or 1 again. Finally, the occupation number of a pair with specific $\mathbf{K}$ is then $N_{\mathbf{K}} \equiv \sum_{\mathbf{k}} \mathcal{N}_{\mathbf{k},\mathbf{K}} = 0, 1, 2, \ldots, QED$.

A Cooper pair is a pair of fermions bound just outside the momentum-space Fermi surface enclosing $N-2$ background, inert, spectator fermions of the N-fermion system. It has partner wave vectors $\mathbf{k}_1$ and $\mathbf{k}_2$ which may or may not add up to a zero center-of-mass wave number $\mathbf{K} \equiv \mathbf{k}_1 + \mathbf{k}_2$. From (18), such a ("bosonic") pair

has an excitation energy which is *linear* [25] in K for small K (long wavelength limit), namely,

$$\varepsilon_K \equiv \Delta_0 - \Delta_K \xrightarrow[K\to 0]{} \frac{1}{2} v_F \hbar K, \tag{19}$$

which is valid provided the coupling is small, where Δ_K is the (positive) binding energy of a Cooper pair with net center-of-mass momentum $\hbar K$, and v_F is the Fermi velocity defined by $E_F \equiv \hbar^2 k_F^2/2m^* = \frac{1}{2} m^* v_F^2$.

Although it has been traditionally argued, correctly, in the literature since 1957 that $K = 0$ Cooper pairs are overwhelmingly tighter-bound that $K > 0$ pairs, Fujita and co-workers [24] conjecture that it is precisely the latter pairs that pre-exist at $T > T_c$ and that *drive* BEC at $T = T_c$. Indeed, the number of Cooper pairs with a specific $K \geq 0$ is proportional to a number which is *less than* (because of finite-temperature smearing effects at the Fermi surface) the overlap volume in k-space swept out by all possible vectors $\mathbf{k}_1$ and $\mathbf{k}_2$ joined head-to-tail as in Figure 2, but both head and tail *within* the energy-shell $\hbar\omega_D$, to give a specific $\mathbf{K}$. This latter overlap volume V_K is just

$$V_K = \int d^3k \theta(|\mathbf{K}/2 + \mathbf{k}| - k_F)\theta(|\mathbf{K}/2 - \mathbf{k}| - k_F)$$
$$\theta(\sqrt{k_F^2 + k_D^2} - |\mathbf{K}/2 + \mathbf{k}|)\theta(|\mathbf{K}/2 - \mathbf{k}| - \sqrt{k_F^2 + k_D^2}). \tag{20}$$

This integral is exact, though tedious [46], and comprises four distinct regions in the interval $0 < K < 2\sqrt{k_F^2 + k_D^2}$, see below. For $K = 0$ this becomes the volume of the spherical shell, namely

$$V_0 = (4\pi/3)k_F^3[(1+\nu)^{\frac{3}{2}} - 1]. \tag{21}$$

Let $\kappa \equiv K/2\sqrt{k_F^2 + k_D^2} \equiv K/2k_F\sqrt{1+\nu}$. The fractional number of Cooper pairs with a specific value of K, to those with $K = 0$, will then be somewhat less than

$$V_K/V_0 = \frac{(1+\nu)^{\frac{3}{2}}}{[(1+\nu)^{\frac{3}{2}} - 1]}[1 - (1+\nu)^{-3/2} + \kappa^3 - (3/2)\kappa(2+\nu)/(1+\nu)]$$
$$if \;\; 0 < \kappa < (1/2)(1 - 1/\sqrt{1+\nu})$$
$$= \frac{(1+\nu)}{\frac{2}{3}[(1+\nu)^{\frac{3}{2}} - 1]}[3\nu^2/16\kappa(1+\nu)^{\frac{3}{2}}]$$
$$if \;\; (1/2)(1 - 1/\sqrt{1+\nu}) < \kappa < 1/\sqrt{1+\nu}$$
$$= \frac{1}{[(1+\nu)^{\frac{3}{2}} - 1]}[-1 + (3/16)\nu^2/(\kappa\sqrt{1+\nu}) + (3/2)\kappa\sqrt{1+\nu} - (1/2)(1+\nu)^{\frac{3}{2}}\kappa^3]$$
$$if \;\; 1/\sqrt{1+\nu} < \kappa < (1/2)(1 + 1/\sqrt{1+\nu})$$
$$= \frac{(1+\nu)^{\frac{3}{2}}}{[(1+\nu)^{\frac{3}{2}} - 1]}[1 - (3/2)\kappa + (1/2)\kappa^3]$$
$$if \;\; 1/2(1 + 1\sqrt{1+\nu}) < \kappa < 1. \tag{22}$$

Finally, it is clear from Fig. 2 that

$$V_K/V_0 = 0 \quad if \quad \kappa \geq 1. \tag{23}$$

These upper bounds are exhibited in Figs. 3 and 4 for different values of $\nu \equiv \Theta_D/T_F = k_D^2/k_F^2$, including the value of $\nu = 3060$ appropriate for the low-carrier concentration ($\simeq 10^{15} cm^{-3}$) superconducting semiconductor $SrTi0_3$ doped with Zr [47]. For $\nu = \infty$ the problem reduces to that of the overlap volume of two solid spheres [48], p. 28, namely $V_K/V_0 = 1 - \frac{3}{2}\kappa + \frac{1}{2}\kappa^3$, to which the last expression of (22) reduces when $\nu >> 1$. In general, note the (small but nonzero) fraction of $K > 0$ pairs to $K = 0$ pairs, particularly for small ν.

Nonetheless, the premise of Refs.[22, 23, 24] is that, *without abandoning the phonon mechanism* modeled by (7), superconductivity is really a BEC in either 2D or 3D, of excited ($K > 0$) Cooper "pairons" pre-existing *above* T_c. At $T = 0$ *all* "pairons" are at rest ($K = 0$), while a mixture of both kinds ($K = 0$ and $K > 0$) is present for $0 < T < T_c$. The result (19) is correct in 3D. For d dimensions we have the general "excitation energy"

$$\varepsilon_K \equiv \Delta_0 - \Delta_K \xrightarrow[K \to 0]{} a(d) v_F \hbar K \tag{24}$$

where [49] $a(1) = 1$, $a(2) = 2/\pi$ and $a(3) = 1/2$. Using (24) instead of $\varepsilon_k = \hbar^2 k^2/2m$ in (1) and performing the integral implied by (3) one obtains (for $N_0 \simeq 0$, $\mu \simeq 0$) the weak-coupling T_c-formula in d space dimensions

$$T_c = \frac{a(d) v_F \hbar}{k_B} \left[\frac{\pi^{\frac{d+1}{2}} n}{\Gamma(\frac{d+1}{2}) \zeta(d)} \right]^{1/d}. \tag{25}$$

Since $\zeta(1) = \pi^2/6 \simeq 1.64493$ and $\zeta(3) \simeq 1.20206$, this reduces to the T_c formulae of Refs. [22, 23], for 2D and 3D respectively, namely $T_c = 1.244 \hbar k_B{}^{-1} v_F n^{1/2}$ in 2D and $T_c = 1.008 \hbar k_B{}^{-1} v_F n^{1/3}$ in 3D [*except* that the coefficient 1.244 in 2D should replace the coefficient 0.977 of Ref. [22] since $a(2)$ equals $2/\pi$ in 2D instead of the $1/2$ mistakenly assumed there]. Note from (25) that $T_c > 0$ for $d > 1$, a result that might conceivably be relevant in understanding quasi-1D organic superconductors [50]. Organic superconductors comprise $(1 + \epsilon)$D materials such as the Bechgaard salts, $(2 + \epsilon)$D materials like the ET salts and fully-3D materials such as the alkali- and alkaline-earth-doped fullerene systems called "fulleride" superconductors [51]. The $(1 + \epsilon)$D and $(2 + \epsilon)$D compounds consist of *coupled* parallel chains and planes, respectively, of molecules.

The large dot in Figure 5 on the $d = 3$ ordinate denotes the previously mentioned BEC value of T_c, in units of T_F, for a 3-dimensional fermion gas in which we imagine *all* the fermions paired into quadratic-dispersion-relation bosons, i.e., (6) with $n = n_F/2$ and $m = 2m^*$, with $n_F = k_F^3/3\pi^2$ the 3D fermion-number density. In d-dimensions, using (3) for the number of fermions $N_F = 2\sum_{\mathbf{k}} \theta(k_F - k)$ one obtains $n_F = k_F^d/2^{d-2}\pi^{d/2} d\Gamma(d/2)$. On the other hand, the number of bosons n actually formed under interaction (7) is $g(E_F)\hbar\omega_D$, where $g(\varepsilon) \equiv (L/2\pi)^d d^d k/d\varepsilon = (m^*/2\pi\hbar^2)^{d/2}$. $L^d \varepsilon^{\frac{d}{2}-1}/\Gamma(d/2)$. Thus, instead of the upper bound $n/n_F = 1/2$ used before, one really has only $n/n_F = d\nu/4$. Using this for n/n_F we have plotted (5)

and (25) [assuming $a(d) = 1$] in units of T_F, *vs.* d in Fig. 5 (for the special case $\nu = 10^{-3}$ appropriate for conventional superconductors). Both curves will be raised somewhat for ν values appropriate for cuprates, namely, $0.03 \leq \nu \leq 0.07$.

5. Zero-sound phonons, plasmons and Cooper pairs contrasted

Cooper pairs are *entities distinct* from zero-sound phonons or plasmons since the former: a) are bounded in number, and b) carry a fixed constituent-fermion-number (namely two), while phonons or plasmons *do not* share either property.

Fig. 6 compares and contrasts them in the longwavelength limit ($K \to 0$). The dashed quadratic curve is the plasmon dispersion relation [48], p. 180,

$$\omega_K = \omega_P[1 + \frac{9}{10}(K/K_{TF})^2 + \ldots] \tag{26}$$

in the "ring (RPA) approximation" valid for $r_s \equiv r_0/a_0 \equiv (\frac{4\pi}{3}n_F)^{-1/3}/(\hbar^2/me^2) << 1$, where r_0 is an average electron spacing, $n_F \equiv k_F^3/3\pi^2$ being the electron number-density, a_0 the first Bohr radius $\hbar^2/me^2$ with m the electron mass, while the plasmon frequency is $\omega_P \equiv \sqrt{4\pi n_F e^2/m}$ and the "Thomas-Fermi inverse screening length" is $K_{TF} \equiv \sqrt{6\pi n_F e^2/E_F}$ with $E_F \equiv \hbar^2 k_F^2/2m$ as before. The dot-dashed curve is the weak-coupling zero-sound phonon dispersion curve for repulsive interactions between fermions at $T = 0$, and is given by [48] p. 183,

$$\omega_K \simeq [1 + 2e^{-(2\pi^2\hbar^2/mk_F\nu(0)\ +\ 2)}]v_F K \tag{27}$$

for $\nu(0) << \hbar^2/mk_F$, where $\nu(\mathbf{q}) \equiv \int d^3r e^{-i\mathbf{q}\cdot\mathbf{r}}V(\mathbf{r})$ and $V(\mathbf{r})$ the (repulsive) interparticle interaction potential. The slope of this straight line *rises* as coupling is increased, and assumes the form

$$\omega_K \simeq [\nu(0)/3\pi^2(\hbar^2/mk_F)]^{1/2}v_F K \tag{28}$$

for $\nu(0) >> \hbar^2/mk_F$. Note that (28) can be rewritten as

$$\omega_K^2 \simeq \frac{\nu(0)}{3\pi^2(\hbar^2/mk_F)}v_F^2 K^2 \tag{29}$$

and becomes the plasmon frequency squared ω_P^2 if $\nu(K)$ is taken as the Fourier integral of the Coulomb interaction, $4\pi e^2/K^2$.

On the other hand, for attractive interactions $V < 0$ between the fermions one has the so-called "Anderson mode" [52],

$$\omega_K \simeq [1 - 4g(E_F)|V|]\frac{1}{\sqrt{3}}v_F K \tag{30}$$

in the weak-coupling limit, which is shown as the dotted curve in Fig. 6. Finally, the weak-coupling Cooper pair dispersion relation (19) is represented by the full curve. In 2D, the Anderson mode (30) carries [53] a factor $1/\sqrt{2}$ instead of the $1/\sqrt{3}$ of 3D; it thus also lies higher than the Cooper pair dispersion relation (15) since $1/\sqrt{2} > 2/\pi$.

Using the computer-algebra packages MATHEMATICA and MAPLE, we have verified that the K^2 term in both 2D (15) and 3D (18) *diverges* in the weak coupling limit; curiously, this behavior also occurs for the plasmon, since the quadratic term in (26) can be written as $\hbar K^2/2M_P$ in terms of a "plasmon mass" M_P. This mass

$$M_P \sim \hbar K_{TF}^2/\omega_P \sim \frac{m^{3/2}e}{k_F^{1/2}} \xrightarrow[e\to 0]{} 0, \tag{31}$$

so that it also vanishes in the weak-coupling ($e \to 0$) limit, in perfect accord with the fact that (zero-) sound phonons are massless.

6. BCS ground state *à la* Davydov

A surprising property of the BCS theory of the ground ($T = 0$) state of a many-fermion system interacting via the model potential (7) is that the energy shift of the superfluid state E_S with respect to the normal state E_N is, *for any coupling strength*, just the total energy of an *ideal gas* of bosonic Cooper pairs. This astounding conclusion had not been adequately stressed, to our knowledge, before Davydov [54] (see also Ref. [23] as well as in Refs. [30]). It follows directly from the well-known result [55] for the energy shift between the superconducting (S) and normal (N) total many-body energies (per unit volume)

$$\frac{E_S - E_N}{\Omega} = 2g(E_F)\int_0^{\hbar\omega_D} d\varepsilon \left[\varepsilon - \frac{1}{2}\frac{2\varepsilon^2 + \Delta^2}{\sqrt{\varepsilon^2 + \Delta^2}}\right], \tag{32}$$

where Ω is the system volume, $g(E_F)$ is defined as in (11), and $\Delta = \hbar\omega_D/\sinh[1/g(E_F)V]$ is the BCS gap energy which is *distinct* from the binding energy (11), both being valid for *any* coupling. As with Eq. (11), in arriving at (32) only $\hbar\omega_D \ll E_F$ has been assumed—*not* weak coupling. Recall, however, that in 2D the assumption $\hbar\omega_D \ll E_F$ is superfluous, since then $g(E_F)$ is a *constant* independent of E_F. The integral (32) can be performed exactly [55], and gives

$$\frac{E_S - E_N}{\Omega} = g(E_F)(\hbar\omega_D)^2\left[1 - \sqrt{1 + \left(\Delta/\hbar\omega_D\right)^2}\right] \tag{33}$$

$$= -\left[g(E_F)\hbar\omega_D\right]\frac{2\hbar\omega_D}{e^{2/g(E_F)V} - 1} \tag{34}$$

$$= -n_0\Delta_0 \xrightarrow[\lambda\to 0]{} -\frac{1}{2}g(E_F)\Delta^2, \tag{35}$$

where Δ was eliminated in the second step, where $g(E_F)\hbar\omega_D$ is precisely the *pairon* number density n_0 at $T = 0$, provided $\hbar\omega_D \ll E_F$, and use was made of (11) in the last equality. Ironically, (33) and (34) are found in Ref. [55], but *not* the all-important, remarkably simple, and far-reaching equality (35) implying that the BCS ground state corresponds precisely to an ideal gas of composite bosons embedded in an ideal gas of unpaired fermions, for *all* coupling. The final expression in (35) is

the well-known and familiar weak-coupling [$\lambda \equiv g(E_F)V \ll 1$] result, where Δ is again the BCS gap energy. Note the crucial difference between Δ and Δ_0 (which in weak coupling reduce to $2\hbar\omega_D e^{-1/\lambda}$ and $2\hbar\omega_D e^{-2/\lambda}$, respectively) that was *required* to arrive at (35), and that is rather frequently neglected in the original and in the textbook literature on the subject. This striking conclusion about the ideal pairon gas—though *not* self-consistent since even at $T = 0$ BCS predicts a *smeared* (not sharp) Fermi surface—supplements the more common interpretation of the BCS *excited* states as an ideal gas of *fermionic* ("bogolon") excitations—a picture, however, valid only in the limit of weak coupling. Note that weak coupling $\lambda \equiv g(E_F)V \ll 1$ is distinct and unrelated to the limit $\hbar\omega_D \ll E_F$.

Besides striking, the conclusion that the BCS ground-state is an ideal (i.e. *interactionless*) gas of Cooper pairs embedded in an ideal gas of (unpaired) fermions at *all* couplings, is remarkable because it holds *regardless of how severely the pairs overlap.* At weak coupling pairs will individually be huge and overlap considerably; for strong coupling pairs are small and well-separated. Within the BCS-Bose crossover picture [32] these two extremes are respectively known as the BCS and Bose (or BE) limits.

In essence, therefore, BCS theory is an elegant generalization to *two* particles of the Hartree-Fock (*one*-particle) theory of a many-particle system, both being fundamentally "mean-field" theories.

7. Four-fluid statistical model in 2D

In this section we merely sketch a 2D model to be discussed in greater detail by N. J. Davidson in his contribution to this workshop, and which is motivated by the Davydov interpretation of the BCS ground-state just discussed.

The total number of fermions $N = L^2k_F^2/2\pi$ equals the number of unpaired fermions N_1, plus the number of pairable ones N_2, where $N_2 = 2g(E_F)\hbar\omega_D$ with $g(E_F) = L^2m^*/2\pi\hbar^2$ as before. At finite temperature let $N_{20}(T)$ be the number of pairable but (because of thermal pair-breaking) unpaired fermions; this is given by

$$N_{20}(T) = 2\int_{\mu-\hbar\omega_D}^{\mu+\hbar\omega_D} \frac{d\varepsilon g(\varepsilon)}{e^{\beta(\varepsilon-\mu_2)}+1} \quad ; \quad \beta \equiv (k_BT)^{-1}, \tag{36}$$

if μ_2 is the fermion chemical potential of the unpaired but pairable fermions. Since in 2D $g(\varepsilon)$ is a constant, the integral is exact so that

$$N_{20}(T) = \frac{2g(E_F)}{\beta}\Big\{2\beta\hbar\omega_D + \ln\Big[\frac{1+e^{\beta(\mu-\mu_2-\hbar\omega_D)}}{1+e^{\beta(\mu-\mu_2+\hbar\omega_D}}\Big]\Big\}. \tag{37}$$

The relevant *number equation* is then

$$N_2 = N_{20}(T) + 2[N_{B,0}(T) + N_{B,K>0}(T)] \tag{38}$$

where $N_{B,0}(T)$ is the number of ("bosonic") Cooper pairs with $K = 0$ at temperature T, while $N_{B,K>0}(T)$ the number with $K > 0$. The latter in turn is just

$$N_{B,K>0}(T) = \sum_{K>0}^{K_0} [e^{\beta\{\bar{\varepsilon}_{B,K}(T)-2\mu_2\}} - 1]^{-1} \tag{39}$$

where

$$\bar{\varepsilon}_{B,K}(T) \equiv 2\mu - \Delta_K(T) \tag{40}$$

is the (thermal) average total energy of a Cooper pair, in analogy with the $T = 0$ equation $E_T = 2E_F - \Delta_K$ introduced just below (9). The cutoff K_0 in (39) is defined as $\Delta_{K_0} \equiv 0$ and is illustrated in Figure 1. The T-dependent Cooper-pair (positive) binding energy $\Delta_K(T)$ is given [21], chapter 10, in the 2D linear approximation in weak coupling by

$$\Delta_K(T) \simeq \Delta_0 - \epsilon_g(T) - \frac{2}{\pi}\hbar v_F K + O(K^2) \tag{41}$$

where $\epsilon_g(T)$ is defined as the *pairon gap*, distinct from the quasi-fermion (BCS) gap $\Delta(T)$ but alike in that both $\epsilon_g(T)$ and $\Delta(T)$ are nonnegative and vanish for $T \geq T_c$. The pairon gap $\epsilon_g(T)$ results from solving the BCS hamiltonian generalized [21], chapter 10, to include $K > 0$ Cooper pairing. Analogous to (15) and (19), one can then define a T- and K-dependent excitation energy $\varepsilon_K(T) \equiv \Delta_0 - \Delta_K(T) \simeq \epsilon_g(T) + \frac{2}{\pi}\hbar v_F K$ allowing one to identify $\varepsilon_K(T) - \mu_B$, where μ_B is the bosonic chemical potential, with the factor multiplying β in (39), namely $\varepsilon_{B,K}(T) - 2\mu_2 = \varepsilon_K(T) - \mu_B = \Delta_0 - \Delta_K(T) - \mu_B$ so that (40) leads to

$$\mu_B = 2(\mu_2 - \mu) + \Delta_0. \tag{42}$$

The BEC transition temperature T_c is then given by $\mu_B \simeq 0$ and $N_{B0}(T_c) \simeq 0$, where from (42) $\mu - \mu_2$ in (37) is just $\Delta_0/2$. Hence (38) leads to the transcendental equation

$$N_2 = N_{20}(T_c) + 2N_{B,K>0}(T_c). \tag{43}$$

The last quantity in (43) then becomes, since $\epsilon_g(T_c) = 0$,

$$N_{B,K>0}(T_c) = \frac{L^2}{2\pi}\int_0^{K_{01}} \frac{dK\,K}{e^{\beta_c \frac{2}{\pi}\hbar v_F K} - 1} \tag{44}$$

where $K_{01} = \pi\Delta_0/2\hbar v_F$ in the linear approximation (15) since $\Delta_{K_{01}} \equiv 0$, and $\beta_c \equiv 1/k_B T_c$. Since for weak coupling $\Delta_0 \simeq 2\hbar\omega_D e^{-2/\lambda}$ vanishes, so does K_{01}, allowing the exponential under the integral sign to be expanded to first order, leaving

$$N_{B,K>0}(T_c) \underset{\lambda\to 0}{\simeq} \frac{L^2\pi\Delta_0 m^*}{16\hbar^2}\frac{T_c}{T_F} \tag{45}$$

Note that for quadratic-dispersion-relation bosons one has K^2 instead of K in the exponential, making the integral in (44) diverge in the lower limit so that $T_c \equiv 0$ as expected in 2D. Since $N_2 = 2g(E_F)\hbar\omega_D$, (38) with $\mu - \mu_2 = \Delta_0/2$ in the log in (37) expanded in powers of Δ_0, gives the T_c equation

$$T_c \underset{\Delta_0\to 0}{\simeq} \frac{\sqrt{2}}{\pi}\sqrt{\Theta_D T_F} \quad - \quad \ldots \tag{46}$$

assuming $\Theta_D/2T_c << 1$, the correction term left out tending to *reduce* T_c. Table 1 shows values of T_c/T_F resulting from (46) for three cuprates for which empirical Θ_D and T_F values are taken from [56]. These calculated T_c/T_F values are somewhat higher than the empirical Uemura [26] range of $0.01 < T_c/T_F < 0.06$.

A factor α further reducing T_c can be introduced and called a "pairon-formation suppression factor" (with respect to the ideal spherical, or circular, Fermi surface), and has three possible origins. i) Elemental superconductors have partially hyperboloid Fermi surfaces were electron-electron or hole-hole [22, 23] pairons are formed via acoustic phonons. Since these surfaces are only small parts of the total Fermi surface, α is expected to be quite small. ii) Pairons (either positively- or negatively-charged) are formed in equal numbers from the physical vacuum, meaning that the density of states for the non-predominant [22, 23] fermions, e.g. "holes" in Pb, is the relevant density-of-states entering in (11), thus making α even smaller. iii) "Necks" in the Fermi surface are more favorable for pairon formation than "inverted double caps" since the density-of-states is larger around a "neck". This feature appears to explain why face-centered-cubic Pb has a higher T_c than face-centered-cubic Al. For these and possibly other reasons the pairon density n_0 or n_B in actual superconductors is smaller than that associated with a spherical Fermi surface. On the other hand, if the Fermi surface is spherical or even ellipsoidal but in the first Brillouin zone as in Na, K or other alkali metals, then $\alpha = 0$ exactly; this agrees with the observed fact that alkali metals remain normal down to absolute zero temperature. If a metal Fermi surface is known to contain "necks" and "inverted double caps" (as in Al, Pb, Be, W, etc.) such a metal has a finite, nonzero α and hence $T_c > 0$. An accurate determination of α for a specific substance might conceivably be based on low temperature specific heat comparisons with ideal Fermi gas values corresponding to spherical Fermi surfaces.

Finally, interactions are expected to further lower T_c, though perhaps minimally, as suggested by the slight reduction of T_c in liquid ^{4}He compared with the ideal boson gas.

8. Conclusions

Bose-Einstein condensation (BEC) T_c-formulae for any positive space dimensionality $d > 0$ are readily derived for a pure gas of bosons with either a quadratic or linear dispersion relation. For the former one recovers the well-known result that $T_c > 0$ only for $d > 2$. On the other hand, for the latter $T_c > 0$ for $d > 1$. This significant difference has a profound impact in the theory of superconductivity. The reason is simply that standard BCS theory can be generalized to include nonzero-center-of-mass-momentum Cooper pairs. In general, Cooper pairs propagate with a *linear* energy-momentum dispersion relation, and can thus undergo BEC not only in 2D but also for any dimension greater than unity. As a result, robustly enhanced T_c values are possible with linear (but not quadratic) dispersion-relation bosons, and the BCS "phonon barrier" of $T_c \leq 46$K can be "broken" without discarding phonon-mediated interactions and *without assuming strong coupling.*

Another remarkable conclusion, not entirely new but scarcely mentioned or un-

derstood in the literature, is the fact that the BCS ground state describes an *ideal* gas of bosonic Cooper pairs for *all* values of the BCS interaction model coupling. This picture motivates a simple four-fluid mixture statistical model in 2D which continues to give enhanced T_c values even in weak coupling.

M. C. and M. de Ll. acknowledge partial support from grant PB95-0492 and SAB95-0312 (Spain). M. de Ll. thanks R. M. Carter, N. J. Davidson and D. M. Eagles for extensive discussions and/or correspondence, NATO (Belgium) for a research grant, as well as the U. S. Army Research Office for a travel grant.

References

[1] R. A. Hein *et al*, Phys. Rev. Lett. **12**, 320 (1964); J. F. Schooley *et al*, Phys. Rev. Lett. **12**, 474 (1964).

[2] R. L. Greene *et al*, Phys. Rev. Lett. **34**, 577 (1975).

[3] J. G. Bednorz and K. A. Müller, Z. Phys. **B 64**, 189 (1986).

[4] D. M. Eagles, Physica **C 225**, 222 (1994).

[5] J. Wilks and D. S. Betts, *An Introduction to Liquid Helium* (Clarendon Press, Oxford, 1987).

[6] N. D. Mermin and D. M. Lee, Sci. Am. (Dec. 1976) p. 56; O.V. Lounasmaa and G. R. Pickett, Sci. Am. (June 1990); R. C. Richardson, Phys. Today (Aug. 1981) p. 46; *Helium Three*, ed. by W. P. Halperin and L. P. Pitaevskii (North-Holland, Amsterdam, 1990); A. J. Leggett, Revs. Mod. Phys. **47**, 331 (1975).

[7] R. A. Ogg, Jr., Phys Rev. **69**, 243 (1946).

[8] V.L. Ginzburg, Ups. Fiz. Nauk. **48**, 25 (1952); Fortschr. Phys. **1**, 101 (1953).

[9] M. R. Schafroth, Phys. Rev. **96**, 1442 (1954); M. R. Schafroth, S. T. Butler and J. M. Blatt, Helv. Phys. Acta **30**, 93 (1957); J. M. Blatt, *Theory of Superconductivity* (Academic, N.Y. 1964) and refs. therein.

[10] R. Micnas *et al*, Revs. Mod. Phys. **62**, 113 (1990).

[11] P. W. Anderson, Science **235**, 1196 (1987); P. W. Anderson, G. Baskaran, Z. Zou and T. Hsu, Phys. Rev. Lett. **58**, 2790 (1987).

[12] X. G. Wen and R. Kan, Phys. Rev. **B 37**, 595 (1988).

[13] J. R. Schrieffer, X. G. Wen and S. C. Zhang, Phys. Rev. Lett. **60**, 944 (1988).

[14] R. Friedberg and T. D. Lee, Phys. Rev. **B 40**, 6745 (1989); R. Friedberg, T. D. Lee and H. C. Ren, Phys. Lett. **A 152**, 417 and 423 (1991).

[15] Y. J. Uemura *et al.*, Phys. Rev. Lett. **62**, 2317 (1989).

[16] J. D. Gunton and M.J. Buckingham, Phys. Rev. **166**, 152 (1968); R. M. Ziff, G. E. Uhlenbeck and M. Kac, Phys. Rep. **32**, 169 (1977).

[17] D. E. Farrell, R. G. Beck, M. F. Booth, C. J. Allen, E. D. Bukowski and D. M. Ginsberg, Phys. Rev. **B 42**, 6758 (1990).

[18] R. K. Pathak and P. V. Panat, Phys. Rev. **B 41**, 4749 (1990).

[19] A. S. Alexandrov and N. F. Mott, Rep. Progs. Phys. **57**, 1197 (1994) and refs. therein; *Polarons and Bipolarons in High-T_c Superconductors and Related Materials*, ed. by E. K. H. Salje, A. S. Alexandrov and W. Y. Liang (Cambridge University Press, Cambridge, 1995)

[20] J. Ranninger, in *Bose-Einstein Condensation* (ed. by A. Griffin, D.W. Snoke and S. Stringari) (Cambridge University Press, Cambridge, 1995).
[21] S. Fujita and S. Godoy, *Quantum Statistical Theory of Superconductivity* (Plenum, N. Y.) (in press).
[22] S. Fujita and S. Watanabe, J. Supercond. **5**, 219 (1992).
[23] S. Fujita, J. Supercond. **5**, 83 (1992); **4**, 297 (1991).
[24] S. Fujita, T. Kimura and Y. Zheng, Found. Phys. **21**, 1117 (1991).
[25] J. R. Schrieffer, *Theory of superconductivity* (Benjamin, NY, 1964) p. 33.
[26] Y. J. Uemura *et al.*, Nature **352**, 605 (1991); Phys. Rev. Lett. **66**, 2665 (1991); Y. J. Uemura and G. M. Luke, Physica **B 186-188**, 223 (1993).
[27] D. M. Eagles, Phys. Rev. **186**, 456 (1969).
[28] A. J. Leggett, J. Phys. (Paris) Colloq. **41**, C7-19 (1980).
[29] K. Miyake, Prog. Theor. Phys. **69**, 1794 (1983).
[30] M. Randeria, J. M. Duan and L. Y. Shieh, Phys. Rev. **B 41**, 327 (1990); Phys. Rev. Lett. **62**, 981 (1989).
[31] J. Labbé, S. Barisic, and J. Friedel, Phys. Rev. Lett. **19**, 1039 (1967).
[32] M. Randeria, in *Bose-Einstein Condensation* (ed. by A. Griffin, D. W. Snoke and S. Stringari) (Cambridge University Press, Cambridge, 1995).
[33] D. van der Marel, Physica **C 165**, 35 (1990).
[34] M. Drechsler and W. Zwerger, Ann. der Physik **1**, 15 (1992).
[35] M. Casas, J. M. Getino, M. de Llano, A. Puente, R. M. Quick, H. Rubio and D. M. van der Walt, Phys. Rev. **B 50**, 15945 (1994); R. M. Carter, M. Casas, J. M. Getino, M. de Llano, A. Puente, H. Rubio, and D. M. van der Walt, Phys. Rev. **B 52**, 16149 (1995).
[36] P. Nozières and S. Schmitt-Rink, J. Low. Temp. Phys. **59**, 195 (1985); F. Pistolesi and G. C. Strinati, in *Bose-Einstein Condensation* (ed. by A. Griffin, D. W. Snoke and S. Stringari) (Cambridge University Press, Cambridge, 1995), and in Phys. Rev. **B 49**, 6356 (1994) and **B 53**, 15168 (1996).
[37] R. Haussmann, Z. Phys. **B 91**, 291 (1993).
[38] R. Haussmann, Phys. Rev. **B 49**, 12975 (1994).
[39] D. Dzhumanov, P. J. Baimatov, A. A. Baratov and N. I. Rahmatov, Physica **C 235-240**, 2339 (1994).
[40] D. J. Thouless, Ann. Phys. (N.Y.) **10**, 553 (1960); L. P. Kadanoff and P. C. Martin, Phys. Rev. **124**, 670 (1961).
[41] R. Carter *et al.*, in *Condensed Matter Theories* , vol. 11, ed. by R. F. Bishop *et al.* (Nova, N.Y., 1996) (in press).
[42] R. M. May, Phys. Rev. **135**, 1515 (1964); R. Aldrovandi, Fortschr. Phys. **40**, 631 (1992); A. Haerdig and F. Ravndal, Eur. J. Phys. **14**, 17 (1993); S. Viefers, F. Ravndal, and T. Haugset, Am. J. Phys. **63**, 369 (1995).
[43] R. K. Pathria, *Statistical Mechanics* (Pergamon, Oxford, 1972) p. 177, 211 and 501.
[44] M. H. Anderson *et al.*, Science **269**, 198 (1995); G. Taubes, *ibid*, p. 152; K. Burnett, *ibid*, p. 182; G. P. Collins, Phys. Today **48** [No. 8], 17 (1995); C. C. Bradley *et al.*, Phys. Rev. Letters **75**, 1687 (1995).
[45] L. N. Cooper, Phys. Rev. **104**, 1189 (1956).
[46] M. G. López and M. A. Solís, to be published

[47] D. M. Eagles *et al*, Physica **C 157**, 48 (1989).
[48] A. L. Fetter and D. Walecka, *Quantum Theory of Many-Particle Systems* (McGraw-Hill, N.Y., 1971)
[49] S. Fujita, unpublished.
[50] D. Jérome *et al.*, Physica **B 206 & 207**, 559 (1995); N. Dupuis and G. Montambaux, Phys. Rev. **B 49**, 8993 (1994); J. M. Williams *et al.*, Science **252**, 1501 (1991); D. Jérome, *ibid*, p. 1509; A. Khurana, Phys. Today **43** [No. 9], 17 (1990).
[51] A. Hebard, Phys. Today **45** [No. 11], 26 (1992).
[52] P. W. Anderson, Phys. Rev. **110**, 827 (1958)
[53] L. Belkhir and M. Randeria, Phys. Rev. **49**, 6829 (1994).
[54] A. S. Davydov, Phys. Reps. **190**, 191 (1990), see esp. p. 208.
[55] J. Bardeen, L. N. Cooper and J. R. Schrieffer, Phys. Rev. **108**, 1175 (1957); For an elementary treatment see D. R. Tilley and J. Tilley, *Superfluidity and Superconductivity* (Adam Hilger, Bristol, 1986).
[56] D. R. Harshman and A. P. Mills, Phys. Rev. **B 45**, 10684 (1992).

Figure caption

Figure 1: Exact 2D Cooper-pair dispersion relation calculated numerically from (13) for $\lambda = 0.5$ and $\nu = 10^{-2}$, compared with its linear approximation (14).

Figure 2: Cross-section of overlap volume (cross-hatched) giving an upper bound as explained in text to the number of Cooper pairs with a definite center-of-mass momentum $\hbar\mathbf{K}$, if the pair partners interact via the BCS model interaction (7).

Figure 3: Overlap volume (20) to (22) of two spherical shells of Fig. 2 as function of K, relative to volume when $K = 0$, for various values of $\nu \equiv \Theta_D/T_F \equiv k_D^2/k_F^2$: $\nu = 10^{-3}$ applies to *conventional* superconductors; $0.03 \leq \nu \leq 0.07$ to cuprates; $\nu = 3060$ to Zr-doped $SrTiO_3$ [46]; and the limit $\nu = \infty$ refers to overlap volume of two solid spheres [48], p. 28.

Figure 4: Same as Fig. 3 but on a semilog plot.

Figure 5: Full curve refers to BEC in d dimensions according to (5), while dashed curve refers to BEC according to (25) if $a(d) = 1$ is used, for $\Theta_D/T_F = 10^{-3}$, and $n/n_F = d\nu/4$, $m = 2m^*$ as explained in text. The dot at $d = 3$ refers to (5) with $n/n_F = \frac{1}{2}$ and $m = 2m^*$, namely *all* fermions paired. Light and dark crosshatchings comprise Uemura plot [26] data for *exotic* and *conventional* superconductors, respectively. The thin horizontal line marked BCS "phonon barrier" corresponds to Eq. (12) with $\lambda \leq 1/2$, namely $T_c/T_F \leq (1.13e^{-2})\Theta_D/T_F \simeq 0.153\Theta_D/T_F$ for the case $\Theta_D/T_F = 10^{-3}$.

Figure 6: Dispersion curves for: the plasmon (26) (dashed); the weak-coupling (repulsive interaction) zero-sound phonon (27) (dot-dashed); the weak-coupling (attractive interaction) Anderson mode (30) (dotted); and the weak-coupling 3D Cooper pair (18) (full curve).

Table Caption

Table 1: BEC critical temperatures T_c, in units of the Fermi temperature T_F, predicted by (46) in the four-fluid statistical model discussed in text, for three cuprates. Data on T_F and Θ_D are taken from [56].

Table 1

	$T_F(K)$	$\Theta_D(K)$	T_c/T_F (Eq. 46)
YBaCuO	2190-2390	368	0.17 to 0.19
TlCaBaCuO	1640-2020	458	0.21 to 0.24
BiSrCaCuO	580-1360	246	0.19 to 0.29

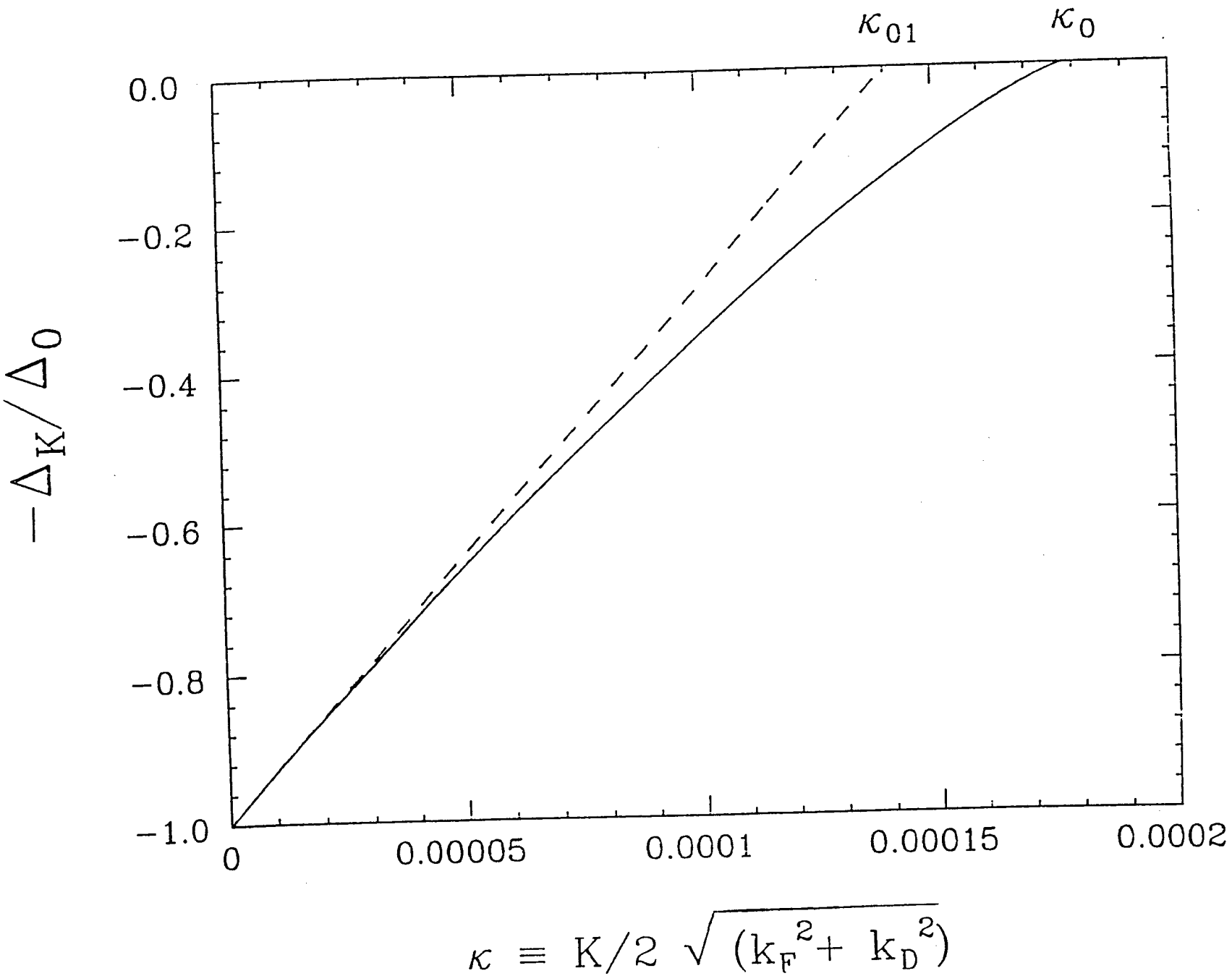
κ_{01}
κ_0
0.0
−0.2
−0.4
−0.6
−0.8
−1.0
$-\Delta_K/\Delta_0$
0
0.00005
0.0001
0.00015
0.0002
$\kappa \equiv K/2\sqrt{(k_F^2 + k_D^2)}$

Fig. 1

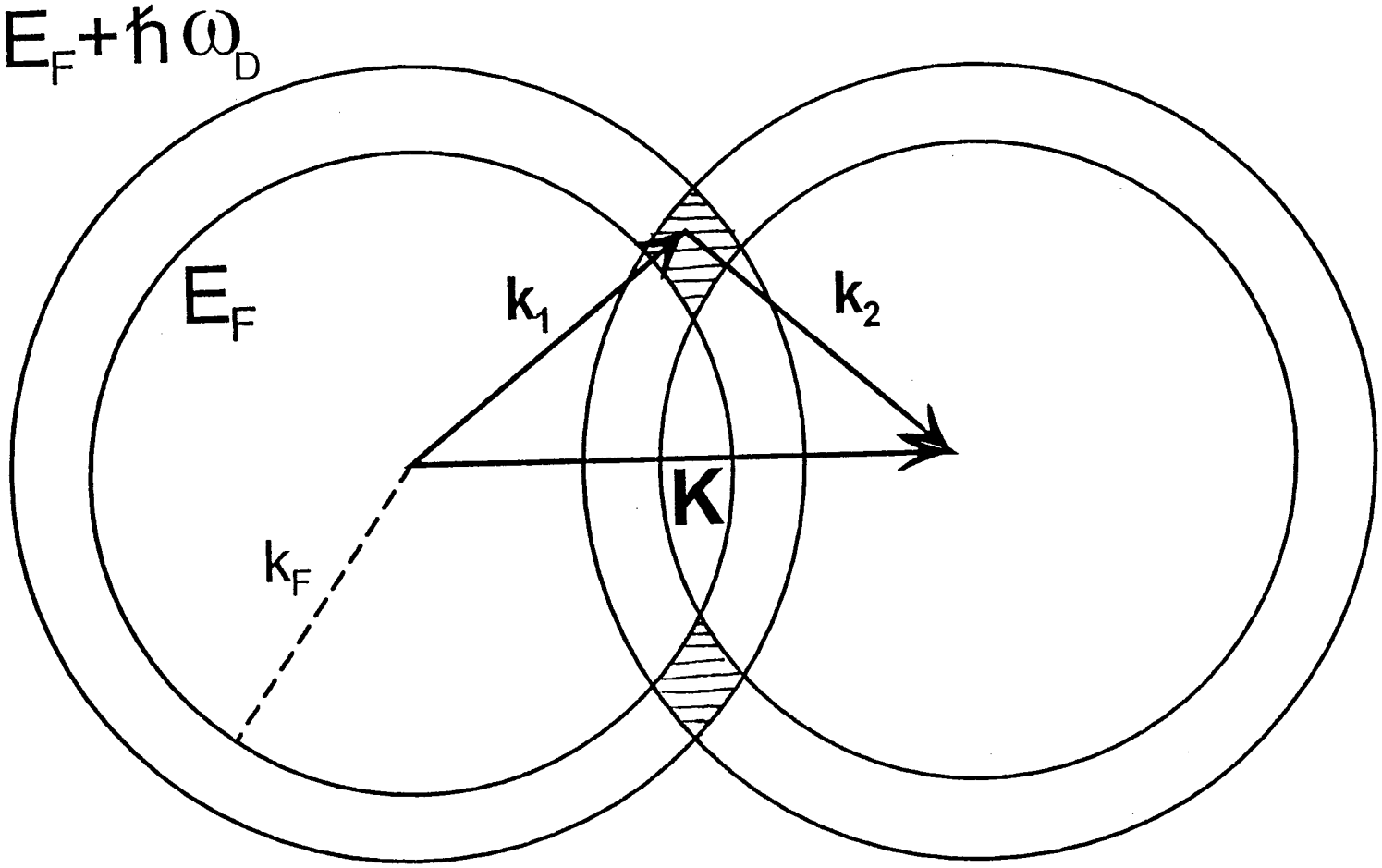

Fig. 2

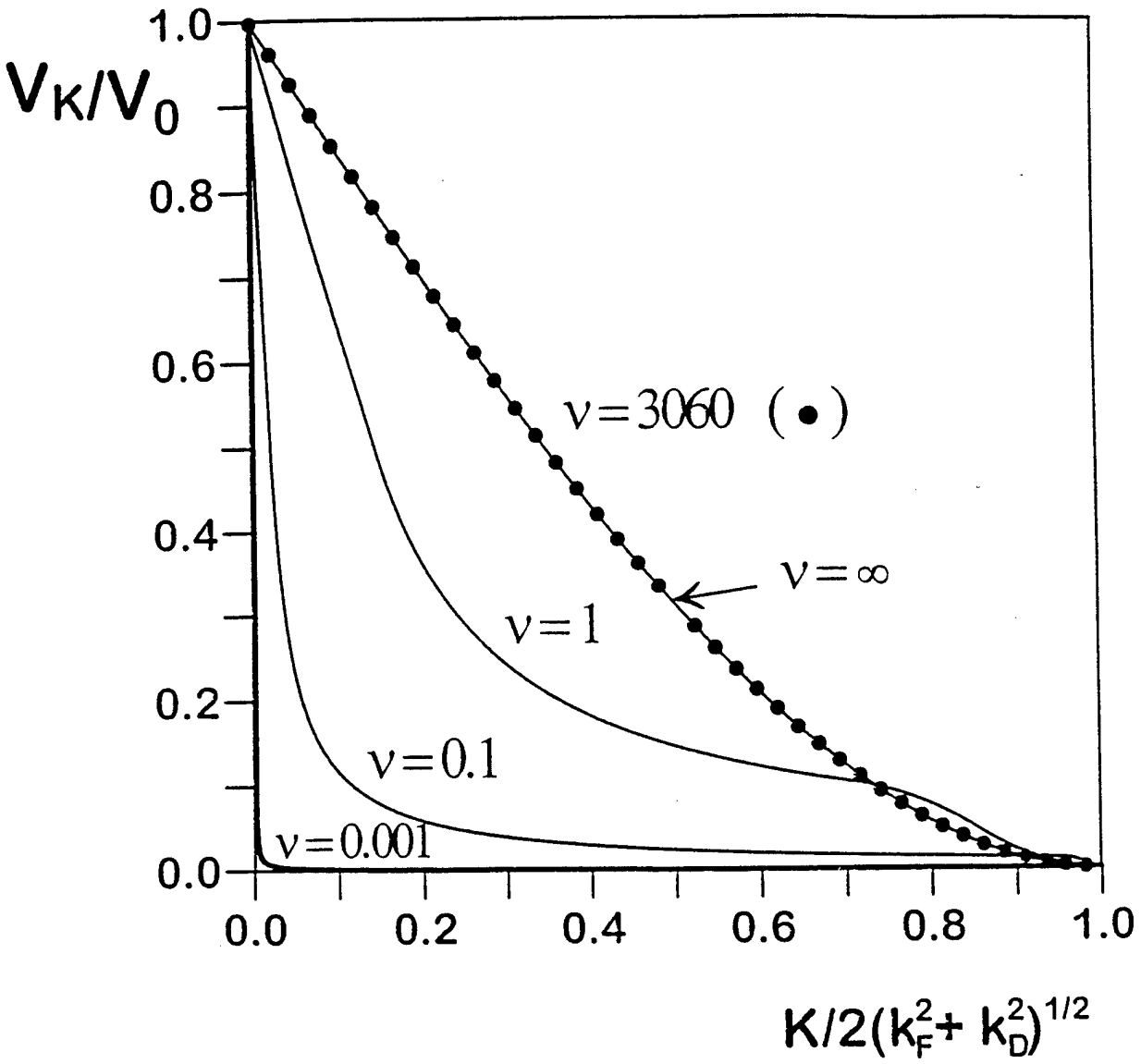
1.0
V_K/V_0
0.8
0.6
0.4
0.2
0.0
0.0
0.2
0.4
0.6
0.8
1.0
$\nu=3060$ (•)
$\nu=\infty$
$\nu=1$
$\nu=0.1$
$\nu=0.001$
$K/2(k_F^2+ k_D^2)^{1/2}$

Fig. 3

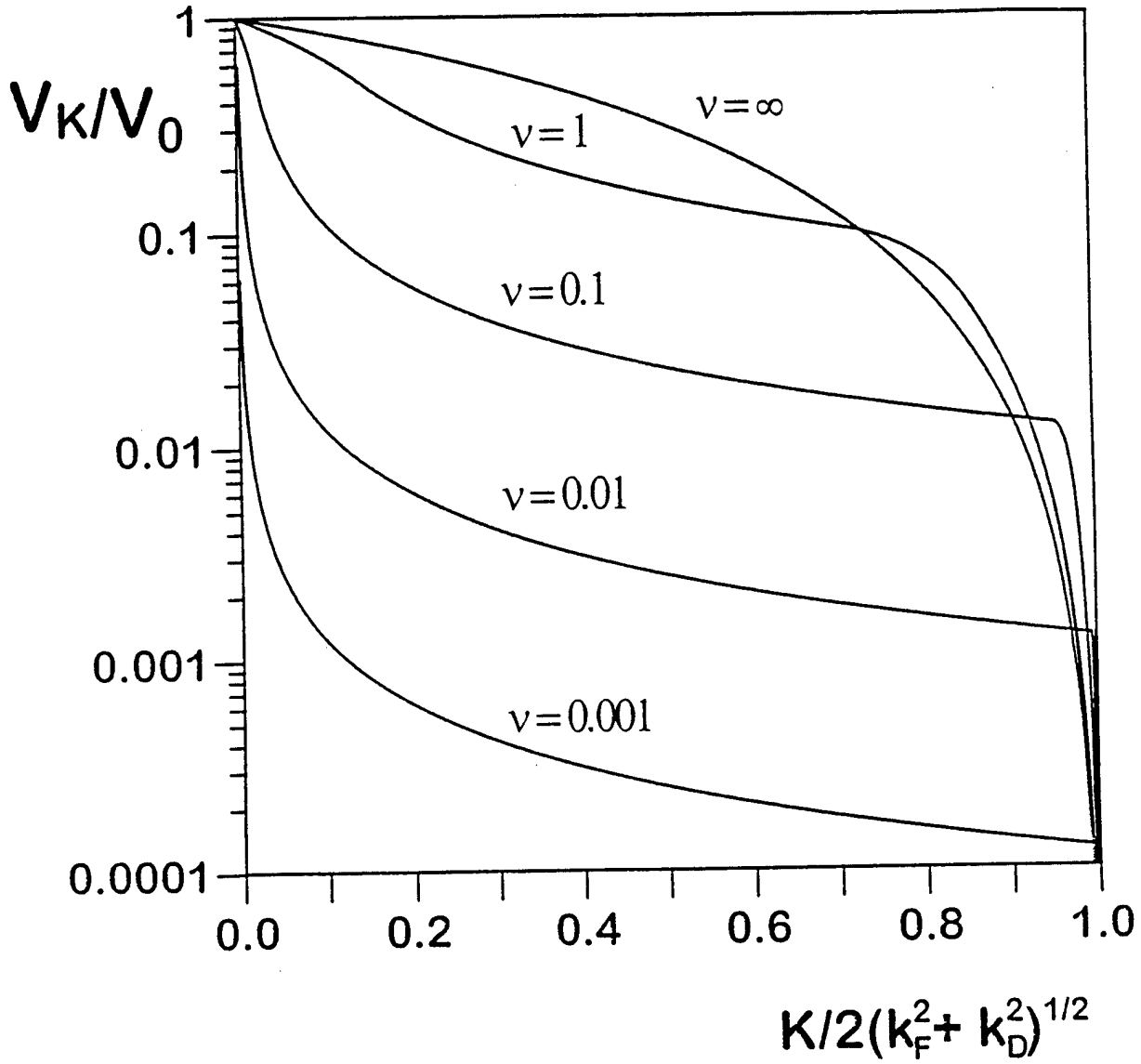
1
0.1
0.01
0.001
0.0001
V_K/V_0
$\nu=\infty$
$\nu=1$
$\nu=0.1$
$\nu=0.01$
$\nu=0.001$
0.0
0.2
0.4
0.6
0.8
1.0
$K/2(k_F^2+ k_D^2)^{1/2}$

Fig. 4

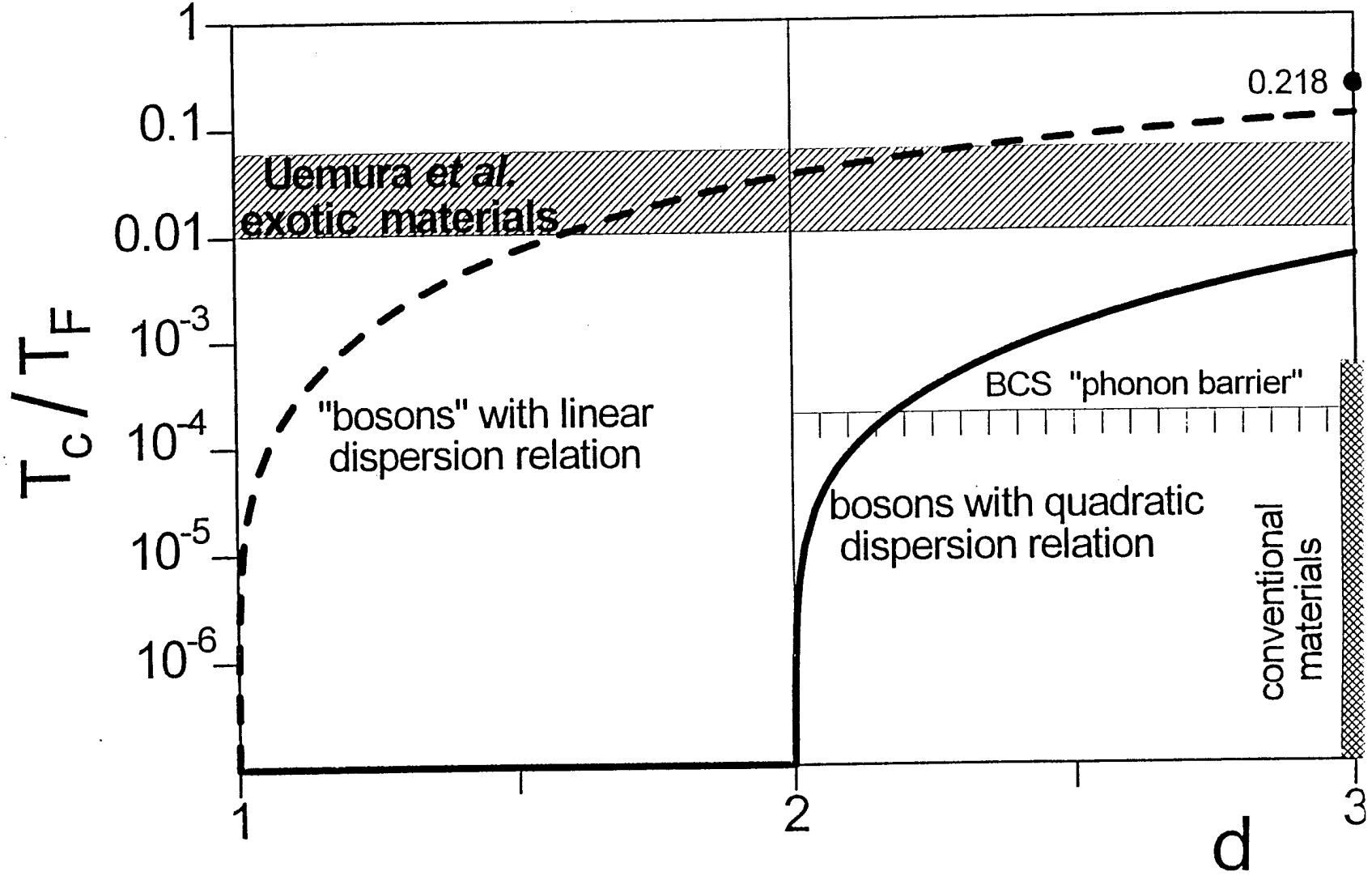
1
0.1
0.01
10^{-3}
10^{-4}
10^{-5}
10^{-6}
T_c / T_F
0.218
Uemura *et al.*
exotic materials
"bosons" with linear
dispersion relation
BCS "phonon barrier"
bosons with quadratic
dispersion relation
conventional
materials
1
2
3
d

Fig. 5

Fig. 7

MATHEMATICAL SIGNATURES OF PLASMA INSTABILITIES IN LOW DIMENSIONAL SOLID STATE SYSTEMS

P. Bakshi and K. Kempa

Department of Physics, Boston College, Chestnut Hill, MA 02167, USA

1. INTRODUCTION

Plasma waves and instabilities have been extensively studied for gaseous plasmas for over four decades now, many of these phenomena have been experimentally observed and some have led to device applications as well. Analogous phenomena in solid state plasmas have been much less explored. Early attempts in this direction were unsuccessful due to the high collisionality of solid state systems. The advent of molecular beam epitaxy and other technological advances have made possible the creation of low dimensional systems (quasi two dimensional electron gas layers, quasi one dimensional quantum wires) with much reduced collisionalities, raising again the question, whether plasma instabilities can be generated in such systems, and if so, whether they can be utilized for practical device applications.

This is an important issue, both scientifically and for technological applications. If a nonequilibrium carrier distribution is (somehow) created, there are three distinct channels available to the excited carriers for relaxation to equilibrium: *phonons*, *photons* and *plasmons*. While the first two have been studied extensively, the third possibility has not received adequate attention. Plasmon generation, which is the result of net downwards (in energy) single particle transitions arising from a population inversion in the carrier distribution function, can indeed be a faster channel for relaxation in some situations, and significant energy transfer into growing plasma waves (plasma instabilities) may be possible under suitable conditions. This mode of energy relaxation will then be the preferred route for the carriers to lose their excess energy. The ensuing buildup in plasma wave (plasmon) energy can be directly (through dipole charge oscillations in a bounded plasma) or indirectly (through a grating coupler) converted into electromagnetic radiation at the frequency of the plasma mode, leading to radiation emission devices. For typical low dimensional semiconductor systems, these frequencies are in the terahertz range (meV in terms of energies: millimeter or submillimeter waves). Development of compact, coherent radiation

sources in this range would fill an important gap, and would be relevant for various scientific and technological applications [1].

We have examined the problem of generating plasma instabilities in low dimensional solid state systems for some time now [2-14], and shown theoretically the feasibility of these phenomena in a variety of situations through detailed calculations at the level of Random Phase Approximation. Here we ask the question whether some common features emerge, that presage the possibility of plasma instabilities. In classical plasmas, the mathematical signature for plasma instabilities is the Penrose criterion based on the global properties of the velocity space distribution function. We have generalized this criterion to quantum plasmas [13] in terms of a suitably averaged distribution function (Section 2). This generalized criterion explains many of the features found in our earlier studies of uniform systems [2-11] and can even be extended to periodically modulated systems [12]. For bounded systems with discrete energy levels, the resonant energy denominators play a major role in determining the criteria for plasma instabilities, and a different approach is required. The plasma mode frequencies are shifted from the inter-level frequencies by the collective effects (depolarization shifts). When an adequate population inversion is maintained, and an allowed downward transition frequency is slightly higher than an allowed upward transition frequency, a resonance of the depolarization shifted downward and upward frequencies occurs leading to a plasma instability. A new formalism (Energy Level-Pairs Formalism) is developed in Section 3 to analyze the Random Phase Approximation response of the system. This approach makes clear the basic mechanism for the generation of the plasma instability. It also shows how this criterion can be generalized to a group of levels (minibands in quantum wells or superlattices), and even to continua of levels, thereby providing a uniform explanation for plasma instabilities we have explored in several solid state systems [2-14].

2. CRITERIA FOR PLASMA INSTABILITIES

Plasma is a collection of charged particles where Coulomb interactions lead to collective behaviour. At the simplest (hydrodynamic) level of description, the plasma state is described [15] by the fluid density, velocity and the pervading electric field, and the corresponding perturbed quantities n_1, v_1 and E_1 undergo oscillations proportional to $e^{i\mathbf{q}\cdot\mathbf{x}}\, e^{-i\omega t}$, representing plasma waves. Equations of motion and continuity, along with Poisson's equation relate these variations and provide the dispersion relation $\omega = \omega(q)$ for the plasma mode. The unperturbed n_0, v_0 and E_0 need not be uniform, and a non equilibrium state can lead to complex frequencies with $\gamma(\equiv \mathrm{Im}\omega) > 0$ implying a growing wave amplitude proportional to $e^{\gamma t}$; this is the manifestation of a plasma instability.

The hydrodynamic description does not provide for wave particle interactions; for a proper description thereof one must employ the more general distribution function approach [15-18] in phase space with $f = f(\mathbf{x}, \mathbf{v}, t)$. The Vlasov equation for f, supplemented by the Poisson or Maxwell equations, leads to an effective dielectric function

$$\varepsilon(\mathbf{q},\omega) = 1 - v_q\chi(\mathbf{q},\omega), \tag{1}$$

where v_q is the Coulomb factor and $\chi(\mathbf{q},\omega)$ the susceptibility function. The solutions of $\varepsilon(\mathbf{q},\omega) = 0$ represent the allowed plasma modes $\omega = \omega(\mathbf{q})$, and if ω is complex with $\gamma > 0$, that plasma mode is unstable. The dielectric function for a *classical* 3D uniform equilibrium plasma is given by [16]

$$\varepsilon(\mathbf{q},\omega) = 1 - \frac{\omega_p^2}{q^2}\int_L \frac{q(\partial f_o/\partial u)}{qu - \omega}\,du, \tag{2}$$

where $f_o(u)$ is the equilibrium (Maxwellian) effective distribution function [16] as a function of u, the velocity component in the direction of $\mathbf{q}$, obtained by integrating out the perpendicular velocities. This leads to the standard plasma mode $\omega^2 = \omega_p^2 = 4\pi ne^2/m$ for small q with a small imaginary ω, ($\gamma < 0$), representing Landau damping due to the wave particle interactions [16].

For a nonequilibrium plasma with a two peaked distribution function $f_o(u)$ (e.g. as shown in Fig. 1 of Ref. 13, maintained by a net current), a *population inversion* occurs which allows a transfer of energy from the particles to the plasma wave giving rise to a plasma instability. The particles faster than the wave ($v > \omega/q$) impart energy to the wave, the particles slower than the wave ($v < \omega/q$) gain energy from the wave, and when the faster particles have a larger population than the slower ones ($\partial f/\partial u > 0$, for some $u > 0$) a plasma instability may become feasible. Thus the shape of $f_o(u)$ determines whether a plasma instability will occur.

There are two well known theorems in classical plasma instability theory [16]. (1) Gardner's Theorem: If for all directions $\mathbf{q}$, the effective distribution function decreases monotonically away from its maximum at $u = 0$, ($u(\partial f_o/\partial u) \le 0$), such a plasma remains stable. (2) Penrose Theorem: For a given $f_o(u)$, with one minimum at u_o, instability occurs if and only if

$$\int_{-\infty}^{\infty} \frac{f_o(u_o) - f_o(u)}{(u - u_o)^2}\,du < 0. \tag{3}$$

Gardner's theorem rules out plasma instabilities for single peaked distributions. Penrose criterion (3) provides a quantitative method for an *a priori* determination of whether an instability will occur, based on the shape of the effective distribution function. A simple corollary is that a distribution function with a velocity gap (no particles in some velocity range, i.e. $f_o(u_o)=0$) will necessarily be unstable.

For *quantum* plasmas, the Random Phase Approximation (RPA), which provides a very good description for most systems, leads to an effective dielectric function

$$\varepsilon(\mathbf{q},\omega) = 1 - \frac{4\pi e^2}{q^2} \sum_{\mathbf{p}} \frac{f(\mathbf{p} + \hat{\mathbf{q}}) - f(\mathbf{p})}{\varepsilon_{\mathbf{p}+\hat{\mathbf{q}}} - \varepsilon_{\mathbf{p}} - \hbar\omega}, \tag{4}$$

where $\hat{\mathbf{q}} = \hbar\mathbf{q}$, $f(\mathbf{p})$ is the momentum distribution function and $\varepsilon_{\mathbf{p}} = p^2/2m$. The structural similarity to the classical expression (2) is evident, and can be made more precise by a simple construction [13]. Rewrite the sum in Eq. (4) by shifting $\mathbf{p} \rightarrow \mathbf{p} - (\hat{\mathbf{q}}/2)$ as

$$\sum_{\mathbf{p}} \frac{f(\mathbf{p} + \hat{\mathbf{q}}/2) - f(\mathbf{p} - \hat{\mathbf{q}}/2)}{\varepsilon_{\mathbf{p}+\hat{\mathbf{q}}/2} - \varepsilon_{\mathbf{p}-\hat{\mathbf{q}}/2} - \hbar\omega}. \tag{5}$$

The denominator is simply

$$\frac{1}{2m}\{(\mathbf{p} + \hat{\mathbf{q}}/2)^2 - (\mathbf{p} - \hat{\mathbf{q}}/2)^2\} - \hbar\omega = \hbar(\mathbf{v}\cdot\mathbf{q} - \omega) = \hbar(qu - \omega), \tag{6}$$

where $\mathbf{p} = m\mathbf{v}$ and u is the velocity component in the direction of $\hat{\mathbf{q}}$. The numerator can be re-expressed in terms of a $\hat{\mathbf{q}}$-averaged distribution function by defining

$$f_{\hat{\mathbf{q}}}(\mathbf{p}) \equiv \int_{-1/2}^{1/2} d\xi\, f(\mathbf{p} + \xi\,\hat{\mathbf{q}}). \tag{7}$$

Then

$$\hat{\mathbf{q}} \cdot \frac{\partial}{\partial \mathbf{p}} f_{\hat{\mathbf{q}}}(\mathbf{p}) \equiv \int_{-1/2}^{1/2} d\xi \frac{\partial}{\partial \xi} f(\mathbf{p} + \xi\,\hat{\mathbf{q}}) = f(\mathbf{p} + \hat{\mathbf{q}}/2) - f(\mathbf{p} - \hat{\mathbf{q}}/2). \tag{8}$$

Thus Eq. (4) reduces to

$$\varepsilon(\mathbf{q},\omega) = 1 - \frac{4\pi e^2}{q^2} \sum_{\mathbf{p}} \frac{\hat{\mathbf{q}} \cdot \frac{\partial}{\partial \mathbf{p}} f_{\hat{\mathbf{q}}}(\mathbf{p})}{\hbar(qu - \omega)}. \tag{9}$$

Taking into account the different normalizations of $f(\mathbf{p})$ and $f_o(u)$, Eq. (9) reduces precisely to Eq. (2). This leads to the general result

$$\chi_{\text{quant}}[f(\mathbf{p})] = \chi_{\text{class}}[f_{\hat{\mathbf{q}}}(\mathbf{p})], \tag{10}$$

where $f_{\hat{q}}(\mathbf{p})$, Eq. (7), is just the original momentum distribution $f(\mathbf{p})$ averaged symmetrically over the range $\hat{\mathbf{q}} = \hbar\mathbf{q}$ centered at $\mathbf{p}$. While the derivation of Eq. (10) above was for 3D, the same result is obtained in 2D and 1D systems as well.

With this mapping, it is now possible to infer the properties of a quantum plasma from those of a classical plasma with the q-averaged distribution. In particular, the theorems of classical plasma theory can now be applied to determine the instability criteria for quantum plasmas. Since the mapping is q-dependent, a quantum plasma which is unstable for small q, may become stable for large q, as the corresponding classical distribution has less pronounced minima and maxima due to the extended averaging. This explains why in all our earlier studies on a variety of systems, the instability disappeared beyond some characteristic q_{max}. Also, it becomes apparent on reviewing our previous scenarios [2-12] for obtaining instabilities that those were different ways of achieving two peaked distributions in velocity space. Where the peaks were close, and the minimum between them was shallow, the Penrose condition (as applied to the q-averaged distribution) was not satisfied. Increasing the separation between the peaks by increasing the relative drift velocity led to the onset of instability at some threshold drift, usually of the order of the Fermi velocity v_F. This is easy to understand in the light of the discussion in this section: increased separation of the two peaks deepens the minimum, and when the two peaks are separated by a drift velocity exceeding their combined spread (typically of the order of v_F), the Penrose condition is satisfied. Increasing the drift increases the range of q over which the instability persists.

The Penrose criterion, and its generalization to quantum plasmas, are restricted to uniform systems. Periodically modulated systems with small density modulation can be approximately described in terms of effective velocity distributions as in [12], and the Penrose type criteria can be applied to these distributions. Bounded systems, which give rise to discrete energy levels, however, require a different approach. Plasma instability criteria for such systems are discussed in the next section.

3. ENERGY LEVEL PAIRS FORMALISM

We have shown elsewhere [13,14] the advantage of using bounded systems (or quasi bounded systems such as finite length quantum wires or finite width slabs or superlattices) for generation of plasma instabilities. Bounded systems have discrete energy levels, and the considerations of the previous section, based as they are on continuous distribution functions, are not applicable. Nevertheless, can one obtain some general, *a priori criteria* for plasma instabilities in such systems? It is clear even from the expression for the dielectric function for uniform systems, Eq. (4), that energy denominators will play a strong role for systems with discrete energy levels and the susceptibility will become large for frequencies which resonate with the interlevel separations. We develop in this section a formalism, which explicitly recognizes the role of interlevel separations, and which demonstrates what the essential criterion is for achieving an instability in such systems. This approach is then generalized to quasi bound systems and to systems with continuous

energy spectra as well, thus providing a unifying explanation for plasma instabilities in all systems.

The density response to an external potential perturbation at frequency ω, $V_e(\mathbf{r},t) = V_e(\mathbf{r})e^{-i\omega t}$ is given in the RPA by [13,14],

$$\delta\rho(\mathbf{r},\omega) = \int d\mathbf{r}'\chi_o(\mathbf{r},\mathbf{r}';\omega)V_T(\mathbf{r}',\omega)\,, \tag{11}$$

where χ_o is the single particle susceptibility,

$$\chi_o(\mathbf{r},\mathbf{r}';\omega) = 2\sum_{\varepsilon}\sum_{\varepsilon'}\frac{f_\varepsilon - f_{\varepsilon'}}{\varepsilon-\varepsilon'+\hbar\omega}\psi^*_\varepsilon(\mathbf{r})\psi_{\varepsilon'}(\mathbf{r})\psi^*_{\varepsilon'}(\mathbf{r}')\psi_\varepsilon(\mathbf{r}'). \tag{12}$$

χ_o is determined by the single particle energy levels ε and wave functions $\psi_\varepsilon(\mathbf{r})$ of the ground state (i.e. the unperturbed state, $V_e = 0$) of the system. The occupation numbers f_ε are prescribed by the external conditions imposed on the system. For example, for the equilibrium situation at temperature T = 0, all $f_\varepsilon = 1$ for $\varepsilon < \varepsilon_F$ the Fermi energy and $f_\varepsilon = 0$ for all $\varepsilon > \varepsilon_F$. Non equilibrium distributions $\{f_\varepsilon\}$ can be generated, and maintained in a steady state ground state, by selective injection and extraction techniques [14] or by applying an external electric field, etc. Plasma instabilities can arise for suitably arranged non equilibrium populations $\{f_\varepsilon\}$. The total potential $V_T = V_e + V_H$, where V_H is the Hartree potential,

$$V_H(\mathbf{r},\omega) = \frac{e^2}{\kappa}\int d\mathbf{r}'\,\frac{\delta\rho(\mathbf{r}',\omega)}{|\mathbf{r}-\mathbf{r}'|}\,, \tag{13}$$

κ being the dielectric constant of the material. This system of equations, (11) to (13) has to be solved self consistently, and those frequencies that make the response $\delta\rho(\mathbf{r},\omega)$ exceptionally large are the *normal modes* of the system. These are the oscillations that can arise spontaneously in the system. If ω is complex, and $\gamma > 0$, this will be a plasma instability with density response and other related quantities growing in time as $e^{\gamma t}$.

Depending on the nature of the system under consideration, these standard RPA equations can be solved in a variety of ways. We introduce here yet another point of view; it has the merit of explicitly recognizing the importance of the interlevel energy separations, and being particularly well suited to answer the question raised at the beginning of this section.

Let us first consider, for the sake of illustration, a system which has only two energy levels ε_1 and ε_2, with corresponding wave functions ψ_1 and ψ_2, taken to be real. Then Eq. (12) simplifies to

$$\chi_o(\mathbf{r},\mathbf{r}';\omega) = C_{21}(\omega)\,\psi_1(\mathbf{r})\psi_2(\mathbf{r})\psi_1(\mathbf{r}')\psi_2(\mathbf{r}'), \tag{14}$$

$$C_{21}(\omega) = \frac{4\Delta_{21}(f_2 - f_1)}{\Delta_{21}^2 - \omega^2}\ , \tag{15}$$

$\Delta_{21} = \varepsilon_2 - \varepsilon_1 > 0$, and $\hbar$ has been absorbed in ω (now measured in energy units). The self consistent set of Eqs. (11 to 13) reduces to

$$\delta\rho(\mathbf{r},\omega) = C_{21}(\omega)\psi_1(\mathbf{r})\psi_2(\mathbf{r})\,[\langle 1\,|V_{ext}|\,2\rangle + (e^2/\kappa)\,A_{12}], \tag{16}$$

with

$$A_{12} = \int \psi_1(\mathbf{r}')\psi_2(\mathbf{r}')\,\frac{\delta\rho(\mathbf{r}'',\omega)}{|\mathbf{r}' - \mathbf{r}''|}\,d\mathbf{r}'\,d\mathbf{r}''\ . \tag{17}$$

Now multiplying eq. (16) by $\psi_1(\mathbf{r}')\psi_2(\mathbf{r}')/|\mathbf{r}' - \mathbf{r}|$ and integrating over $\mathbf{r}'$ and $\mathbf{r}$ leads to a linear equation for A_{12},

$$A_{12} = C_{21}(\omega)G_{12,12}\,[(V_{ext})_{12} + (e^2/\kappa)\,A_{12}], \tag{18}$$

with

$$G_{12,12} = \int \psi_1(\mathbf{r})\psi_2(\mathbf{r})\,\frac{1}{|\mathbf{r} - \mathbf{r}'|}\,\psi_1(\mathbf{r}')\psi_2(\mathbf{r}')\,d\mathbf{r}\,d\mathbf{r}'. \tag{19}$$

The explicit solution is

$$A_{12}(\omega) = [\,1 - C_{21}(\omega)\,(e^2/\kappa)\,G_{12,12}]^{-1}\,C_{21}(\omega)\,G_{12,12}(V_{ext})_{12}. \tag{20}$$

The density response $\delta\rho(\mathbf{r},\omega)$ becomes exceptionally large at all $\mathbf{r}$ when ω is such that the square bracket in eq. (20) vanishes, or

$$\omega^2 = \Delta_{21}^2 - 4\Delta_{21}\,(f_2 - f_1)\,(e^2/\kappa)\,G_{12,12}. \tag{21}$$

This is the collective response frequency of the plasma composed of a two level system with occupation numbers f_1 and f_2. Eq. (21) is the fundamental equation describing the depolarization shift for the energy pair (ε_1, ε_2) due to the Coulomb interactions of the occupants of those levels. If we absorb the factor (e^2/κ) into the Coulomb matrix element G, it becomes an averaged Coulomb energy which provides a quantitative measure of those interactions. It is easy to show that this energy G is positive definite, by using an integral representation for the Coulomb factor in Eq. (19),

$$\frac{e^2}{\kappa|\mathbf{r} - \mathbf{r}'|} = \int d\mathbf{q} e^{i\mathbf{q} \cdot (\mathbf{r} - \mathbf{r}')} v_q, \tag{22}$$

where the specific form of v_q depends on the dimensionality of the system, but is positive definite in all cases. Then

$$G_{12,12} = \int d\mathbf{q}\ v_q\ |\langle 1\ |e^{i\mathbf{q}\cdot\mathbf{r}}|\ 2\rangle|^2 \tag{23}$$

is also, obviously, positive definite. Thus Eq. (21) shows that for normal population distribution ($f_2 < f_1$) the plasma response is at an energy $\omega > \Delta_{21}$, the pair energy separation. On the other hand, with population inversion ($f_2 > f_1$), $\omega < \Delta_{21}$ and the depolarization shift is negative.

What is the physical mechanism behind these depolarization shifts? The matrix element and its complex conjugate in Eq. (23) represent a (virtual) plasmon emission with momentum $\mathbf{q}$ followed by its absorption. The Fourier transformed Coulomb factor v_q represents the relative probability for this process (at momentum $\mathbf{q}$), and the full integration takes into account all possible scenarios. Thus intrapair (virtual) plasmon emission and reabsorption is the basic mechanism for the depolarization shifts in a single pair.

Based on this physical picture, it is easy to see what will happen if more energy levels are introduced into the system. Each energy pair, by itself, will create its own depolarization shifts as in Eq. (21). But in addition there will be interpair Coulomb interactions (coupling different pairs) where the plasmon is emitted by one pair but absorbed by another. Thus the consistency condition will be some appropriate generalization of the vanishing of the square bracket in Eq. (20), representing the modification of the intrapair shifts due to all the interpair interactions.

Before displaying the general result, let us consider a three levels system, which proves to be a paradigm for the generation of plasma instabilities. There are three energy pairs in a three level system, represented by (12), (23) and (31) as indices for the quantities Δ, C, A and G in the previous discussion. The self consistency condition leads to coupled equations for A_{12}, A_{23} and A_{31} and the condition for an exceptionally large response $\delta\rho(\mathbf{r},\omega)$ for any external perturbation leads to a 3 x 3 determinantal condition for the normal modes ω^2. Besides the intrapair elements like $G_{12,12}$, we also have interpair $G_{12,23}$, $G_{12,31}$

and $G_{23,31}$ defining the full response. If we consider the special case where only the middle level is occupied ($f_2 = 1$) and the other two are empty ($f_1 = f_3 = 0$), all entities with index (13) drop out. Physically this is so, since the only transitions can be from 2 to 1 or 2 to 3, represented by the pair indices (21) and (23). Algebra similar to Eqs. (14) to (20) leads to a pair of coupled equations for A_{12} and A_{23}, and the condition for a large response is the 2 x 2 determinantal condition

$$\begin{vmatrix} 1 - C_{21}G_{21,21} & - C_{23}G_{21,23} \\ - C_{21}G_{23,21} & 1 - C_{23}G_{23,23} \end{vmatrix} = 0. \qquad (24)$$

This provides a quadratic equation for ω^2,

$$(\Delta_{21}^2 - 4\Delta_{21}G_{21,21} - \omega^2)(\Delta_{23}^2 - 4\Delta_{23}G_{23,23} - \omega^2) - 16\Delta_{21}\Delta_{23}|G_{23,21}|^2 = 0, \qquad (25)$$

where $\Delta_{21} = \varepsilon_2 - \varepsilon_1 > 0$, but $\Delta_{23} = \varepsilon_2 - \varepsilon_3 < 0$, and with real wave functions,

$$G_{23,21} = \int dr\, dr'\, \psi_2(r)\psi_3(r) \frac{e^2/\kappa}{|r - r'|} \psi_2(r')\psi_1(r') \qquad (26)$$

$$= \int dq\, v_q \langle 2|\, e^{iq\cdot r}\, |3\rangle \langle 2|\, e^{-iq\cdot r'}\, |1\rangle = G_{21,23}.$$

Without the interpair processes (i.e. neglecting the last term in Eq. (25) we simply recover the two depolarization shifted individual pair modes at frequencies

$$\omega_{21}^2 = \omega_{21}^2 - 4\Delta_{21}G_{21,21} \;;\; \omega_{23}^2 = \Delta_{23}^2 - 4\Delta_{23}G_{23,23} \qquad (27)$$

where the down transition frequency is reduced ($\omega_{21} < \Delta_{21}$), and the up transition frequency is enhanced ($\omega_{23} > |\Delta_{23}|$), from the corresponding interlevel (single particle transition) values. If we can arrange the energy levels so that $\Delta_{21} > |\Delta_{23}|$, it may be possible to bring ω_{21} and ω_{23} into resonance (i.e. make $\omega_{21} = \omega_{23} = \omega_R$) through the collective effects. Then Eq. (25) becomes

$$(\omega^2 - \omega_R^2)^2 = 16\Delta_{21}\Delta_{23}\, |G_{23,21}|^2, \qquad (28)$$

or

$$\omega^2 = \omega_R^2 \pm 4i\Delta_{21}\,|\Delta_{23}|\,|G_{23,21}|, \tag{29}$$

since Δ_{21} and Δ_{23} have opposite signs. This, then, is the essential mechanism that generates plasma instabilities. Arrange the energy differences and populations of two pairs such that the down transition frequency is larger than the up transition frequency. If the collective effects are strong enough to bring them into resonance, Eq. (29) will prevail and the root with $\gamma > 0$ creates the plasma instability. The strength of the instability (size of γ) at resonance is governed by the interpair processes implied by the Coulomb matrix element G of Eq. (26). The emission of a (virtual) plasmon $\mathbf{q}$ in one pair coupled with its absorption in another pair is the essential physical mechanism for the generation of plasma instability.

For the general system with M energy levels, there are $\frac{1}{2}$ M(M-1) = N energy pairs, labelled by (ij) where $i \neq j$ and (ij) is the same as (ji). Analysis similar to the preceding special cases leads to the eigenmode condition in the *energy pair representation*,

$$\det\,[\delta_{ij,k\ell} - G_{ij,k\ell}C_{k\ell}] = 0, \tag{30}$$

with definitions of C and G analogous to Eqs. (15) and (26), and where the determinant has dimension N. By multiplying each column in Eq. (30) by $(\Delta_{k\ell}^2 - \omega^2)$, we obtain the standard form

$$\det\,[\Delta_{k\ell}^2 - \omega^2)\delta_{ij,k\ell} - G_{ij,k\ell}\,\hat{C}_{k\ell}] = 0, \tag{31}$$

where the ω-dependence has been made explicit, and $\hat{C}_{k\ell} = C_{k\ell}(\Delta_{k\ell}^2 - \omega^2)$ does not depend on ω. It is clear that the number of modes predicted by Eq. (31) is the same as the dimensionality N. The density response for any one of these normal modes, $\omega^2 = \omega_n^2$, is given by

$$\delta\rho(\mathbf{r},\omega_n) = \sum_{(ij)} A_{(ij)}(\omega_n)(e^2/\kappa)C_{(ij)}(\omega_n)\psi_i(\mathbf{r})\psi_j(\mathbf{r}) \equiv \sum_{(ij)} \delta\rho_{(ij)}(\mathbf{r},\omega_n), \tag{32}$$

which displays explicitly the relative contribution of each pair (ij). The relative weights are given by $A_{(ij)}(\omega_n)C_{(ij)}(\omega_n)$. Thus this formalism is capable of describing the full RPA response of any system in a convenient form. The dimensionality is reduced considerably if all levels are either completely filled ($f_i = 1$) or empty ($f_i = 0$). If there are M_o occupied

levels and M_e empty levels, the dimension of the determinant in (30) is reduced to $N = M_o M_e$.

Significant simplifications occur if the interpair Coulomb energies $G_{ij,k\ell}$ are small. Then a systematic expansion of the determinant in Eq. (31) is possible,

$$1 + \sum_{ij,k\ell}{}' \frac{|G_{ij,k\ell}|^2 \hat{C}_{ij}\hat{C}_{k\ell}}{(\omega_{ij}^2 - \omega^2)(\omega_{k\ell}^2 - \omega^2)} + \ldots = 0, \tag{33}$$

where the depolarization shifted ω_{ij}^2 are the analogs of Eq. (21) or (27), and the summation excludes $(ij) = (k\ell)$ and also avoids repetition of terms. If we ignore the higher order terms, and resolve the second term into partial fractions, we obtain

$$1 + \sum_{ij} \frac{B_{ij}}{\omega_{ij}^2 - \omega^2} = 0, \tag{34}$$

a form reminiscent of the atomic polarizability expression. The coefficients B_{ij} can be given explicitly in terms of the G's and $\hat{C}$'s. Eq. (34) represents the effective dielectric function for the system. It may be noted that there is no plasmon $\mathbf{q}$, nor any dispersion $\omega = \omega(\mathbf{q})$ in any of these expressions. This is so because a bounded plasma does not admit plane waves and thus $\mathbf{q}$ is not a characterizing parameter for a mode. The numerical order of the mode approximately plays the role of $\mathbf{q}$ in a bounded plasma, and in the limit of large sized systems, a clear correspondence to the free system limit can be established. In principle Eq. (33) can be expanded in the higher order denominators involving ω^2, which can all be resolved into simple partial fractions (assuming no degeneracies, $\omega_{ij} \neq \omega_{k\ell}$). Then the B_{ij} in Eq. (34) would be replaced by more involved coefficients D_{ij} in terms of chain products of the interpair elements (G's). These remarks are only intended to show the generality of this approach; the details and practical applications will be provided elsewhere.

A special case of practical importance for plasma instabilities is that of a finite width slab (a quantum well), limited in the x direction to length L, and open in the y and z directions. Now the wave functions in Eq. (12) have the form

$$\psi_\varepsilon(\mathbf{r}) = e^{ik_y y}\, e^{ik_z z}\, \psi_{\varepsilon_x}(x). \tag{35}$$

The plane waves in y and z directions allow plasmons of specific wave numbers q_y and q_z ($\equiv \mathbf{q}_\perp$) through momentum conservation, and the more general χ_o of Eq. (12) can now be represented through its Fourier transform

$$\chi_o(x,x';\omega,q_\perp) = 2\sum_{\varepsilon_x}\sum_{\varepsilon_x'}\sum_{p_\perp}\frac{f_{\varepsilon_x,p_\perp+q_\perp}-f_{\varepsilon_{x'},p_\perp}}{\varepsilon_x-\varepsilon_{x'}+\varepsilon_{p_\perp+q_\perp}-\varepsilon_{p_\perp}+\hbar\omega}\psi_{\varepsilon_x}(x)\psi_{\varepsilon_x'}(x)\psi_{\varepsilon_x'}(x')\psi_{\varepsilon_x}(x'). \quad (36)$$

The response at $q_\perp = 0$ can be related to that of a one dimensional problem, since the transverse energies drop out from the denominator and the distributions in the numerator can be summed over $p_\perp$. Thus the formalism discussed above is directly applicable with the advantage that the summed f's provide strong collective effects. All the particles with different perpendicular momenta respond coherently to enhance various collective effects. Strong plasma instabilities can be expected for this scenario, a prediction we have confirmed by detailed calculations. All the vertical transitions ($q_\perp = 0$) between the x-energy levels have the *same* matrix elements and these add up coherently to scale the effective G's from their one dimensional quantum well (i.e. finite length wire, Ref. 14) values to much larger values for the case of a slab. Thus much stronger plasma instabilities are to be expected from the slab systems.

The same technique of summing the f's over perpendicular momenta can be used for small $q_\perp$, even though the energy denominators are not exactly the same. This remains a good approximation for a significant range of $q_\perp$, since the energy denominators are primarily governed by the well separated x-energy levels.

Extending these approximation techniques a step further, several closely spaced energy denominators can be grouped together into an average denominator and treated as a single energy pair. This is clearly applicable to minibands in multiple quantum wells or superlattices. Even for a continuum of energies such as the two peaked distribution of section 2, one can consider that to be an effectively three level system, with the two peak energies well occupied and the intermediate energy level (at the velocity minimum) almost empty. This three level system will lead to a determinantal condition defining the parameter range for a plasma instability. This type of approach, emphasizing the grouping of almost similar energy denominators may provide a practical method for a quick evaluation of whether a given system will generate a plasma instability. We are already able to relate qualitatively the main results of our previous studies [2-14] to simple considerations outlined in this section.

4. CONCLUDING REMARKS

In view of the importance of using the plasma instabilities approach (which can also be characterized as stimulated plasmon emission or a plasmon laser) to generate electromagnetic radiation in the terahertz range, obtaining *a priori* indications of their feasibility is very valuable. We have shown (Section 2) how the classical criteria can be generalized to quantum systems described within the RPA. We have also developed (Section 3) a new formalism, especially suited to bounded systems, which enables one to see the potential for plasma instabilities in such systems. In addition, it provides a unifying approach which can explain the main features of our earlier results in several different types

of systems. The basic, universal criterion that emerges is that the plasma instability is created by an interplay of matching up and down transitions. The latter necessarily require some *population inversion* in part of the energy spectrum. The strength of the *collective effects* has to be sufficient to *reduce* the (single particle) down transition frequency *and increase* the (single particle) up transition frequency to bring them into resonance to create the instability. The *strength* of the instability at this resonance is governed by the *interpair* Coulomb interactions. Grouping of pairs with similar energy denominators into a single effective pair with a coherently enhanced interaction strength is permissible, and provides a simple explanation of several of our earlier results. This broad understanding makes it possible to *design* systems with appropriate energy and distance scales that enhance the instabilities. For example, in a quantum well the energy separations Δ scale as $(1/L^2)$ while the Coulomb interactions G scale as (1/L), providing an *a priori* assessment of the size of the system that may generate a plasma instability. It is also clear from this formalism that higher temperatures do not create any limitations, in principle, on obtaining plasma instabilities. Even broad band population inversion (as is commonly the case in classical plasmas) will lead to a plasma instability. The mode is sharp and is *not* broadened due to thermal effects. Essentially, this is so because all the electrons participating in the creation of the plasma mode are moving coherently amongst the participating pairs. Further elaborations of the formalisms and various applications will be given elsewhere.

ACKNOWLEDGMENTS

We thank Dr. Mikael Ciftan for many valuable discussions. This work was supported by U.S. Army Research Office Grant No. DAAH04-94-G-0052. Participation at the Condensed Matter Theory 20th Workshop and presentation of this paper were facilitated by U.S. Army Research Office Grant No. DAAH04-96-1-0184.

REFERENCES

[1] See, for example, in Proceedings of SPIE, Vol. **2145**, eds. N. Peygambarian, *et al* . (1994): Session 9, on "Invited Papers on Systems Applications for THz Sources," M.A. Freking, p. 222; T.G. Phillips, p. 230; F.C. DeLucia and T.M. Goyette, p. 239; R.A. McGee, p. 248; and Session 5, Keynote Address on "Terahertz Sources" by B.D. Guenther, p. 120.

[2] P. Bakshi, J. Cen and K. Kempa , J. Appl. Phys. **64**, 2243 (1988).

[3] J. Cen, K. Kempa and P. Bakshi, Phys. Rev. B**38**, 10051 (1988).

[4] K. Kempa, P. Bakshi and J. Cen, Proceedings of SPIE , vol. **945**, 62 (1988).

[5] K. Kempa, J. Cen and P. Bakshi, Rapid Communication, Phys. Rev. B**39**, 2852 (1989). Also see, for experimental verification, F. Dong, M.J. Graf and P.M. Mankiewich, Solid State Commun. **84**, 785, (1992); and M.J. Graf, P. Bakshi, F. Dong and K. Kempa, Physica B, **194-196**, 2377 (1994).

[6] P. Bakshi and K. Kempa, Rapid Communication, Phys. Rev. B**40**, 3433 (1989).

[7] P. Bakshi, J. Cen and K. Kempa, Solid State Commun. **76**, 835-837, (1990).

[8] J. Cen, K. Kempa and P. Bakshi, Solid State Commun. **78**, 433-437 (1991).
[9] K. Kempa, P. Bakshi, J. Cen and H. Xie, Phys. Rev. B**43**, 9273-9274 (1991).
[10] H. Xie, K. Kempa and P. Bakshi, J. Appl. Phys. **72**, 4767 (1992).
[11] K. Kempa, P. Bakshi, H. Xie and W.L. Schaich, Phys. Rev. B**47**, 4532 (1993).
[12] K. Kempa, P. Bakshi and H. Xie, Rapid Communication, Phys. Rev. B**48**, 9158 (1993).
[13] P. Bakshi and K. Kempa, Superlattices and Microstructures, **17**, 363 (1995).
[14] K. Kempa, P. Bakshi and E. Gornik, Phys. Rev. B**54**, 8231 (1996).
[15] F.F. Chen, *Introduction to Plasma Physics and Controlled Fusion*, (Plenum Press, New York, 1984).
[16] N. Krall and A. Trivelpiece, *Principles of Plasma Physics*, (McGraw-Hill, New York, 1973).
[17] S. Ichimaru, *Basic Principles of Plasma Physics*, (Benjamin/Cummings, Reading, MA, 1973).
[18] A.B. Mikhailovskii, *Theory of Plasma Instabilities, Vol. 1*, (Consultant Bureau, New York, 1974).

BOSE-EINSTEIN CONDENSATION, PAIRING AND ODLRO: A VIEW FROM COORDINATE SPACE

C. E. Campbell

Institute for Theoretical Physics
University of Linz, A-4040 Linz, AUSTRIA

and

School of Physics and Astronomy
University of Minnesota, Minneapolis, MN 55455 USA †

1. INTRODUCTION

In this contribution we discuss a few old results on Bose-Einstein condensation (BEC), off-diagonal long range order (ODLRO), and pairing, with an orientation to coordinate space in order to deal with realistic hamiltonians for strongly correlated systems.

Superfluidity and superconductivity are manifestations of quantum mechanics at a macroscopic level. The most direct connection with the microscopic physics is through the nature of off-diagonal order in reduced density matrices. With these density matrices one can define a macroscopic order parameter or wave-function which obeys a Schrödinger-like equation and contains the quantum mechanical phase and density information concerning superfluidity or superconductivity.

It is possible and useful to arrive at this information from the microscopic description of the system just as one does when using statistical physics to obtain thermodynamic and transport properties of macroscopic systems. In particular, the existence of a macroscopic wavefunction describing some of the quantum properties of the many-body system is an indication that the macroscopic state depends on average on only one or a few coordinates. Information about the multiparticle correlations can be discarded by tracing out nearly all of the many-body degrees of freedom, keeping only the off-diagonal dependence of the remaining few coordinates. Thus it should not be surprising that it is only necessary to have the one-body density matrix to describe boson superfluidity and the two-body density matrix to describe fermion superfluidity.

In the case of strongly correlated systems, it is advantageous, and sometimes necessary, to formulate this in coordinate space. Contrary to a common view, there

is no serious disadvantage to working in coordinate space representation, and there are some additional advantages since the very notions of reduced density matrices and the off-diagonal limit are coordinate space concepts.

2. OFF-DIAGONAL LONG RANGE ORDER IN BOSE FLUIDS

The relationship between ODLRO in boson fluids and BEC was first shown by Oliver Penrose in 1951 by considering the properties of the one-body density matrix for a boson fluid [1]:

$$\rho_1(\mathbf{r},\mathbf{r}') \equiv \langle \psi^\dagger(\mathbf{r})\,\psi(\mathbf{r}')\rangle$$

where $\psi^\dagger(\mathbf{r})$ is the creation operator for a particle at $\mathbf{r}$, and the expectation value is either an appropriate ensemble average at finite temperature or the ground state average at zero temperature. Clearly this is the amplitude for the simultaneous removal of a particle at $\mathbf{r}$ and addition of a particle at $\mathbf{r}'$ as long as $\mathbf{r} \neq \mathbf{r}'$, and is closely related to one-body Green functions. The relationship to the condensate fraction is given by taking the off-diagonal limit:

$$\lim_{|\mathbf{r}-\mathbf{r}'|\to\infty} \rho_1(\mathbf{r},\mathbf{r}') = N_0 \Phi_0(\mathbf{r}')\Phi_0^\star(\mathbf{r}) \ ,$$

where this may be taken as the definition of $\Phi_0(\mathbf{r})$ if such a limit exists and $\Phi_0(\mathbf{r})$ is normalized. The existence of ODLRO is determined by the order of magnitude of N_0: If N_0 is macroscopic in the thermodynamic limit, then the system is said to possess ODLRO, and $\Phi_0(\mathbf{r})$ is the macroscopic wavefunction of the system (or, more commonly, $\sqrt{N_0}\Phi_0(\mathbf{r})$ is the order parameter of the system). Thus the order parameter is of order unity in the thermodynamic limit; equivalently, the condensate number N_0 is macroscopic, and the condensate fraction (defined by $n_0 = N_0/N$ for an N-body system) is of order unity. This describes the situation for liquid ^4He in a bulk geometry below the lambda temperature, including the case when there is spatial inhomogeneity, leading to a non-trivial $\Phi_0(\mathbf{r})$ [2].

The macroscopic wavefunction is often exhibited as the solution of a non-linear Schrödinger equation, known as the Gross-Pitaevskii or Ginzberg-Landau equation when done at the mean-field level or including spatial fluctuations. Such an equation for Φ_0 may be formally obtained from the full microscopic hamiltonian H by taking the following limit:

$$\lim_{|\mathbf{r}-\mathbf{r}'|\to\infty} \langle \psi^\dagger(\mathbf{r})\, H\, \psi(\mathbf{r}')\rangle \, .$$

However the resultant equation is not terribly practical for our purposes; it appears much more useful for strongly correlated systems (especially when they are inhomogeneous) to find $\rho_1(\mathbf{r},\mathbf{r}')$ by first solving the many-body problem and then using the resultant ρ_1 to obtain Φ_0 and N_0 by treating $\rho_1(\mathbf{r},\mathbf{r}')$ as a non-local one-body operator and solving for its eigenvalues and eigenfunctions. The largest eigenvalue is then N_0 and the corresponding eigenfunction is our macroscopic wavefunction $\Phi_0(\mathbf{r})$ [3].

The situation is quite different in reduced dimensions at finite temperatures. Quantum fluctuations eliminate the possibility of a non-zero condensate fraction in one-dimension, and at non-zero temperatures in two-dimensions; with a sufficiently long-ranged interaction, the condensate fraction is zero even in the ground-state in

two-dimensions [4,5]. However superfluidity exists in liquid helium films in spite of the fact that the condensate fraction vanishes in the thermodynamic limit (defined for films to be the limit as the lateral dimensions diverge). This may be understood in terms of the existence of quasi-ODLRO (QODLRO), whereby the off-diagonal limit of the one-body density matrix vanishes in the thermodynamic limit, but sufficiently slowly (algebraically) that the integral over $|\mathbf{r}-\mathbf{r}'|$ diverges in the thermodynamic limit, signifying the divergence of the order-parameter susceptibility.

This QODLRO actually gives some life to the condensate fraction as long as one takes the thermodynamic limit carefully. In particular one finds that in this ordered phase, $N_0 \propto N^c$ where $0 < c < 1$ in a QODLRO phase. In that case one may still define the condensate wavefunction $\Phi_0(\mathbf{r})$ as above.

In liquid helium, the coherence length is rather short-ranged: the off-diagonal limit in the case of the bulk is achieved well before $|\mathbf{r}-\mathbf{r}'|$ reaches $10\mathring{A}$. At equilibrium density for zero temperature, the condensate fraction is approximately $N/N_0 = 0.085$ as determined by quantum Monte Carlo simulations [6], a number that is consistent with deep inelastic neutron scattering at low temperatures [7].

The spatially quick onset of the ODLRO limit leads to the possibility of superfluid-like behavior in systems as small as a few hundred particles Ref. [3] and references cited therein).

3. OFF-DIAGONAL LONG RANGE ORDER IN FERMION FLUIDS

By examining the possibility of ODLRO in *ideal* Bose and Fermi gases, it is clear immediately that there is a fundamental difference imposed by the statistics: the ideal Bose gas has a Bose-Einstein condensate at and below a well-defined transition temperature, while the ideal Fermi gas does not. While the introduction of interactions produces fundamental differences for both statistics, nature shows us that this qualitative difference is robust: a gas or liquid of interacting bosons will have a BEC and ODLRO if the temperature is low enough or the density is high enough, but fermion fluids apparently do not possess ODLRO unless there is an attractive interaction present, and even then it is not guaranteed.

The absence of ODLRO in the one-body density matrix for a fermion system is a trivial consequence of the Pauli exclusion principle: the condensate number N_0 is in every case the occupation number of a one-body state (specifically, Φ_0) [3], which cannot be greater than one when spin is included.

The solution to this old puzzle has long been known [8,9]. Stated in terms of the reduced density matrices, the lowest order reduced density matrix in which one may find ODLRO in fermion fluids is the two-body density matrix, which is defined by [10]

$$\rho_2(\mathbf{r_1},\mathbf{r_2},\mathbf{r_1}',\mathbf{r_2}') \equiv \left\langle \psi^\dagger(\mathbf{r_2})\psi^\dagger(\mathbf{r_1})\psi(\mathbf{r_1}')\psi(\mathbf{r_2}')\right\rangle .$$

and has a similar interpretation as the one-body density matrix except in this case for pairs of particles. The ODLRO that corresponds to superconductivity in fermion systems (and fermion superfluidity in liquid ^3He) is obtained by taking the off-diagonal limit wherein both unprimed coordinates approach an infinite distance from the primed coordinates:

$$\lim_{OD} \rho_2(\mathbf{r_1},\mathbf{r_2},\mathbf{r_1}',\mathbf{r_2}') = M_0\Phi_0(\mathbf{r_1},\mathbf{r_2})\Phi_0^\star(\mathbf{r_1}',\mathbf{r_2}')$$

where now we have a macroscopic, normalized pair wavefunction $\Phi_0(\mathbf{r_1}, \mathbf{r_2})$ which is short-ranged in $\mathbf{r}_1 - \mathbf{r}_2$, a dependence that can otherwise be ignored in the analysis of ODLRO. Indeed, in a uniform system, one may decompose Φ_0 into a "center of mass" factor depending on $(\mathbf{r}_1 + \mathbf{r}_2)/2$ multiplied by a "relative" factor. If the relative factor falls off fast enough to be normalized in a volume of order unity, then one has ODLRO in the two-body density matrix if M_0 is macroscopic. It is relatively simple to calculate this two-body wavefunction in a translationally invariant BCS superconductors, where it is seen that $\sqrt{M_0}\Phi_0(\mathbf{r})$ is just the fourier transform of $u_k v_k^*$, and

$$M_0 = \frac{1}{\Omega} \sum_{\mathbf{k}} |u_k|^2 \, |v_k|^2$$

where u_k and v_k are the BCS-Bogoliubov parameters determined by diagonalizing the BCS hamiltonian.

Another possible form of superfluidity appearing in the two-body density matrix is a bound-state pairing, wherein this two-body function is exponentially short-ranged[11-13]. That would be a composite boson picture, where the two-body bound state essentially satisfies Bose statistics. This type of pairing could occur at a higher temperature than the onset of ODLRO, unlike the BCS transition where the Cooper pairs are formed at the superconducting transition temperature. Of course the onset of ODLRO in the two-body density matrix in the bound-state pairing case could be described just as well by ODLRO in the one-body density matrix of the composite bosons. In that case the maximum value of M_0 would be $N/2$. It should be noted, however, that such bound-state pairing would require an attractive interaction over the distance scale of the exponential, which suggests that there must be involved additional bodies in the pairing if when the two bound particles are identical "elementary" particles, such as two electrons. (Composite fermions such as deuterium and ^{3}He can have a "bare" attractive interaction leading to unassisted pairing.)

4. ADDITIONAL PROPERTIES OF FEW-BODY DENSITY MATRICES

There are a few properties of ρ_2 that are worth noting, and when combined with the corresponding properties of ρ_1 point to general properties for higher order reduced density matrices (though the latter are not important for present purposes), and again give some insight in to the relationship between boson and fermion ODLRO. It is obvious that the two-body density matrix is symmetric or antisymmetric in the unprimed coordinates (as well as the primed coordinates) for boson and fermion statistics respectively, and it follows that for both statistics it is symmetric under simultaneous exchange of indices 1 and 2. All reduced density matrices are linked by sequential relationships whereby the lower order density matrices may be obtained from the higher order ones by tracing out an appropriate number of coordinates. In particular,

$$\int \rho_1(\mathbf{r}_1, \mathbf{r}_1) d\mathbf{r}_1 = N$$

and

$$\int \rho_2(\mathbf{r}_1, \mathbf{r}_2', \mathbf{r}_1, \mathbf{r}_2) d\mathbf{r}_1 = (N-1)\rho_1(\mathbf{r}_2', \mathbf{r}_2)$$

Finally the fully on-diagonal n-body reduced density matrix is precisely the n-body reduced density. Thus, in the common notation:

$$\rho_1(\mathbf{r}, \mathbf{r}' = \mathbf{r}) = \rho(\mathbf{r})$$

which is the one-body density, while

$$\begin{aligned}\rho_2(\mathbf{r_1}, \mathbf{r_2}, \mathbf{r_1}, \mathbf{r_2}) &= \rho_2(\mathbf{r_1}, \mathbf{r_2}) \\ &= \rho(\mathbf{r_1})\rho(\mathbf{r_2})g_2(\mathbf{r_1}, \mathbf{r_2})\end{aligned}$$

where g_2 is the well-known pair distribution from the theory of fluids. (Having the correct behavior of $g_2(\mathbf{r_1}, \mathbf{r_2})$ as $|\mathbf{r_1} - \mathbf{r_2}| \rightarrow 0$ is crucial to a good theory of strongly correlated fluids.) One also has occasion to use the partially off-diagonal two-body density matrix, which appears under the integral sign in the $2 \Rightarrow 1$ sequential relationship above, and which also plays an important role in the theory of final state interactions in deep inelastic neutron scattering.

When there is ODLRO in an $n-body$ density matrix, it implies the presence of ODLRO in a higher-order density matrix as long as both reduced density matrices have have indices n of $O(N^0)$ [10]. In particular, ODLRO in the one-body density matrix in a boson system leads immediately to ODLRO in the two-body density matrix:

$$\lim_{OD} \rho_2(\mathbf{r_1}, \mathbf{r_2}, \mathbf{r_1}', \mathbf{r_2}') = N_0^2 \Phi_0(\mathbf{r_1}, \mathbf{r_2}) \Phi_0^*(\mathbf{r_1}', \mathbf{r_2}')$$

Thus the two-body condensate number $M_0 = N_0^2$, but at the same time the pair wavefunction $\Phi_0(\mathbf{r_1}, \mathbf{r_2})$ is no longer short-range in $|\mathbf{r_1} - \mathbf{r_2}|$, instead satisfying:

$$\lim_{|\mathbf{r_1} - \mathbf{r_2}| \rightarrow \infty} \Phi_0(\mathbf{r_1}, \mathbf{r_2}) = \Phi_0(\mathbf{r_1}) \Phi_0(\mathbf{r_2})$$

Thus there is an extra factor of the volume in the denominator of the right-hand side, making the entire right-hand side of the off-diagonal limit of the two-body density matrix again of order unity in this case. Nevertheless one can see that the ODLRO in the two-body density matrix of a system which has ODLRO in the one-body density matrix is fundamentally different than the possible ODLRO in the two-body density matrix of a fermion system. The full off-diagonal limit in the former case is then

$$\lim_{DOD} \rho_2(\mathbf{r_1}, \mathbf{r_2}, \mathbf{r_1}', \mathbf{r_2}') = N_0^2 \Phi_0(\mathbf{r_1}) \Phi_0(\mathbf{r_2}) \Phi_0^*(\mathbf{r_1}') \Phi_0^*(\mathbf{r_2}')$$

where the "DOD" limit means that all coordinates are distant from one another, not just primed from unprimed.

Note that there is no reason in principle that a boson fluid should not *first* show ODLRO in the two-body density matrix, in which case this last equation is no longer valid and $M - 0$ is $O(N)$ instead of $O(N^2)$. However that would produce a factor of two in the quantum of circulation, which is definitely not seen in liquid ^{4}He. I.e., the quantum of circulation is confirmation that the ODLRO first appears in the one-body density matrix in liquid ^{4}He, while the presence of the factor of two in the quantum of magnetic flux is confirmation that ODLRO first appears in the two-body density matrix in superconductors.

5. FROM MANY TO FEW: REDUCING THE INFORMATION

More general possibilities for ODLRO were detailed by C.N. Yang in his 1962 global analysis of ODLRO [10] in terms of reduced density matrices $\rho_n(\mathbf{R}^n, \mathbf{R}^{n\prime})$ for indices $n \geq 1$ (where for conciseness we use the shorthand notation $\mathbf{R}^n = \{\mathbf{r}_1, \ldots, \mathbf{r}_n\}$ and similarly for the primed coordinates):

$$\rho_n(\mathbf{R}^n, \mathbf{R}^{n\prime}) \equiv \langle \psi^\dagger(\mathbf{r_n}) \cdots \psi^\dagger(\mathbf{r_1}) \psi(\mathbf{r_1}') \cdots \psi(\mathbf{r_n}') \rangle \,.$$

This leads naturally back to the full (or $N-body$) density matrix and its relation to the reduced density matrices.

Since we wish to work in coordinate space, it is most convenient to employ the canonical ensemble for the description of the system at finite temperatures; then the zero-temperature limit produces the $N-$body ground state wavefunction.

For the N-body system, the N-body density matrix is proportional to the coordinate space representation of the statistical density operator:

$$W(\mathbf{R}^N, \mathbf{R}^{N\prime}) = \langle \mathbf{R}^N | \hat{\rho} | \mathbf{R}^{N\prime} \rangle = \frac{1}{N!} \rho_N(\mathbf{R}^N, \mathbf{R}^{N\prime})$$

where $\mathbf{R}^N \equiv \{\mathbf{r}_1, \ldots, \mathbf{r}_N\}$, $\mathbf{R}^{N\prime} \equiv \{\mathbf{r}'_1, \ldots, \mathbf{r}'_N\}$ and the statistical density operator is

$$\hat{\rho} = exp[-\beta(H - F)]$$

where H is the hamiltonian, and F is the Helmholtz free energy which serves to normalize the density matrix. This statistical density operator contains all of possible information about the N-body system in thermodynamic equilibrium in the sense that the most probable measured value of an observable $\hat{B}$ is given by

$$\langle \hat{B} \rangle = Tr \hat{B} \hat{\rho}.$$

$W(\mathbf{R}^N, \mathbf{R}^{N\prime})$ may be expressed as an $N-$body operator in terms of its own eigenvalues and eigenfunctions, which are of course the eigenfunctions of the hamiltonian. Thus the $N-$body density matrix may be written in diagonal form:

$$\rho_N(\mathbf{R}^N, \mathbf{R}^{N\prime}) = \sum_\alpha N! e^{-\beta(E_\alpha - F)} \Phi_\alpha(\mathbf{R}^{N\prime}) \Phi^*_\alpha(\mathbf{R}^N)$$

where β is the inverse temperature and E_α and Φ_α are respectively the eigenvalues and eigenfunctions of the hamiltonian. Thus we see that the eigenvalues of the $N-$body density matrix are are $N! \exp[-\beta(E_\alpha - F)]$.

At zero temperature the $N-$body density matrix becomes

$$\rho_N(\mathbf{R}^N, \mathbf{R}^{N\prime}) = N! \Phi_0(\mathbf{R}^{N\prime}) \Phi^*_0(\mathbf{R}^N)$$

where Φ_0 is the ground state wavefunction of the hamiltonian.

The $N!$ is obviously a nuisance here, and in any case is just a convention. However it does serve as an illustration of several points. Obviously the $T = 0$ density matrix has maximum possible quantum coherence since it is a single quantum state.

But the maximum condensate number is $N!$, not N^N as one might guess by extending the the pattern that we observed above in the reduced density matrix cases. Moreover it was this pattern that produced an off-diagonal limit for the reduced density matrices that was of order unit when the system has ODLRO. This is just an indication that it is the dominance of a single term in the diagonal representation of the density matrices which is the important property for producing ODLRO. At $T = 0$ there is only one term in this diagonal representation.

We wish to elaborate further on the replacement of the full density matrix by the reduced density matrix for most purposes in a macroscopic system. In particular, while the average value of an observable B is given by $\langle B \rangle = TrB\rho_N/N!$, nearly all observables are few-body operators. (The most important exception is the entropy.) Thus if B is an $n-$body operator, its average value is given by:

$$\begin{aligned}\langle B \rangle &= Tr(B_n\rho_n)/n! \\ &= \frac{1}{n!}\int B_n(\mathbf{r}_1,\ldots\mathbf{r}_n;\mathbf{r}'_1,\ldots\mathbf{r}'_n)\rho_n(\mathbf{r}'_1,\ldots\mathbf{r}'_n;\mathbf{r}_1,\ldots\mathbf{r}_n)d\mathbf{r}'_1\cdots d\mathbf{r}'_n d\mathbf{r}_1\cdots d\mathbf{r}_n\end{aligned}$$

where this reduced density matrix is given by the first equation in this section. (Note that if B_n is a coordinate space operator, i.e. if it is diagonal in coordinate space, then it includes a factor of a permanent or determinant of Dirac delta functions $\delta(\mathbf{r}_i - \mathbf{r}_j)$ for bosons or fermions, respectively, which draws the entire expression on diagonal via the integral over the primed coordinates, replacing the $n-$body density matrix by the $n-$body density. On the other hand, the most common examples of non-coordinate space operators are the momentum and kinetic energy operators, both of which are one-body operators.)

The reduced density matrices obviously carry less information about the system than the $N-$body density matrix, since the former cannot be used to calculate expectation values of the higher order operators. Moreover, at finite temperature the measure of the reduction of information compared to a single state of the system (or the $T = 0$ state) is the information entropy, given by

$$S_I = -Tr[WlnW]$$

which of course is related to the thermodynamic entropy S by the Boltzmann constant: $S = k_B S_I$. A measure of the *further* reduction of information as the $N-$body density matrix is traced down to reduced density matrices is the information entropy of the reduced density matrix. To define this we first define a normalized reduced density matrix:

$$w_n(\mathbf{r}'_1,\ldots\mathbf{r}'_n;\mathbf{r}_1,\ldots\mathbf{r}_n) = \frac{(N-n)!}{N!}\rho_n(\mathbf{r}'_1,\ldots\mathbf{r}'_n;\mathbf{r}_1,\ldots\mathbf{r}_n)$$

which satisfies Trw_n=1. The average value of an $n-$body operator then becomes

$$\langle B \rangle = \frac{N!}{(N-n)!\,n!}Tr(B_n w_n)$$

The information entropy for this reduced density matrix is then

$$S_{I,n} = -Tr(w_n\, ln\, w_n)$$

Except for the ideal Bose gas at $T = 0$, this information entropy is non-zero for $n < N$ even at $T = 0$. This is made clear by expressing ρ_n in its own diagonal representation, or equivalently w_n, which is diagonal in the same representation:

$$w_n(\mathbf{R}^n, \mathbf{R}^{n\prime}) = \sum_\lambda P_{n,\lambda} \Phi_{n,\lambda}(\mathbf{R}^n) \Phi^*_{n,\lambda}(\mathbf{R}^{n\prime})$$

where $P_{n,\lambda} = \frac{(N-n)!}{N!} M_{n,\lambda}$ where $M_{n,\lambda}$ are the eigenvalues of the $n-$body reduced density matrix ρ_n. Thus the information entropy at this level is:

$$S_{I,n} = -\sum_\lambda P_{n,\lambda} \, ln \, P_{n,\lambda}$$

We conjecture that this is a monotonically increasing function of $N-n$ in conformance with the fact that the information is decreasing with each successive step downward through the reduced density matrices.

We know of no use of this particular formulation, though we are currently exploring this further.

In conclusion we have summarized a number of facts related to Bose-Einstein condensation, pairing, ODLRO, and the properties of reduced density matrices. The literature is rich with many other properties of these density matrices. We also note that there has been recent attention to bound-state pairing as a possible explanation for some of the unusual properties of high temperature superconductors.

ACKNOWLEDGMENTS

Some of the research discussed here was funded in part by the U. S. National Aeronautics and Space Administration under Grant NAGW-3324 and by the Minnesota Supercomputer Institute. We also acknowledge the hospitality and support of E. Krotscheck and his colleagues at the Institute for Theoretical Physics of the University of Linz, and of the Fulbright Commission and Austrian-American Educational Commission. We are pleased to acknowledge travel support provided in part through a grant from the Army Research Office, Research Triangle Park, to Southern Illinois University.

REFERENCES

† Present and permanent address.

[1] O. Penrose, Phil. Mag. **42**, 1373 (1951).

[2] G. V. Chester, in *Quantum Fluids and Nuclear Matter*, Vol. XI B of *Lectures in Theoretical Physics*, edited by K. T. Mahanthappa and W. E. Britten (Gordon and Breach, New York, 1969), pp. 253–296.

[3] C. E. Campbell, J. Low Temp. Phys. **93**, 907 (1993).

[4] C. E. Campbell, in *Progress in Liquid Physics*, edited by C. A. Croxton (Wiley, London, 1977), Chap. 6, pp. 213–308.

[5] W. R. Magro and D. M. Ceperley, Phys. Rev. Lett. **73**, 826 (1994).

[6] P. M. Whitlock and R. M. Panoff, Can. J. Phys. **65**, 1409 (1987).
[7] P. E. Sokol and W. M. Snow, in *Excitations in Two-Dimensional and Three-Dimensional Quantum Fluids*, Vol. 257 of *NATO Advanced Study Institute, Series B: Physics*, edited by A. F. G. Wyatt and H. J. Lauter (Plenum, New York, 1991), pp. 47–58.
[8] M. R. Schafroth, Phys. Rev. **100**, 463 (1955).
[9] J. Bardeen, L. N. Cooper, and J. R. Schrieffer, Phys. Rev. **108**, 1175 (1957).
[10] C. N. Yang, Rev. Mod. Phys. **34**, 694 (1962).
[11] A. Leggett, Rev. Mod. Phys. **47**, 331 (1975).
[12] A. Leggett, *Modern Trends in the Theory of Condensed Matter*, Vol. 115 of *Lecture Notes in Physics* (Springer, Berlin, Heidelberg, and New York, 1981), p. 13.
[13] A. Leggett, J. Physique. C **7**, 19 (80).

Conditions of Superfluidity in Molecular Hydrogen

D. M. Ceperley and M. C. Gordillo

National Center for Supercomputer Applications
and Department of Physics
University of Illinois Urbana-Champaign, IL 61821 USA

1. INTRODUCTION

Over the last few decades, there has been a search for bose-condensed systems. Until a little over one year ago, liquid helium below 2 K was the only elemental system which was observed to be Bose-Einstein condensed. Elsewhere we have heard about the successes in seeing BEC in atomic vapors and the attempts to cool spin-polarized atomic hydrogen to sufficiently low temperatures to BEC. [1]

Molecular hydrogen H_2 is a natural candidate for superfluidity since it is composed of two pairs of fermions (electrons and protons) in singlet bound states (in para-hydrogen). (This is different than the system Silvera discussed: spin polarized *atomic* hydrogen.) A hydrogen molecule has half the mass of helium, hence the ideal bose condensation temperature would be double that of helium. Hydrogen is a spherical molecule, stable and commonly found, possessing an internal structure (para/ortho hydrogen)that is easily accessible to experiment. At low temperatures and pressures the density of the triplet state, (ortho-hydrogen) is very low in equilibrium. Because of the light mass, one might expect that exchange effects in hydrogen would be more important than in helium. However nature is not so accommodating. Because a hydrogen molecule is more polarizable than helium, the attractive Van der Walls interactions between two molecules are stronger. Its attractive well depth is 37K instead of 10K between helium atoms. As a consequence, the zero pressure density is somewhat higher in hydrogen (0.026 Å^{-3}) than in helium (0.022 Å^{-3}). In helium, when one compresses by this much, one forms a solid at 25 bars. Unfortunately, from the point of view of superfluidity, this has already happened in hydrogen at zero pressure. To make molecular hydrogen into a superfluid all one needs to do is to lower the density by a small amount (10% to 20%.)

Maris[2] tried to form supercooled droplets of liquid hydrogen since the interior of a droplet would be at a negative pressure. One might hope that there would be a barrier to the nucleation of the solid phase as a droplet cools by evaporation. However, both liquid and solid hydrogen are highly mobile, so that if there is a tendency for

solidification, it is likely that solid hydrogen would form quickly. Several groups[3] initially reported superfluid-like signals of hydrogen in vycor, a substance with a porous fractal geometry. While it is plausible that disorder might favor the liquid over the solid, the temperature where the anomalous signals were seen was well above the expected temperature for BEC. The experiments have now been explained as due to movement of hydrogen in and out of the vycor as the temperature is changed.

We have simulated molecular hydrogen in clusters[4] and found that in clusters of fewer than 20 molecules the superfluid density is high. We have also simulated bare hydrogen surfaces and found surface melting of two layers down to 5.5K and delocalization of the topmost layer at even lower temperatures. Simulations of systems with an incomplete topmost layer are superfluid but incomplete layers are not thermodynamically stable. We see thermally activated vacancies in the top layer below the melting temperature, but too few to Bose condense. Vacancy motion is however responsible for relaxation of hydrogen surfaces.

We speculate that in certain "dirty" hydrogen films, the tendency for solidification might be suppressed enough for the film to undergo a Kosterlitz-Thouless transition at low temperatures. Recent simulations[5] of 2D hydrogen with repulsive potassium impurities support this idea, exhibiting superfluid properties at 1K.

2. PATH INTEGRAL MONTE CARLO METHOD

The method of choice for investigating superfluidity of bosonic systems is Path Integral Monte Carlo (PIMC). For bosonic systems, PIMC is an exact numerical method and computers and methods are fast enough that one can begin to "design" the superfluid. (By that, all that is meant is that one can quickly investigate the effect of changing some of the parameters in the model with enough reliability that an experimentalist might try to see the effect.) Only PIMC is capable of accurately predicting the two transitions in condensed ^{4}He: the transition to the superfluid state below 2.2K and the transition to a localized solid above 25 bars pressure. Thus we can use it with confidence to predict what would happen to molecular hydrogen in various situations.

Feynman[6] introduced imaginary time path integrals. Each molecule is mapped into a "polymer", the molecules trace a path in imaginary time which returns to its starting position. Bose statistics corresponds to exchange of polymers where different molecules end up in exchanged positions. Superfluidity corresponds to a macroscopic exchange.

There are several classic manifestations of superfluidity which can be calculated with PIMC. The first effect to be observed and explained by Feynman was the peak in the specific heat resulting from the enlarged phase space of the permuting paths. The second effect, the non-zero superfluidity density is defined in terms of the response of the system to moving the boundaries. This is calculated in PIMC as the mean squared winding number in periodic boundary conditions, or the mean squared area in a cluster. The third effect is a momentum condensation, where a non-zero fraction of the atoms has precisely zero momentum. This is observed by inelastic neutron scattering as discussed by Silver. The momentum distribution is a delta function in 3D and has an algebraic singularity in 2D, resulting from the Kosterlitz-Thouless transition. The momentum distribution is calculated in PIMC by cutting open a

polymer and seeing if the two ends separate or remain bound. The theory and numerical methods of PIMC are discussed in detail in ref [7].

The calculations reviewed here treat the hydrogen molecule as a spherical particle, which is a good approximation for para-hydrogen at low pressures and temperatures. This is because two interacting molecules, both in the J=0 state, are rotating quickly enough that they appear spherical. We have used the semi-empirical Silvera-Goldman[8] potential. Comparisons to experimental data have errors on the order of a few degrees (K) per molecule.

The only unusual feature of our calculation is the special care that needs to be taken at the boundaries for a surface or cluster. Clusters were enclosed in a spherical cavity (radius about 20 Å) to keep molecules from evaporating. Surfaces were modeled with an external potential in the z direction and periodic boundary conditions in the x and y directions. Typical simulation boxes are roughly cubical, 20Åon a side, containing on the order of one hundred molecules. The external potential is constructed so that the particles are attracted to one wall with precisely the force exerted by a semi-infinite slab of hydrogen at the equilibrium density. In some calculations a "frozen" layer of hydrogen was inserted next to the attracting wall to better model the underlying layers. More details are given in refs. [9-11].

Once the Hamiltonian is specified, the exact pair action of two molecules is calculated, so that long imaginary-time steps can be used. Tests have established that we need an imaginary-time step $\tau \leq 0.025K^{-1}$ so that the time-step error is much smaller that the statistical error and the error from the assumed potential energy. This means that we need 20 "time-slices" to achieve a physical temperature of 2 K. Use of the primitive action would require hundreds of time steps for equivalent accuracy. A generalized Metropolis procedure is used to sample the combined path and permutation space. Statistics are gathered on properties such as energy, density, structure factor, exchange probability and superfluid density. We have used the MPI (message passing interface) language to speed up the calculations by doing several runs in parallel[11]. One can go directly from the Hamiltonian to physical properties with a run of less than 1 day on workstations; less for thermodynamic properties, more for the superfluid density. PIMC is unique as a numerical technique in its accuracy, ability to deal with complex situations, and efficient use of the powerful computers that are available.

3. THE SURFACE OF SOLID HYDROGEN

Molecular hydrogen is unique among the elements in having an interface between a highly quantum solid and a vacuum at low temperature. Scaling from simulations of classical liquids would give a triple point temperature of about 26K; in fact the freezing temperature is 13.8K. Because of the effects of quantum motion, the sublimation energy (*i. e.* the chemical potential) depends very strongly on the isotopic mass. It changes from 95 K for H_2 to 140 K for D_2. We calculate an energy of 87 K for H_2 with PIMC, thus verifying that our potential is reasonably accurate. Errors come from the assumed potential not the path integral method.

The breakdown between kinetic and potential energy is interesting. The kinetic energy is 69 K at low temperatures, showing that quantum effects are very large and explaining the large isotope effect in the sublimation energy. We estimate[9]

the Lindeman's ratio (rms deviation from lattice site divided by nearest neighbor separation) in the bulk as 0.21, in agreement with the experimental estimate of 0.18. Also, the equilibrium solid density is calculated correctly. We calculate a surface tension of 3.4 KÅas compared to extrapolation of measurements in the liquid phase of 5.3 KÅ.

From our PIMC studies[9], it is clear that bare H_2 surfaces are very different from bulk solid because of delocalization and, below $\approx$ 1K, bose statistics. We find the top layer of solid hydrogen to be very fluffy: the rms displacement of the atoms on the surface in the normal direction is almost twice what it is deep inside the sample. This fluffiness is greatly reduced[10] if helium atoms are on top; even though the helium atoms sit well above the hydrogen surface they serve to pack it down and increase the localization of the hydrogen: thus helium poisons any hydrogen superfluidity.

Surface melting is the formation of a stable liquid layer at the solid/vapor interface below the bulk melting temperature. Most bulk materials are believed to be wet by a film of their own melt, a few atomic or molecular layers thick at temperatures very near the melting temperature. For a single molecular H_2 layer, a solidification temperature of 5.74K has been seen in experiment[12]. This is more than a factor of two below the bulk melting temperature, but is still too high to expect that liquid H_2 will become superfluid. The question arises whether quantum surface melting is qualitatively or only quantitatively different than that of classical surface melting.

Figure 1 shows a rough "phase diagram" of the surface layers of solid hydrogen as determined with PIMC[11]. Depending on the surface density and temperature, a layer of hydrogen can be either in a 2D gas, 2D liquid or solid or coexistence between those three phases. We defined the phase of a layer with simple structural criteria. They are not necessarily rigorous (but could be made so.)

1. The spatial extent of a *layer* is identified by the minima in the vertical density. A molecule belongs to that layer if its centroid is between those minima.
2. A *solid* has large peaks in the transverse structure factor. Normally these are commensurate with the underlying solid hydrogen lattice but near melting we see evidence of other incommensurate solid structures.
3. We identify a *liquid* as a layer with a smooth transverse structure function.
4. A *superfluid* has many non-trivial exchanges and windings around the periodic boundaries. The number of superfluid atoms is proportional to the mean squared winding number.
5. A *liquid /gas coexistence* has a very large compressibility, as computed by the structure factor extrapolated to zero wave vector.

Using these definitions of liquid and solid, we find[11] that the top layer remains liquid down to about 6K, in agreement with experiments[12]. We examined the liquid-gas coexistence by doing simulations with a half-filled top layer. That top half layer never froze but below the liquid/gas critical point the resulting superfluid formed a 2D drop. This phase is however not stable in the thermodynamic limit. For a large enough system, the density of the droplet would become large enough for it to solidify. The molecules near a surface step are delocalized even at low temperatures, but it is unlikely that they can connect up with other steps in such a way as to propagate the phase of the wavefunction (the order parameter) across a macroscopic distance.

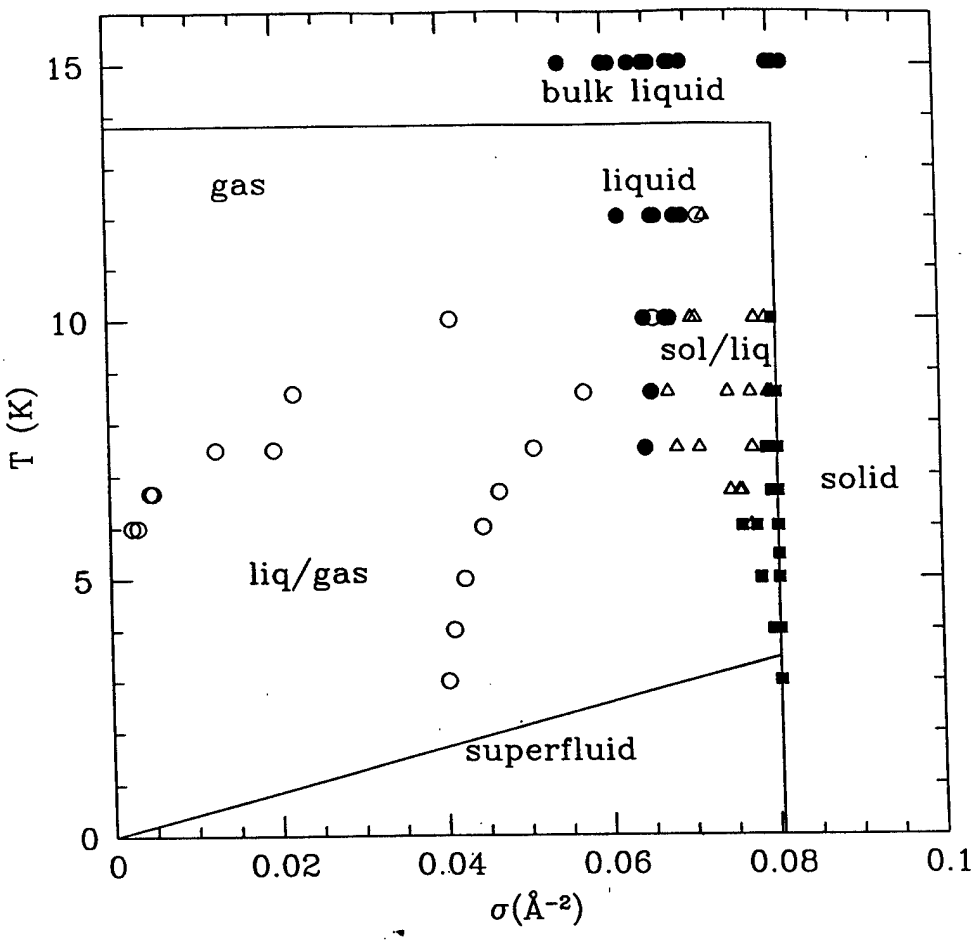

Figure 1. The dependence of layer density on temperature. Each point represents the layer density and temperature. The solid circles are identified as a liquid; open circles as the coexistence between a 2D liquid and a 2D gas; solid squares are a 2D solid; the open triangles are a very disordered 2D solid, possibly the coexistence between 2D liquid and 2D solid. The solid line at 0.0804 $\AA^{-2}$ is the coverage deep inside the solid. The line at 13.8K is the bulk melting temperature. If the system remains a liquid to sufficiently low temperature it will become superfluid as marked.

There is one way in which a solid can become a superfluid: if vacancies in the solid were numerous enough they could bose condense. This is called a "super-solid": a system with a spontaneously broken translational order and momentum condensation. In our simulation we see that top layer expand before it melts. Hence, it must contain vacancies but the question is whether there will there be enough of them to become superfluid. We find[11] that the vacancies are thermally activated. Their concentration is given by:

$$c(T) = D_0 \exp(-\Delta E/(k_B T)) \quad . \tag{1}$$

Bose condensation occurs when a bosonic exchange percolates through the sample. To find the transition temperature one needs a relationship between exchange and the density. The two dimensional superfluid transition (Kosterlitz-Thouless) transition occurs at a temperature when :

$$T_c = 1.8c(T)\sigma_0\hbar^2/m^* \quad , \tag{2}$$

where m^* is the effective mass of the vacancy and the coefficient in front has been determined for 2D ^{4}He by Ceperley and Pollock[13]. The precise value of these two parameters will not matter. The question is whether these two equations have a solution for T_c. They do iff:

$$E_l \leq [1.8D_l\sigma^*\hbar^2]/[m^*e] \quad . \tag{3}$$

Putting in rough estimates for $m^* \approx 2m$ and D_l for the first layer the LHS of the inequality is 25K and the RHS is 2.3K so one never has Bose condensation. The concentration of vacancies drops too fast as the temperature is lowered so that the thermal wavelength (growing as $T^{-1/2}$) never reaches a neighboring vacancy.

Even though vacancies do not Bose condense on the surface of hydrogen, apparently, they are responsible for mass transport at the surface. Classen et al.[14] recently described measurements of surface acoustic waves on hydrogen surfaces at low temperature. They prepared a thick homogeneous layer of hydrogen on silver. Upon raising the temperature the film forms bulk crystallites because the bulk has a lower chemical potential; this is called dewetting. However, the process of dewetting is diffusion-limited and can be sensitively observed by monitoring the changing signature of the surface waves. By varying the temperature, one can determine that the mass diffusion is thermally activated with an energy of 23 $\pm$ 2 K. It is plausible that the mechanism for surface diffusion of hydrogen films is thermally activated vacancies since the creation energy of the vacancy that we estimated matches what is measured. We are currently calculating of vacancy energies for the other hydrogen isotopes to further compare with experiment.

4. DIRTY HYDROGEN SURFACES

We have seen that hydrogen at a surface has a tendency to become a superfluid[10]. However, if hydrogen is placed on top of another solid layer of hydrogen, the situation favors too much the solid and the top layer freezes at 6K. One must modify, in some way, the substrate on which a layer of hydrogen sits.

The basic idea of our most recent simulations is to favor the liquid state by putting down an array of impurities, incommensurate with the solid hydrogen structure. This lowers the density and the melting point by lowering the free energy of the liquid phase, relative to the solid phase. To simplify the problem, to date, we have only considered a two dimensional model where the hydrogen molecules were restricted to lie in a plane. In that plane, we placed a number of static impurities. We have varied the density and type of impurities to try to favor the liquid state as much as possible. Figure 2 shows a representation of our best superfluid 2D hydrogen. It is composed of a square lattice of impurities, spaced about 10Åapart. We have yet

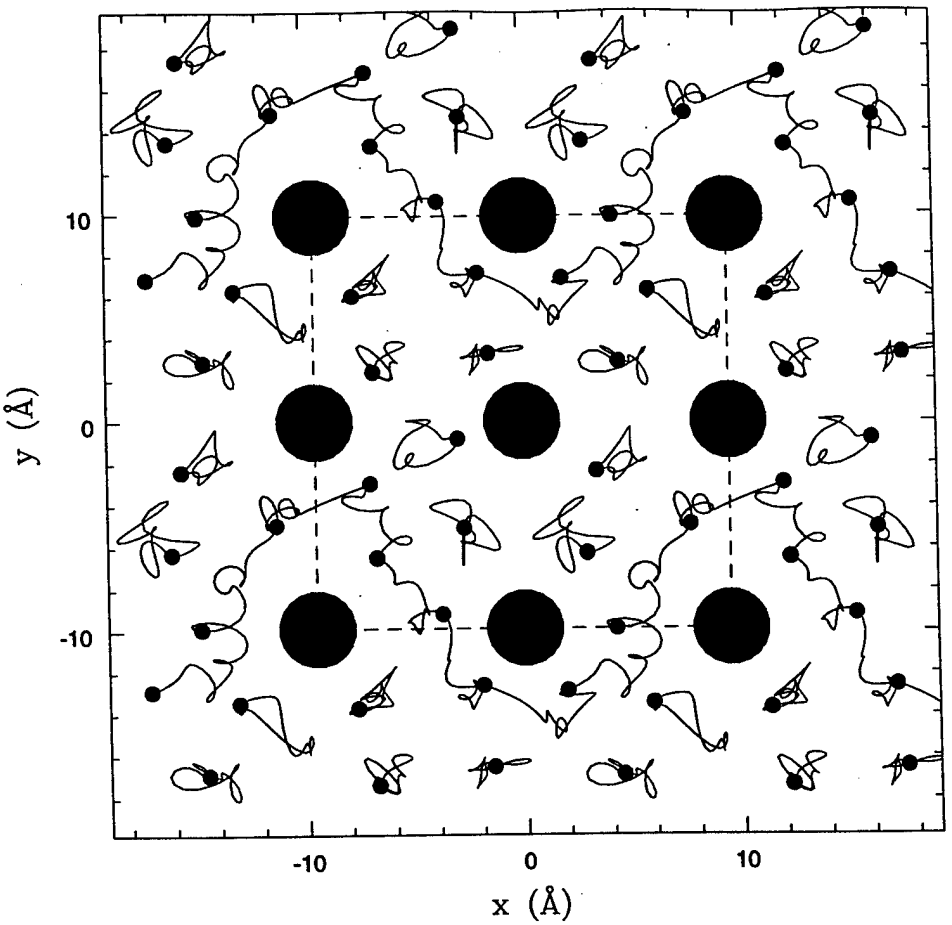

Figure 2. A typical path of hydrogen molecules in the superfluid state. The nine large circles represent the K impurities: the small circles are the positions of the hydrogen molecules at a single time slice. The imaginary time trajectory of the particles has been Fourier smoothed for clarity. A single unit cell of the simulation box is shown as the dashed rectangle. One can see that the path winds around the periodic boundary conditions in the x direction, thus it is superfluid.

to examine other ways of putting down the impurities, we have only varied their spacing. We have found that large impurities which repel the hydrogen molecules work best. Attractive impurities form a skin of solid hydrogen around them and "seed" a localized, non-superfluid, glassy hydrogen phase.

Figure 4 shows the energy versus coverage of the clean system (no impurities) and the dirty (impurity) system. The effect of the impurities is to lower the binding energy, but it also lowers the density at the minimum. The system at the minimum is a liquid (solid in the clean system) as evidenced by the structure factor. The superfluid density, calculated from the mean-squared winding number, versus coverage is shown in figure 3. The minimum in the energy corresponds to a maximum of the superfluid response. One half of the atoms are superfluid at temperatures below 1K, the other atoms make a normal liquid skin around the impurities. We predict a superfluid transition at about 1.2K.

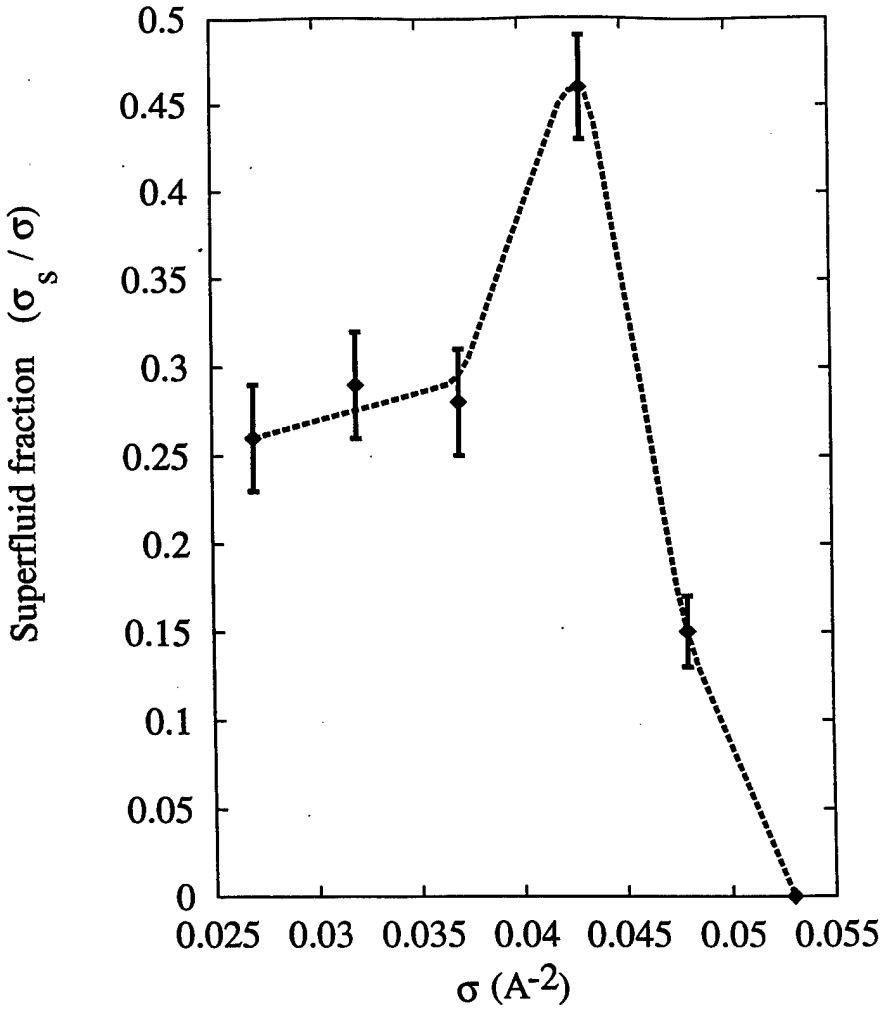

Figure 3. The superfluid fraction versus hydrogen coverage (in molecules per $Å^{-2}$) at 1K for the 2D system with potassium impurities present. At the optimal coverage, roughly half of the molecules participate in superfluid flow. At higher coverages the system becomes localized.

We have examined the spacing between the impurities and determined that if they are closer together the superfluid cannot propagate between the cracks. If they are further apart, small hydrogen crystallites can form in the area between the impurities. A spacing of roughly 10 Å is optimal for stabilizing the liquid.

We are now studying the 3D models as we did with pure hydrogen surfaces. Once the Hamiltonian is constructed the calculations are relatively routine, though potentially time consuming because of the large number of substrate/impurity combinations. An important physical consideration to take into account in looking for an appropriate substrate is that hydrogen must wet the surface at low temperature: hydrogen must prefer to absorb on the surface, rather than form a pure crystal. The chemical potential of bulk hydrogen at low temperature is around 90K and we see that the binding within the 2D layer with impurities present is about 10K. Thus the binding energy of a single molecule to the substrate should be more than 80K. If it is much greater than 80K the hydrogen molecules will be trapped into pockets on the surface and unable to move around and exchange. Amongst the rare gas substrates, Neon has close to this value of binding. However, it is not clear how one would be

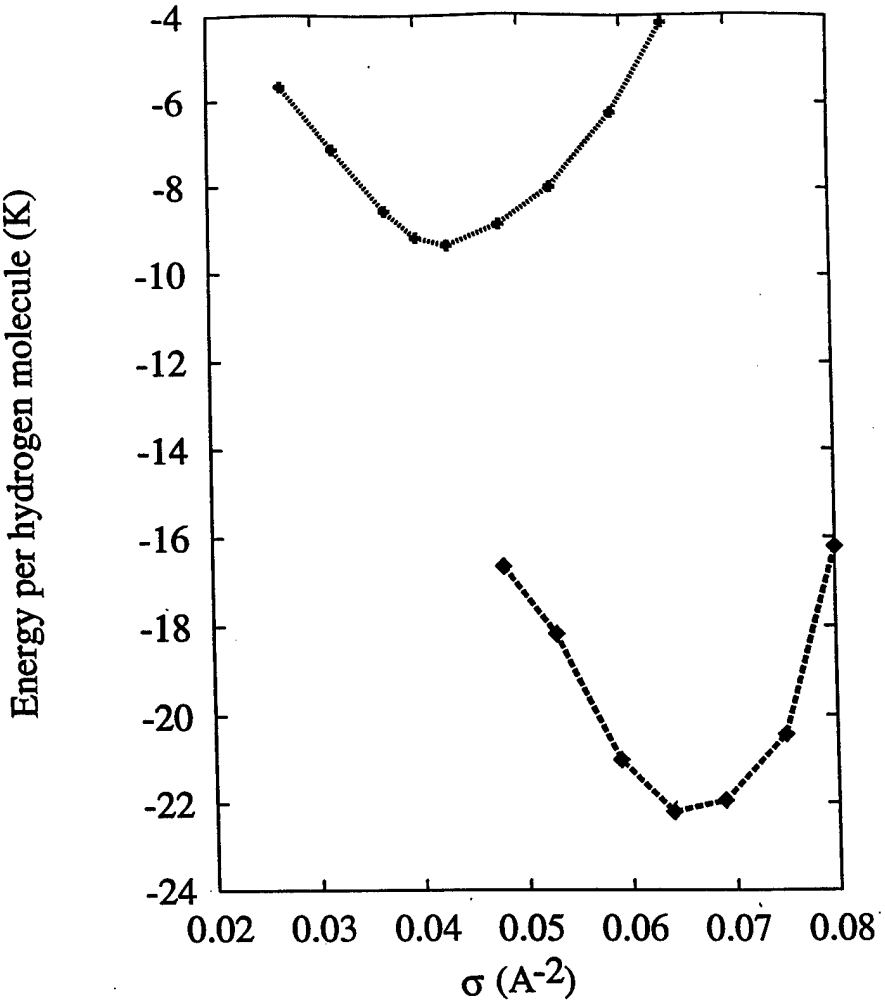

Figure 4. The energy/molecule versus the coverage for the "clean" (translationally invariant) systems (lower points and curve) and system with potassium impurities (upper points and curve) at a temperature of 1K. Because of the repulsive interaction of the impurities, the zero pressure coverage is lowered and fluid at all temperatures, while the "clean system" is solid for the lowest energy coverage.

able to place impurities on a neon surface.

5. CONCLUSION

PIMC for systems of bosons is an exact numerical method and is now to the point that we can use it to explore novel systems for superfluidity or other quantum properties. PIMC is past the point where one is simply reproducing the results of experiment but instead we are trying to make predictions that will guide experimentalists. This progress has come about because of the development of accurate robust numerical many-body techniques, and of ever faster computers. The methodology has grown synergestically with other many-body methods. Of course, experiments are crucial to verify the predictions.

We are using the same code to study hydrogen in a completely different regime: at much high temperatures and pressures, to study what happens as the atoms and

molecules become ionized and dissociated. Full details of these and other calculations are on our WWW page: *www.ncsa.uiuc.edu/Apps.CMP/index.html*

ACKNOWLEDGMENTS

We used the computational facilities at the National Center for Supercomputing Applications and at the Cornell National Supercomputer Center for this work. This research was supported by NSF-DMR94-224-96, by the Spanish Ministry of Education and Culture, and by a travel grant from the U.S. Army Research Office.

REFERENCES

[1] M. H. Anderson, J. R. Ensher, M. R. Matthews, C. E. Wieman and E. A. Cornell, Science **269**, 198 (1995).
[2] H. J. Maris, G. M. Seidel and T. E. Huber, J. Low. Temp. Phys. **51**, 471 (1983).
[3] M. Schindler, A. Dertinger, Y. Kondo and F. Pobell, Phys. Rev. B **53**, 11451 (1996). D. F. Brewer, J. C. N. Rajendra and A. L. Thomson, J. Low. Temp. Phys. **101**, 317 (1995).
[4] P. Sindzingre, D. M. Ceperley and M. L. Klein, Phys. Rev. Letts. **67**, 1871 (1991).
[5] M. C. Gordillo and D. M. Ceperley, to be published.
[6] R. P. Feynman, Phys. Rev. **90**, 1116 (1953).
[7] D. M. Ceperley, Rev. Mod. Phys. **67**, 279 (1995).
[8] I. F. Silvera and V. V. Goldman, J. Chem. Phys. **69**, 4209 (1978).
[9] M. Wagner and D. M. Ceperley, J. Low Temp. Phys. **94**, 147 (1994).
[10] M. Wagner and D. M. Ceperley, J. Low Temp. Phys. **94**, 171 (1994).
[11] M. Wagner and D. M. Ceperley, J. Low Temp. Phys. **102**, 275 (1994).
[12] O. E. Vilches, J. Low. Temp. Phys. **89**, 267 (1992).
[13] D. M. Ceperley and E. L. Pollock, Phys. Rev. **B 39**, 2084 (1989).
[14] J. Classen, K. Eschenroder and G. Weiss, Ann. Physik **4**, 1 (1995).

PAIRING FORCES IN NUCLEI

R. R. Chasman
Physics Division
Argonne National Laboratory
Argonne, IL 60439-4843 USA

1. INTRODUCTION

In this contribution, I shall mention some features of pairing forces that are unique to nuclei and cover some areas of major interest in nuclear structure research, that involve pairing. At the level of most nuclear structure studies, nuclei are treated as consisting of two kinds of fermions (protons and neutrons) in a valence space with rather few levels. These features give rise to unique aspects of pairing forces in nuclei: 1) n-p pairing in T=0 as well as the usual T=1 pairing that is characteristic of like fermions, 2) a need to correct pairing calculations for the (1/N) effects that can typically be neglected in superconducting solids. An issue of current concern is the nature of the pairing interaction; several recent studies suggest a need for a density dependent form of the pairing interaction. There is a good deal of feedback between the questions of accurate calculations of pairing interactions and the form and magnitude of the pairing interaction. Finally, I discuss some many-body wave functions that are a generalization of the BCS wave function form, and apply them to a calculation of energy level spacings in superdeformed rotational bands.

One expects n-p pairing to be important mainly in light nuclei, where the valence orbitals for neutrons and protons are the same. Nuclear forces are short range and one can get reasonable estimates of matrix element sizes by using a δ interaction. In light nuclei, L-S coupling provides a good description of nuclear level structure, and the standard pairs consist of partners in time reversed orbitals (N,L,M,Ms) and (N,L,-M,-Ms), giving rise to L=0, S=0, J=0 pairs. Exactly the same spatial overlap exists for orbital pairs consisting of (N,L,M,Ms) and (N,L,-M,M_s) giving rise to L=0, S=1, J=1 pairs. Such an antisymmetrized δ matrix element vanishes for like particle pairs of this type. However, this matrix element does not vanish [1,2] for n-p pairs. It is large and gives rise to collective J=1, T=0 pairs. Strong evidence for the importance of such pairing comes from the spectroscopy of p-shell nuclei. The ground states of the odd-odd nuclei ^{6}Li and ^{14}Ni are $J^{\pi} = 1^{+}$. Recent studies [3] of f-p shell nuclides suggest that T=1 n-p pairing also plays an important role in describing the properties of the neutron-deficient nuclides of this region.

2. BEYOND MEAN FIELD

As we attempt to describe nuclear properties more accurately, details of the calculational method become more and more important. The inadequacies of nuclear structure calculations, arising from the non-conservation of particle number in BCS wave functions, has become an important issue recently. The problem is particularly serious in deformed nuclei, where the number of active valence orbitals is ~5, i.e. (1/N) effects are almost as important as the leading terms. One of the approaches for dealing with this problem in a quasi-particle formalism is the Lipkin-Nogami [4,5] method. A clear discussion of this method has been given [6] and has been recently implemented in several calculations [7,8]. One could do exact particle number projection and solve the problem, with the penalty of giving up the simplicity of quasi-particle solutions.

In the Lipkin-Nogami method, one augments the pairing Hamiltonian with the usual $\lambda_1 N$ term and adds an additional term $\lambda_2 N^2$ term. The quantities λ_1 and λ_2 are determined by using reasonable, but arbitrary conditions [6] on the BCS wave function. What is going on is obscure. Here, I would like to show a much simpler way [9] to understand these issues, based on exact sum rules. For any wave function, with good particle number, the following sum-rules are exact.

$$\sum_{\ell} N_\ell \, |\psi\rangle = N_0 |\psi\rangle \tag{1}$$

where N_0 is the number of nucleon pairs in the state of interest and $\langle O \rangle$ is the expectation value of an operator in state $|\psi\rangle$.

$$\Big\langle N_k \sum_{\ell \neq k} N_\ell \Big\rangle = (N_0 - 1)\langle N_k \rangle \tag{2}$$

$$\langle N_k \rangle \Big\langle \sum_{\ell \neq k} N_\ell \Big\rangle = \Big(N_0 - \langle N_k \rangle\Big)\langle N_k \rangle \tag{3}$$

Combining Eqs. (2) and (3), we get the exact correlation sum rule

$$\Big\langle N_k \sum_{\ell \neq k} N_\ell \Big\rangle - \langle N_k \rangle \Big\langle \sum_{\ell \neq k} N_\ell \Big\rangle = -\langle N_k \rangle \langle 1 - N_k \rangle \tag{4}$$

This correlation is exactly the same in magnitude as the correlation between the two nucleons induced by the pairing interaction. $\langle N_k N_{-k} \rangle = \langle N_k \rangle$ in a pairing wave function so

$$\langle N_k N_{-k} \rangle - \langle N_k \rangle \langle N_{-k} \rangle = \langle N_k \rangle \langle 1 - N_k \rangle \tag{5}$$

The correlations of Eq. (5) are exactly included in a BCS wave function, but those of Eq. (4) are absent. We can include the effects of these correlations, by setting

$$\langle a_i^+ a_{-i}^+ a_{-j} a_j \rangle = \Big[\langle N_i (1 - N_j) \rangle \cdot \langle N_j (1 - N_j) \rangle \Big]^{1/2} \tag{6}$$

and introduce an approximation based on the sum-rule correlation. We set

$$\langle N_i N_j \rangle = \langle N_i \rangle \langle N_j \rangle - \beta_i \beta_j / \sum_k \beta_k \tag{7}$$

where

$$\beta_k = \langle N_k \rangle \langle 1 - N_k \rangle \tag{7a}$$

and one solves in the usual way. This approximation gives fairly good agreement with exact results, but underestimates the anti-correlation between pairs on opposite sides of the fermi level. We improve the approximation by taking this special anti-correlation into account, setting

$$\langle N_i N_j \rangle = -\eta \beta_i \cdot \beta_j \cdot S(i,j) \tag{8}$$

where

$$S_{i,j} = \langle N_i \rangle \langle 1 - N_j \rangle + \langle N_j \rangle \langle 1 - N_i \rangle \tag{8a}$$

$$\eta = \left[\bar{N} \sum_r \beta_r \langle 1 - N_r \rangle + (1 - \bar{N}) \sum_r \beta_r \langle N_r \rangle \right]^{-1} \tag{8b}$$

Solving, with this approximation, we get extremely good agreement with exact solutions obtained[10] for equally spaced levels. Not only are the energies almost exact, the occupation probabilities are also almost exact. In Fig. 1, we compare the exact and BCS energies and occupation probabilities [10] for a system having 32 equally spaced, doubly degenerate levels, and 16 pairs, with the results obtained in our approximation. This clearly shows the effects of ignoring the correlation effects in small systems. In condensed matter systems, this should not be much of a problem because the anti-correlations are distributed over many levels. In typical nuclear systems, the number of active orbitals is ~ 5; $\langle 1/N \rangle$ effects are crucial.

It is important to note that no wave function based on the BCS structure (a product form) is appropriate in the RPA regime. One useful way of dealing with such problems is a configuration interaction diagonalization procedure that uses the pairing interaction strength as a generator coordinate. This can be considered a discretization of the Hill-Wheeler equation [11,12]. In this approach, one varies the interaction strength, and obtains a many-body solution for each value of the strength. Such solutions are not orthogonal, and the overlaps must be included in a generalized diagonalization procedure. We set

$$|\psi\rangle = \sum_i A_i \phi_i(G) \tag{9}$$

and the amplitudes are determined diagonalizing the Hamiltonian using the physical value of G. Approximate solutions can be obtained, using the Gaussian overlap approximation.

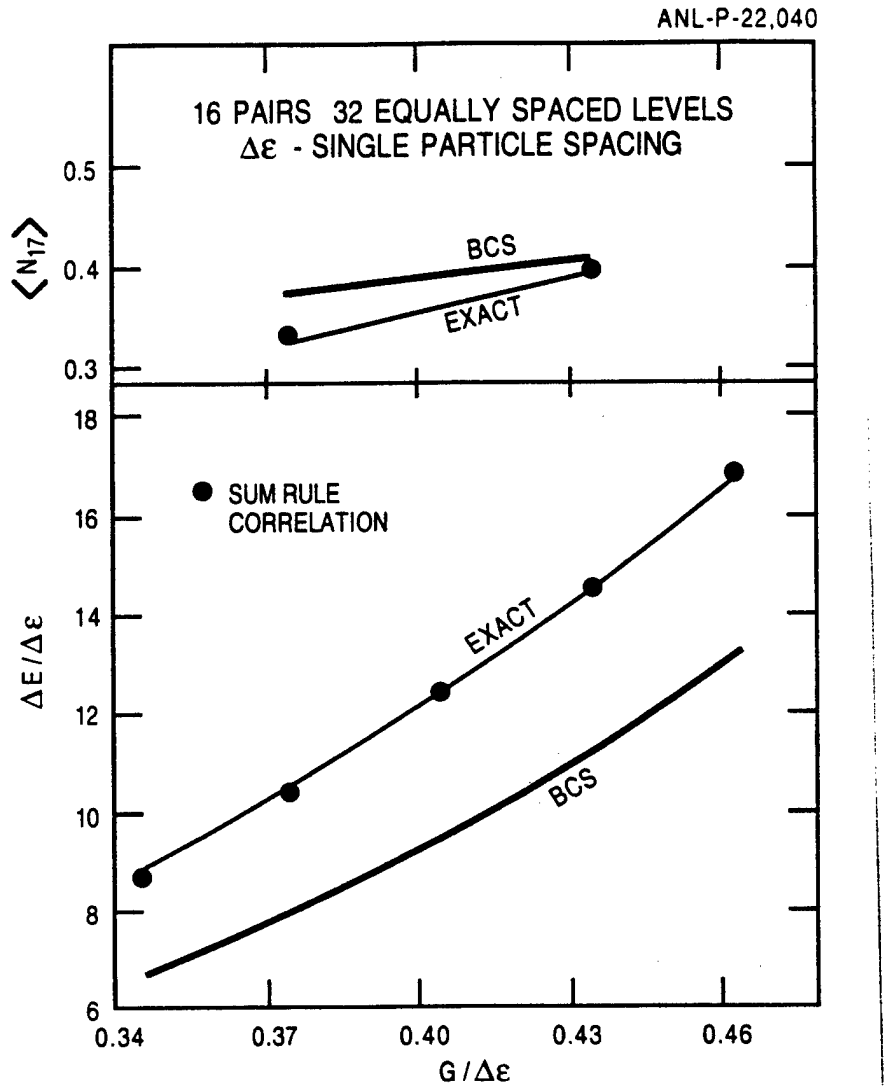

Figure 1. A comparison of exact, BCS and correlation corrected wave functions. In the upper panel, we show the occupation probability of level 17 obtained in the three calculations, as a function of interaction strength. In the lower panel, we compare energy shifts as a function of the interaction strength. The unit of energy is the energy difference between successive levels. Because of the particle-hole symmetry in this example, $\langle N_{16}\rangle = 1 - \langle N_{17}\rangle$.

We emphasize the need to go beyond simple treatments of pairing in deformed and superdeformed nuclear systems. In the deformed heavy elements, average single particle spacings are ~200 keV, i.e. it takes ~400 keV to promote a pair of neutrons and the interaction constant is just ~100 keV. This is the reason that there are so few active orbitals in nuclear pairing calculations, and one must go beyond BCS wave functions. Superdeformed shapes are associated with particularly low level densities and one must get far beyond BCS to get results that are meaningful.

3. EFFECTIVE PAIRING INTERACTIONS

Only with accurate calculational methods in hand, can we turn to the question of what is the effective pairing interaction. The simplest and most often used form of the interaction is to assume a constant G interaction. The magnitude of the interaction depends on the number of levels used in the calculation, as there is a divergence problem. Typically, one uses ~30 doubly degenerate Nilsson levels in such calculations. The strength of the interaction is $\sim(21\pm1)/A$ for neutrons, where A is the nuclear mass. Considerable controversy has developed in the literature about the magnitude of the proton pairing interaction; with values of Gp=1.1 Gn, 1.3 Gn, 1.4 Gn and 1.6 Gn appearing [7,13-17] in the literature.

In all of these cases, pairing interaction strengths were obtained from fits to experimental data. It should be noted that different calculational techniques are used by different authors, and this gives rise to some of the differences. However, there are differences for calculations in different regions using a given method. It would be interesting to make a systematic study of pairing interaction strengths in different mass regions, using the density dependent pairing force discussed below. At this point in time, one must be wary of simple extrapolations of pairing strengths. Rather, it appears more reasonable to fit the strength to some relevant experimental data in the mass region of interest.

If one uses a δ-interaction for calculating pairing matrix elements, the quality of agreement with experiment is about the same as with a constant G interaction. It was noted [18] that a density dependent δ interaction provides a much improved description of nuclear features. The main argument [19] for a density mediated interaction is that the free interaction is too strong to be consistent with observed nuclear features. It should be noted that one in fact must adjust the overall strength of constant G, δ or density dependent δ interactions to reproduce spectroscopic observables such as gaps or two quasi-particle excitation energies. The form of the interaction introduced [18] is

$$V(\vec{r}_{ij}) = -V_0\delta\left(\vec{r}_i - \vec{r}_j\right)\left[1 - \left(\rho\left(r\right)/\rho_0\right)^{2/3}\right] \tag{10}$$

where ρ_0 is roughly equal to the nuclear density. In some cases, it is taken as slightly smaller than the interior density and the interaction is repulsive in the nuclear interior. The power of 2/3 is also not crucial. We have found that any power between 2/3 and 1 gives essentially the same results, so long as one adjusts the overall strength, V_0, to give the same gap. The effect of this interaction is that orbitals that are concentrated in the nuclear surface and exterior regions have large pairing matrix elements. One might think that the overall pairing strength might be substantially larger when nuclei are superdeformed as compared to when they are normally deformed because the surface to volume ratio is substantially larger for superdeformed shapes.

If one adjusts the strength, what are the observable differences between the different forms of the pairing interaction? One way of differentiating between different interactions is to look at level spacings between orbitals as the fermi level moves from

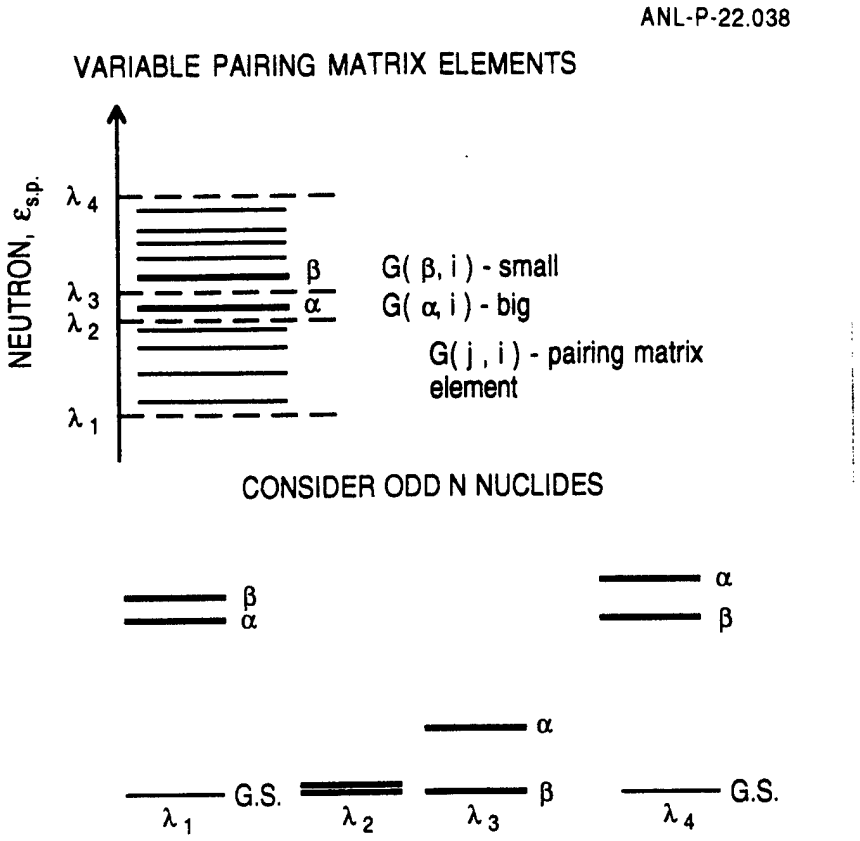

Figure 2. Schematic Change of Level Spacing with change of Fermi Level. λ indicates the Fermi level. At λ_1, the orbitals α and β are far above the Fermi level; at λ_4 far below.

far below them to far above them. This can be done conveniently [20] in the actinides, where the changes in deformation are relatively small. In Fig. 2. we indicate how this spacing changes with the position of the fermi level when one of the two levels (α) has large pairing matrix elements and the other (β) has small ones. When α is blocked, the energy costs are high and when β is blocked the costs are low. When both levels are far above the fermi level or far below, pairing changes their relative spacings slightly. The level β will be somewhat closer to the ground state. However, when the levels are near the fermi level, there may be apparent spacing changes of several hundred keV when the number of of the relevant nucleons is increased by two. In Fig. 3, we display the single particle level spacings for actinide neutrons, as extracted [20] from experiment using: a) a constant pairing interaction, and b) a density dependent interaction. Clearly, the latter interaction appears to give a better description of the data. Most of the large shifts in extracted level spacings disappear, when one uses the density dependent interaction.

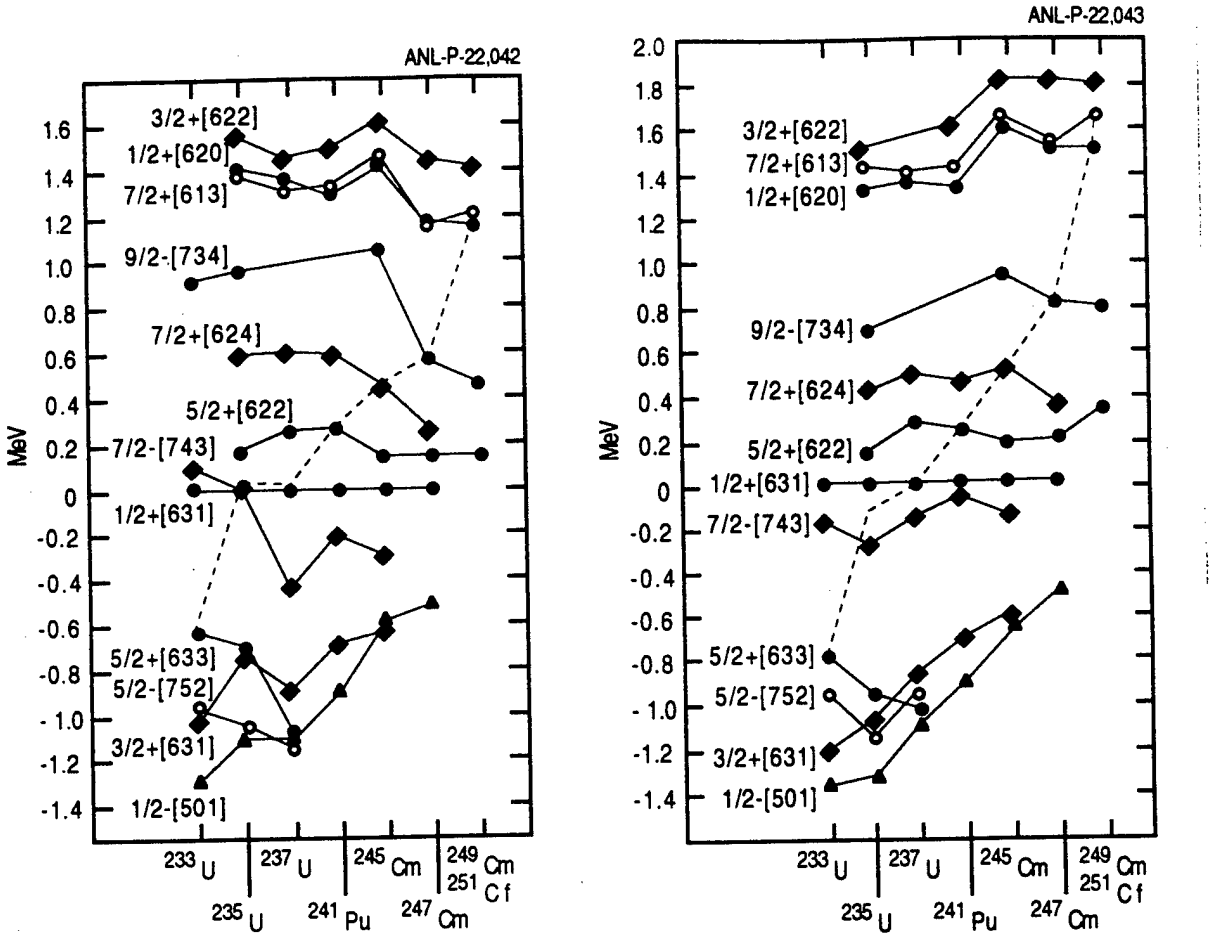

Figure 3. Single Particle Level Spacings Extracted from Observed Level Spacings in the Actinides. (a) using constant G pairing interaction. (b) using a density dependent δ interaction. The dashed line connects the ground states. All energies are relative to the $1/2^+[631]$ orbital.

A density dependent pairing interaction has been used for a study of the halo nucleus ^{9}Li [19]. Recently, density dependent pairing has been used to calculate [21] the properties of the Pb isotopes, ranging from A=190 to A=214, using several versions of a density dependent pairing interaction. They can account quite well for neutron separation energies using several variations on density dependent pairing. When they examine the changes in nuclear radii, however, they get somewhat better agreement with experiment using a term depending on the gradient of the density (more surface peaking) in their interaction. Using the standard version of density dependent pairing, one does not reproduce [22] the changes of charge radii quite so well.

4. ROTATIONAL BANDS IN SUPERDEFORMED NUCLEI

Superdeformation was first discovered [23] in the heavy elements, when a short fission lifetime was measured in ^{242}Am, that had a known fission lifetime. The lifetimes of these fission isomers were explained in terms of a second, superdeformed[24] minimum in the nuclear energy surface. Typically deformed nuclei are characterized by axis ratios of ~1.3:1. The fission isomers are characterized by axis ratios of ~2:1. See the article of Bjornholm and Lynn [25], for an excellent review of fission isomers.

One of the exciting developments in nuclear structure studies in the past decade has been the discovery [26] of superdeformation at high spins. The superdeformed bands in the A 150 region are characterized by axis ratios of 1.85:1. Superdeformation at high spin in this region was predicted [27,28] in calculations. An island of superdeformation near N~88 was found in calculations at I=0 [29] and used to explain many of the features found in fission mass yields.

A few years after the discovery of superdeformation in the A~150 mass region, our calculations [30] indicated that there were accessible superdeformed states in the A~190 region. Such states were shortly thereafter found [31-33] in ^{191}Hg and ^{192}Hg. In this region, the axis ratios characteristic of superdeformed shapes are ~1.65:1. Superdeformed minima are characterized by extremely low single-particle level densities near the fermi level. From the point of view of pairing calculations, this means that it not sufficient to develop product wave functions, even those with particle number projection before doing a variational calculation. One way [34] to deal with such problems is configuration interaction, using the generator coordinate method. It was found in the Hg region that the dynamic moment of inertia is a moderately increasing function of angular momentum, for angular momenta $10\hbar < I < 40\hbar$. The dynamic moment of inertia is defined as the moment of inertia that one would infer for a perfect rotor by looking at the the difference between successive transitions in a rotational band; i.e. for a rotor the energy is

$$E(I) = \frac{\hbar^2}{2\mathcal{J}}\left[I(I+1)\right] \tag{11a}$$

so

$$\mathcal{J} = 4\hbar^2(\mathrm{MeV})^{-1}/\left[\left\{\mathrm{E(I+2)-E(I)}\right\}-\left\{\mathrm{E(I)-E(I-2)}\right\}\right] \tag{11b}$$

Note that one does not need to know the angular momenta of the states involved in the transitions to define a moment of inertia in this way. This is appealing for experimentalists, as the spins may be hard to determine. In the Hg region, calculations that ignore pairing, give estimates of the moment of inertia that are constant with angular momentum. By including pairing, one gets variations [35] in the moment of inertia.

A second motivation for accurate calculations of the properties of superdeformed rotational bands was the discovery [36] of "identical bands"; i.e. sequences of transitions with the same energies, in different nuclei (^{151}Tb and ^{152}Dy). This is particularly strange as Dy has an even number of protons and Tb has an odd number of protons.

The phenomenon of identical bands was also found in the superdeformed bands [37] of the Hg region, and even in normally deformed nuclei [38]. Before worrying about identical bands, it seems necessary to understand what is involved in the accurate calculation of transition energies in a single band.

5. MANY BODY WAVE FUNCTIONS

Here, we consider the calculation of rotational energies in the cranking approximation[34] using a many-body wave function. Specifically, we consider the following questions: 1) how important are configuration interaction effects, and 2) what are the differences between constant G pairing and density dependent pairing in superdeformed nuclei.

The cranking [39,40,41] Hamiltonian is

$$H = \sum_k \epsilon_k N_k - \omega \sum_{i,j} (J_x)_{i,j} a_i^+ a_j - \sum_{i,j>0} G_{i,j} a_i^+ a_{-i}^+ a_{-j} a_j \tag{12}$$

where ω is a Lagrange multiplier and Jx is angular momentum about an axis perpendicular to the symmetry axis. The pairing matrix elements that we consider are: a) constant G, and b) density dependent delta interactions.

The many-body wave functions that we use are products of sums of terms. We set

$$|\psi\rangle = \prod^{\pi, T_z, \alpha} \sum_i \phi_i(\pi, T_z, \alpha) \tag{13}$$

where α is an unspecified quantum number such as the projection of angular momentum on the nuclear symmetry axis. Each of the terms in the sum is in turn a product of creation and annihilation operators and $|0\rangle$ is the particle vacuum. For purposes of illustration, we consider a group, i, consisting of three doubly degenerate Nilsson orbitals and having an even number of neutrons in the group. There are four ways that the number parity can be portioned among the levels, keeping an overall even number parity. In general, there are 2^{N-1} terms when there are N levels in the group. There are the same number of terms when the number parity is odd. Making a tabulation of the possibilities, we have

	Orbital Number		
	1	2	3
Term Number 1	*e*	*e*	*e*
2	*e*	*o*	*o*
3	*o*	*e*	*o*
4	*o*	*o*	*e*

When we have an 'e' associated with a level in a given term. we put in a factor $(1+Ba^{\dagger}a^{\dagger}_{-})$ and when we see an 'o' associated with a level. we put in the factor $(a^{\dagger}+Ca^{\dagger}_{-})$ where B and C are variational parameters. In total, there are $(N+1)(2^{N-1})$ variational parameters in a group with N orbitals. To illustrate. we have for the third term in the table

$$\phi_3 = A_3\left(a^{\dagger}_1 + T_{31}a^{\dagger}_{-1}\right)\left(1 + T_{32}a^{\dagger}_2 a^{\dagger}_{-2}\right)\left(a^{\dagger}_3 + T_{33}a^{\dagger}_{-3}\right) \tag{14}$$

The parameter A_3 is usually 1.0. The first term corresponds to a BCS-like wave function. Before solving for the variational parameters, we project from Eq. (13) a state of exact proton number, exact neutron number, good parity and good signature. For a group with 5 levels, there are 80 variational parameters to be determined and 448 in a group of 7 levels (where we neglect those like A_3). The solutions are obtained by iterating the set of coupled non-linear algebraic equations obtained by minimizing H with respect to the variational parameters. In our typical calculation, there are ~1500-2000 variational parameters, taking both neutrons and protons into account.

6. ROTATIONAL SPACINGS IN THE SUPERDEFORMED BAND OF ^{192}Hg

We apply these wave functions to the lowest superdeformed band in ^{192}Hg. As we are considering superdeformed shapes, where the single particle level densities are very low, we anticipate that configuration interaction effects are important. Calculations of rotational spacings that include pairing without configuration interaction effects have been carried out in this mass region by several authors [7,16,42-44]. A very nice feature of our wave functions is that off-diagonal matrix elements and overlaps are easy to calculate. We have used both the neutron and proton pairing strengths as generator coordinates. Further, we have carried out diagonalizations where the cranking frequency is treated as an additional generator coordinate. In the latter case, the solutions consist of ~70 different configurations. In Fig. 4, we show the neutron and proton pairing correlation energies as a function of angular momentum, calculated with constant G pairing

$$G_N = .118 \text{ MeV} \quad G_p = 1.4G_N \tag{15}$$

when we consider just the single wave function that minimizes the energy. When we include configuration interaction, there is a considerable improvement in the total energy. In Fig. 5, we show the gain in energy, when Gn and Gp are used as generator coordinates (solid line) and the energy gains obtained by using the cranking frequency (dashed line) as a generator coordinate in addition. The improvements in the energy are substantial, on the order of 0.5 MeV at the higher spins.

To what extent are transition energies are affected by the inclusion of configuration interaction. In Fig. 6, we display the difference between calculated and experimentally

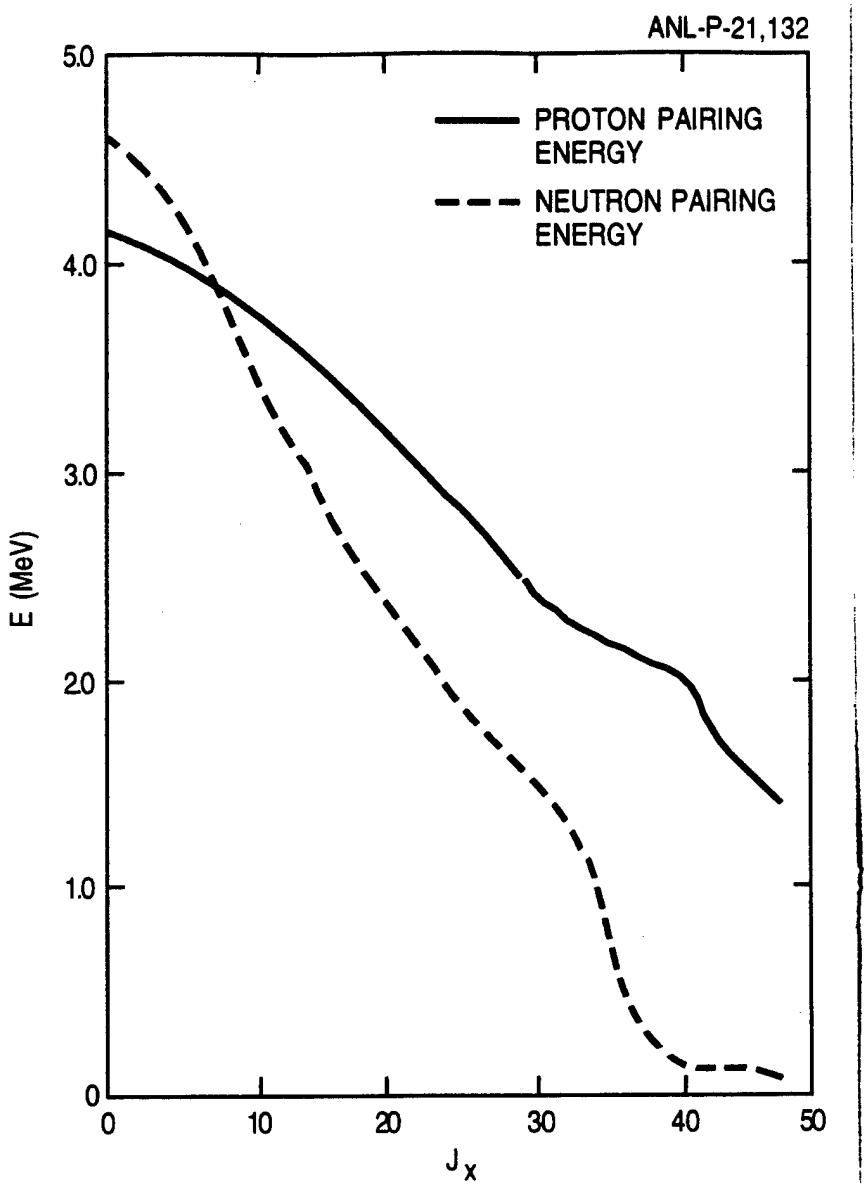

Figure 4. Proton and neutron pairing correlation energies as a function of angular momentum.

observed transition energies in ^{192}Hg. Perfect agreement would be the straight line at 0 keV. The dashed curve shows the difference when configuration interaction effects are not included and the line shows the difference when configuration interaction effects are included. There is a substantial improvement in the agreement with exper-

iment in the latter case. Apart from the question of the adequacy of our calculation. this result illustrates most emphatically the need to go beyond mean-field (BCS) when the interaction is weak. We believe that this result has universal relevance for superdeformed rotational bands, because one gets superdeformation only when the level density is low near the fermi level. The issue of weak pairing interactions is always exacerbated with increasing angular momentum, as can be seen from Fig. 4.

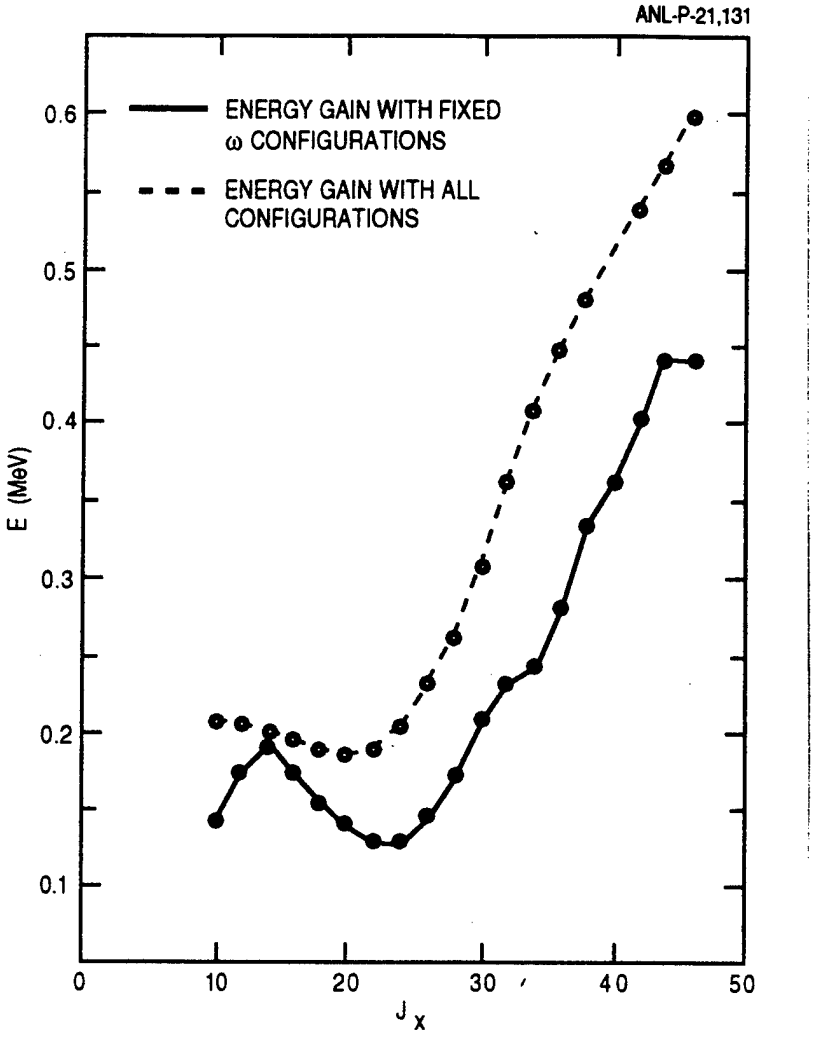

Figure 5. Gains in Energy as a Function of Angular Momentum. (a) using Gn and Gp as generator coordinates. (b) using ω as a generator coordinate in addition to Gn and Gp.

We next consider the following question: to what extent does the density dependent delta pairing interaction improve our results? In Fig. 7, we compare the rotational spacings obtained with a constant G pairing force and a density dependent

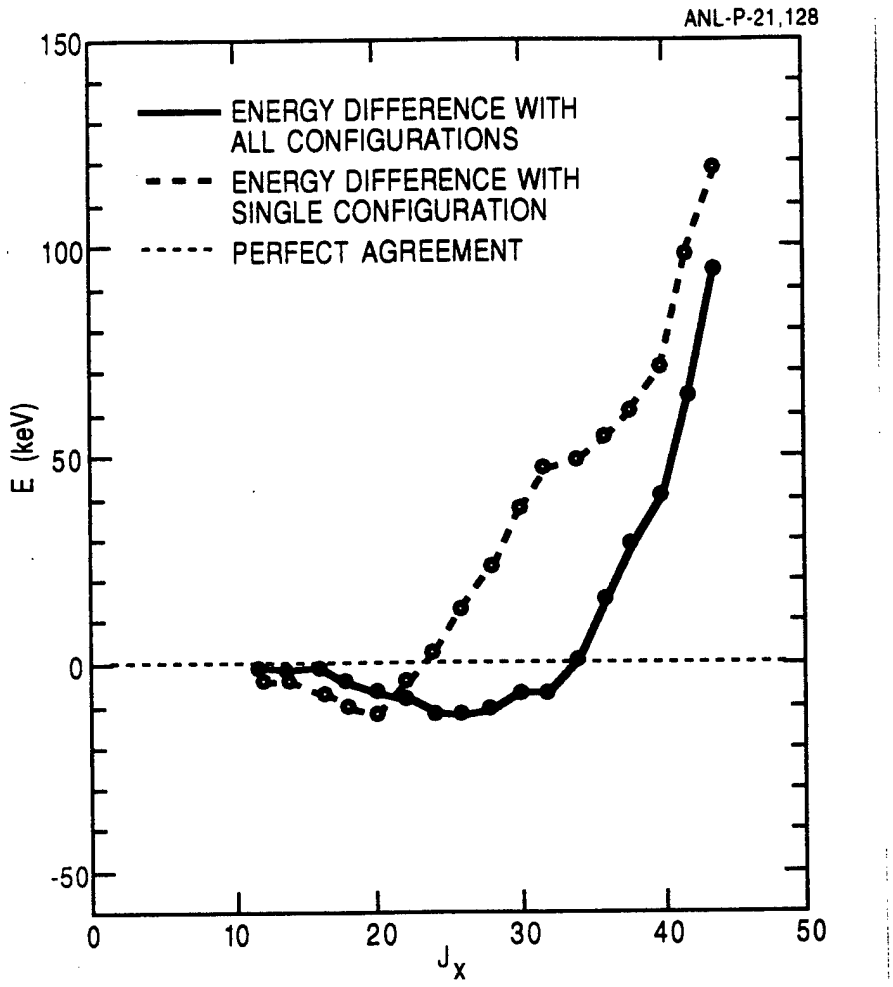

Figure 6. Difference between Measured Transition Energies and Observed Transition Energies in Superdeformed Rotational Band of ^{192}Hg calculated without and with configuration interaction.

δ pairing force. We have adjusted the strengths of the density dependent proton and neutron pairing interactions to have the same overall strength as the constant G interaction at I=10$\hbar$. Configuration interaction is included in both calculations. In this calculation, the value of Gp was taken as 1.3Gn to look at the sensitivity to small changes in pairing strength. We have subtracted the energy differences of an ideal rotor with a moment of inertia of 100 $\hbar^2$ MeV^{-1} from the calculated energies, in order to see the energy differences clearly. We also show the experimental energy differences in this figure. The obvious result here is that both choices of pairing interaction give substantially the same result. On this scale, it appears that they disagree with experiment. We have also looked at the relative shifts of single-particle orbitals, in odd-mass superdeformed bands in analogy to our study of the actinides.

Here, the relative shifts of levels with large and small average pairing matrix elements is on the order of 100 keV as we vary the fermi level. This is to be contrasted with the ~500 keV shifts in the actinides. The reason that density dependent pairing effects are attenuated in superdeformed minima is that the overall pairing is reduced because of the low single particle level densities associated with superdeformed minima.

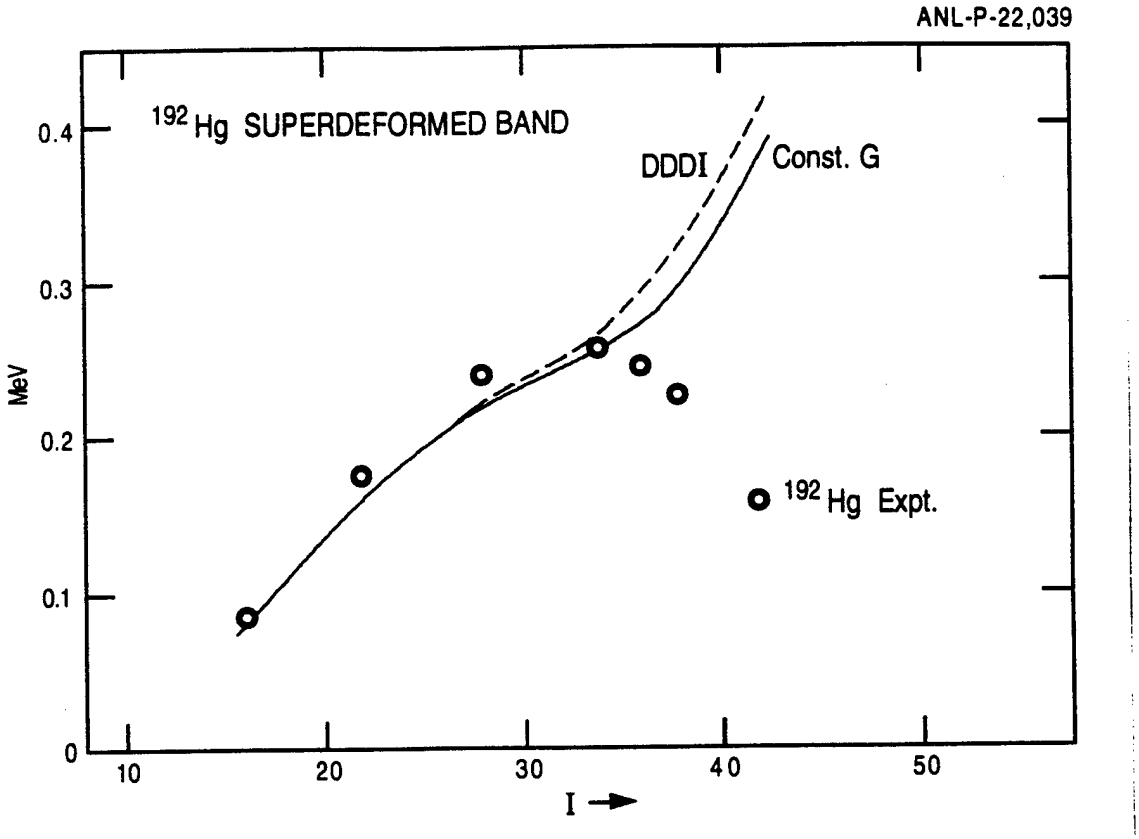

Figure 7. Excitation Energies Calculated with Constant G Pairing, Density Dependent Pairing and Experimental Excitation Energies relative to an Ideal Rotor with a moment of inertia of $100\hbar^2$ MeV^{-1}.

To retain some sense of perspective, it is useful to compare the calculated and observed level spacings in ^{192}Hg, without subtracting any reference energies. This amounts to an integration over the energy differences of Fig. 6, obtained with configuration interaction. In Fig. 8, we make such a comparison. The calculated and experimental energies are adjusted to be the same for the $I=10^+$ level. The absolute value of this energy depends on the excitation of the superdeformed minimum relative to the ground state at I=0. Looking at the energies in this way, we see an impressive agreement over an interval of 9 MeV. The differences between experimental and observed energies are less than 200 keV from I=10 $\hbar$ to I=42 $\hbar$. This indicates that we have a reasonable understanding of superdeformed bands in the Hg region. The ~500 keV improvements, that we get by including configuration interaction, are noticeable even on this scale.

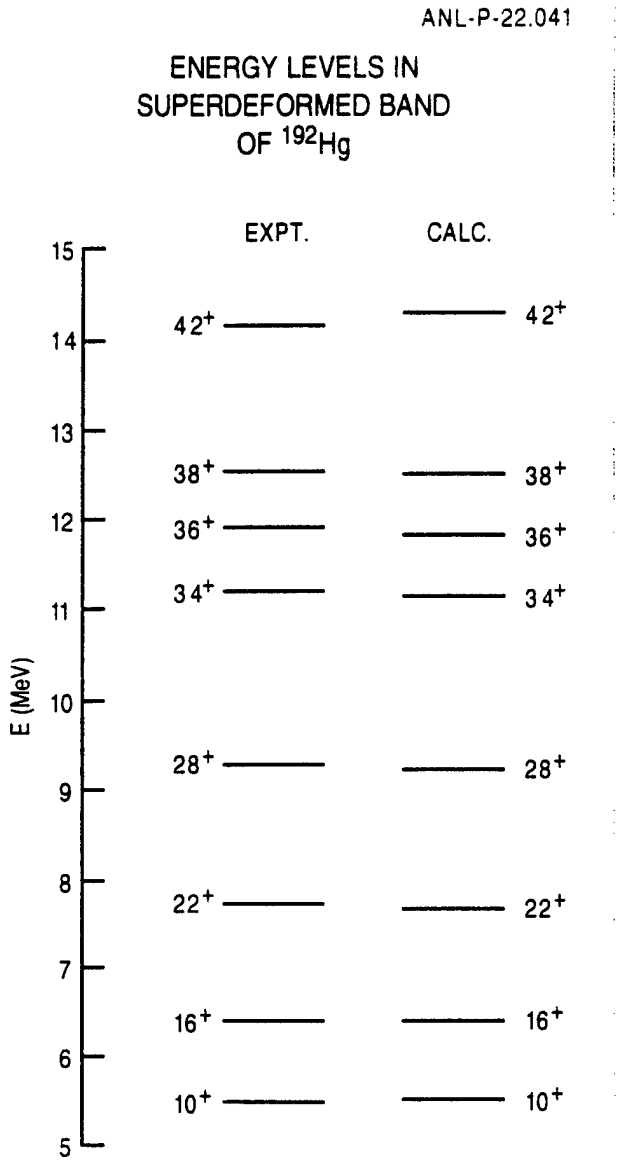

Figure 8. A direct comparison of calculated and observed rotational excitation energies (adjusted to agree at I=10$\hbar$).

7. SUMMARY

We have discussed the important role that the small number of valence particles play in nuclear spectroscopic pairing calculations. We have shown, using exact sum rules, how correlations arise from going beyond the BCS wave function. We have tried to show the importance of taking many-body correlation effects into account with a detailed consideration of level spacings in superdeformed rotational bands.

ACKNOWLEDGMENTS

This research is supported by the U.S. Department of Energy under contract W-31-109-ENG-38. The calculations reported here were carried out on the SP computer of the MCS Division of Argonne National Laboratory and at the NERSC facility at Berkeley. I thank the Army Research Office for subsidizing a portion of the expenses involved in my participating in the CMT20 Workshop.

REFERENCES

1. A. Goswami and L.S. Kisslinger, Phys. Rev. **B140**, 26 (1965).
2. A.L. Goodman, G.L. Struble, J. Bar-Touv, and A. Goswami, Phys. Rev. **C2**, 380 (1970).
3. J. Engel, K. Langake, and P. Vogel, Phys. Lett. **B389**, 211 (1996).
4. H.J. Lipkin, Ann. Phys. N.Y. **9**, 272 (1960).
5. Y. Nogami, Phys. Rev. **B134**, 313 (1964).
6. P. Quentin, N. Redon, J. Meyer, and N. Meyer, Phys. Rev. **C41**, 341 (1990).
7. G. Gall *et al.*, Z. Phys. **A348**, 183 (1994).
8. A. Valor, L.M. Robledo, and J.L. Egido, Phys. Rev. **C53**, 172 (1996).
9. R.R. Chasman, Phys. Rev. **C5**, 29 (1972).
10. R.W. Richardson, Phys. Rev. **141**, 949 (1966).
11. D.L. Hill and J.A. Wheeler, Phys. Rev. **89**, 1102 (1953).
12. P. Ring and P. Schuck, in *The Nuclear Many–Body Problem*, Springer-Verlag, (New York 1980) pp. 398-437.
13. W. Ogle *et al.*, Rev. Mod. Phys. **43**, 424 (1971).
14. R.R. Chasman *et al.*, Rev. Mod. Phys. **49**, 833 (1977).
15. R.R. Chasman, Phys. Rev. **C21**, 456 (1980).
16. J. Terasaki *et al.*, Nucl. Phys. **A593**, 1 (1995).
17. S.J. Krieger *et al.*, Phys. Rev. **C54**, 2399 (1996).
18. J.W. Ehlers and S.A. Moszkowski, Phys. Rev. **C6**, 217 (1972).
19. G.F. Bertsch and H. Esbensen, Ann. Phys. **209**, 327 (1991).
20. R.R. Chasman, Phys. Rev. **C14**, 1935 (1976).
21. S.A. Fayans and D. Zawischa, Phys. Lett. **B383**, 19 (1996).
22. N. Tajima *et al.*, Nucl. Phys. **A551**, 434 (1993).
23. S.M. Polikanov *et al.*, Zh. Ekxp. Teor. Fiz. **42**, 1016 (1962).
24. V.M. Strutinsky, Nucl. Phys. **A95**, 420 (1967).
25. S. Bjornholm and J.E. Lynn, Rev. Mod. Phys. **52**, 725 (1980).
26. P.J. Twin *et al.*, Phys. Rev. Lett. **57**, 811 (1986).
27. K. Neergard, V.V. Paskevich, and S.Frauendorf, Nucl. Phys. **A262**, 61 (1976).
28. J. Dudek and W. Nazarewicz, Phys. Rev. **C31**, 298 (1985).
29. B. D. Wilkins *et al.*, Phys. Rev. **C14**, 1832 (1976).
30. R.R. Chasman, Phys. Lett. **B219**, 227 (1989).
31. E.F. Moore *et al.*, Phys. Rev. Lett. **63**, 360 (1989).

32. D. Ye *et al.*. Phys. Rev. **C41**. R9 (1990).
33. J.A. Becker *et al.*, Phys. Rev. **C41**. R13 (1990).
34. R.R. Chasman, Phys. Lett. **B319**. 41 (1993).
35. M.J.A de Voigt, J. Dudek, and Z. Szymanski, Rev. Mod. Phys. **55**, 949 (1983).
36. T. Bryski *et al.*, Phys. Rev. Lett. **64**, 1650 (1990).
37. F.S. Stephens *et al.*, Phys. Rev. Lett. **66**, 1378 (1991).
38. I. Ahmad *et al.* Phys. Rev. **C44**, 1204 (1991).
39. D.R. Inglis, Phys. Rev. **96**, 1059 (1954).
40. P. Ring, R. Beck, and H.J. Mang, Z. Phys. **231**, 10,26 (1970).
41. M. Brack and B.K. Jennings, Nucl. Phys. **A258**, 264 (1976).
42. M.A. Riley *et al.*, Nucl. Phys. **A512**, 178 (1990).
43. M. Girod *et al.*, Phys. Rev. **C45**, 1420 (1992).
44. R.R. Chasman, Phys. Lett. **B242**. 317 (1990).

Invited talk presented at the *XX International Workshop on Condensed Matter Theories - Joint U.S.-India Seminar on Bose-Einstein Condensation and Pairing Phenomena*, 9-14 December, 1996, University of Pune, Pune, India.

GROUND STATE CALCULATIONS OF LI ATOMS IN A HARMONIC TRAP

Siu A. Chin[†], *Harald A. Forbert*[†], *and E. Krotscheck*[†‡]

[†]Center for Theoretical Physics and Department of Physics
Texas A&M University, College Station, TX 77843 USA

[‡]Institut für Theoretische Physik
Johannes Kepler Universität, Linz, Austria

1. INTRODUCTION

The recent observations of Bose-Einstein condensation in ^{87}Rb [1], ^{7}Li [2] and ^{23}Na [3] have renewed much theoretical interest in the study of low density bose systems. The importance of these experiments is not, as some press coverage would seem to suggest [4], that low density systems allow a cleaner theoretical determination of the Bose condensate. While this may well be true, there are no serious theoretical disagreements over the condensate fraction in liquid Helium (all within 8%-11%), which is about a billion times as dense as these atomic systems. The continuous debate has always been whether neutron scattering experiments, as a probe of liquid Helium, despite strong final-state-interactions, can directly signal the presence of the condensate. Thus the importance of these recent observations lies not only in their novel techniques of condensate production, but also of its detection.

The fundamental energetics of a dilute, uniform, bose gas with positive scattering length has long been elucidated in a series of seminal papers by Huang and Yang [5], Lee, Huang and Yang [6], and others [7]. More recently, P. A. Ruprecht *et al.* [8], have solved numerically, and Baym and Pethick [9] have shown analytically, how the mean-field theory of Gross and Pitaevskii can be applied to the case of a non-uniform bose gas confined in a harmonic trap. In contrast, since a bose gas with negative scattering length, such as ^{7}Li, will collapse in the bulk limit, little is known about its ground state properties. When trapped in a harmonic well, this instability is postponed by the confinement kinetic energy. However, both the onset and the dynamics of this instability is not well understood. The initial Li experiment [2], which suggested that there may be more particle in the ground state than can be accounted for by the Gross-Pitaevskii mean-field theory, has triggered new theoretical efforts in the study of overall attractive bose systems [10] . The revised experimental estimate of

the condensate particle number [11] has removed a basic discrepancy, however, it has not lessened the urgency to understand this fundamental bose system better.

In this work, we outline some fundamental steps necessary for a microscopic study of bose systems with negative scattering length. In the case of positive scattering length, it is well known that perturbation theory is not directly applicable. One key observation of this work is that for negative scattering length, the use of the Moszkowski-Scott [12] separated potential once again renders perturbation theory useful. We will discuss in detail the properties of the full Li-Li potential and the resulting finite size corrections when this potential in a harmonic well is approximated by the scattering length.

2. THE NON-INTERACTING BOSE GAS

The onset of the Bose-Einstein condensation in an ideal Bose gas is characterized by a critical temperature

$$T_c = 3.31 \left(\frac{\hbar^2}{mk_B}\right)\left(\frac{N}{V}\right)^{2/3}. \tag{1}$$

For liquid Helium, where $N/V = 0.0218$ Å^{-3} and $\hbar^2/mk_B = 12.12$ KÅ^2, this gives $T_c = 3.13$ K, which is quit close to the superfluid lambda transition temperature $T_\lambda = 2.17$ K. For a non-interacting Bose gas confined to a harmonic potential

$$V(r) = \frac{1}{2}m\omega^2 r^2,$$

the situation is more complicated. Let b be the characteristic radius of the potential defined by the frequency ω via

$$\hbar\omega = \frac{\hbar^2}{m}\frac{1}{b^2}. \tag{2}$$

The ground state wavefunction is then simply

$$\psi_0(r) = \frac{1}{(\pi b^2)^{3/4}}\exp(-\frac{1}{2}\frac{r^2}{b^2}). \tag{3}$$

The corresponding condensation temperature [13] is

$$bT_c = (1.202)^{-1/3}\left(\frac{\hbar^2}{k_B m}\right)\left(\frac{N}{b^3}\right)^{1/3}. \tag{4}$$

Note that in thermodynamic limit of $N \to \infty$, $b \to \infty$, such that $N/b^3 \to const.$, $T_c \to 0$! Thus strictly speaking, there is no finite critical temperature. Nevertheless, for finite values of b and N, the above defined T_c does characterized a narrow range of temperature over which rapid changes associated with condensation are observed. To illustrate this, we consider the density profile (or the momentum profile) of a

harmonically trapped ideal Bose gas as the temperature is lowered below T_c. For an anisotropic trap with $\omega_x = \omega_y = \omega_\perp$, its excitation spectrum is given by

$$\epsilon_{i,j,k} = \hbar\omega_\perp(i+j) + \hbar\omega_z k.$$

At a given particle number N and temperature T, the fugacity $\lambda = e^{\mu/kT}$ is determined implicitly via

$$N = \sum_{i,j,k} N_{i,j,k} = \sum_{i,j,k} \frac{\lambda \exp[-\epsilon_{i,j,k}/kT]}{1 - \lambda \exp[-\epsilon_{i,j,k}/kT]}.$$

Once λ is known, the integrated two dimensional density profile is given by

$$\begin{aligned} \rho(x,z) &= \int dy \sum_{i,j,k} N_{i,j,k}\, \psi_i^2(x)\psi_j^2(y)\psi_k^2(z) \\ &= \sum_{i,k} \widetilde{N}_{i,k}\, \psi_i^2(x)\psi_k^2(z), \end{aligned} \tag{5}$$

where

$$\widetilde{N}_{i,k} = \sum_j \frac{\lambda \exp[-\epsilon_{i,j,k}/kT]}{1 - \lambda \exp[-\epsilon_{i,j,k}/kT]}.$$

We have carried out the sum over states in (5) with i and k ranged over 400 states. The resulting density profiles for $N = 20,000$ as a function of temperature is shown in Fig. 1. T_c in this case is 71 nK. The geometry is chosen to mimic that of the Rb experiment [1]. As the temperature is lowered below T_c, the density profile develops a sharp peak corresponding to the macroscopic occupation of the ground state. Since the momentum eigenstates are also Gaussians, a similar peaking would also occur in the momentum density distribution.

3. THE TRIPLET LI POTENTIAL

The triplet potential between two ^{7}Li atoms has been extensively studied by many groups [14-21]. The potential is weak by atomic standards, but it is 10 times as deep as that between two ^{4}He atoms. Whereas two ^{4}He atoms can barely form a bound state, two triplet ^{7}Li atoms can sustain 11 bound states, 9 of which have been observed experimentally [16,21], including the topmost one [21]. By fitting and amalgamating the short, medium and long range results of [17,18], we have obtained a simple analytic potential which is adequate for our computational needs. This is shown in Fig. 2. The potential is characterized by a hard core at $r = 3$ Å, a well depth of ≈ -480 K, and an attractive range of ≈ 20 Å. The horizontal lines indicate bound state energies; their values are given in Table 1. These are compared with experimental values [16,21] and with that of Côté, Dalgarno and Jamieson's potential [20]. Also included are comparisons of the scattering length a and the effective range r_e. While there are excellent agreements in the bound state energies, there are substantial variations in the scattering length and the effective range. To

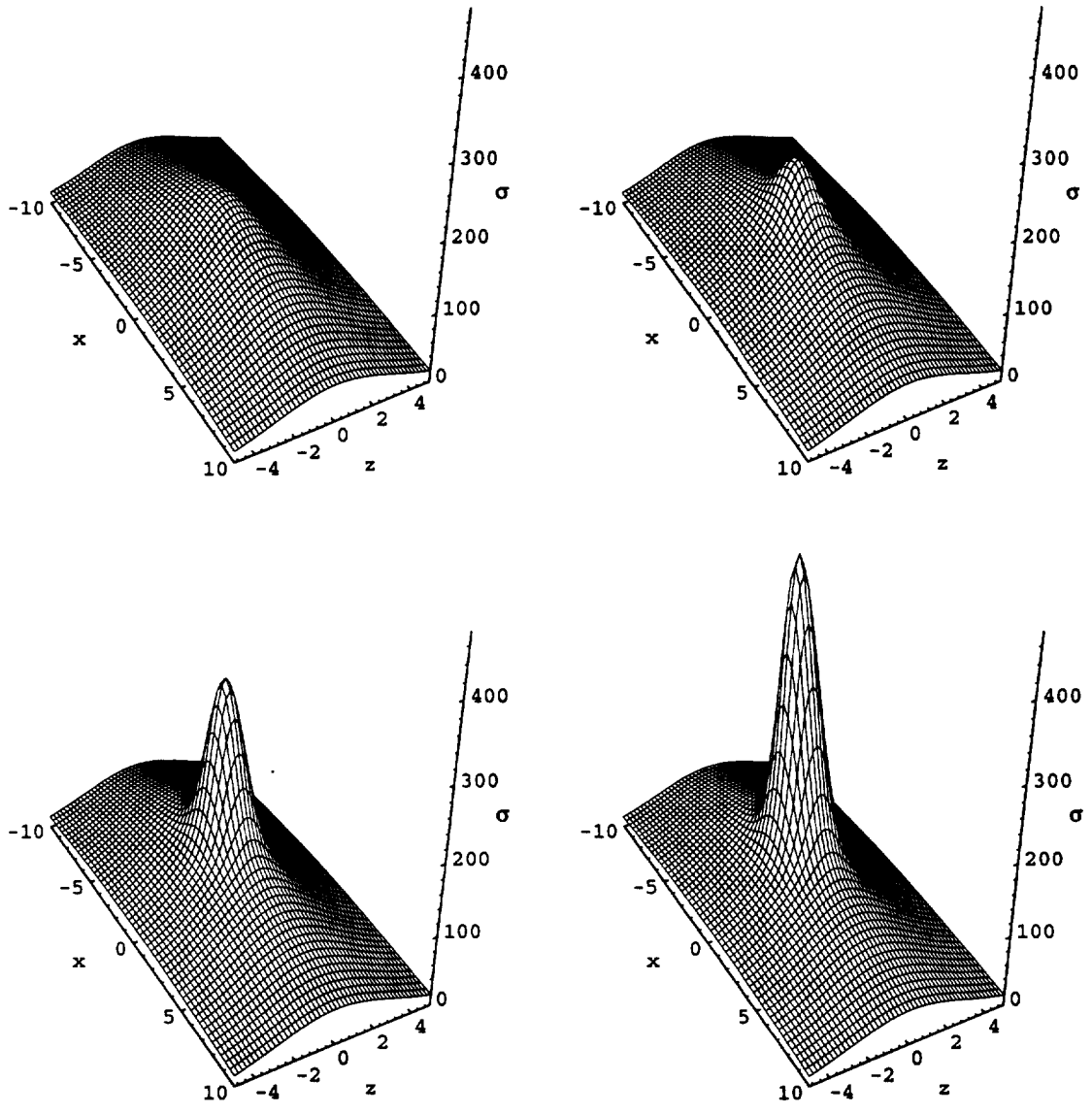

Figure 1. The integrated two dimensional density profile of 20,000 non-interacting bosons in a harmonic trap with b_z=0.9845 μm and $b_\perp$=1.655 μm. x and z are measured in units of μm. The temperatures are, from left to right and from top to bottom, 72, 71, 70, and 69 nK respectively. The condensation temperature is 71 nK.

the extent that some predictions are sensitive to the actual value of the scattering length, one must remember that the scattering length remains an theoretical inference

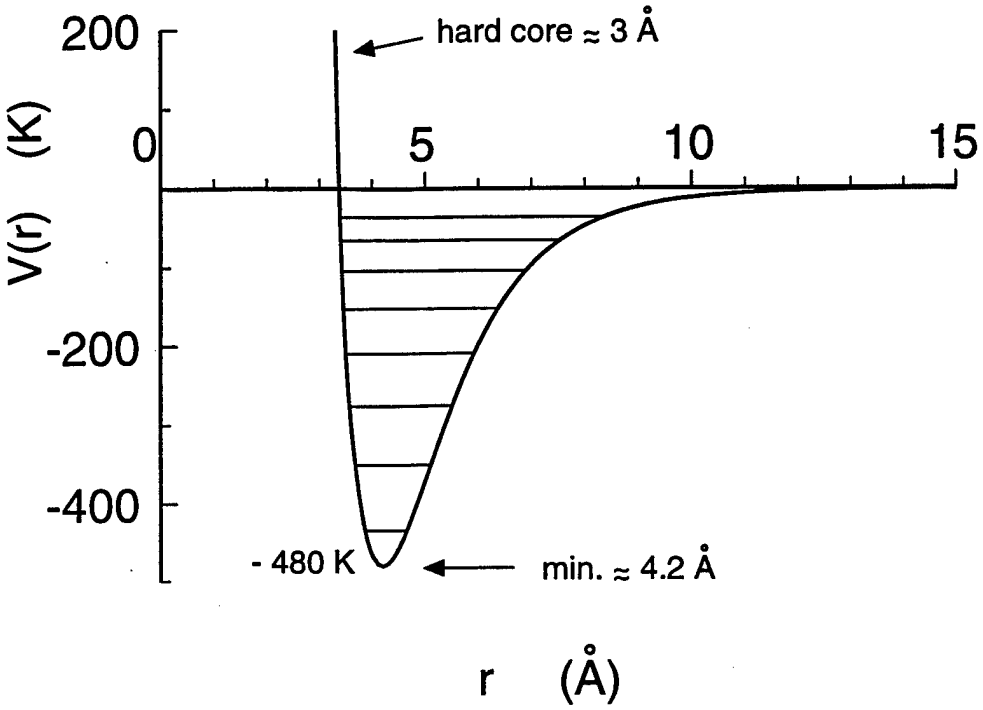

Figure 2. The triplet ^{7}Li potential from our own fit to the RKR data of Ref. [17]. For clarity, only the lowest 8 of 11 bound states are indicated.

rather than an experimentally observable.

The existence of the hard core and bound states make it difficult to do a microscopic many-body calculation using the bare two-body potential. The hard core precludes the use of perturbation theory and the formation of bound states does not correspond to the experimental situation. Experimentally, since the density is extremely low, bound states can form only by rare three-body collisions. If bound states are formed, they are then likely to be ejected from the shallow trap by releasing their binding energy. Thus the trapped atoms are in a metastable many-body ground state with no two-body bound states. One way out of this difficult is to use the delta function pseudopotential, which only takes account of the scattering length of the bare potential. However, this approach cannot address the adequacy of the scattering length approximation itself, nor can it be used to higher orders to assess many-body correlation effects. In this work, we will introduce another kind of effective potential long familiar from nuclear physics, which eliminates both the hard core and the bound state problem.

Table 1

The 11 bound state energies (in K) of triplet ^{7}Li of our potential as compared with experiment and another calculation. a is the scattering length and r_e is the effective range. The more refined calculation of Ref. [2] gives $a = -14.447$ Å. *The top most level was determined in Ref. [21].

Expt. [16]	Côté *et al.* [20]	This Work
-0.598*	-0.550	-0.572
-	-4.886	-5.005
-	-16.204	-16.612
-36.210	-36.253	-36.842
-65.633	-65.713	-65.813
-104.222	-104.327	-104.029
-151.925	-151.998	-151.672
-208.678	-208.719	-208.625
-274.460	-274.547	-274.754
-349.370	-	-349.991
-433.684	-	-434.396
a	-9.102 Å	-11.35 Å
r_e	537.0 Å	387 Å

4. THE MOSZKOWSKI-SCOTT SEPARATION METHOD

A basic idea for dealing with a potential having a strongly repulsive core is to separate it into two parts,

$$V(r) = V_S(r) + V_L(r),$$

with the short range part $V_S(r)$ to be treated exactly and the long range part $V_L(r)$ perturbatively. The choice of $V_S(r)$ and $V_L(r)$ is arbitrary, and can be chosen according to physical insights. For an *overall* attractive potential with an infinite hard core at $r = c$, Moszkowski and Scott [12] observed that the exact two-body relative radial wavefunction $u(r)$ must behave as shown in Fig. 3. As compared with the non-interacting two-body wavefunction

$$u_0(r) = \sin kr,$$

$u(r)$ is first pushed out by the hard core and hence must be below the free wavefunction. As its higher points further out are being pulled back by the attraction, it gives

the appearance of rising rapidly and bending over. Thus it must have a "hump" at which it is tangential to the free two-body wavefunction at a distance $r = d$. This is the Moszkowski-Scott separation distance. The tangent condition at d is just the equality of the logarithmic derivatives

$$\frac{u'(d)}{u(d)} = \frac{u_0'(d)}{u_0(d)}. \tag{6}$$

If we simply take

$$V_S(r) = V(r)\theta(d-r) \quad \text{and} \quad V_L(r) = V(r)\theta(r-d),$$

then the wavefunction at $r > d$ is entirely determined by the logarithmic derivative at $r = d$ and $V_L(r)$. Thus if we are only interested in the behavior of the wavefunction at $r > d$, which is the case for low density systems, then we may as well use the simpler wavefunction

$$\widetilde{u}(r) = \begin{cases} u_0(r), & \text{if } r < d\ ; \\ u(r), & \text{if } r \geq d\ . \end{cases}$$

But this wavefunction is produced by $V_L(r)$ only. Hence, we may as well replace the original potential by just $V_L(r)$. In effect, since $V_S(r)$ as defined above gives zero phase-shift, we can take it to be zero, in which case, its exact treatment is trivial. Thus in its simplest form, the Moszkowski-Scott separation method replaces the original two-body potential by just

$$V(r) \to V_L(r).$$

The separation distance d depends on $k = \sqrt{Em}/\hbar$. To study particles confined in a macroscopic harmonic trap with $E = \frac{3}{2}\hbar\omega$ close to zero, we simply take $k = 0$. For ^{7}Li, this separation distance is $d = 36.7008$ Å. The maximum potential at this distance is only $\approx -4\times10^{-3}$ K, which is certainly weak enough for doing perturbative calculations.

5. THE PAIR ENERGY SHIFT IN A HARMONIC TRAP

To test the effectiveness of the Moszkowski-Scott separation method, we will apply it to the case of two Li atoms in a harmonic trap. In order to make a quantitative comparison, we will first compute the pair energy shift analytically. The resulting energy shift contains corrections due to the finite size of the trap, which goes beyond the scattering length approximation. These finite size effects are widely assumed to be negligible; while this may well be the case, it is of interest to demonstrate this directly with an analytic calculation.

For two interacting Li atoms in a harmonic potential, their energy shift is given by the relative Schrödinger equation:

$$\left[-\frac{\hbar^2}{m}\nabla^2 + \frac{1}{4}m\omega^2 r^2 + V(r)\right]\psi(r) = E\psi(r).$$

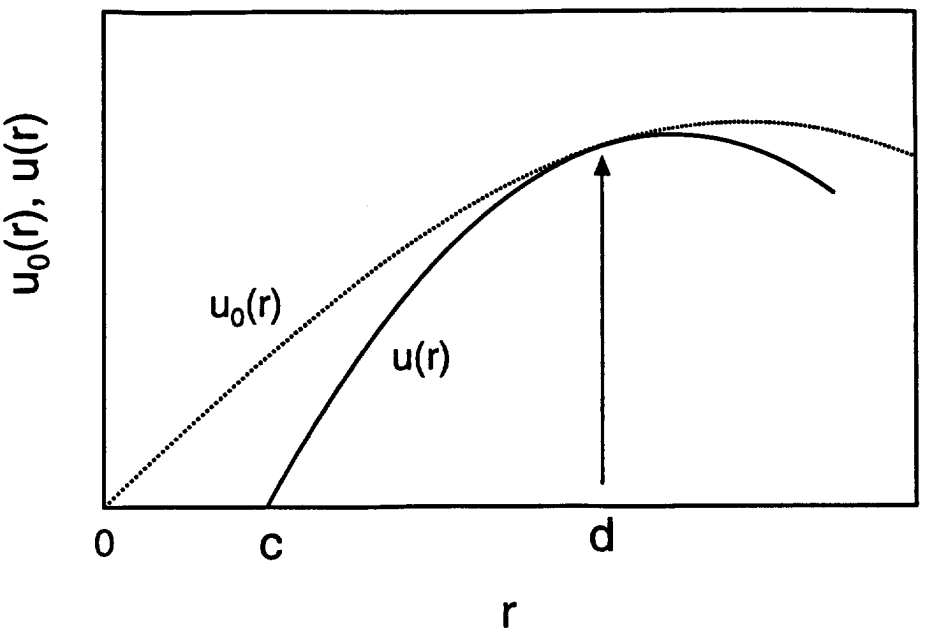

Figure 3. The Moszkowski-Scott separation distance d. $u_0(r)$ and $u(r)$ are free and interacting relative radial wavefunctions respectively. c is the hard core radius.

Introducing dimensionless variables, $\epsilon = E/\hbar\omega = Eb^2/(\hbar^2/m)$, $\widetilde{V}(r) = V(r)/\hbar\omega$, $x = r/b$, and $\psi(r) = u(x)/x$, the above reduces to

$$\left[-\frac{d^2}{dx^2} + \frac{1}{4}x^2 + \widetilde{V}(bx)\right] u(x) = \epsilon u(x). \tag{7}$$

Since b is the size of the magnetic trap on the order of 30,000 Å, whereas the range of the interaction is only 30 Å, on the scale of x, the Li-Li potential is non-vanishing only near $x \approx 0$. If the pair potential is ignored, then the solutions of (7) are just the parabolic cylinder functions [22]:

$$u(x) = U(-\epsilon, x). \tag{8}$$

Since the potential is non-vanishing only near $x \approx 0$, its effect can be incorporate as a boundary condition on the wavefunction. Near $x \approx 0$, but r much greater than the range of the potential, $u(x)$ is the scattered wavefunction oblivious of the trap potential,

$$u(x) = A\sin(bkx + \delta),$$

where $k = \sqrt{\epsilon}/b$. Matching $u'(0)/u(0)$ on both sides of (8) gives the eigen condition for determining the energy:

$$bk\cot(\delta) = -\sqrt{2}\frac{\Gamma(\frac{3}{4} - \frac{\epsilon}{2})}{\Gamma(\frac{1}{4} - \frac{\epsilon}{2})}. \tag{9}$$

To solve this equation for ϵ, we expand in powers of $(1/b)$:

$$k\cot\delta = \frac{-1}{a} + \frac{1}{2}r_e k^2 - Tk^4 + \cdots = -\frac{1}{a} + \frac{1}{2}r_e\epsilon\left(\frac{1}{b}\right)^2 - T\epsilon^2\left(\frac{1}{b}\right)^4 + \cdots$$

$$\epsilon = \frac{3}{2} + \epsilon_1\left(\frac{1}{b}\right) + \epsilon_2\left(\frac{1}{b}\right)^2 + \epsilon_3\left(\frac{1}{b}\right)^3 + \epsilon_4\left(\frac{1}{b}\right)^4 + \epsilon_5\left(\frac{1}{b}\right)^5 + \cdots$$

Matching power coefficients on both sides of (9) then gives:

$$\begin{aligned}
\epsilon_1 &= \sqrt{\frac{2}{\pi}}a \\
\epsilon_2 &= \frac{2\left(1 - \ln 2\right)a^2}{\pi} \\
\epsilon_3 &= \sqrt{\frac{2}{\pi}}a^2\left[\frac{3}{4}r_e + \left[\frac{1}{\pi}\left(3\left(1 - \ln 2\right)^2 - 1\right) - \frac{\pi}{12}\right]a\right] \\
\epsilon_4 &= 0.00844343a^2\left(-48.4124a^2 + 72.4033ar_e\right).
\end{aligned}$$

Thus if we define the energy shift ΔE via

$$E = \frac{3}{2}\hbar\omega + \Delta E$$

then we have

$$\Delta E b^3 = \frac{\hbar^2}{m}\left\{\epsilon_1 + \epsilon_2\left(\frac{1}{b}\right) + \epsilon_3\left(\frac{1}{b}\right)^2 + \epsilon_4\left(\frac{1}{b}\right)^3 + \cdots\right\}$$

$$\Delta E b^3 = -62.563 + 173.717\left(\frac{1}{b}\right) + 202317.0\left(\frac{1}{b}\right)^2 + \cdots .$$

The first term on the right hand side corresponds to the scattering length approximation:

$$\Delta E b^3 = \frac{\hbar^2}{m}\sqrt{\frac{2}{\pi}}a.$$

The rest of the terms are finite size corrections in powers of $1/b$. This analytical determination of the energy shift is compared with the exact numerical solution in Fig. 4. The quadratic approximation is in excellent agreement with the exact solution for trap size as small as a few hundred Å. The scattering length approximation is

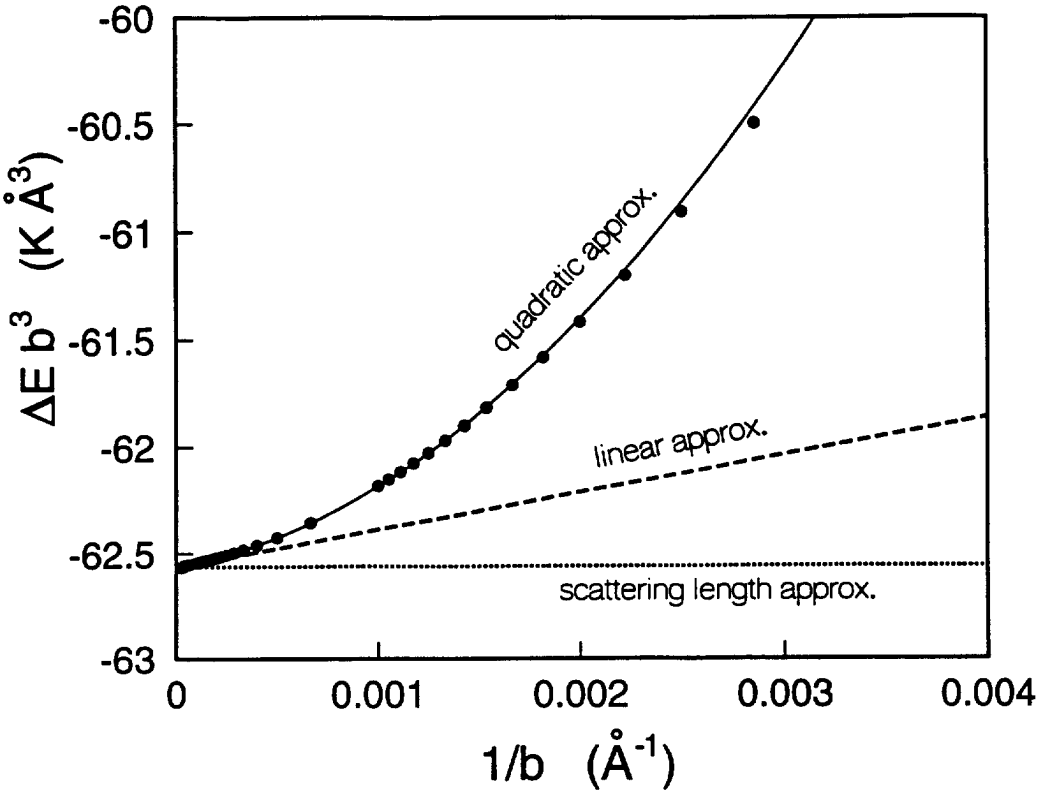

Figure 4. The energy shift of two Li atoms confined in a harmonic trap of size b. The solid circles are exact numerical results.

within 1% of the exact energy for $b > 1000$ Å. Thus its use for experimental trap sizes of $b \approx 30,000$ Å is well justified.

6. PERTURBATIVE CALCULATIONS

The long range part ($r \gtrsim 20$ Å) of the Li-Li triplet potential is known analytically [18],

$$\lim_{r\to\infty} V(r) \to -\left(\frac{C_6}{r^6} + \frac{C_8}{r^8} + \frac{C_{10}}{r^{10}}\right),$$

with coefficients, $C_6 = 9.6244 \times 10^6$, $C_8 = 1.6163 \times 10^8$ and $C_{10} = 4.0046 \times 10^9$. The Moszkowski-Scott separation method suggests that we replace the bare potential by

$$V_L(r) = -\left(\frac{C_6}{r^6} + \frac{C_8}{r^8} + \frac{C_{10}}{r^{10}}\right)\theta(r-d), \tag{10}$$

with $d = 36.7008$ Å. In contrast to the delta function pseudopotential, this potential can be used in higher order calculations. From its definition, this potential is phase-

equivalent to the original at zero energy. Let's see how well this works in computing the pair energy shift.

A. First order

The first order energy shift due to V_L is just

$$\Delta E_0^{(1)} = \ < 0|V_L|0 > \ = \int d^3r \ \psi_0^2(r) V_L(r),$$

where the unperturbed ground state wavefunction ψ_0 is given in (3). Expanding the wavefunction in powers of $1/b$ and keeping only terms up to $1/b^5$, gives

$$\Delta E_0^{(1)} = \sqrt{\frac{2}{\pi}}\gamma_3 b^{-3} - \frac{1}{\sqrt{2\pi}}\gamma_5 b^{-5} = -52.1730 b^{-3} + 105058.1 b^{-5},$$

where

$$\gamma_i = \int_0^\infty V_L(r) r^{i-1} dr$$

The first term here corresponds to the Born approximation of the scattering length, since

$$\gamma_3 = \frac{\hbar^2}{m} a_B,$$

and $a_B = -9.4575$ Å. Higher order contributions will correct this to the exact scattering length.

B. Second order

The second order energy-shift is given by:

$$\begin{aligned}\Delta E_0^{(2)} = \ & < 0|V_L \frac{1 - |0><0|}{E_0 - H} V_L|0 >, \\ & = \int d^3r_1 d^3r_2 \psi_0(r_1) V_L(r_1) \widetilde{G}_0(r_1, r_2; E_0) V_L(r_2) \psi_0(r_2).\end{aligned}$$

The Green's Function $G = 1/(E-H)$ for the harmonic oscillator is known analytically [23]. Since our potential is spherically symmetric, we only need its S-wave component:

$$\begin{aligned}G_0(r_1, r_2; E) = & < r_1 | \left(\frac{1}{E - H} \right)_{l=0} | r_2 >, \\ & = -\frac{1}{4\pi\hbar\omega (r_1 r_2)^{3/2}} \frac{\Gamma(\frac{3}{4} - \nu)}{\Gamma(3/2)} \mathrm{W}_{\nu, \frac{1}{4}} \left(\frac{\mu\omega}{\hbar} r_>^2 \right) \mathrm{M}_{\nu, \frac{1}{4}} \left(\frac{\mu\omega}{\hbar} r_<^2 \right),\end{aligned}$$

where $m\omega/\hbar = 1/b^2$, $\nu = E/(2\omega\hbar)$, $\mu = m/2$, and W and M are the Whittaker functions [22]. The required matrix element involves the ground state projection

operator $1-|0><0|$. This is easily accomplished by isolating and removing the pole term $\propto 1/(E-E_0)$:

$$\widetilde{G}_0(r_1,r_2;E_0) = \lim_{E\to E_0} G_0(r_1,r_2;E) \quad \text{with pole term removed,}$$
$$= \mathrm{e}^{-\frac{\mu\omega}{2\hbar}(r_a^2+r_b^2)}\left[-\frac{\mu}{2\pi\hbar^2}\frac{1}{r_>} + \frac{\mu^{3/2}\omega^{1/2}}{\pi^{3/2}\hbar^{5/2}}(1-\ln 2) + \frac{\mu^2\omega}{2\pi\hbar^3}r_> + \mathrm{O}(\omega^{3/2})\right].$$

The resulting energy shift gives

$$\Delta E_0^{(1)} + \Delta E_0^{(2)} = -60.8265b^{-3} + 120.807b^{-4} + 145750.0b^{-5}.$$

C. Third order

The third order energy-shift is given by:

$$\Delta E_0^{(3)} = \; <0|V_L\left(\frac{1-|0><0|}{E_0-H}\right)V_L\left(\frac{1-|0><0|}{E_0-H}\right)V_L|0>$$
$$- <0|V_L\left(\frac{1-|0><0|}{E_0-H}\right)^2 V_L|0> \cdot <0|V_L|0>.$$

However, since each wavefunction carries a factor of $\omega^{3/4}$, the second term is of order ω^3 or b^{-6} and can therefore be neglected in the present calculation. Skipping over some tedious algebra, one obtains

$$\Delta E_0^{(1)} + \Delta E_0^{(2)} + \Delta E_0^{(3)} = -62.3181b^{-3} + 160.882b^{-4} + 160686.8b^{-5}.$$

The convergence of these perturbative calculations is shown in Fig. 5. The inclusion of results up to third order already gives very good agreement with the exact energy shift over the entire range of $0 < 1/b < 1/200$.

7. A VARIATIONAL HARTREE CALCULATION

As a prelude for doing a microscopic many-body calculation, we will first consider a variational Hartree calculation. As suggested by Baym and Pethick [9], it is sufficient to use Gaussian trial states,

$$\Psi(r_1,r_2\ldots r_N) = \prod_i \phi(r_i) = \prod_i (\pi\alpha^2)^{-3/4}\exp\Big(-\frac{1}{2}\frac{r_i^2}{\alpha^2}\Big),$$

where α is the variational parameter. The variational energy is then

$$E_V = N\frac{\hbar^2}{2m}\int d^3r\phi(r)[-\nabla^2 + \frac{r^2}{b^4}]\phi(r) + \frac{1}{2}N(N-1)\int d^3r_1 d^3r_2\phi^2(r_1)V_L(r_{12})\phi^2(r_2).$$

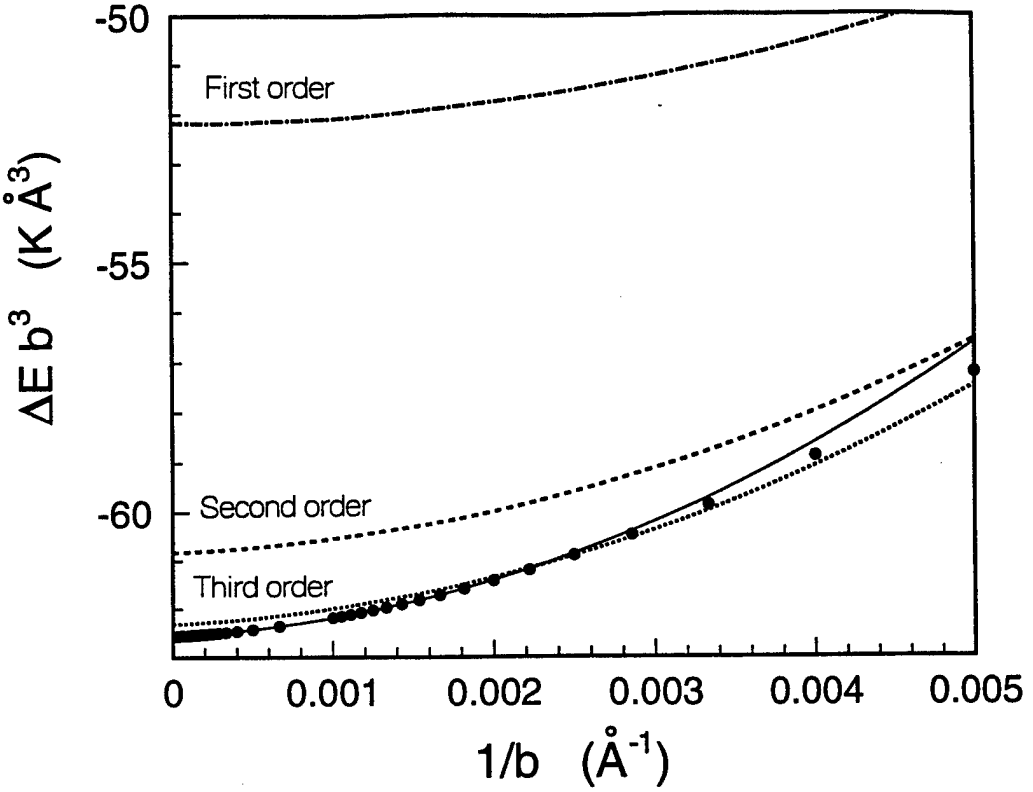

Figure 5. First, second and third order perturbative calculations of the Li pair energy shift in a harmonic well using the Moszkowski-Scott separated potential (10).

Introducing $x = \alpha/b$, the Gaussian integrals can be evaluate to give

$$E_V/N = \frac{3}{4}\frac{\hbar^2}{m}\frac{1}{b^2}[x^{-2} + x^2] + \frac{1}{2}(N-1)(2\pi)^{3/2}\frac{1}{x^3 b^3}\int d^3r V_L(r)\exp(-\frac{1}{2}\frac{r^2}{\alpha^2}) \quad (11)$$

When α is on the order of the trap radius b, since the range of the potential is much smaller than the trap size,

$$\int d^3r V_L(r)\exp(-\frac{1}{2}\frac{r^2}{\alpha^2}) \approx \int d^3r V_L(r) = 4\pi\frac{\hbar^2}{m}a_B.$$

This gives

$$E_V/N = \frac{1}{2}\hbar\omega\left\{\frac{3}{2}[x^{-2} + x^2] + \sqrt{\frac{2}{\pi}}\frac{(N-1)a_B}{b}\frac{1}{x^3}\right\}. \quad (12)$$

This is identical to the equation derived by Fetter [24], except that here we have only a_B rather than a. When the scattering length is negative, the absolute energy

minimum is at $x = 0$, but for

$$N < N_c = (5^{-1/4} - 5^{-5/4})\sqrt{\frac{\pi}{2}}\frac{b}{|a_B|}$$

a local minimum exists near $x \lesssim 1$, corresponding to a metastable state. $N_c \approx 2200$ for $a_B = -9.46$ Å. According to (12), when $N > N_c$, the local minimum disappears and the collapse is absolute, all the way down to $x = 0$. However, according to (11), which knows about the finite size of the trap, this is not the case. When α is reduced, it cuts off the integrated strength of the potential and halts the collapse near $\alpha \approx d$, which is more reasonable. (Note that if one uses the bare potential, then the integral diverges due to the hard core and the Hartree theory is not applicable.)

The N_c determined here is larger than those appeared in the literature. This is due to the use of a_B and the fact that our potential's scattering length is smaller (in absolute value) than that of Ref. [2].

8. CONCLUSIONS AND FUTURE DIRECTIONS

In this work, we have outlined the usefulness of using the Moszkowski-Scott separation method in the study of Bose condensed dilute atomic system with negative scattering lengths. In contrast to systems with positive scattering lengths, where perturbation theory is never directly applicable, the MS separated potential for Li is very weak. We have shown that third order perturbation theory yielded excellent results for the energy shift of two Li atoms in a harmonic trap. The use of the MS potential also allows one to go beyond the scattering length approximation and to compute finite size corrections directly. Work is currently in progress to study the stability of the Li ground state using many-body perturbation theories and variational theories with 2-body correlation functions.

ACKNOWLEDGMENTS

This research was funded, in part, by the U. S. National Science Foundation grants PHY95-12428 (to SAC) and DMR-9509743 (to EK), and by the Austrian "Fondszur Förderung der Wissenschaftlichen Forschung" (FWF) under project number P11098 - PHY, with travel support in part by the U. S. Army Research Office grant DAAH04-96-I-0184 to SAC.

REFERENCES

[1] M. H. Anderson *et al.*, Science **269**, 198 (1995)
[2] C. C. Bradley *et al.*, Phys. Rev. Lett. **75**, 1687 (1995)
[3] K. B. Davis *et al.*, Phys. Rev. Lett. **75**, 3969 (1995)
[4] G. R. Collins, Physics Today **48**, 17 (1995)
[5] Kerson Huang and C. N. Yang, Phys. Rev. **105**, 767 (1957)
[6] T. D. Lee, Kerson Huang and C. N. Yang, Phys. Rev. **106**, 1135 (1957)

[7] K. A. Brueckner and K. Sawada, Phys. Rev. **106**, 1117 (1957)
[8] P. A. Ruprecht, M. J. Holland, K. Burnett and M. Edward, Phys. Rev. **A51**, 4704 (1995)
[9] G. Baym and C. Pethick, Phys. Rev. Lett. **76**, 2477 (1996)
[10] F. Dalfovo and S. Stringari, Phys. Rev. **A53**, 6 (1996)
[11] C. C. Bradley, C. A. Sackett, and R. G. Hulet, Phys. Rev. Lett. **78**, 985 (1997)
[12] S. A. Moszkowski and B. L. Scott, Ann. Phys. (NY), **11**, 65 (1960).
[13] S. R. deGroot, G. J. Hooyman and C. A. ten Seldam, Proc. Roy. Soc. (London) **A203**, 266 (1950).
[14] D. D. Konowalow, R. M. Regan and M. E. Rosenkrantz, J. Chem. Phys. **81**, 4534 (1984)
[15] I. Schmidt-Mink, W. Müller and W. Meyer, Chem. Phys. **92**, 263 (1985)
[16] C. Linton, T. L. Murphy, F. Martin, R. Bacis and J. Verges, J. Chem. Phys. **91**, 6036 (1989)
[17] W. T. Zemke and W. C. Stwalley, J. Phys. Chem. **97**, 2053 (1993)
[18] M. Marinescu, H. R. Sadeghpour and A. Dalgarno, Phys. Rev. A **49**, 982 (1994)
[19] A. J. Moerdijk, W. C. Stwalley, R. G. Hulet and B. J. Verhaar, Phys. Rev. Lett. **72**, 40 (1994)
[20] R. Côté, A. Dalgarno, and M. J. Jamieson, Phys. Rev. A **50**, 399 (1994).
[21] E. R. I. Abraham, W. I. McAlexander, C. A. Sacket and R. G. Hulet, Phys. Rev. Lett. **74**, 1315 (1995)
[22] M. Abramowitz and I. A. Stegun, *Handbook of Mathematical Functions*, Dover Publications, New York.
[23] Hagen Kleinert, *Path Integrals in Quantum Mechanics, Statistics and Polymer Physics*, (World Scientific Publishing Co., Singapore 1990)
[24] A. L. Fetter, "Ground State and Excited States of a confined Bose Gas," cond-mat/9510037.

BOSE–EINSTEIN CONDENSATION IN LIQUID HELIUM: A CORRELATED DENSITY MATRIX THEORY

J. W. Clark

McDonnell Center for the Space Sciences
and Department of Physics
Washington University, St. Louis, MO 63130 USA

M. L. Ristig, T. Lindenau, and M. Serhan

Institut für Theoretische Physik
Universität zu Köln, D-50937 Köln, Germany

1. INTRODUCTION

A fundamental microscopic understanding of the lambda transition and of the condensed phase in liquid ^{4}He assumes heightened importance in the wake of the observations of Bose–Einstein condensation in ultracold atomic vapors [1–3]. Although computer simulations of the transition have produced many valuable insights [4], a satisfactory *ab initio* theory remains to be achieved [5]. The work to be described is offered as a step in that direction.

We present a microscopic many–body analysis of the Bose–Einstein condensation phenomenon in a strongly interacting boson fluid within the framework of correlated density matrix theory [6–14]. The approach is based on a trial density matrix of the form $W(\mathbf{R},\mathbf{R}') \propto \Phi(\mathbf{R})P(\mathbf{R},\mathbf{R}')Q(\mathbf{R},\mathbf{R}')\Phi(\mathbf{R}')$. Effects of virtual collective excitations are included through temperature–dependent correlated wave function factors $\Phi(\mathbf{R})$ and $\Phi(\mathbf{R}')$; effects of real collective excitations, through the incoherence factor $P(\mathbf{R},\mathbf{R}')$; and effects of real quasiparticle excitations, through the statistical incoherence factor $Q(\mathbf{R},\mathbf{R}')$. An appropriate choice of the form of $Q(\mathbf{R},\mathbf{R}')$, involving a condensation strength parameter B_{cc}, properly accounts for the infinite range of the statistical correlations in the condensed phase, and, with $B_{cc} = 0$, serves to extend the applicability of the proposed trial density matrix to the normal phase. In the spirit of the method of correlated basis functions (CBF) [15–20], such a trial density matrix incorporates the dynamical and statistical correlations essential to a viable description of the strongly interacting, strongly quantal system found in liquid ^{4}He.

Implementation of this description requires the evaluation of the free energy

corresponding to the trial density matrix so constructed. Practical evaluation is made possible by application and adaptation of the techniques of hypernetted chain theory. Invoking the Gibbs–Delbrück–Moliére minimum principle [11], an optimal description is attained by functional variation of the free energy.

In the simplified version of the theory developed here, we adopt a restricted optimization scheme suitable for the target case of liquid ^{4}He. Numerical results have been obtained for several key properties of the system at low temperature. Among these properties is the condensation strength B_{cc}, which is nonzero only in the condensed phase and may be interpreted as the modulus of the two–dimensional order parameter characterizing the Bose broken symmetry [21] associated with Bose–Einstein condensation in liquid ^{4}He. As portions of the free energy functional, the internal energy and the entropy of the system have been calculated. The latter contains portions attributable to collective phonon–roton excitations and to quasiparticle excitations. The nature of the quasiparticle excitation has been investigated in some detail. Remarkably, the theory predicts the existence of two quasiparticle branches which follow different dispersion relations in the condensed phase. One quasiparticle branch shows conventional behavior, with a dispersion relation that is sensibly approximated by a quadratic dispersion law without an energy gap. The second branch is characterized by a spectrum containing a gap and displaying a strong temperature dependence. Population of the second branch with increasing temperature is apparently linked with the degradation of the condensate.

In more quantitative terms, we find a theoretical condensation temperature (λ point) $T_c \simeq 2.3$ K for liquid ^{4}He at particle density $\rho = 0.02185$ Å^{-3} equal to the equilibrium density of the ground state. The first–branch quasiparticles (technically, quasiparticles of cyclic or cc type) have zero chemical potential in the temperature range $T_\lambda^- \leq T \leq T_\lambda^+$, with $T_\lambda^- \simeq 1.2$ K and $T_\lambda^+ \simeq 3.2$ K. Correspondingly, the correlation length of the cyclic distribution function [10] $G_{cc}^{(0)}(r)$ diverges in the same range. At temperatures $T_\lambda^- \leq T \leq T_c$, the second–branch (or c–type) quasiparticles exert a crucial influence in destroying the ^{4}He condensate. In the normal phase, the quasiparticle branches are indistinguishable. At higher temperatures above T_λ^+, the quasiparticles behave essentially like free ^{4}He atoms moving in a nonzero, negative chemical potential, with kinetic energies close to the bare value $\hbar^2 k^2/2m$.

The organization of the paper is as follows. Section 2 reviews the basic strategy of correlated density matrix theory. In Section 3 we assemble a trial density matrix that is equipped to describe the principal features of both normal and superfluid phases of strongly interacting Bose systems. In Sec. 4 we address the problem of evaluating the associated free energy and introduce the diagonal approximation [9,11] for the entropy. The form of the approximate entropy is indicative of the existence of two quasiparticle branches along with the expected collective mode. Section 5 outlines the process of full optimization of the trial density matrix through solution of Euler–Lagrange equations derived from the Gibbs–Delbrück–Moliére minimum principle. In Sec. 6 we specify the restricted optimization scheme that is adopted for a preliminary numerical study of liquid ^{4}He. The results are presented and discussed in Sec. 7, with special attention to the behavior and possible significance of the two quasiparticle branches. Section 8 describes planned improvements upon this first effort toward a microscopic understanding of the lambda transition within CBF theory.

2. ELEMENTS OF CORRELATED DENSITY MATRIX THEORY

Consider a homogeneous system of N bosons at density ρ and temperature T, described by a Hamiltonian

$$H = T + V = -\sum_{j}^{N} \frac{\hbar^2}{2m} \Delta_j + \sum_{i<j}^{N} v(r_{ij}) \quad . \tag{1}$$

We have in mind the case, typified by liquid ^{4}He, in which the two–body interaction is strongly repulsive at small interparticle separations r and then turns weakly attractive, falling off rapidly in magnitude with increasing r. An interaction of this kind induces strong correlations in configuration space, and the system cannot be adequately described by a mean–field theory. Correlations must be introduced explicitly. At zero temperature, this has been done efficiently and with great success through CBF theory at its variational level – or simply correlated-wave-function theory [15-20]. The natural extension of this variational approach to finite temperature is correlated density matrix theory [6–14], in which the Rayleigh–Ritz minimum principle for the expected energy E is replaced by the Gibbs–Delbrück–Moliére minimum principle [11] for the Helmholtz free energy,

$$F = E - TS_e \quad . \tag{2}$$

The essential new quantity to be evaluated is the entropy S_e, while the expected internal energy E becomes temperature dependent.

The energy and entropy are defined as functionals of the N–body density operator W,

$$E[W] = \mathrm{Tr}[WH] \tag{3}$$

$$S_e[W] = -k_B \,\mathrm{Tr}[W \ln W] \quad . \tag{4}$$

Since we do not know (and will never know) the exact density matrix W for a nontrivial many–body system, we consider trial density matrices belonging to a restricted class. The choice of this class is dictated by two criteria. It must be broad and flexible enough, in critical aspects, to permit quantitative explanation of a given set of physical measurements, yet it must somehow be simple enough that accurate evaluation of the internal energy and entropy is practical. The free–energy functional is to be minimized under variation of W within the chosen class, thus under variation of the structural ingredients specifying a member of that class.

Generalizing variational–CBF theory for strongly interacting systems at zero temperature, W is to be chosen, in coordinate space, so as to incorporate the most important features of the prevailing dynamical and statistical correlations as well as any underlying symmetries of the system.

Exact Product Decomposition. To this end, we employ the exact product decomposition of W in the coordinate–space representation [6,9,10,14]:

$$W(\mathbf{R},\mathbf{R}') = \frac{1}{I} \Phi(\mathbf{R}) P(\mathbf{R},\mathbf{R}') Q(\mathbf{R},\mathbf{R}') \Phi(\mathbf{R}') \quad . \tag{5}$$

The vectors $\mathbf{R}$, $\mathbf{R}'$ denote the configurations of the N particles, and the denominator

$$I = \int d\mathbf{R}\ \Phi^2(\mathbf{R}) Q(\mathbf{R}, \mathbf{R}) \tag{6}$$

imposes the unit–trace condition on W.

The *coherence factors* $\Phi(\mathbf{R})$ and $\Phi(\mathbf{R}')$ have the form of correlated N–body wave functions and, for identical bosons, are required to be fully symmetric under permutation. The *incoherence factors* $Q(\mathbf{R}, \mathbf{R}')$ and $P(\mathbf{R}, \mathbf{R}')$, which differ from 1 only at $T > 0$, depend in a non–separable manner on both $\mathbf{R}$ and $\mathbf{R}'$. They account, respectively, for the presence of real quasiparticle excitations and real collective excitations, the latter being phonon–roton excitations in the case of liquid ^{4}He. The quantities $\Phi(\mathbf{R})$, $P(\mathbf{R}, \mathbf{R}')$, and $Q(\mathbf{R}, \mathbf{R}')$ all depend on the temperature T. They can be taken to be real and nonnegative when there is no flow.

3. ASSEMBLY OF THE TRIAL DENSITY MATRIX

To describe the analog of Bose–Einstein condensation in a strongly interacting Bose system, we make the following choices of coherence and incoherence factors in the general product decomposition (5).

- For the coherence factor we assume a temperature–dependent wave function of Jastrow form

$$\Phi(\mathbf{R}) = \exp\left\{\frac{1}{2}\sum_{i<j}^{N} u(r_{ij})\right\} \tag{7}$$

  defined by two–body pseudopotentials $u(r_{ij})$. This choice, which accounts for the strong dynamical spatial correlations, may be extended to a Feenberg form containing triplet, quadruplet, ... pseudopotentials.

- To describe the effects of collective excitations generated by density fluctuations, we adopt an incoherence factor $P(\mathbf{R}, \mathbf{R}')$ having the analogous form

$$P(\mathbf{R}, \mathbf{R}') = \exp\sum_{i,j}^{N}\left\{\gamma\left(|\mathbf{r}_i - \mathbf{r}'_j|\right) - \frac{1}{2}\gamma\left(|\mathbf{r}_i - \mathbf{r}_j|\right) - \frac{1}{2}\gamma\left(|\mathbf{r}'_i - \mathbf{r}'_j|\right)\right\} \quad . \tag{8}$$

- To incorporate the effects of quasiparticle excitations, we employ an incoherence factor $Q(\mathbf{R}, \mathbf{R}')$ constructed as

$$Q(\mathbf{R}, \mathbf{R}') = \frac{1}{A^N}\frac{1}{2\pi \mathrm{i}}\oint \frac{dz}{z}\, \mathrm{e}^{A/z} \operatorname*{Perm}_{i,j}\left\{\Gamma_{cc}\left(|\mathbf{r}_i - \mathbf{r}'_j|\right) + B_{cc} z\right\} \quad , \tag{9}$$

  where the contour is to encircle the origin in the counterclockwise sense. The constant B_{cc} is related to an order parameter defined below, and A is a scale constant. This construction ensures the proper behavior of the theory in the thermodynamic limit [22].

The value of the constant A appearing in Eq. (9) is fixed by the dynamical and statistical correlations, through

$$A = \left\{1 - \rho \int d\mathbf{r}\, \Gamma_{cc}(r)\Big(1 + G_{dd}(r) + G_{dc}(r)\Big)\right\}^2 \quad . \tag{10}$$

The functions $G_{dd}(r)$ and $G_{dc}(r)$ are components of the radial distribution function

$$g(r) = 1 + G_{dd}(r) + 2G_{de}(r) + G_{ee}(r) + 2B_{cc}\left\{2G_{dc}(r) + 2G_{ec}(r) + G^{(2)}_{cc}(r)\right\} \tag{11}$$

associated with the assumed N–body density matrix [10,19].

It has been demonstrated that the trial density matrix so constituted is sufficiently general to describe both normal and superfluid phases of a strongly interacting Bose system [10]. The four defining ingredients, namely the pseudopotential $u(r)$, the function $\gamma(r)$ describing collective excitations, the statistical function $\Gamma_{cc}(r)$, and the parameter B_{cc}, are to be determined by functional minimization of the free energy, subject to any relevant constraints.

Specialization to Noninteracting Bosons. In the absence of dynamical correlations, the pseudopotential $u(r)$ vanishes identically. Moreover, collective excitations are absent, implying

$$\gamma(r) \equiv 0 \qquad \text{and} \qquad P(\mathbf{R}, \mathbf{R}') \equiv 1 \quad . \tag{12}$$

The quasiparticle excitations are evidently free bosons with kinetic energy $\epsilon_0(k) = \hbar^2 k^2/2m$. In this special case, the exact N–body density matrix at arbitrary temperature is correctly reproduced with a statistical function $\Gamma_{cc}(r)$ of Gaussian form [9,10,22], $\Gamma_{cc}(r) \sim \exp[-\pi(r/\lambda_{\rm th})^2]$, where $\lambda_{\rm th}$ is the thermal wave length. The normal phase of the free–boson system is recovered by setting the parameter B_{cc} equal to zero. For $B_{cc} > 0$, the independent bosons are condensed into a Bose–Einstein phase and B_{cc} may be identified with the condensate fraction.

Interacting Bosons. Dynamical spatial correlations are now present and hence the two–body pseudopotential no longer vanishes identically. However, no long–range spatial order exists, so $u(r) \to 0$ as $r \to 0$. The ground state is a pure state and hence the correlations occurring in it correspond to *virtual* excitations. Therefore the function $\gamma(r)$, which describes the effects of *real* collective excitations, must be identically zero at $T = 0$. However, at nonzero T, real collective excitations are present and consequently $\gamma(r)$ plays an essential role. This function goes to zero at large r and has a Fourier transform satisfying $\gamma(k) \geq 0$.

With the choice (9) for the incoherence factor $Q(\mathbf{R}, \mathbf{R}')$, the statistical correlation function $\Gamma_{cc}(r)$ still vanishes as $r \to \infty$ at any given temperature, i.e., in the superfluid as well as in the normal phase. However, it will in general deviate from Gaussian form.

Off–Diagonal Long–Range Order and Bose Broken Symmetry. The parameter B_{cc} appearing in the incoherence factor $Q(\mathbf{R}, \mathbf{R}')$ is interpreted as a *condensation strength*, the normal phase being characterized by $B_{cc} \equiv 0$. Bose–Einstein condensation can be said to occur for $0 < B_{cc} \leq 1$, since the density matrix then exhibits off–diagonal long–range order [23].

To establish this behavior, take the limit

$$\lim_{|\mathbf{R}-\mathbf{R}'|\to\infty} W(\mathbf{R},\mathbf{R}') = \frac{1}{I}\Phi(\mathbf{R})P(\mathbf{R})B_{cc}^{N}P(\mathbf{R}')\Phi(\mathbf{R}') \quad . \tag{13}$$

This limit has the simple product form

$$\lim_{|\mathbf{R}-\mathbf{R}'|\to\infty} W(\mathbf{R},\mathbf{R}') = \Phi'^{*}(\mathbf{R})\Phi'(\mathbf{R}') \tag{14}$$

in terms of a non–vanishing *coherent wave function*

$$\Phi'(\mathbf{R}) = \frac{B_c^N}{\sqrt{I}}P(\mathbf{R})\Phi(\mathbf{R}), \tag{15}$$

where

$$P(\mathbf{R}) = \exp\left\{-\frac{1}{2}\sum_{i,j}^{N}\gamma(r_{ij})\right\} \tag{16}$$

and

$$B_c = \sqrt{B_{cc}}\mathrm{e}^{\mathrm{i}\phi} \quad . \tag{17}$$

The quantity B_c will serve as a complex order parameter. The property (14) gives rise to ODLRO in the reduced density matrices and specifically in the one–body density matrix.

For the homogeneous Bose system, the complex order parameter B_c of (17) carries a global phase ϕ. More generally, for an inhomogeneous system, the order parameter is characterized by a *local gauge field*

$$B_c^N(\mathbf{R}) = \exp\left\{\sum_{i}^{N}\left[\frac{1}{2}\ln B_{cc}(\mathbf{r}_i) + \mathrm{i}\phi(\mathbf{r}_i)\right]\right\} \quad , \tag{18}$$

where

$$B_c(\mathbf{r}_i) = \sqrt{B_{cc}(\mathbf{r}_i)}\mathrm{e}^{i\phi(\mathbf{r}_i)} \tag{19}$$

may be viewed as a macroscopic wave function.

We now observe the following features. At $T = 0$, the coherent wave function $\Phi'(\mathbf{R})$ for the homogeneous condensed system has a constant phase $\exp\{iN\phi\}$ which may be removed by a global quantum–mechanical gauge transformation that leaves the N–body density matrix invariant (gauge symmetry). However, at finite T where the statistical function $\Gamma_{cc}(r)$ is nonzero, there exists no gauge transformation that can eliminate the dependence of the density matrix on B_c in the condensed phase where $B_c \neq 0$. Thus, in the Bose–condensed phase at $T > 0$, the assumed density matrix breaks the gauge symmetry of the Hamiltonian [21].

Particle Sum Rule. In general, one can calculate the particle density of a uniform system as the diagonal limit of the (suitably normalized) one–body density matrix $\rho(|\mathbf{r}-\mathbf{r}'|)$, i.e., as the limit of this quantity for $\mathbf{r}-\mathbf{r}' \to 0$. The result agrees necessarily

with the particle density specified at the outset. This condition is called the *particle sum rule* [9–11]. For the trial density matrix assumed here, it can be given the form

$$B_{cc}\left\{1+\frac{1}{N}\sum_{\mathbf{k}}\Gamma_{cc}(k)\left[S_{dc}(k)+S_{cc}^{(1)}(k)\right]\right\}+\frac{1}{N}\sum_{\mathbf{k}}\Gamma_{cc}(k)\left[1+S_{cc}^{(0)}(k)\right]=1 \quad (20)$$

in terms of the components $S_{dc}(k)$, $S_{cc}^{(0)}(k)$, and $S_{cc}^{(1)}(k)$ of the static structure function $S(k)$ (see Refs. [10,11]).

At this point we introduce the definitions

$$n_{cc}(k)=\Gamma_{cc}(k)\left[1+S_{cc}^{(0)}(k)\right] \quad , \quad (21)$$

$$n_c(k)=\Gamma_{cc}(k)\left[1+S_{cc}^{(2)}(k)\right]+2B_{cc}\Gamma_{cc}(k)\left[S_{dd}(k)+2S_{dc}(k)\right] \quad , \quad (22)$$

$$R=\frac{1}{N}\sum_{\mathbf{k}}\Gamma_{cc}(k)\left[S_{dd}(k)+S_{dc}(k)\right] \quad , \quad (23)$$

with the intent that $n_{cc}(k)$ and $n_c(k)$ will later be interpreted as (average) occupation numbers of elementary excitations. The quantity $S_{dd}(k)$ is the direct–direct component [10,11,19] of $S(k)$. The particle sum rule may then be written in the more convenient form

$$B_{cc}(1-R)+\frac{1}{2N}\sum_{\mathbf{k}}n_{cc}(k)+\frac{1}{2N}\sum_{\mathbf{k}}n_c(k)=1 \quad . \quad (24)$$

In the normal phase, we have $B_{cc}\equiv 0$ and $n_{cc}(k)=n_c(k)$, so the sum rule reduces simply to

$$\frac{1}{N}\sum_{\mathbf{k}}n_{cc}(k)=1 \quad . \quad (25)$$

At $T=0$, the statistical function $\Gamma_{cc}(k)$ vanishes identically and hence the condensation strength B_{cc} is unity.

4. EVALUATION OF THE ENTROPY AND INTERNAL ENERGY

Diagonal Approximation for the Entropy. To explore the practical consequences of the trial density matrix assembled and examined in Sec. 3, we must be able to evaluate the free energy F explicitly for the given Hamiltonian. Of the two extensive ingredients of F, namely the internal energy E and the entropy S_e, the latter is by far the more difficult to treat.

Following [7,9,11] the construction of the entropy is based on a replica construction,

$$TS_e=-\beta^{-1}\frac{\partial}{\partial\sigma}\,\mathrm{Tr}\,\{W^\sigma\}\,\Big|_{\sigma\to 1} \quad . \quad (26)$$

Traces of integral powers σ of the density matrix W are analyzed using hypernetted–chain (HNC) techniques and the results analytically continued to non–integral values

of σ. Analytic continuation is performed in *diagonal approximation*: an approximation that reduces the matrix equations resulting from the HNC analysis to simple one–component equations. This approximation, which ignores the coupling between quasiparticle and collective modes, yields an entropy expression having a transparent physical interpretation (cf. [6,9,11]).

The resulting total entropy is made up of three parts:

$$S_e = S_e^{(ph)} + S_e^{(cc)} + S_e^{(c)} \quad . \tag{27}$$

The individual parts of the entropy may be expressed in a familiar form in terms of quantities $n(k)$, $n_{cc}(k)$, and $n_c(k)$ that behave like occupation numbers of elementary excitations:

$$S_e^{(ph)} = k_B \sum_{\mathbf{k}} \Big\{ [1+n(k)] \ln [1+n(k)] - n(k) \ln n(k) \Big\} \quad , \tag{28}$$

$$S_e^{(cc)} = \frac{1}{2} k_B \sum_{\mathbf{k}} \Big\{ [1+n_{cc}(k)] \ln [1+n_{cc}(k)] - n_{cc}(k) \ln n_{cc}(k) \Big\} \quad , \tag{29}$$

$$S_e^{(c)} = \frac{1}{2} k_B {\sum_{\mathbf{k}}}' \Big\{ [1+n_c(k)] \ln [1+n_c(k)] - n_c(k) \ln n_c(k) \Big\} \quad . \tag{30}$$

The diagonal approximation to the entropy then becomes a sum of contributions from three types of noninteracting elementary excitations. The occupation numbers $n_{cc}(k)$ and $n_c(k)$ have already been defined by Eqs. (21) and (22), while $n(k)$ is determined by the relation

$$n(k)\,[1+n(k)] = \gamma(k) S(k) \quad , \tag{31}$$

where $S(k)$ is the static structure function associated with the assumed trial density matrix. The prime in Eq. (30) restricts the summation to those $\mathbf{k}$ regions where $n_c(k) \geq 0$.

The contribution $S_e^{(ph)}$ represents the entropy of the collective density fluctuations – phonons and rotons – and corresponds to a thermal distribution $n(k)$ of noninteracting collective elementary excitations having wave number k.

The second and the third terms of the entropy decomposition (27), i.e. $S_e^{(cc)}$ and $S_e^{(c)}$, represent the entropy contributions from two branches of noninteracting quasiparticles. The two quasiparticle branches predicted by the theory are distinct only in the case of an interacting system in its condensed phase. In the normal phase, the two terms $S_e^{(cc)}$ and $S_e^{(c)}$ become identical and their sum correctly reproduces the entropy derived earlier [9] for a system of normal bosons.

In the case of noninteracting bosons, dynamical correlations are absent, implying $S_{dd}(k) \equiv S_{dc}(k) \equiv 0$ and $S_{cc}^{(0)}(k) = S_{cc}^{(2)}(k)$, so that $n_c(k) = n_{cc}(k) = \Gamma_{cc}(k)(1 + S_{cc}^{(0)}(k))$. Thus the entropies $S_e^{(cc)}$ and $S_e^{(c)}$ coincide in both normal and condensed phases. However, the slightest interaction $v(r)$ lifts the twofold degeneracy of the quasiparticle excitations in the condensed phase.

The form obtained for the entropy therefore leads us to distinguish two different kinds of quasiparticles, designated type c and cyclic type cc. The two types of

quasiparticles in general follow different dispersion relations. Their partial densities are given by

$$\varrho_c = \sum_{\mathbf{k}}{}' n_c(k)/2N \qquad \text{and} \qquad \varrho_{cc} = \sum_{\mathbf{k}} n_{cc}(k)/2N \quad . \tag{32}$$

The interaction–induced symmetry–breaking phenomenon that lifts the degeneracy of the cc and c excitations is measured by the order parameter

$$M = \frac{\varrho_{cc} - \varrho_c}{\varrho_{cc} + \varrho_c} \quad . \tag{33}$$

For the noninteracting system, $M \equiv 0$ at all T. When interactions are present, $M \equiv 0$ in the normal phase and $M > 0$ in the condensed phase, with $M \to 1$ as $T \to 0$.

Once we have interpreted the components $S_e^{(ph)}, S_e^{(cc)}$, and $S_e^{(c)}$ as partial entropies of noninteracting elementary excitations of Bose character, it is natural to introduce the corresponding excitation energies through the Bose distributions

$$n(k) = \{\exp \beta\omega(k) - 1\}^{-1} \quad , \tag{34}$$

$$n_{cc}(k) = \{\exp \beta\omega_{cc}(k) - 1\}^{-1} \quad , \tag{35}$$

$$n_c(k) = \{\exp \beta\omega_c(k) - 1\}^{-1} \quad . \tag{36}$$

The energies $\omega(k)$ of the collective phonon–roton excitations have the proper long–wavelength behavior $\omega(k) \simeq \hbar ck$ as $\mathbf{k} \to 0$, while the excitations belonging to the cyclic branch manifest characteristic quasiparticle behavior. Consider first the energies of the cc quasiparticle branch, which may be written as $\omega_{cc}(k) = \epsilon^{(0)}(k) - \mu$, introducing the chemical potential μ as a reference level. The energies $\epsilon^{(0)}(k)$ go like $\hbar^2k^2/2m^*$ at small momenta, where m^* is a temperature–dependent effective mass.

The energies $\omega_c(k)$ of the second quasiparticle branch are not independent of those of the cyclic branch. In liquid ^{4}He at low temperature, they are found to exhibit a large finite energy gap, with a minimum in the maxon–roton region of momenta.

Internal Energy Decomposition. The internal energy corresponding to the chosen trial density matrix may also be decomposed into contributions arising from the three elementary excitation branches (plus a term of the same form as in the ground state at $T = 0$). The result for the total energy is [10]

$$E = \sum_{\mathbf{k}} \epsilon_{ph}(k)n(k) + \frac{1}{2}\sum_{\mathbf{k}} \epsilon_{cc}(k)n_{cc}(k) + \frac{1}{2}\sum_{\mathbf{k}} \epsilon_0(k)n_c(k) + N\frac{\rho}{2}\int d\mathbf{r}\, v^*(r)g(r) \quad . \tag{37}$$

Here $v^*(r) = v(r) - (\hbar^2/4m)\Delta u(r)$ is the Jackson–Feenberg effective potential, $\epsilon_0 = \hbar^2k^2/2m$, and we have set $\epsilon_{ph}(k)n(k) = \epsilon_0(k)\gamma(k)$. In the normal phase, the energy result derived in Ref. [9] is regained.

The single–particle energies $\epsilon_{cc}(k)$ appearing in Eq. (37) are given, in terms of HNC quantities, by

$$\epsilon_{cc}(k) = \epsilon_0(k)\Big\{1 - X_{cc}^{(0)}(k) + \tilde{X}_{cc}^{(0)}(k) - B_{cc}\big[1 - X_{cc}^{(0)}(k)\big]\Big[1 + n_{cc}(k)\Big]^{-1}$$

$$\times\big[S_{dd}(k) + 2S_{dc}(k) + S_{cc}^{(1)}(k) - \tilde{S}_{dc}(k) - \tilde{S}_{cd}(k) - \tilde{S}_{cc}^{(1)}(k)\big]\Big\} \quad . \tag{38}$$

Explicit definitions of the various functions that enter this structural formula are given in Refs. [10,11]. At $T = 0$, where the occupation numbers $n(k)$, $n_c(k)$, and $n_{cc}(k)$ all vanish, the first three terms in Eq. (37) drop out and we are left with the standard Jastrow variational result for the ground–state energy of a Bose fluid [16–18].

5. OPTIMIZATION OF TRIAL DENSITY MATRIX

Having constructed working functional expressions for the entropy and internal energy and hence the Helmholtz free energy F, the last formal step is optimization of the four ingredients $u(r)$, $\gamma(r)$, $\Gamma_{cc}(r)$, and B_{cc} of the trial density matrix by means of a minimum principle.

Incorporating the particle sum rule (24) as a constraint, we introduce the generalized Helmholtz free energy

$$F_\nu = E - TS_e + \nu(N - \Sigma) \tag{39}$$

at prescribed total number N of bosons, where

$$\Sigma = NB_{cc}(1 - R) + \frac{1}{2}\sum_{\mathbf{k}} n_{cc}(k) + \frac{1}{2}\sum_{\mathbf{k}} n_c(k) \quad . \tag{40}$$

It may be noted that, by virtue of the particle sum rule, the quantity B_{cc} is itself a functional of the three variational functions $u(r)$, $\gamma(r)$, and $\Gamma_{cc}(r)$. However, it is operationally more convenient to treat these four quantities as independent and impose the sum rule via the Lagrange multiplier ν.

Employing the Gibbs–Delbrück–Moliére minimum principle for the free energy, variation of F_ν with respect to $u(r)$, $\gamma(r)$, $\Gamma_{cc}(r)$, and B_{cc} leads to four coupled Euler–Lagrange equations for the optimal density matrix,

$$\frac{1}{N}\frac{\delta F_\nu}{\delta u(r)} = 0 \quad , \tag{41}$$

$$\frac{1}{N}\frac{\delta F_\nu}{\delta \gamma(r)} = 0 \quad , \tag{42}$$

$$\frac{1}{N}\frac{\delta F_\nu}{\delta \Gamma_{cc}(r)} = 0 \quad , \tag{43}$$

$$\frac{1}{N}\frac{\partial F_\nu}{\partial B_{cc}} = 0 \quad . \tag{44}$$

Solution of these equations yields the optimal functions $u(r)$, $\gamma(r)$, and $\Gamma_{cc}(r)$, and the optimal condensation strength B_{cc}, all as functions of the Lagrange parameter ν, which is determined by the particle sum rule.

We next present and interpret each of these Euler–Lagrange (E–L) equations.

Paired–Phonon Equation. The E–L equation (41) arising from variation of F_ν with respect to the pseudopotential $u(r)$ may be written as a finite–temperature paired–phonon (PPA) equation [24, 18] for the optimal static structure function $S(k)$,

$$\frac{\epsilon_0(k)}{2}\left[S(k) - 1\right] + \dot{S}_\nu + 2\nu B_{cc}\dot{R} = 0 \quad . \tag{45}$$

This equation involves the variational derivatives $\dot{R} = \delta R/\delta u(k)$ and $\dot{S}_\nu = \delta S_\nu/\delta u(k)$, the quantity S_ν being a generalized structure function [9,16,18] that will be made explicit elsewhere.

Generalized Feynman Equation. The E–L equation (42) arising from variation of F_ν with respect to the function $\gamma(r)$ (which introduces thermal effects of collective excitations) is the generalized Feynman equation (cf. Ref. [25])

$$\omega(k) = \epsilon_0(k)S^{-1}(k)\coth\frac{\beta}{2}\omega(k) \tag{46}$$

for the phonon–roton energy. This equation is familiar from the original correlated–density–matrix analysis of Campbell *et al.* [6].

Quasiparticle Equation. The third Euler–Lagrange equation, Eq. (43), determines the optimal statistical function $\Gamma_{cc}(k)$. Equivalently, it determines the quasiparticle distribution function $n_{cc}(k)$, and therewith (via Eq. (35)) the quasiparticle energy $\omega_{cc}(k)$ of the cyclic elementary excitations. In momentum space, this equation may be written

$$\begin{aligned}\mathring{S}_\nu + \epsilon_0\left\{B_{cc}S_{dd} + \left(S_{cc} - S_{cc}^{(0)} - \tilde{S}_{cc} + \tilde{S}_{cc}^{(0)}\right)\right\}n_{cc} + (\epsilon_{cc} - \omega_{cc} - \nu)\left(1 + S_{cc}^{(0)}\right) \\ + (\epsilon_0 - \omega_c - \nu)\,\Theta(n_c)\left\{1 + S_{cc}^{(0)} + 2\left(S_{cc} - S_{cc}^{(0)}\right)\right\} + 2\nu B_{cc}\mathring{R} = 0 \quad ,\end{aligned} \tag{47}$$

where the variational derivatives $\mathring{R} = \delta R/\delta\Gamma_{cc}(k)$ and $\mathring{S}_\nu = \delta S_\nu/\delta\Gamma_{cc}(k)$ will be explicated elsewhere.

Renormalized Hartree Equation. The fourth E–L equation, Eq. (44), may be interpreted as a renormalized Hartree equation that serves to fix the optimal condensation strength B_{cc}, which is a kind of self–consistent field. This equation may be given the expression

$$\frac{\rho}{2}\int d\mathbf{r}\left[v^*(r) + v_{ph}^*(r)\right]\frac{\partial g(r)}{\partial B_{cc}} + \frac{1}{2N}\sum_{\mathbf{k}}\epsilon_{cc}^*(k)n_{cc}(k) + \frac{1}{2N}{\sum_{\mathbf{k}}}'\epsilon_c^*(k)n_{cc}(k) = \Lambda \tag{48}$$

in terms of the Jackson–Feenberg effective potential and a collective effective-potential component

$$v_{ph}^*(r) = \frac{1}{(2\pi)^3\rho}\int d\mathbf{k}\left\{-2\epsilon_{ph}(k)n(k)S^{-1}(k)\right\}\mathrm{e}^{-i\mathbf{k}\cdot\mathbf{r}} \quad . \tag{49}$$

The Hartree potential in the condensed phase is

$$\Lambda = \nu \left(1 - R - B_{cc} \frac{\partial R}{\partial B_{cc}} \right) \quad . \tag{50}$$

Explicit expressions for the single–particle energies $\epsilon^*_{cc}(k)$ and $\epsilon^*_c(k)$ have been obtained in terms of HNC building blocks.

6. RESTRICTED OPTIMIZATION FOR LIQUID ^{4}He

In a preliminary effort to gain insights into the λ transition in liquid ^{4}He, we adopt parametrized forms for the pseudopotential $u(r)$ and for the statistical function $\Gamma_{cc}(r)$ (or dispersion relation $\omega_{cc}(k)$), and make a simple ansatz for the condensation strength B_{cc}. This may be considered as the first step toward a full optimization, in that the results of the restricted optimization may be used as input for an iterative solution of the E–L equations.

- Assuming the standard Lennard–Jones potential for $v(r)$, we employ a pseudopotential of Schiff–Verlet [26] type

$$u(r) = -(b/r)^5 \tag{51}$$

  with $b = 2.965$ Å. Although it fails to account for the long–range effects of virtual phonons, this choice suffices for a semi–quantitative account of the spatial correlations at zero temperature, and it is useful as a first approximation in iterative solution of the PPA equation.

- The optimal solution of the E–L equation (47) for the thermal occupation number $n_{cc}(k)$, or equivalently for the cyclic quasiparticle energy, is approximated in terms of the two–parameter trial form

$$\omega_{cc}(k) = \frac{\hbar^2 k^2}{2m^*} - \mu \quad , \tag{52}$$

  which is specified by an effective mass m^* and a chemical potential μ.

- The renormalized Hartree equation is only relevant in the condensed phase where $B_{cc} \neq 0$. Rather than attempt an exact solution of this equation, we assert the plausible form

$$B_{cc} = 1 - \frac{1}{N} \sum_{\mathbf{k}} n(k) \quad , \tag{53}$$

  motivated by the expectation that B_{cc} is closely related to the superfluid density of the condensed phase. This assumption is in accord with Landau's picture, in which the normal component is defined by the total number of phonon–roton excitations.

Having prescribed or parametrized the key components $u(r)$, $\omega_{cc}(k)$, and B_{cc} of the density matrix, there remains the question of how to treat the collective dispersion law. For strict consistency, the generalized Feynman relation should be used to evaluate the energies $\omega(k)$ of the collective excitations. However, this treatment

would ignore backflow effects, which cannot be neglected because of the very strong correlations present in liquid ^{4}He.

More specifically, the roton minimum in the Feynman approximation is located at a wave number $k_R \simeq 1.9\,\text{Å}^{-1}$, with an energy of about 20 K (depending on temperature). Due to neglect of backflow effects, this theoretical energy estimate is much too high compared with the experimental value $\omega(k_R) \simeq 8\,K$ for the energy of the roton minimum.

In the interest of a meaningful comparison with experiment, we therefore apply an apparently drastic scaling approximation. To mimic the influence of backflow in a simple fashion, we multiply the bare energy values given by the Feynman equation by a factor 1/3 and employ the scaled data as input to calculate the thermal distribution $n(k)$ that enters the proposed formula for B_{cc}. With this scaling procedure, the collective phonon–roton excitation energies are brought close to the experimental phonon–roton spectrum.

7. NUMERICAL RESULTS

Within the restricted optimization scheme described in Sec. 6, we have carried out a numerical study of liquid ^{4}He in a temperature range $0 \leq T \leq 4.5\,\text{K}$ embracing the lambda transition. Results are available for:

(i) The condensation strength B_{cc} and the order parameter M that characterize the condensed phase.

(ii) The internal energy and the entropy generated by the collective phonon–roton excitations and the quasiparticle branches.

(iii) The effective mass and chemical potential characterizing the cyclic branch and the unusual dispersion properties of the second quasiparticle branch.

The partial distribution functions needed for the calculation have been evaluated by solving the appropriate hypernetted chain equations in the HNC/0 approximation, which neglects elementary or bridge diagrams [10,11,19].

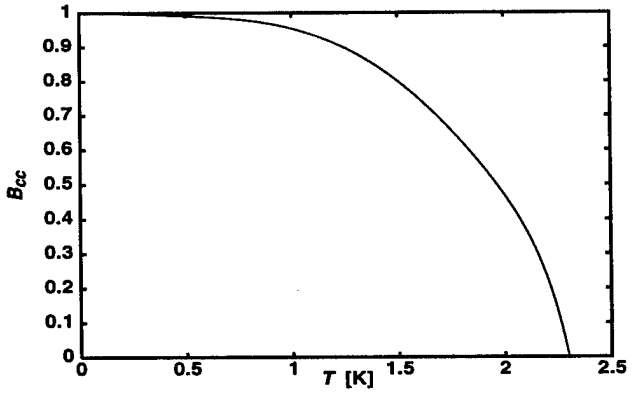

Figure 1. The condensation strength B_{cc} as a function of temperature T. The numerical results for the restricted optimal treatment yield a critical temperature $T_c \simeq 2.3$ K, at and below which the liquid condenses into its Bose–Einstein phase.

The results for the temperature dependence of the condensation strength B_{cc} in the condensed phase are presented in Fig. 1. This quantity, the absolute square of the two–dimensional order parameter (17), deviates from unity by less than 10% in the temperature range $0 \leq T \leq 1.2$ K. At temperatures $T \geq 1.2$ K, it falls off rapidly, until the condensed portion of the liquid disappears at a critical temperature $T_c \simeq 2.3$ K. This prediction for the critical temperature for destruction of the condensate is fairly close to the experimental value $T_\lambda \simeq 2.18$ K of the λ–transition temperature.

The nature of the λ transition may be further analyzed within our microscopic model by examining the behavior of the energies $\omega_{cc}(k)$ and $\omega_c(k)$ of the two branches of quasiparticle excitations. The excitation energy (52) of the cyclic branch is specified by the effective mass m^*/m of the corresponding quasiparticles and the chemical potential μ they experience. The optimal results for these quantities are plotted as functions of temperature in Figs. 2 and 3. The effective–mass parameter m^*/m shows a sensitive temperature dependence, with a maximum of about 1.36 at the critical temperature $T_c \simeq 2.3$ K. Below T_c, the mass decreases rather rapidly with increasing condensation strength down to temperatures around 1 K, where m^* reaches a value of about half the mass of a bare ^{4}He atom. At still lower temperatures, $T \leq 0.5$ K, the effective mass again declines rapidly, levels off, and approaches a value $m^* = m/3$ as $T \to 0$.

In the normal phase above T_c, the effective mass m^* of the cyclic–branch quasiparticles falls from its maximum at the critical point to a minimum of about one bare mass, $m^* \simeq m$, at a temperature $T_\lambda^+ \simeq 3.2$ K. Thereafter m^* increases slowly with temperature. It is interesting to observe that as the temperature is decreased through the range $T_c \leq T \leq T_\lambda^+$, the system tends to resist condensation by an appropriate increase of the quasiparticle mass. This feature will be addressed more fully below.

Figure 3 displays the temperature dependence of the chemical potential μ felt by a quasiparticle of the cyclic branch. At high temperatures, the chemical potential is negative. With decreasing temperature, its absolute value decreases rapidly until the temperature $T_\lambda^+ \simeq 3.2$ K is reached. The most striking result is the vanishing of the optimal chemical potential in the temperature range $T_\lambda^- \leq T \leq T_\lambda^+$, with $T_\lambda^- \simeq 1.2$ K. This behavior is very similar to, but distinct from, what is seen in the familiar case of noninteracting bosons having the bare ^{4}He atomic mass [27]. In the noninteracting case, the particles *both* attain zero chemical potential *and* condense at a critical temperature very close to $T_\lambda^+ \simeq 3.2$ K. However, in contrast to the uninhibited condensation of a system of free bosons, the interacting system reacts as the temperature is reduced below T_λ^+ by increasing the quasiparticle mass m^*. As a result, the actual transition temperature is depressed to $T_c \simeq 2.3$ K. At temperatures T below $T_\lambda^- \simeq 1.2$ K where the system is strongly condensed, a quasiparticle of the cyclic type has, instead, a small effective mass (see Fig. 2) and experiences a nonzero, negative chemical potential. The chemical potential reaches a minimal value $\mu \simeq -0.12$ K at $T \simeq 0.7$ K and vanishes once again as the ground state is approached $(T \to 0)$.

This and other properties of the chemical potential are related to the behavior of the cyclic structure function $S_{cc}^{(0)}(k)$ at zero momentum $\hbar\mathbf{k}$ (Fig. 4). The quantity $S_{cc}^{(0)}(0)$ is a measure of the correlation length of the associated cyclic distribution function $G_{cc}^{(0)}(r)$ (see Refs. [10,11] for detailed definitions).

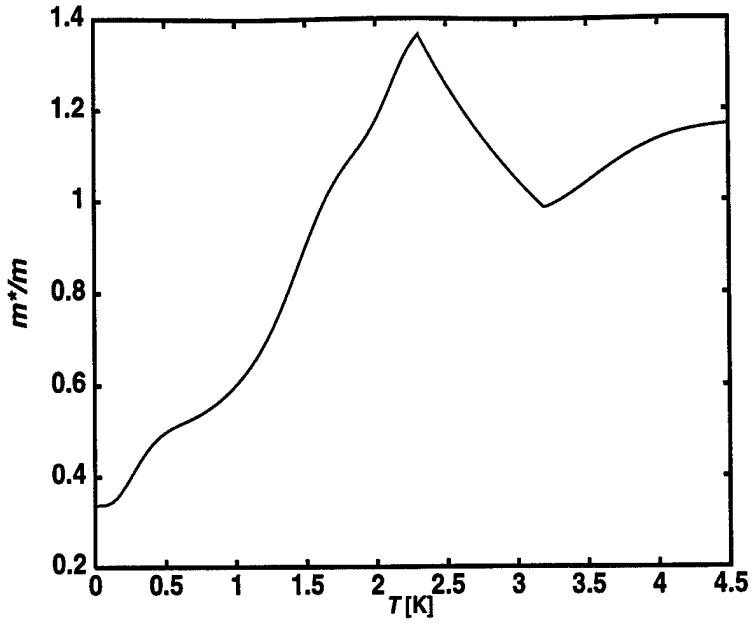

Figure 2. The effective mass m^* of the (cyclic) quasiparticle spectrum (52) as a function of temperature T. The effective mass has a maximum at the critical temperature $T_c \simeq 2.3$ K and decreases rapidly with decreasing temperature in the range $0 \leq T \leq T_c$ where the condensed phase exists.

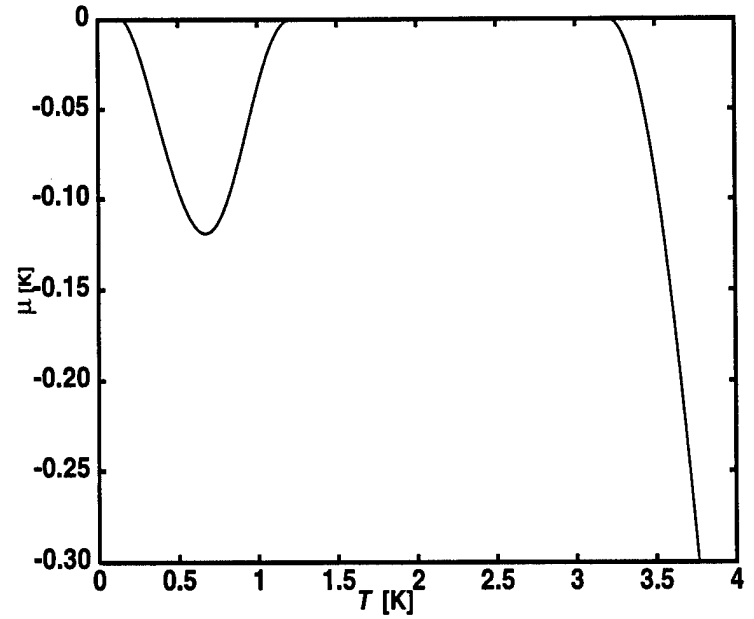

Figure 3. The chemical potential μ of the (cyclic) quasiparticle spectrum (52) versus temperature T. The chemical potential vanishes in the temperature range $T_\lambda^- \leq T \leq T_\lambda^+$, with $T_\lambda^- \simeq 1.2$ K and $T_\lambda^+ \simeq 3.2$ K.

The results shown in Fig. 4 imply that $G_{cc}^{(0)}(r)$ is a short–range function in the low–temperature region $0 < T < T_\lambda^- \simeq 1.2$ K and at temperatures $T > T_\lambda^+$. As the temperature $T_\lambda^+ \simeq 3.2$ K is approached from above, $1/S_{cc}^{(0)}(0) \to 0$ and the correlation length associated with $G_{cc}^{(0)}(r)$ diverges and remains infinite throughout the temperature range $T_\lambda^- \leq T \leq T_\lambda^+$, including the critical temperature T_c for Bose condensation.

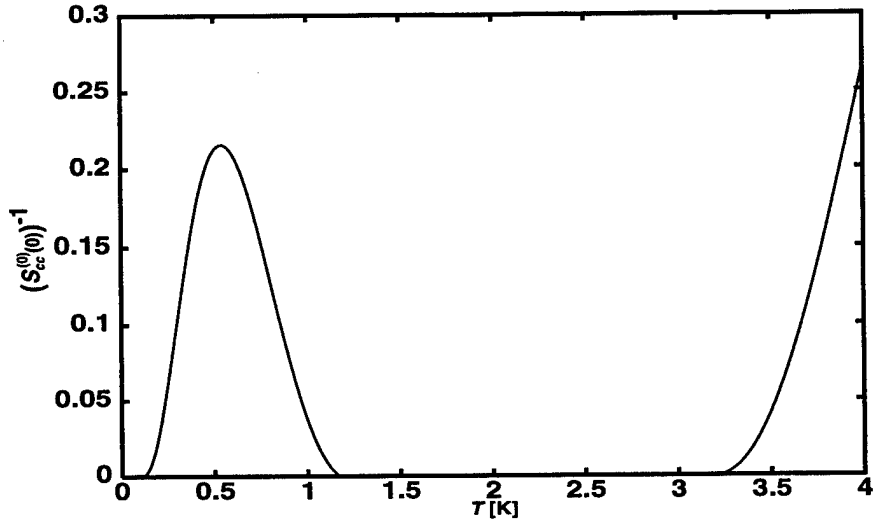

Figure 4. Temperature dependence of the inverse of the cyclic structure function $S_{cc}(k)$ at zero wave number k. This quantity vanishes in the region $T_\lambda^- \leq T \leq T_\lambda^+$ where the chemical potential μ of the quasiparticle branch (52) is zero, signaling that the corresponding cyclic spatial distribution function has infinite correlation length.

We next discuss the results obtained for the second branch of quasiparticle excitations. The energies $\omega_c(k)$ of these excitations are calculated from the average occupancy $n_c(k)$ through the defining relation (36). In turn, Eq. (22) is used to determine $n_c(k)$ from the numerical results for the partial structure functions and the exchange function $\Gamma_{cc}(k)$. In the normal phase, the excitation energies $\omega_c(k)$ are the same as the energies $\omega_{cc}(k)$ parametrized by Eq. (52) and the two branches are indistinguishable. However, in the condensed phase the branches follow quite different dispersion relations. Plots of $\omega_c(k)$ versus k are given at selected temperatures in Figs. 5 and 6. At low temperatures $T \leq T_\lambda^- \simeq 1.2$ K where the condensation strength is approximately unity, there is a gap of some 20 K or more between the ground state and the c–branch excitations. Moreover, as seen in Fig. 5, there is a forbidden wave–number zone, $0 \leq k \leq k_0 \simeq 1.3$ Å^{-1}, where quasiparticles associated with the second, type–c branch cannot exist. Consequently, the second quasiparticle energy branch is practically unpopulated in the temperature region $0 \leq T \leq T_\lambda^-$, and therefore one has $\rho_c \simeq 0$.

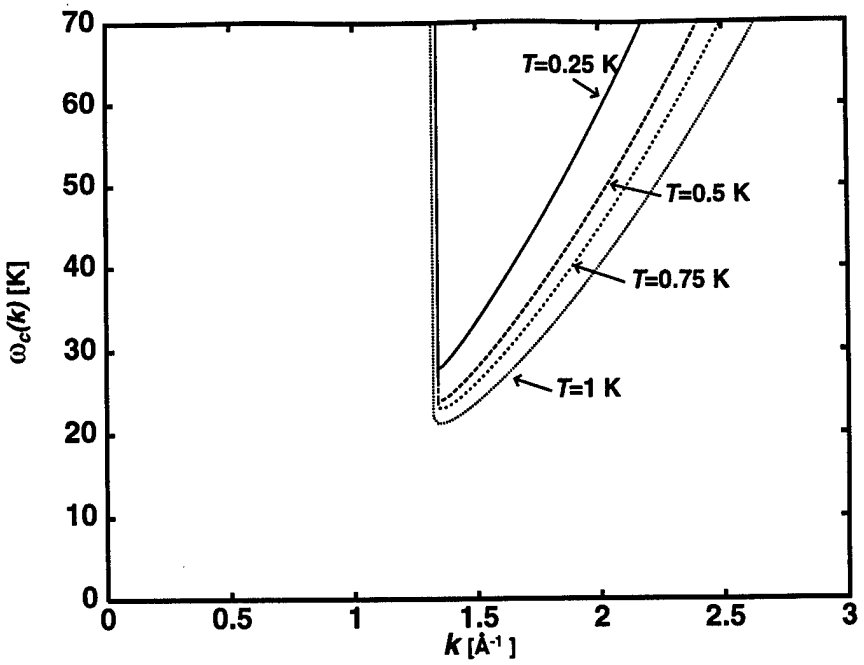

Figure 5. Numerical results for the excitation energy $\omega_c(k)$ of the quasiparticle branch c at various temperatures $T < T_\lambda^- \simeq 1.2$ K. Due to the large excitation energies, the $c-$type quasiparticle levels are essentially unpopulated at these temperatures.

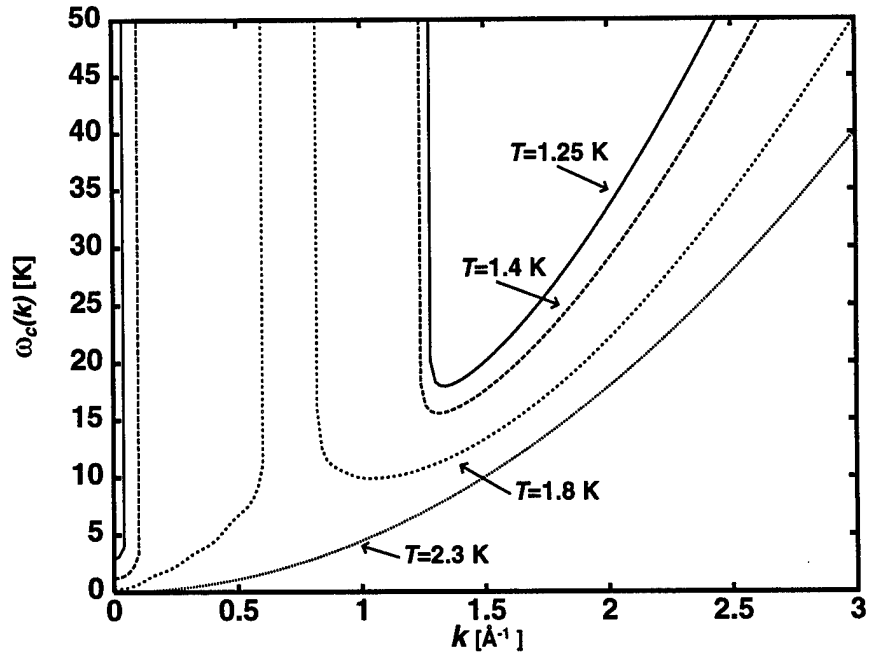

Figure 6. Numerical results for the excitation energy $\omega_c(k)$ of the quasiparticle branch c at temperatures $T_\lambda^- < T < T_c$. In this temperature range, the branch c admits low–lying excitations at small wave numbers. Upon approaching the critical temperature $T_c \simeq 2.3$ K from below, the forbidden region of energies disappears and the excitation branches c and cc become identical.

When the temperature exceeds T_λ^-, a channel of low–energy c-type quasiparticle excitations with small momenta $\hbar\mathbf{k}$ opens up, as seen in Fig. 6. With increasing temperature, the width of the forbidden zone shrinks drastically. Approaching the λ–point from below, the excluded region vanishes completely, and thereafter the dispersion law $\omega_c = \omega_c(k)$ is coincident with that obeyed by the quasiparticles of the cyclic branch. Thus, for $T_\lambda^- \leq T \leq T_c$, the number of quasiparticle excitations increases rapidly with increasing temperature. This causes a dramatic reduction of the condensation strength and leads, finally, to the disappearance of the condensate at $T = T_c \simeq 2.3$ K.

The pivotal role in the decay of the condensate that these considerations attribute to the c–type quasiparticles may be measured quantitatively by the order parameter M defined by Eq. (33). The numerical results for the optimal values of $M(T)$ are plotted in Fig. 7. Since $\rho_c \simeq 0$ at temperatures $0 \leq T \leq T_\lambda^- \simeq 1.2$ K, the excitations of the cyclic branch dominate in this range; accordingly both M and B_{cc} are close to unity. However, when the temperature rises to T_λ^-, population of the c branch becomes possible. With further increase of temperature, the number ρ_c of c–type quasiparticles increases rapidly, bringing to an end the dominant influence of the cyclic quasiparticle branch. The two types of quasiparticles become indistinguishable at the critical point $T_c \simeq 2.3$ K, and hence M is identically zero in the non–condensed normal phase.

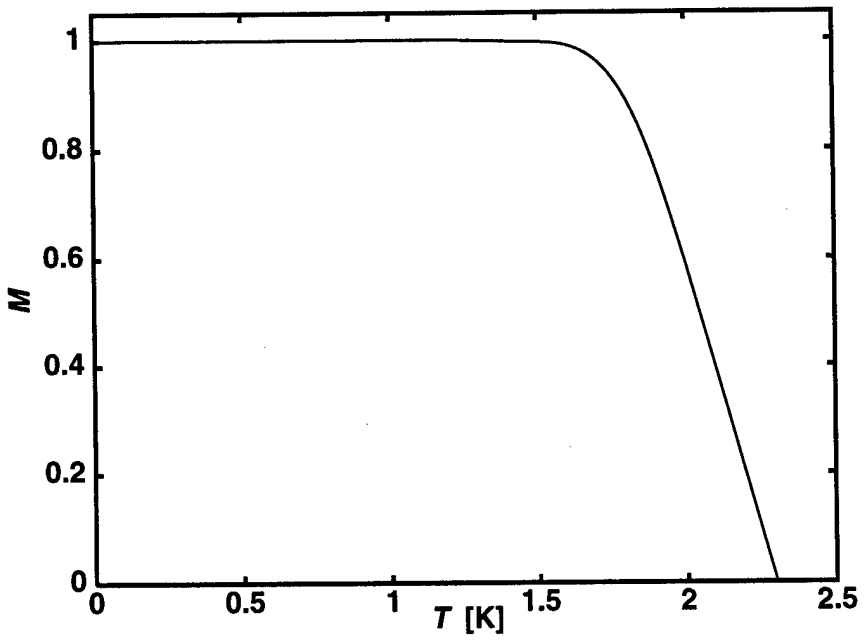

Figure 7. The order parameter M of Eq. (33) as a function of temperature, showing rapid falloff in the region $T_\lambda^- < T \leq T_c$ due to the open channel of low–energy excitations of the quasiparticle branch c. The parameter M vanishes at the critical temperature $T_c \simeq 2.3$ K since the two quasiparticle branches become indistinguishable in the normal phase.

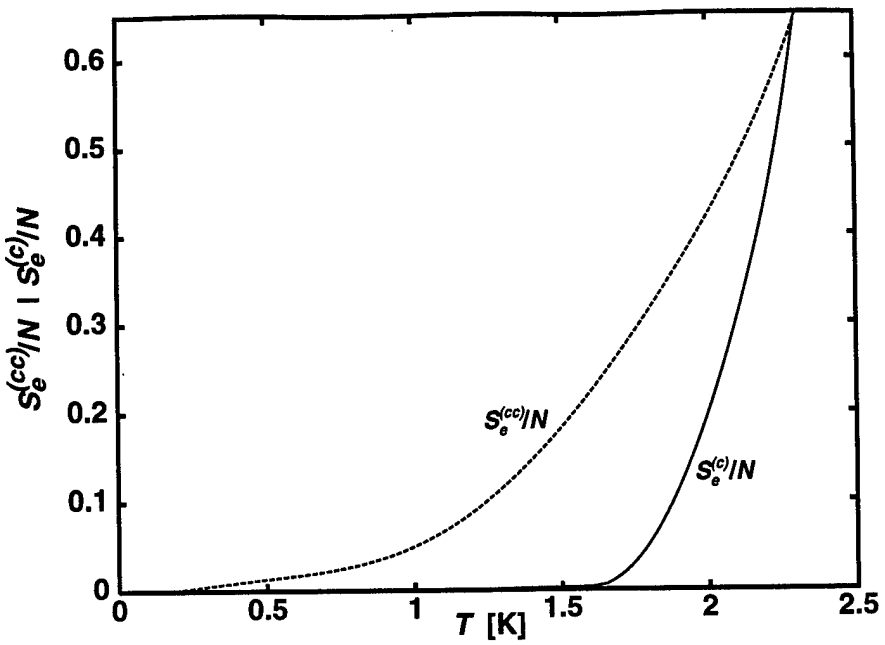

Figure 8. Dependence on temperature T of the entropies of the quasiparticle excitations associated with the cyclic branch cc and with branch c.

The results obtained for the entropy components (29) and (30) associated with the two quasiparticle branches in the Bose–condensed phase are displayed in Fig. 8. The behavior of the entropy component $S_e^{(c)}$ arising from c–type quasiparticle excitations conforms to what we would expect from the preceding discussion. This component is effectively zero at temperatures $T < T_\lambda^-$, but increases rapidly with temperature once the channel for type–c quasiparticles of small momenta opens up (i.e., once $T > T_\lambda^-$). Since the quasiparticle branches merge into a single branch at the predicted λ point, the inequality $S_e^{(c)} < S_e^{(cc)}$ becomes an equality in the normal phase where $\rho_c = \rho_{cc}$.

In the above we have dealt in some detail with the quantitative predictions of our microscopic model of Bose–Einstein condensation in helium. To conclude the discussion, due attention should be given, at a more qualitative, interpretative level, to the unusual features of this model. In particular, what is the origin of the second quasiparticle branch? Does the appearance of two quasiparticle branches have some underlying physical significance, or is it an artifact of our ansatz for the trial density matrix or of the approximations made? To begin the discussion, it is our position that the c–type quasiparticle branch is not an artifact but is instead a manifestation of important physics, operating within the limitations of our approximate description.

One possibility that has been suggested is that the c quasiparticles represent an attempt by the model to simulate the quasiparticle damping of the collective modes and attendant decay of the condensate. Another intriguing picture harks back to an idea of Felix Bloch, that there might exist both particle and hole excitations in a system of identical bosons, much like in a Fermi system. This idea is in harmony with David Pines' persuasive arguments that strongly interacting Bose and Fermi liquids – in particular liquid ^{4}He and liquid ^{3}He – have much more in common than

is normally supposed.

Developing on Bloch's idea, we would view the c branch as the quasi*particle* branch. Its energy $\omega_c(k)$ would then be identified as the energy of an additional ^{4}He atom produced by the action of a creation operator $a_k^\dagger$ on the ground state. Similarly, the cc branch would be considered as the quasi*hole* branch, its states being produced by the action of an annihilation operator a_k, and its dispersion law $\omega_{cc}(k)$ being that of a hole. This interpretation is in fact consistent with, and supported by, the fine structure of the version of correlated density matrix theory outlined herein. Inspecting the diagrammatic cluster expansions of n_{cc} and n_c one sees that the two–body cluster suffices to give $S_{cc}^{(0)}(k)$, and therewith n_{cc}, to lowest nonvanishing order. On the other hand, it is necessary to go to four–body cluster order to obtain the lowest nonvanishing contribution to $S_{cc}^{(2)}(k)$ (and up to three–body cluster order for $S_{de}(k)$). In other words, to describe the c quasiparticle branch, one needs two more particles than for the cc branch – just the difference in particle number between a particle state and a hole state. Within this "Bloch interpretation," the symmetry between particle and hole excitations is broken in the condensed state of an interacting boson system, the particle and hole branches having different dispersion relations. The degree of the symmetry violation is measured by the order parameter $M = (\rho_{cc} - \rho_c)/(\rho_{cc} + \rho_c)$. At low T, particles are bound with an energy gap of about 25 K, but holes can be excited continuously in k. It remains to be seen whether the phonon–roton branch mixes substantially with the hole branch and thereby eradicates the quadratic small–k behavior of the hole spectrum. A consistent solution of the Euler–Lagrange equations in the condensed system in the relevant low–temperature region may cast some light on this question.

8. FURTHER DEVELOPMENT OF THE THEORY

What we have described can only be considered a first tentative step toward full realization of a quantitative and comprehensive correlated density matrix theory of the low–temperature properties of ^{4}He. While the available results show the promise of a fruitful illumination of the microscopic basis of the λ transition, it is clear that substantial improvements upon the current treatment are needed. A convincing and definitive calculation is likely or certain to require: (i) complete functional minimization of the free energy, (ii) the incorporation of backflow correlations, (iii) use of a better approximation for the entropy, and (iv) an account of the coupling between quasiparticle and collective modes. These improvements are being approached stepwise. Some positive results are already available for (i), no consideration yet being given to (ii)–(iv).

Such improvements will enable one to explore, in more realistic detail, the variation of the partial distribution functions and associated structure functions with temperature and density. Among other interesting problems and elaborations that should be pursued we can mention

- Microscopic investigation of the experimentally observed sharpening of the structure function $S(k,T)$ as the temperature of the condensed equilibrium state is increased toward the critical point (cf. Refs. [28–30]).
- Calculation of the optimal condensate fraction to elucidate its relation to the

condensation strength B_{cc} (cf. Refs. [12,31]).

- Extension of the formalism and applications to inhomogeneous Bose systems.

ACKNOWLEDGMENTS

This work has been supported, in part, by the U. S. National Science Foundation under Grant No. PHY-9602127, by the Deutsche Forschungsgemeinschaft under Grant Nos. 267/26/27, by the Graduiertenkolleg "Classification of phase transitions in crystalline materials," and by the EC Human Capital and Mobility Program under Contract No. ERBCHRXCT 940456. Part of this research was carried out while MLR was enjoying the hospitality of the Department of Physics, Washington University, during a leave from the Universität zu Köln. JWC expresses his gratitute to the U. S. Army Research Office, Research Triangle Park, for travel support through a grant to Southern Illinois University–Carbondale, and to the Indian sponsors of CMT20 for local support during the Pune Workshop. We thank C. E. Campbell and L. Reatto for valuable comments bearing on the interpretation of the predicted quasiparticle branches. The current affiliation of MS is: Max–Planck–Institut für Physik komplexer Systeme, Bayreuther Str. 40, Haus 16, 01187 Dresden, Germany.

REFERENCES

[1] M. H. Anderson, J. R. Ensher, M. R. Matthews, C. E. Wieman, and E. A. Cornell, Science **269**, 198 (1995).

[2] C. C. Bradley, C. A. Sackett, J. J. Tollett, and R. G. Hulet, Phys. Rev. Lett. **75**, 1687 (1995).

[3] K. B. Davis, M.–O. Mewes, M. R. Andrews, N. J. van Druten , D. S. Durfee, D. M. Kurn, and W. Ketterle, Phys. Rev. Lett. **75**, 3969 (1995).

[4] E. L. Pollack and D. M. Ceperley, Phys. Rev. B **30**, 2555 (1984); D. M. Ceperley and E. L. Pollack, Phys. Rev. Lett. **56**, 351 (1986); E. L. Pollack and D. M. Ceperley, Phys. Rev. B **36**, 8343 (1987).

[5] D. Kleppner, Physics Today **49**, *8*, 11 (1996).

[6] C. E. Campbell, K. E. Kürten, M. L. Ristig, and G. Senger, Phys. Rev. B **30**, 3728 (1984).

[7] G. Senger, M. L. Ristig, K. E. Kürten, and C. E. Campbell, Phys. Rev. B **33**, 7562 (1986).

[8] C. E. Campbell, in *Condensed Matter Theories*, edited by L. Blum and F. B. Malik (Plenum, New York, 1993), Vol. 8.

[9] G. Senger, M. L. Ristig, C. E. Campbell, and J. W. Clark, Ann. Phys. (N.Y.) **218**, 116 (1992).

[10] M. L. Ristig, G. Senger, M. Serhan, and J. W. Clark, Ann. Phys. (N.Y.) **243**, 247 (1995).

[11] M. Serhan, Doctoral thesis, Universität zu Köln (unpublished, 1996).

[12] M. L. Ristig, R. Pantförder, M. Serhan, and G. Senger, in *Condensed Matter Theories*, edited by M. Casas, M. de Llano, J. Navarro, A. Polls (Nova Science Publishers, Commack, NY, 1995).

[13] K. A. Gernoth, J. W. Clark, and M. L. Ristig, in *Condensed Matter Theories*, edited by M. Casas, M. de Llano, J. Navarro, and A. Polls (Nova Science Publishers, Commack, NY, 1995).
[14] C. E. Campbell, in *Recent Progress in Many-Body Theories*, edited by E. Schachinger, H. Mitter, and H. Sormann (Plenum, New York, 1995), Vol. 4.
[15] J. W. Clark and E. Feenberg, Phys. Rev. **113**, 388 (1959).
[16] E. Feenberg, *Theory of Quantum Fluids* (Academic, New York, 1969).
[17] C.–W. Woo, in *The Physics of Liquid and Solid Helium*, edited by K. H. Bennemann and J. B. Ketterson (Wiley, New York, 1976), Vol. 1.
[18] C. E. Campbell, in *Progress in Liquid Physics*, edited by C. A. Croxton (Wiley, New York, 1978).
[19] J. W. Clark, in *Progress in Particle and Nuclear Physics*, edited by D. Wilkinson (Pergamon, Oxford, 1979), Vol. 2.
[20] M. L. Ristig, in *From Nuclei to Particles*, edited by A. Molinari, Proceedings, International School of Physics Enrico Fermi, Course LVII, Varenna, 1981 (North–Holland, Amsterdam, 1982).
[21] P. W. Anderson, *Basic Notions of Condensed Matter Physics* (Benjamin, New York, 1984).
[22] R. M. Ziff, G. E. Uhlenbeck, and M. Kac, Phys. Rep. **32**, 169 (1977).
[23] C.N. Yang, Rev. Mod. Phys. **34**, 694 (1962).
[24] C. E. Campbell and E. Feenberg, Phys. Rev. **188**, 396 (1969).
[25] R. P. Feynman, Phys. Rev. **94**, 262 (1954).
[26] D. Schiff and L. Verlet, Phys. Rev. **160**, 208 (1967).
[27] F. London, *Superfluids* (Dover, New York, 1964), Vol. 2.
[28] F. W. Cummings, G. J. Hyland, and G. Rowlands, Phys. Kondens. Mater. **12**, 90 (1970).
[29] G. J. Hyland, G. Rowlands, and F. W. Cummings, Phys. Lett. **31**, 465 (1970).
[30] G. Gaglione, G. L. Masserini, and L. Reatto, Phys. Rev. **23**, 1129 (1981).
[31] R. Pantförder, T. Lindenau, and M. L. Ristig, J. Low Temp. Phys., in press.

RELATIVISTIC KINEMATICS AND UNITARITY RELATIONS FOR THE PROPER SELF-ENERGY

David J. Ernst

Department of Physics and Astronomy
Vanderbilt University, Nashville, TN 37235 USA

to appear in

CONDENSED MATTER THEORIES, VOL. 17

Invited Talk given at International Workshop on Condensed Matter Theories XX, Pune, India. December 1996.

RELATIVISTIC KINEMATICS AND UNITARITY RELATIONS FOR THE PROPER SELF-ENERGY

David J. Ernst

Department of Physics and Astronomy
Vanderbilt University, Nashville, TN 37235 USA

1. INTRODUCTION

The question of how to construct a practical many-body theory when some or perhaps all of the constituents are moving at relativistic velocities is discussed. Here, an emphasis is being placed on the *practical.* Techniques are sought which allow all the methodologies developed for the nonrelativistic problem to continue to be used. The emphasis is not on elegance so much as it is on calculability. The remainder of the works presented at this workshop do not fall into the relativistic realm. Furthermore, I do not see any pending need to incorporate relativity in the problems that the people here are addressing. Nevertheless, this work will provide an overview and the necessary references if such a need should arise.

The motivation for this work has been the problem of the interaction of a pion with a finite nucleus. We are interested in pion kinetic energies up to 1 GeV, while the pion's mass is only 140 MeV. The need for a relativistic treatment is obvious. The methodologies and calculational techniques developed for the pion have also been applied to proton induced reactions and, more recently, to kaon induced reactions.

The question being addressed can simply be worded, "What do you have to do to your favorite diagrams to make them covariant?" This question is largely one of kinematics. It, however, leads to the second question, "How do you handle the basic fact that particle number is no longer conserved?" This second question is the source of the 'unitarity relations' in the title of this work. This is an important consideration when you move to the covariant problem even if particle production or absorption is not a significant physical occurrence.

Below, we first discuss how to define invariant norms, phase space, and covariant kinematics. Then we define one-, two-, and three-body states. Utilizing these, the next logical question is how to define the underlying basic interaction. An important point will be to define the invariant amplitude which is free of kinematic singularities. Putting these together, we will provide explicit formulas for the proper self-energy in the lowest order impulse approximation. The proper self-energy is defined in

terms of the inverse of the Green's function, $G(\omega)^{-1} = \omega - h_o - \Sigma(\omega)$, and, as the proper self-energy occurs often throughout many-body theory, this gives a common ground for a multitude of problems. For the specific problem of elastic scattering, the proper self-energy is the optical potential, $\langle \vec{k}' \,|\, \Sigma(\omega) \,|\, \vec{k} \,\rangle$. The optical potential can be inserted into an integral equation and the equation solved numerically to produce elastic differential cross sections. Finally, we show some recent results for K^+–nucleus scattering and discuss their implications.

2. KINEMATICS

The treatment of kinematics is completely straightforward. Covariant normalizations should be used,

$$\langle \vec{k}' \,|\, \vec{k} \,\rangle = 2\omega(k)\,\delta(\vec{k}' - \vec{k}) \ , \tag{1}$$

where $\omega(k) = \sqrt{k^2 + m^2}$. In addition, invariant phase space factors should be used for all integrations,

$$\int \frac{d^3k}{2\omega(k)} \ .$$

It is *not* necessary to utilize this manifestly invariant approach. However, without explicitly inserting the $2\omega(k)$ factors, there is a great risk of misidentifying form factors or interactions with an implicit factor of $2\omega(k)$ implicitly hidden in the model interaction. This can be very misleading in understanding the range of the interaction; an example of this can be found in [1]. The inclusion of the invariant phase space factors and normalizations does limit one to working in momentum space. In momentum space these factors are simple multiplication by a function and are not an operator which is a function of the gradient.

One-body states are simply defined by starting with the particle at rest and then boosting to a frame in which the particle has a momentum $\vec{p}$

$$|\, \vec{p},\, m \,\rangle = \sum_{m'} \ell_{mm'}(\vec{p}) \,|\, 0,\, m' \,\rangle \ , \tag{2}$$

where $\ell_{mm'}(\vec{p})$ is the Lorentz boost operator. This approach was proposed as the basis of a phenomenology of particles of arbitrary spin in [2] and explicit construction of the spinors based on [3] through spin two can be found in [4]. From the one-body states, two-body states are constructed [5] as the direct product of the one-body states and then the total and relative momentum states are defined by,

$$|\, \vec{k}_1\, \vec{k}_2 \,\rangle \equiv |\, \vec{k}_1 \,\rangle\, |\, \vec{k}_2 \,\rangle \rightarrow |\, \vec{K}\, \vec{\kappa} \,\rangle \ , \tag{3}$$

where the total and relative momentum are defined by $\vec{K} = \vec{K}_1 + \vec{k}_2$ and $\vec{\kappa}$ is the momentum of particle one in the frame where the total momentum is zero, $\vec{K} = 0$. The phase space factors are found to transform as

$$\frac{d^3k_1}{2\omega(k_1)} \ \frac{d^3k_2}{2\omega(k_2)} = \frac{d^3K}{2E(k)} \ \frac{d^3\kappa}{2\mu(\kappa)} \tag{4}$$

where $E^2(K) = K^2 + (m_1 + m_2)^2$ and

$$\mu(\kappa) = \frac{\omega_1(\kappa)\omega_2(\kappa)}{\omega_1(\kappa) + \omega_2(\kappa)} \ . \tag{5}$$

In practice, the angular momentum decomposition of these states is also needed,

$$|\,\vec{K}\,\vec{\kappa}\,\rangle \rightarrow |\,K\,J\,M,\,\kappa\,j\,m\,\rangle \ .$$

If the particles have spin, then the spin and orbital angular momentum can be coupled to give a total angular momentum.

The construction of these states allows for a covariant prescription of a phenomenology — the interaction is constructed in the $\vec{K} = 0$ frame and then boosted to the frame where needed. Having explicitly utilized invariant normalizations and phase-space factors, it is imperative that the invariant scattering amplitude [6] which is free of kinematic singularities is also used. This will guarantee that in building the phenomenology the model interactions and form factors will not include hidden phase-space factors. The appropriate amplitude can be found by noticing that the S-matrix, $\langle\,\vec{k}'\,|\,S\,|\,\vec{k}\,\rangle$, when defined as a matrix element between invariantly normalized states, is a Lorentz scalar. Relating the S-matrix to the T-matrix then produces the appropriate invariant amplitude. This invariant amplitude, when angular momentum decomposed, is related to the phase shifts δ_j by

$$T_j = -\frac{4\hbar^2\,\omega(\kappa)}{\pi\,\kappa}\,e^{i\delta_j}\,\sin\delta_j \ , \tag{6}$$

where $\omega(\kappa) = \omega_1(\kappa) + \omega_2(\kappa)$. This is a useful identity as it makes it easy to discover the relationship of the invariant amplitude to whatever normalization convention one is accustomed.

Utilizing these definitions, the Lippman-Schwinger equation, i.e. the integral form of the Schrödinger equation, becomes [6]

$$\begin{aligned}\langle\,\vec{\kappa}'\,|\,T(\omega)\,|\,\vec{\kappa}\,\rangle &= \langle\,\vec{\kappa}'\,|\,\Sigma(\omega)\,|\,\vec{\kappa}\,\rangle \\ &+ \int \frac{d^3\kappa''}{\omega_1(\kappa'')\omega_2(\kappa'')}\,\langle\,\vec{\kappa}'\,|\,\Sigma(\omega)\,|\,\vec{\kappa}''\,\rangle\,\frac{1}{\omega - \omega(\kappa'') + i\eta}\,\langle\,\vec{\kappa}''\,|\,T(\omega)\,|\,\vec{\kappa}\,\rangle \ .\end{aligned} \tag{7}$$

The equation differs from others in the phase-space factors which occur. It is known [7] as the Kadyshevski equation and has been used in the pion-deuteron [8] problem. A covariant definition [6] of the target wave functions can also be derived in this approach. Although the approach is by construction covariant, in practice this elegance cannot always be maintained. For example, bound state wave functions for the target are required and one does not have Galilean invariant let alone Lorentz covariant models to produce these. If a potential model were chosen for the two-body interaction, then causality would be violated by the instantaneous action at a distance inherent in the model. However, simple field theoretic models, such as the Chew-Low [9] model or the Lee [10] model, for meson-nucleon scattering have been generalized [11] to provide field-theoretically motivated input models.

If the interactions are restricted to two-body interactions (they can certainly still contain vertices that absorb and emit particles), then the basic kinematic character of a calculation will be that of a three-body problem. At each interaction there will be the two bodies that are interacting plus the remaining nucleons. For the case we shall calculate, there is the incident meson, a struck nucleon, and $(A-1)$ residual nucleons. Calculations thus require the definition of three-body states. Just as we generated the two-body state

$$|\,\vec{k}_1\,\vec{k}_2\,\rangle \rightarrow |\,\vec{K}_{12}\,\vec{\kappa}_{12}\,\rangle\ ,$$

the three-body state can be constructed from the direct product of a one-body state for particle three and the two-body state,

$$|\,\vec{k}_3\,\rangle\,|\,\vec{K}_{12}\,\vec{\kappa}_{12}\,\rangle \equiv |\,\vec{k}_3\,\vec{K}_{12}\,\vec{\kappa}_{12}\,\rangle \rightarrow |\,\vec{K}_{tot}\,\vec{k}_{3(12)}\,\vec{\kappa}_{12}\,\rangle\ , \tag{8}$$

where the total momentum is $\vec{K}_{tot} = \vec{k}_1 + \vec{k}_2 + \vec{k}_3$, and the momentum $\vec{k}_{3(12)}$ is the momentum of particle three relative to the momentum $\vec{K}_{12} = \vec{k}_1 + \vec{k}_2$, i.e. it is the momentum of particle three in the frame where $\vec{k}_3 + \vec{K}_{12}$ or the total momentum of the system is zero.

The optical potential (or proper self-energy) for meson (here labeled π) nucleus scattering in the impulse approximation is given by

$$\begin{aligned}\langle\,\vec{k}'_\pi\,\vec{k}'_A\,|\,\Sigma(\omega)\,|\,\vec{k}_\pi\,\vec{k}_A\rangle = \sum_\alpha \int \frac{d^3k_{A-1}}{2\bar{E}_{A-1}}\,\frac{d^3k'_N}{2\bar{E}'_N}\,\frac{d^3k_N}{2\bar{E}_N} \\ \times\,\langle\Psi'_{\alpha,\vec{k}'_A}\,|\,\vec{k}'_N\vec{k}_{A-1}\rangle\,\langle\vec{k}'_\pi\vec{k}'_N\,|\,T(\omega)\,|\,\vec{k}_\pi\vec{k}_N\rangle\,\langle\vec{k}_N\vec{k}_{A-1}\,|\,\Psi_{\alpha,\vec{k}_A}\rangle\ ,\end{aligned} \tag{9}$$

where α is the set of quantum numbers that delineates the bound state Ψ_α. For this calculation, the difficulty arises because there is no best choice for particles 1 and 2 whose momenta are to be combined first. The basic ingredients of the impulse approximation are the meson-nucleon scattering amplitude and the target wave functions. The meson-nucleon scattering amplitude is naturally a function of the pion-nucleon relative momentum, indicating that the pion and the nucleon should be chosen as particles 1 and 2. However, the target wave function is a natural function of the relative momentum of the nucleon to the remaining $(A-1)$-nucleons, so that the nucleon and the residual nucleons should be chosen as particles 1 and 2. The solution is to construct not only those states with 1 and 2 paired first but also construct those states with 2 and 3 paired first, $|\,\vec{K}_{tot}\,\vec{k}_{1(23)}\,\vec{\kappa}_{23}\,\rangle$. If we expand the two sets of states in angular momentum eigenstates and then take the overlap of the two different orders of coupling, the result is a unitary transformation [5,12] known as "relativistic three-body recoupling coefficients."

The actual expression calculated results from writing the above in terms of the three-body states by inserting twice two complete sets of states, those with the meson-nucleon coupled first and those with the nucleon and the $(A-1)$ nucleons coupled first and then doing the angular momentum decomposition. The result is

$$\Sigma_J(\omega; q_1' L_1' S_1'; q_1 L_1 S_1) =$$
$$\sum \int dq_3 \, d\cos\epsilon_{13}' \, d\cos\epsilon_{13} \frac{q_3^2}{8 \overline{W}_2' \overline{W}_2 \overline{W}_3}$$
$$\times \Psi^*_{j_A}(p_1' \ell_1' j_3 \alpha_3) \Psi_{j_A}(p_1 \ell_1 j_3 \alpha_3) T_{J_3}(\omega_{(3)}; p_3' \ell_3' s\_3; p_3 \ell_3 s_3)$$
$$\times C_J\{q_3' L_3' S_3'(p_3' J_3' \ell_3' s_3')_{12}; q_1 \ell_1' S_1'(p_1' j_A \ell_1' s_1')_{23}\}$$
$$\times C_J\{q_3 L_3 S_3(p_3 J_3 \ell_3 s_3)_{12}; q_1 \ell_1 S_1(p_1 j_A \ell_1 s_1)_{23}\} \ , \qquad (10)$$

where C_J are the relativistic three-body recoupling coefficients. Although this may look complicated, it is very straightforward. Given a subroutine to calculate the recoupling coefficients, this is simply a matter of multiplying a few functions together, summing over all the indices that appear on the right but not the left, and performing the three dimensional integration. This integration is the "Fermi integral" and averages over the momentum of the struck nucleon. If the two-body T-matrix is modeled as a function of the momentum transfer only, then the T-matrix comes out of the integral. The integration then gives the Fourier transform of the density in place of the full density matrix which appears here.

3. UNITARITY AND TIME-ORDERING

In addition to kinematics, there are several basic differences in the physics that occurs when particles are moving relativistically. One of these is that the underlying interaction need not conserve particle number and, if covariant, will not be instantaneous. A consequence is that the two-body scattering amplitude will be a function of four time variables rather than the two time variables present in potential scattering. To treat this situation, the theory must be developed [13] in terms of diagrams which have not yet had the time integration performed. The question of whether to work with time-ordered Bethe-Goldstone diagrams or Feynman diagrams (in which the time-ordering has been totally removed) has an interesting answer — unitarity constraints say to remove some of the time orderings but others need to be maintained. Examples of when and when not to time-order parts of a diagram are given below.

An example is the set of time-ordered diagrams in Fig. 1. The five diagrams differ only in the time ordering of the vertices. The time associated with vertex D always occurs after the time for vertex A, B occurs always later than A, and D occurs later than C. The sum of the five diagrams removes all other restrictions on the time-orderings. Approximating the nucleon mass as infinite to simplify the algebra, the propagators which arise from these five time-ordered diagrams are

$$\frac{1}{\omega''} \frac{1}{\omega_o^+ - \omega''} \frac{1}{\omega''} + \frac{1}{\omega''} \frac{1}{-\omega'' - \omega_o^+} \frac{1}{\omega''} + \frac{1}{\omega_o} \frac{1}{-\omega'' - \omega_o^+} \frac{1}{\omega_o}$$
$$+ \frac{1}{\omega''} \frac{1}{-\omega_o^+ - \omega''} \frac{1}{\omega_o} + \frac{1}{\omega_o} \frac{1}{\omega_o^+ - \omega''''} \frac{1}{\omega_o} = \frac{1}{\omega_o} \frac{1}{\omega_o^+ - \omega''} \frac{1}{\omega_o} \qquad (11)$$

The first point is obvious. It is as simple, if not simpler, to calculate all of these diagrams as a single entity. The second point arises from the realization that unitarity relations [14] can be used to extract models for inelastic scattering that are implicitly

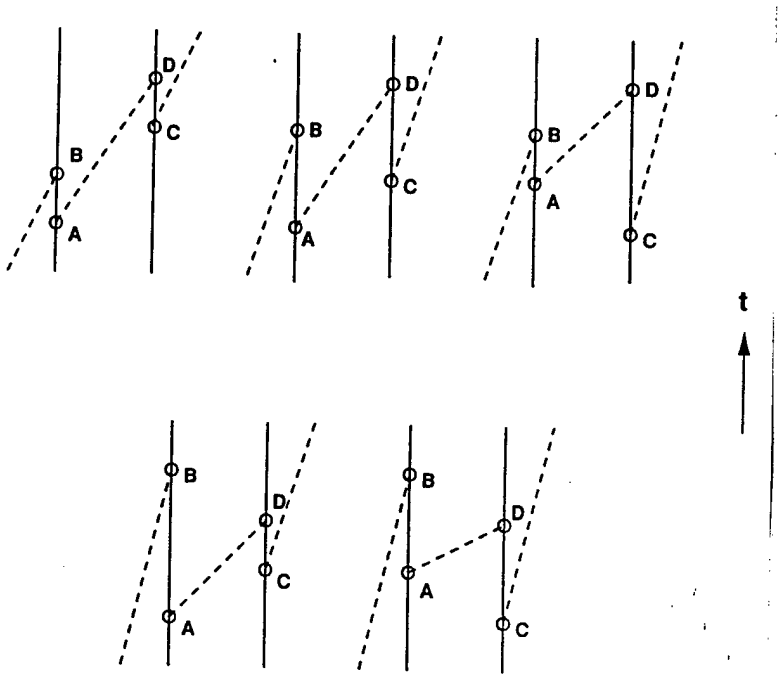

Figure 1. Five time-ordered diagrams, time running from bottom to top. The dashed lines are pons, solid lines nucleons. Note that in all diagrams D is always later than A, B is later than A, and D is later than C. Other than these restrictions, the diagrams sum over all time orderings.

contained in the optical potential. Here all but the first diagram has three mesons present at a given time. The result of the sum of all of these diagrams does not contain any implicit model of pion production, however. The number of particles present at a given time in time-ordered diagrams does not in any way relate to unitarity relations and the implicit model of inelastic channels. Alternate arrangements of the diagrams have also been proposed. One of these [15] is the 'fixed pion-number expansion.' Such an approach works with strictly time-ordered diagrams and arranges the theory according to the number of pions present at any given time. In addition to not making use of the simplification that removing the time-orderings yield and not explicitly including the cancellations that yield meaningful unitarity relations, this approach would stop for its lowest order at the first diagram in Fig. 1 which yields the first term of Eq. 11. The two factors $1/\omega''$ would be associated with the interaction vertices. These would in turn provide very low momentum cutoffs, indicating a very long range for the meson-nucleon interaction. The sum of all the diagrams, however, replaces these factors with $1/\omega_o$. This is the external energy, is completely independent of the integration variable, and thus does not contribute to the range of the interaction.

Next let us allow the time D to come before A. Removing the time ordering of mesons that propagate between the two nucleons adds the backward going meson propagator to the forward going meson propagator

$$\frac{1}{\omega_o^+ - \omega''} \rightarrow \frac{1}{\omega_o^+ - \omega''} + \frac{1}{\omega_o + \omega''} = \frac{2\omega_o}{\omega_o^{+2} - \omega''^2} \ . \tag{12}$$

This simply converts the self-energy [16] from being the optical potential for the

relativisitic Schrödinger equation to being the optical potential for the Klein-Gordon equation.

The next question that would then arise is can we allow the time B to come before A (or D before C)? The diagrams as drawn always have the produced meson leaving before the incident meson arrives. This means that the piece of the meson-nucleon two-body scattering amplitude included is the crossed or U-channel pole. Allowing B to come before A would introduce the direct or S-channel pole part of the two-body amplitude. In the limit of an infinite nucleon mass, the two contributions produce indistinguishable results and simply combine. Keeping a finite mass for the nucleon, however, produces an interesting and important difference [17] between the crossed and uncrossed pole contributions. The crossed pole gives a contribution proportional to

$$\frac{1}{-\omega_o - E_N(k'') - |E_B|} \ ,$$

while the direct pole gives

$$\frac{1}{\omega_o - E_N(k'') - |E_B|} \ ,$$

where $E_N(k'')$ is the kinetic energy of the nucleon and E_B is the binding energy of the nucleon. These factors replace the $1/\omega_o$ that occurs in the infinite nucleon mass case as in Eq. 11. The change in sign of ω_o has physical consequences. In integrating over the momentum k'', the integration for the direct pole is singular. This is because this diagram can contribute to true meson absorption. On the other hand, the crossed pole propagator is never singular; it can never contribute to true meson absorption. Not distinguishing between the different off-shell behavior between the direct channel and the crossed channel led to some unusual results in [18] and posed a question which went unanswered until [17]. This different off-shell behavior for the direct and crossed parts of the amplitudes means that the two time orderings for times A and B must be treated separately.

There remains some very interesting questions that can be addressed within the framework developed in [14]. Only the simplest uncrossed and crossed diagrams, the S-channel and U-channel nucleon pole diagrams, were examined in [17]. How does this off-shell behavior generalize to any U-channel and S-channel singularities? How important in the calculation of cross sections is this off-shell behavior? What does this imply for crossing symmetry in the many-body problem? The general scattering amplitude is a function of four time variables, while the non-relativistic amplitude is a function of only two time variables. What are the off-shell implications of this quite general feature? Work is under way to understand each of these questions.

4. RESULTS FOR K^+-NUCLEUS SCATTERING

The physics question we would like to address is whether the nucleon changes its character when embedded in the nuclear medium. The best probe to address this question is a short-ranged and weakly (in the sense of 'strength' not 'type') interacting projectile. In the limit of a very weak interaction, the total cross section on a nucleus would become just A times the spin-isospin averaged two-body total

cross section. Deviations would imply a modification of the two-body interaction by the nuclear medium. The closest nature comes to this ideal situation is the K^+. The K^+–nucleon total cross section is in the 10 to 20 mb range. Pions above the Δ_{33} are the second weakest of the strongly interacting particles. Although there are broad resonance peaks, the total interaction is relatively independent of energy and has a typical total cross section in the range of 20 to 30 mb.

Working with a probe where the meson-nucleus total cross section is near A times the two-body cross section has a great advantage for the theorist. In this region, the second-order corrections, which are proportional to the square of the two-body amplitude, are small. Since the higher-order corrections are the largest uncertainty in the theory, it is best to keep them as small as possible. In addition, the second-order corrections contain an additional propagator so that going to high energies will also help to minimize the theoretical uncertainties. A simple estimate of the ratio of the second-order optical potential to the first-order is given by [19]

$$R = \frac{U^{(2)}}{U^{(1)}} = \sqrt{\sigma}\frac{\ell_c}{k}\rho \ , \tag{13}$$

where σ is the total two-body cross section, ℓ_c is the correlation length, and ρ is the density at which the projectile interacts. The factor $1/k$, where k is the incident pion momentum, arises from the extra propagator in the second-order potential. For pions on resonance, we find $R \approx 0.1$. R is less than one only because the density at which the interaction is taking place is small. For K^+, $R \approx .01$, and for pions at 500 MeV, $R \approx .04$, and at 1 GeV, $R \approx .02$. We thus expect second-order correlation corrections to be only a few percent. For other corrections, one can substitute the appropriate two-body cross section σ and the appropriate length scale ℓ to achieve a similar estimate.

Another advantage of a weak two-body interaction is that the projectile will penetrate further into the nucleus. Because the modifications to the nucleon should increase with nuclear density, it is important that the projectile see nucleons in a region where the density is substantial. A simple estimate of how far a projectile penetrates into the nucleus can be found from the arguments [20]. This argument states that the radius of deepest penetration is equal to the impact parameter where the profile function of the target just equals one mean free path for the projectile. In [21] it is shown that the K^+ can just penetrate to the center of ^{40}Ca and to the half density point of ^{208}Pb. The pion at 700 MeV makes it to the center of ^{12}C but only to the half density point of ^{40}Ca.

Thus the high-energy pion and the K^+ are the best possible probes among the strongly interacting particles to investigate the possibility that the nucleon is modified in a fundamental way when it finds itself in the nuclear medium. To examine modifications of the properties of excited hadrons in the nuclear medium, the projectile must create these hadrons in the nucleus. These excited hadrons were discovered by their production in the pion-nucleon reaction. Thus high-energy pions are again a logical choice for the projectile. Electrons and photons can also be used.

Although the K^+ is the best probe, there is a limited amount of K^+-nucleus data. Elastic data [22] led to the first indications [23,24] that theories would consistently under-predict the data. However, there is a 17% systematic error in the normalization

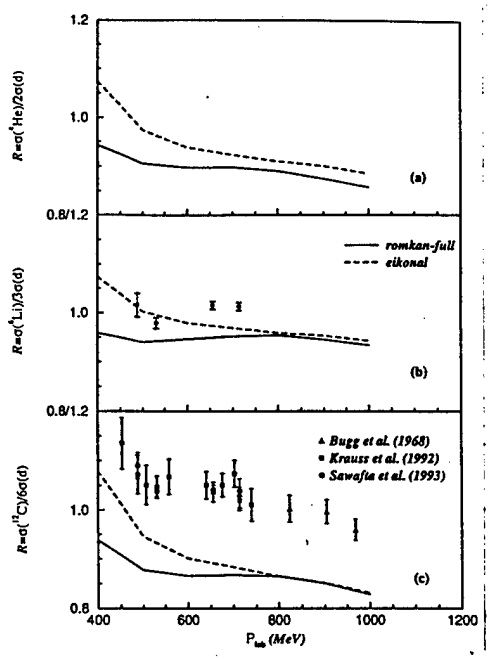

Figure 2. The total cross section ratio defined in Eq. (14) for ^{4}He, ^{6}Li, and ^{12}C as a function of the laboratory momentum of the K^+, P_{lab}. The data are from [25] and the curves are the results of the first-order optical potential utilizing the relativistic momentum-space code ROMKAN.

of the data and a discrepancy of about twenty to 30% between experiment and theory. The short lifetime of the K^+ makes it very difficult to ascertain the absolute normalization of data. Ratios of cross sections are thus much more reliable. The total cross section for a nucleus divided by the total cross section for the deuteron is such a measurement. In Figs. 1 and 2, we present results for K^+ scattering from a variety of nuclei. The data are from [25]. Presented is the ratio

$$r = \frac{\sigma_t(A)/A}{\sigma_t(D)/2} \ . \tag{14}$$

We see that there is an energy independent and nearly target independent discrepancy between the theory and the data. The discrepancy found is almost independent of the details of the theoretical calculation. Indeed, a calculation [26] based on the Kemmer-Duffin-Petiau equation also produces rather similar results. This can be understood by noticing that a simple eikonal model [27] produces results that are close to the full momentum space calculation. This implies that off-shell effects, the Fermi integration, and other features of the momentum-space calculation are not overwhelmingly important. This is supported by noting that the ratios of cross sections in Figs. 1 and 2 are all close to one. What the theorist is calculating is actually the difference from one. A constraint on a reasonable theoretical calculation is that the Born approximation to the optical potential gives for the total cross section nearly

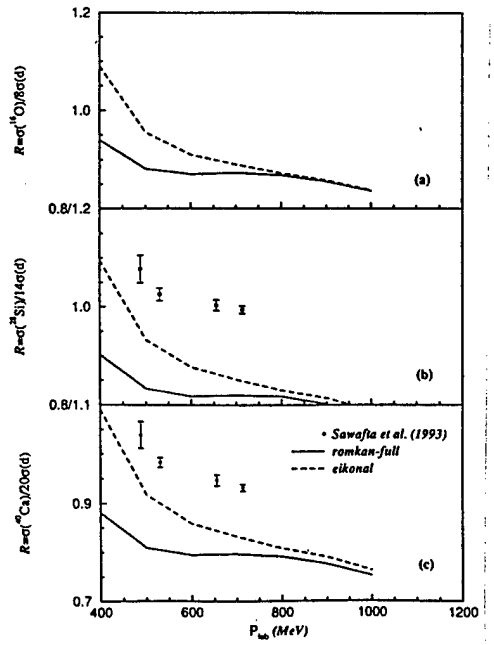

Figure 3. The same as Fig. 1 except the targets are ^{16}O, ^{28}Si, and ^{40}Ca.

A times the spin-isopin averaged two-body total cross section (in the absence of Coulomb-nuclear interference). This is trivially true for the eikonal model. For the momentum-space approach the Born approximation to the optical potential contains a Fermi-averaging over the two-body total cross section. If the Fermi averaging is approximated [28] according to the 'optimal factorization' prescription, then the momentum-space results yield, in Born approximation, A times the two-body cross section evaluated at a small energy shift given by the difference between the average binding energy of the nucleons and the mean spectral energy. Given that the theories are only calculating these small differences from A times the two-body cross section and the shadowing that results from iterating the optical potential in an integral equation (only about a 5% effect), the agreement among theorists is not surprising.

The discrepancy which we find is about 20%. This may be viewed as caused by a modification of the nucleon when in the nuclear medium. Total cross section measurements cannot discriminate among models [24] which would simply increase the two-body scattering amplitude in the medium in an energy independent way.

Mesons exchange currents are a possible mechanism that could account for this discrepancy. The results of [29] would indicate that this is not the case. There it was found that exchange currents are both too small and would have a rapid energy dependence as the energy is increased above the threshold for pion production. Enhanced mesonic clouds resulting from reduced mesonic masses in the nucleus [30] would increase this contribution. but the pronounced energy dependence, not seen in the data, would remain. A calculation which removes the static approximation in calculating the exchange currents and adds scattering from short and mid range correlations [31] yields a much larger effect, an effect that is of the order of the discrepancy between the theory and the data. Further investigation is needed to

understand if the approach of [31] can produce results which are quantitatively in agreement with the energy and target dependence of the data.

Elastic differential cross sections would provide additional information on the origin of the observed discrepancy. It was the differential cross sections measured in [22] that lead to the original observation [23,24] of a possible discrepancy. However, the systematic error in the data is given as 17% and the discrepancy [27] is nearly independent of angle. The possibility of a systematic normalization error somewhat larger than that quoted would resolve the problem. Thus, this data did not provide a clear and convincing argument for a discrepancy. The measurement of elastic differential cross sections with an absolute normalization of 5% would be most useful. However, the short lifetime of the K^+ has so far prevented measurements with absolute normalizations at this level.

Recent data [32] takes an interesting approach to this problem. The rms radius of ^{6}Li and ^{12}C are nearly equal, with ^{6}Li having the slightly larger radius. Roughly ^{12}C is twice as dense as ^{6}Li. In the forward direction the details of the density should make little difference. Thus one can take the ratio of elastic differential cross sections between these two nuclei and in the forward direction one would be examining the density dependence of the mechanism that is causing the discrepancy. In Fig. 1 we see that the less dense ^{6}Li appears to produce a smaller discrepancy for the total cross section than is seen in other more dense nuclei. The measurements of [32] confirm this observation.

Similar results have been found [33] for high-energy pions. There does not exist a phenomenological explanation for this discrepancy that is consistent with all existing data. A model which is predictive in character is needed. The application we have used for our covariant many-body theory has lead to some intriguing results. We have been interested in the elastic scattering problem. However, the approach is quite general and can be used in any many-body problem.

This work was supported, in part, by the US Department of Energy and the US Office of Army Research.

REFERENCES

[1] M. Hirata, F. Lenz, and K. Yazaki, Ann. Phys. (N.Y.) **108**, 116 (1977).

[2] D. V. Ahluwalia and D. J. Ernst, Phys. Rev. C**45**, 3010 (1992).

[3] S. Weinberg, Phys. Rev. B**133** 1318 (1964).

[4] D. V. Ahluwalia, Ph.D. thesis, Texas A&M University (1991), unpublished.

[5] D. R. Giebink, Phys. Rev. C**32**, 502 (1985); C**25**, 2133 (1983).

[6] D. R. Giebink and D. J. Ernst, Comp. Phys. Commun. **48**, 407 (1988).

[7] V. G. Kadyshevski, Nucl. Phys. **B6**, 125 (1981).

[8] L. Mattelitsch and H. Garcilazo, Phys. Rev. C**32**, 1635 (1985).

[9] C. F. Chew and F. E. Low, Phs. Rev. **101**, 1570 (1956).

[10] T. D. Lee, Phs. Rev. **95**, 1329 (1954).

[11] C. B. Dover, D. J. Ernst, R. A. Friedenberg, and R. M. Thaler, Phys. Rev. Lett. **33**, 728 (1974); K. K. Bajaj and Y. Nogami, *ibid.* **34**, 701 (1975); D. J.

Ernst and M. B. Johnson, Phys. Rev. C**17**, 247 (1978); C**20**, 1064 (1979); C**22**, 651 (1980); R. J. McLeod and D. J. Ernst, Phys. Rev. C**23**, 1660 (1981); R. J. McLeod and I. R. Afnan, Phys. Rev. C**32**, 222 (1985); D. J. Ernst, G. E. Parnell, and C. Assad, Nucl. Phys. **A518**, 658 (1990); R. J. McLeod and D. J. Ernst, Phys. Rev. C**49**, 1087 (1994).

[12] H. Garcilazo, unpublished.

[13] M. B. Johnson and D. J. Ernst, Ann. Phys. (N.Y.) **219**, 266 (1992); Phs. Rev. C**27**, 790 (1983).

[14] D. J. Ernst, C. M. Shakin, and R. M. Thaler, Phys. Rev. C**9**, 1374 (1974); P. C. Tandy, E. F. Redish, and D. Bolle, Phys. Rev. Lett. **35**, 921 (1975); Phys. Rev. C**16**, 1924 (1977).

[15] G. A. Miller, Phys. Rev. Lett. **38**, 753 (1977); Phys. Rev. C**16**, 2325 (1977); G. A. Miller and E. M. Henley, Ann. Phys. (N.Y.) **129**, 131 (1980).

[16] J. B. Cammarata and M. Banerjee, Phys. Rev. Lett. **31**, 610 (1973); Phys. Rev. C**13**, 299 (1976); M. B. Johnson and D. J. Ernst, Phys. Rev. C**20**, 1064 (1979).

[17] R. J. McLeod and D. J. Ernst, submitted to Phys. Lett. B.

[18] F. Myhrer and A. W. Thomas, Nucl. Phys. **A326**, 497 (1979).

[19] D. J. Ernst, J. T. Londergan, G. A. Miller, and R. M. Thaler, Phys. Rev. C **16**, 537 (1977).

[20] D. J. Ernst, Phys. Rev. C **19**, 896 (1979).

[21] C. M. Chen, D. J. Ernst, and M. B. Johnson, Phys. Rev. C **48**, 841 (1993).

[22] D. Marlow *et al.*, Phys. Rev. C **25**, 2619 (1982).

[23] M. J. Páez and R. H. Landau, Phys. Rev. C **24**, 1120 (1981).

[24] P. B. Siegel, W. B. Kaufman, and W. R. Gibbs, Phys. Rev. C **30**, 1256 (1984); C **31**, 2184 (1985).

[25] E. Mardor *et al.*, Phys. Rev. Lett. **65**, 2110 (1990); R. A. Krauss *et al.*, Phys. Rev. C **46**, 655 (1992); Sawafta *et al.*, Phys. Lett. B **307**, 293 (1993); R. Weiss *et al.*, Phys. Rev. C **49**, 2569 (1994).

[26] B. C. Clark, S. Hama, G. R. Kälbermann, R. L. Mercer, and L. Ray, Phys. Rev. Lett. **55**, 592 (1985); L. Kurth and B. C. Clark, private communication.

[27] C. M. Chen and D. J. Ernst, Phys. Rev. C **45**, 2011 (1992); M. F. Jiang and D. J. Ernst, *ibid.* **51**, 1037 (1995); M. F. Jiang, D. J. Ernst, and C. M. Chen, *ibid.* **51**, 857 (1995).

[28] D. J. Ernst and G. A. Miller, Phys. Rev. C **21**, 1472 (1980); D. L. Weiss and D. J. Ernst, Phys. Rev. C **26**, 605 (1982).

[29] M. F. Jiang and D. S. Koltun, Phys. Rev. C **46**, 2462 (1992).

[30] G. E. Brown, C. B. Dover, P. B. Siegel, and W. Weise, Phys. Rev. Lett. **26**, 2723 (1988).

[31] C. García-Recio, J. Nieves, and E. Oset, Phys. Rev. C **51**, 237 (1995).

[32] R. Micjael *et al.*, Phys. Lett. **B382**, 29 (1996).

[33] C. M. Chen, D. J. Ernst, M. F. Jiang, and M. B. Johnson, Phys. Rev. C **52** R485 (1995).

ON THE THERMODYNAMIC PHASE TRANSITIONS RELEVANT TO SUPERCONDUCTIVITY AND COLOSSAL MAGNETO-RESISTIVITY FOR A HUBBARD TYPE OF HAMILTONIAN

S. Picozzi[1] , A. N. Proto[2] and F. B. Malik[1]

[1]Physics Department, Southern Illinois University, Carbondale, Illinois, 62901, U.S.A.

[2]Grupo de sistemas dinámicos, Centro Regional Norte, Universidad de Buenos Aires, C.C. 15, SUC-1 (1640) Martinez, Argentina

ABSTRACT

This paper presents the explicit temperature evolution of a modified Hubbard Hamiltonian pertinent to the understanding of superconducting, anti-ferromagnetic and ferromagnetic phases of a system within the framework of the Maximum Entropy Principle and without making any a priori assumption about the pair formation or alignment probabilities at a site. In this paper we discuss two cases, which depend on whether or not the ratio of the strength of magnetization to twice the hopping term prevails over the combined influence of the mean field plus the pairing term. In the former case (situation 1), the system prefers to be ferromagnetic below a critical temperature, while in the latter (situation 2) the system tends to form pairs below a critical temperature. Calculations are presented for sets of parameters corresponding to both situations. In situation 1, the system changes from a ferromagnetic phase to an anti-ferromagnetic phase with the increase of temperature. The model predicts that the critical temperature for this transition increases with the introduction of an external magnetic field as observed experimentally. On the other hand, adjustment of the controlling parameters leads the system to situation 2 when pair formation is preferred below critical temperature which may be relevant to superconductivity.

1. INTRODUCTION

Traditionally, materials have been classified as conductors, semi-conductors and insulators depending upon their electric transport properties. While a great many materials can be ascribed to one or the other category, others instead, when properly doped, seem to cross lines and move from one category to another. In particular, certain compounds of perovskite structure have, in the last decade, acquired prominence in light of their ability to undergo modulations of their electric transport properties over an unprecedented variety of scales as a function of temperature. More specifically, it is remarkable and intriguing that seemingly diametrically opposite phenomena, such as high-temperature superconductivity [1] and colossal magnetoresistance [2-7] may find manifestation in the same class of materials, depending on the concentration of certain specific dopants. From a theoretical point of view, therefore, it would be of interest to devise a framework capable of encompassing both aspects, allowing one to shift continuously from one

type of behavior to the other simply by modulating suitable controlling parameters.

Hence, in the present paper, we examine the possibility of developing a unitary description of a system which may be transformed from one type to another by a set of controlling parameters. We note that both superconductivity and colossal magneto-resistivity or CMR deal with dramatic variations of resistance as a function of temperature and applied magnetic field. Consequently, one is to develop a theory that explicitly allows for the temperature evolution of a dynamic system. The Maximum Entropy Principle or MEP allows one to reach that goal. In section 2 we describe a model relevant to study the relation between these controlling parameters and the occurrence of ferromagnetic, anti-ferromagnetic and paired states at different temperatures. We investigate the probability of pair formation as a function of temperature without any assumption of their existence a priori. The controlling parameters that determine whether the system at low temperature manifests pair formation or spin alignment are discussed for specific cases in section 3.

2. THE MODEL

We adopt the following Hamiltonian, which may be regarded as an extended version of Hubbard's, in the sense of [8]:

$$\hat{H} \equiv \sum_i E(i)\hat{n}_i + (B_o\Delta(i) + M)\hat{n}_{di} + U(i)\hat{r}_i + t\Delta^2(i) \qquad (1)$$

where we have used the following notation:

$$\hat{n}_i \equiv \hat{n}_{i\uparrow} + \hat{n}_{i\downarrow}\,; \quad \hat{n}_{di} \equiv \hat{n}_{i\uparrow} - \hat{n}_{i\downarrow}\,; \quad \hat{r} \equiv \hat{n}_{i\uparrow}\hat{n}_{i\downarrow}\,; \quad \hat{n}_{i\uparrow} \equiv c_{i\uparrow}^{\dagger}c_{i\uparrow}\,; \quad \hat{n}_{i\downarrow} \equiv c_{i\downarrow}^{\dagger}c_{i\downarrow}$$

The c, $c^{\dagger}$, in terms of which all of the above operators are expressed, are creation and annihilation operators obeying canonical anti-commutation rules, namely:

$$\left\{c_{i\uparrow}, c_{j\uparrow}^{\dagger}\right\} = \left\{c_{i\downarrow}, c_{j\downarrow}^{\dagger}\right\} = \delta_{ij}$$

while all the other anti-commutators vanish.

As for the subscripts below the c's, the up and down arrows refer, respectively, to the (½)ħ and (-½)ħ value for a spin's component along an arbitrarily chosen direction, whereas the *i* subscript denotes the *i*-th "site," in the following, generalized, sense: let a complete set of commuting observables be associated to each spin-carrying "particle," including the spin degrees of freedom themselves. As it is well known, all such observables can, simultaneously, possess well defined values. Any set of such values, minus the spin degrees of freedom, constitute, in the present context, a "site." Clearly, one may regard a site in physical space as but a particular case of the above. The quantities in (1) yet undefined are all scalars, whose meaning and units are indicated subsequently, where we elucidate the role of the individual terms of the Hamiltonian.

As we intend to develop a finite-temperature theory, the relevant physical quantities are to be

calculated by the methods of statistical mechanics. We choose to analyze (1) by means of a procedure stemming from the Maximum Entropy Principle (MEP), in the manner of Proto and her collaborators [9-11]. The gist of the MEP may be enunciated as follows:

Among all density matrices $\hat{\rho}$ compatible with the information available about the physical system under scrutiny, one is to select the one which maximizes the information-theoretic entropy, S:

$$S = -k_B Tr(\hat{\rho}\ln\hat{\rho}) \tag{2}$$

k_B, in (1) is Boltzmann's constant and is henceforth set equal to 1. The basis for the latter requirement is that such a density matrix would lead to the **least biased estimates** (in the sense of estimation theory) of the relevant physical quantities. In general, the density matrix derived from the solution of the above extremization problem acquires the following form:

$$\hat{\rho} = \exp(-\sum_{k=0}^{n} \lambda_k \hat{A}_k) \tag{3}$$

In (3) the $\hat{A}$'s are designated as the **Relevant Operators** relative to the problem being studied and the λ's are Lagrange multipliers corresponding to the auxiliary conditions whereby the density matrix is to yield the desired expectation value of the operators.

In our case, we select the following as the Relevant Operators (I ≡ unit operator):

$$\hat{A}_0 = \hat{I}; \quad \hat{A}_1 = \hat{h}_i \equiv E(i)\hat{n}_i + (B_0\Delta(i) + M)\hat{n}_{di} + U(i)\hat{r}_i + t\Delta^2(i);$$

$$\hat{A}_2 = \hat{n}_i; \quad \hat{A}_3 = \hat{r}_i; \quad \hat{A}_4 = \hat{n}_{di}$$

In terms of these Relevant Operators, we can write (3) in the form:

$$\hat{\rho} = \exp(-\lambda_0\hat{I} - \beta\hat{h}_i - \lambda_2\hat{n}_i - \lambda_3\hat{r}_i - \lambda_4\hat{n}_{di}) \tag{4}$$

As the subscript i is being held fixed, (4) cannot represent the density matrix of the overall system. However, our way of proceeding is still meaningful in that, being the total Hamiltonian (1) a sum of uncoupled terms, the overall density matrix acquires a diagonal-block structure, of which (4) simply constitutes the i-th block, also associated with the i-th site. Henceforth, the subscript i is going to be dropped. The mean values (or thermodynamic averages) of the relevant operators are given by:

$$\langle\hat{h}\rangle = -\frac{\partial\lambda_0}{\partial\beta} \tag{5a}$$

$$\langle \hat{n} \rangle = -\frac{\partial \lambda_0}{\partial \lambda_2} \tag{5b}$$

$$\langle \hat{r} \rangle = -\frac{\partial \lambda_0}{\partial \lambda_3} \tag{5c}$$

$$\langle \hat{n}_d \rangle = -\frac{\partial \lambda_0}{\partial \lambda_4} \tag{5d}$$

Identifying $\hat{h}$ as the energy leads to the interpretation of its corresponding multiplier, β, as the reciprocal of the absolute temperature T. Considering that (2) represents nothing but the mean value of the operator $(-\ln\hat{\rho})$, the expression (4) permits us to write the entropy S as:

$$S = \lambda_0 + \beta\langle \hat{h} \rangle + \lambda_2\langle \hat{n} \rangle + \lambda_3\langle \hat{r} \rangle + \lambda_4\langle \hat{n}_d \rangle \tag{6}$$

On the other hand, combining (6) with the thermodynamic expression for the Helmholtz free energy F given by

$$F = U - TS = \langle \hat{h} \rangle - \frac{S}{\beta} \quad , \tag{7}$$

we are able to obtain:

$$F = -\frac{\lambda_0}{\beta} - \lambda_2\langle \hat{n} \rangle - \lambda_3\langle \hat{r} \rangle - \lambda_4\langle \hat{n}_d \rangle \tag{8}$$

For the purpose of evaluating the preceding mean values, and thereby the relevant thermodynamic functions, the following basis is chosen:

$$|3\rangle \equiv c_\uparrow^\dagger c_\downarrow^\dagger |0\rangle ; \quad |2\rangle \equiv (1/\sqrt{2})(c_\uparrow^\dagger - c_\downarrow^\dagger)|0\rangle ; \quad |1\rangle \equiv (1/\sqrt{2})(c_\uparrow^\dagger + c_\downarrow^\dagger)|0\rangle ; \quad |0\rangle \tag{9}$$

where $|0\rangle$ is such that

$$c_\uparrow|0\rangle = c_\downarrow|0\rangle = 0 \tag{10}$$

After expressing the relevant operators in matricial form, the MaxEnt density matrix can be readily written down by means of (4). Its diagonalization is straightforward, as the only off-diagonal terms belong to a two-by-two submatrix. The subsequent step is to impose the normalization condition $Tr\hat{\rho} = 1$, whence λ_0 can promptly be extracted as a function of the remaining multipliers, as such:

$$\lambda_0 = -\beta t\Delta^2 + \ln\left\{1 + e^{-2\lambda_2 - \lambda_3 - \beta(2E+U)} + 2e^{-\lambda_2 - \beta E}\cosh[\beta(B_o\Delta + M) + \lambda_4]\right\} \quad (11)$$

At this point, a brief discussion is in order as regards the Lagrange multipliers. Among the latter, β has already been discussed and is considered, henceforth, as an independent variable. As for the others, they are associated with mean values about which no information is available a priori. The least biased estimates of such mean values are obtained, in general, by setting their respective multipliers equal to zero.

According to (5a) to (5d), we obtain the following mean values by differentiating λ_0 given by (11) and setting $\lambda_2 = \lambda_3 = \lambda_4 = 0$ afterwards:

$$\langle\hat{n}\rangle = 2\frac{e^{-\beta(U+2E)} + e^{-\beta E}\cosh[\beta(B_0\Delta + M)]}{1 + e^{-\beta(U+2E)} + 2e^{-\beta E}\cosh[\beta(B_0\Delta + M)]} \quad (12)$$

$$\langle\hat{r}\rangle = \frac{e^{-\beta(U+2E)}}{1 + e^{-\beta(U+2E)} + 2e^{-\beta E}\cosh[\beta(B_0\Delta + M)]} \quad (13)$$

$$\langle\hat{n}_d\rangle = -2\frac{\sinh[\beta(B_0\Delta + M)]e^{-\beta E}}{1 + e^{-\beta(U+2E)} + 2e^{-\beta E}\cosh[\beta(B_0\Delta + M)]} \quad (14)$$

$$\langle\hat{h}\rangle = E\langle\hat{n}\rangle + (B_0\Delta + M)\langle\hat{n}_d\rangle + U\langle\hat{r}\rangle + t\Delta^2 \quad (15)$$

The parameters E, B_0, U, M, and t in (15) refer, respectively, to the strength of the average values of relevant operators multiplying them and are to be chosen from the physics of the materials to be studied. They are either given in energy units or in a dimensionless form. We may note that some of these parameters could be a function of momentum, k.

The parameter Δ merits special attention. Unlike its peers, it is to be **determined** by imposing that the Helmholtz free energy, as a function thereof, be a minimum. To that end, we express F by combining (6), (7), (12), (13), (14) and (15), obtaining the following expression:

$$F = \frac{\beta t\Delta^2 - \ln[1 + e^{-\beta(U+2E)} + 2e^{-\beta E}\cosh(\beta(B_0\Delta + M))]}{\beta} \quad (16)$$

By minimizing F with respect to Δ, one obtains the following transcendental equation:

$$\Delta = -\frac{B_0}{2t}\langle \hat{n}_d \rangle \tag{17}$$

Now, in order to facilitate the interpretation of the numerical results presented in section 3, we proceed to comment on the various terms in the Hamiltonian. $E(i)\langle \hat{n}_i \rangle$ is a term proportional to the total number of particles located at the *i-th* site, and hence, may be interpreted as the mean field energy of a state in general. In the absence of an average field, this represents the kinetic energy alone. $\hat{n}_{di}$ is proportional to the net spin's component, at the *i-th* site, along an arbitrary direction in space, and the term involving it may be viewed as the energy relative to the coupling between the net spin and the local magnetic field. M refers to the external field, while $B_0\Delta(i)$ is relative to the effective field "seen" by the spin at the *i-th* site, minus the external field. $t\Delta^2$ is proportional to the energy of such effective field. $\langle \hat{r}_i \rangle$ is the number of pairs at the *i-th* site, and the term $U(i)\langle \hat{r}_i \rangle$ is meant to represent energetic "incentive" for the formation of anti-aligned spin pairs. Its origin resides in the physical fact that electron pairs in an entangled state can access regions of the system's phase space, lower in energy, from which they would be otherwise precluded as free electrons, as a result of the Pauli principle [11].

3. RESULTS

Assuming that the Hamiltonian (1) provides a reasonable model for electrons in a material, the objective of this study is to determine the conditions on the strengths of controlling parameters that allow a substance to exhibit superconducting or colossal magnetoresistive behaviors. We note that the superconducting behavior is related to the formation of pairs below a critical temperature T_c, whereas for CMR the system tends to be ferromagnetic below a critical temperature while it is anti-ferromagnetic above it. Thus, the critical point is to determine whether by changing the relative strengths of the parameters, one could induce a system which allows pair formation relevant to superconductivity below T_c, to switch to a system that prefers a ferromagnetic state i.e. aligned states of fermions below T_c and anti-ferromagnetic state, i.e. aligned state above T_c. One is, further, to investigate the role of an external magnetic field in the latter situation pertinent to CMR. To this end, we note that the parameters determining the general physical properties allowing a substance to be characterized as an insulator or metal or semi-conductor are the strength of the mean field or dispersion term, E(k), and the correlation strength U(k). This is because the average behavior of electrons in a system is given by (E(k) + U(k)/2) terms in the Hamiltonian. The change in physical properties of a material could likely to be caused by changing these terms relative to the hopping and internal magnetization term. In this paper, we, therefore, investigate the system's dependence on the value of B/2t relative to |U + 2E|. We find that the said value determines whether a system prefers to be superconducting, i.e. anti-aligned, or ferromagnetic, i.e., aligned, below a critical temperature. These cases are illustrated and discussed subsequently. We may note that the relative values of these parameters are critical to the transition from a ferromagnetic to anti-ferromagnetic state and the division of B/2t and |U + 2E| is germane only to this study.

3.1 Case when B/2t is greater than |U + 2E|

Aside from these four parameters, the system's behavior at a particular temperature T is determined by the Helmholz free energy, F. As noted earlier, the thermodynamic stability of a system corresponds to the absolute minimum of the free energy in terms of Δ. Hence, the investigation of temperature evolution of a system is tantamount to studying the dependence of the absolute minimum as a function of temperature. In the first case the key parameters E and U are taken to be 0.9eV and -1.84 eV which is typical for an insulator or semi-conductor at zero temperature. B and t are, then, taken to be 1.84×10^{-2}eV and 9.0×10^{-5}eV and at first we consider the system in the absence of any external magnetic field i.e., we set M=0. In dimensionless form, these parameters are E = 200, U = -410, B = 4.1, t = 0.02 and M = 0. Thus, B/2t = 102.5 is much greater than |2E + U| = 10.

The free energy F, for this case, is exhibited in Fig. 1, as a function of Δ at T = 26.1°K or in dimensionless units T = 0.5. The symmetric pattern of F about Δ = 0, simply reflects the spatial symmetry between the upward and downward directions; the solutions for positive and negative Δ correspond, respectively, to $\langle \hat{n} \rangle_{di} = -1$ and +1. For the purpose of this discussion, it is, therefore, sufficient to consider the dependence of F on either positive or negative Δ. F has clearly a number of local minima but the absolute minimum occurs at a large value of ±Δ. An analysis of (13) and (14) implies that the system is ferromagnetic for large Δ. In fact for a large value of Δ, $\langle \hat{r}_i \rangle \approx 0$ *and* $\langle \hat{n}_{di} \rangle \approx 1$ implying a net alignment.

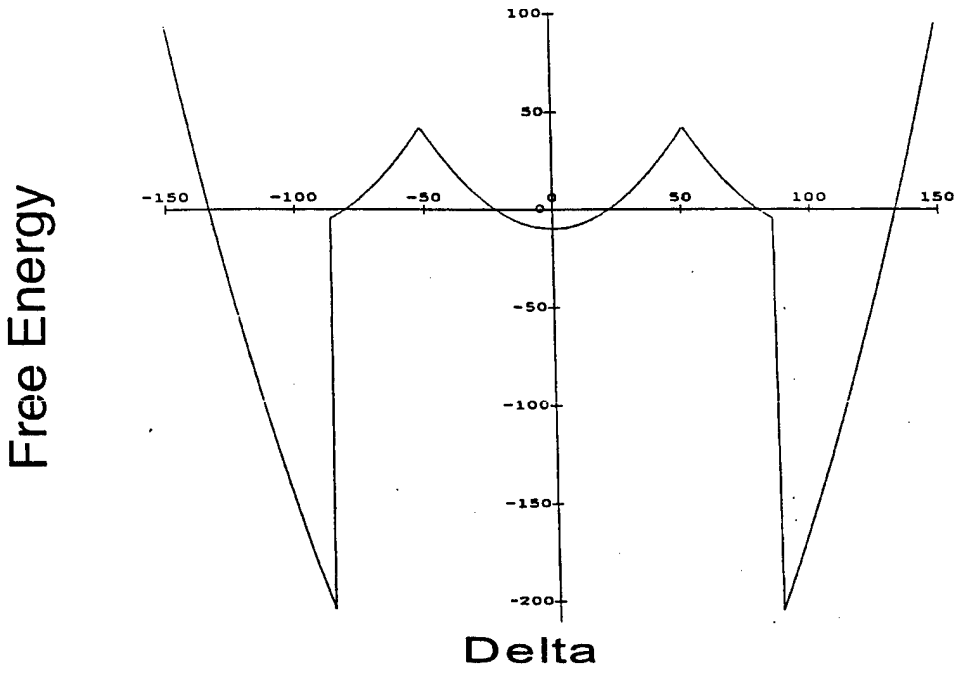

Figure 1. Free energy as a function of Δ for the case 3.1 at 26.1°K where ferromagnetic phase is preferred.

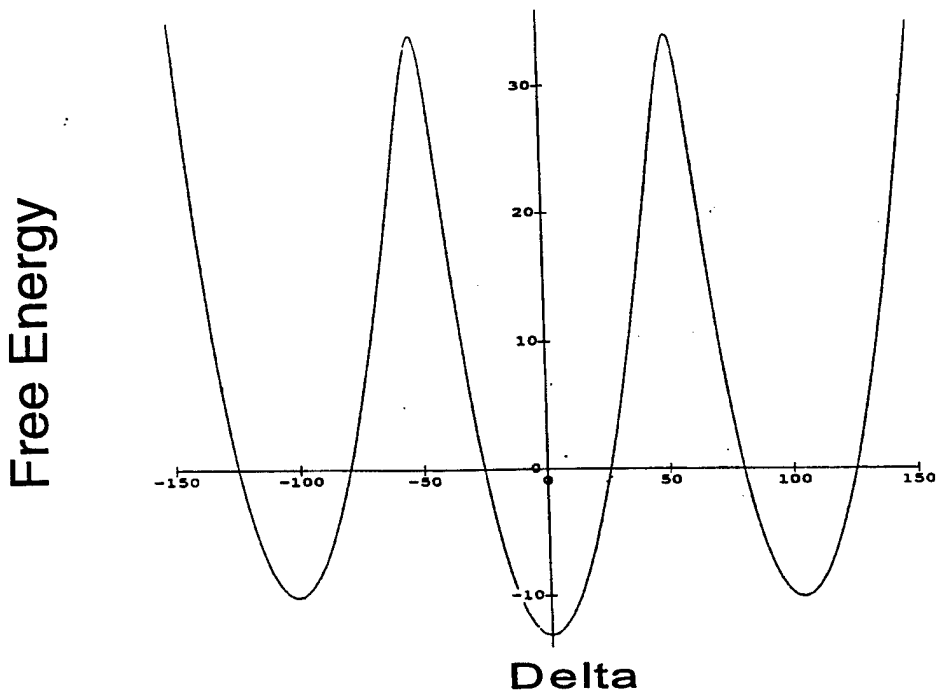

Figure 2. Free energy as a function of Δ at the transition or critical temperature 162.2°K for the case 3.1.

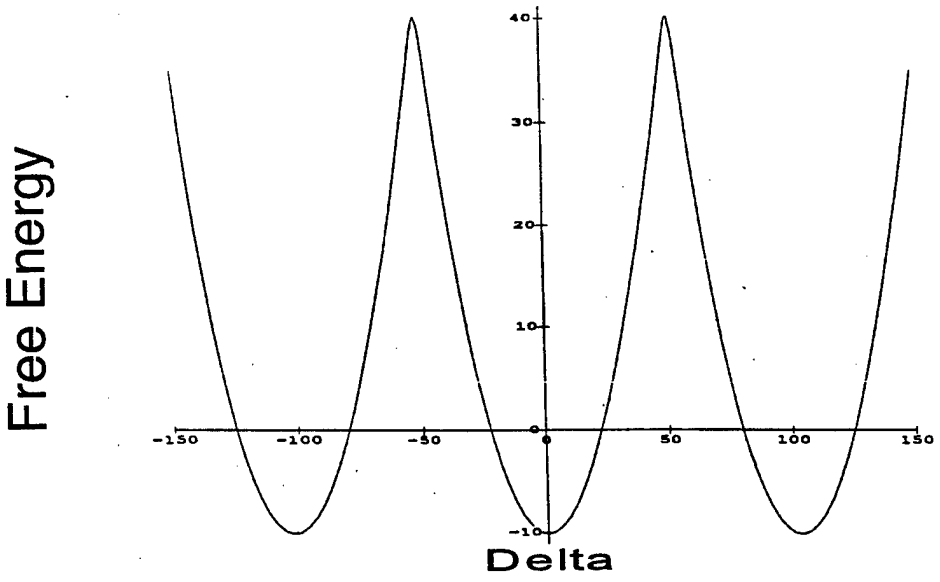

Figure 3. Free energy as a function of Δ at 523°K, i.e. above the transition temperature for the case 3.1.

In Fig. 2, the free energy plotted as a function of Δ for a higher temperature T = 162.2°K indicates three equal minima including one at $\Delta = 0$. The minimum of $\Delta = 0$ becomes an absolute one at a still higher temperature T = 187.8°K or in dimensionless form T = 3.59 as shown in Fig. 3. The insertion of $\Delta \simeq 0$ into (13) and (14) leads to $\langle \hat{r}_i \rangle \neq 0$ *and* $\langle \hat{n}_{di} \rangle \simeq 0$ signifying a vanishing net spin and partial or total anti-alignment at the *i*-th site. The transition or critical temperature is the one corresponding to the situation depicted in Fig. 2 and is 162.2°K or in dimensionless form T = 3.1 for this system. Experimentally, the ferromagnetic and anti-ferromagnetic phases are characterized by low and high resistivity.

The introduction of an external magnetic field, corresponding to a non-zero value for M, removes the symmetry of F about $\Delta = 0$ because it favors one spatial direction over the other and, and more importantly causes an upward shift of the transition temperature. The magneto-resistive effect, in our model, can thus be observed in the temperature domain between the lower T_c corresponding to the absence of an external magnetic field and the higher T_c obtained when a field is present. This is because in this temperature zone, an anti-ferromagnetic system exhibiting high resistivity in the absence of an external magnetic field can be driven into a ferromagnetic phase characterized by low resistivity by a sufficiently intense applied magnetic field. The introduction of such a field would have, on the other hand, little effect on the resistivity below the Curie temperature.

The suddenness of the transition from one phase to another appears to be in contrast to the gradual change observed in experiments. One may, however, note that the calculations presented here refer to a single site while actual measurements reflect bulk properties. The transition temperature is very sensitive to the input parameters and a modest variation of these from site to site could well account for the observed graduality of T_c by performing an appropriate averaging procedure.

3.2. Case where B/2t is smaller than |U + 2E|

Turning our attention to a case where B/2t is less than |U + 2E|, we choose $E = 1.032 \times 10^{-2}$ eV, $U = -4.128 \times 10^{-2}$eV, $B = 1.548 \times 10^{-2}$ eV and $t = 0.516 \times 10^{-2}$ eV and M = 0. In dimensionless units this corresponds to E = 1, U = -4, B = 1.5, t = 0.5 and M = 0. Thus, B/2t = 1.5 which is less than |U + 2E| = 2. In this situation, the system manifests itself in an anti-aligned state below a critical temperature. In this circumstances, the system evidently possesses a vanishing net spin at the *i*-th site, which may be interpreted as pair formation characteristic to a superconducting phase. This is depicted in Fig. 4 where the free energy at T = 1.2°K is plotted as a function of Δ and exhibits an absolute minimum at $\Delta = 0$. Fig. 5 displays the number of pairs per site as a function of temperature, with the pair formation probability dropping sharply at a temperature greater than T = 1 in dimensionless units corresponding to T = 120°K.

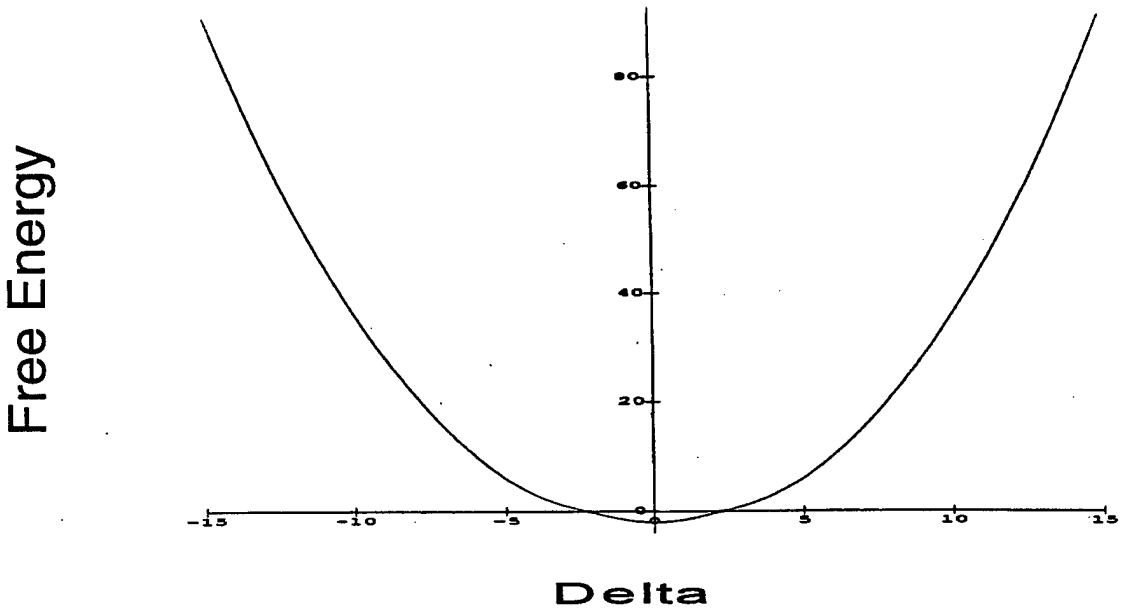

Figure 4. Free energy as a function of Δ at 1.2°K, i.e. below the transition temperature for the case 3.2 where anti-alignment or pairing is preferred.

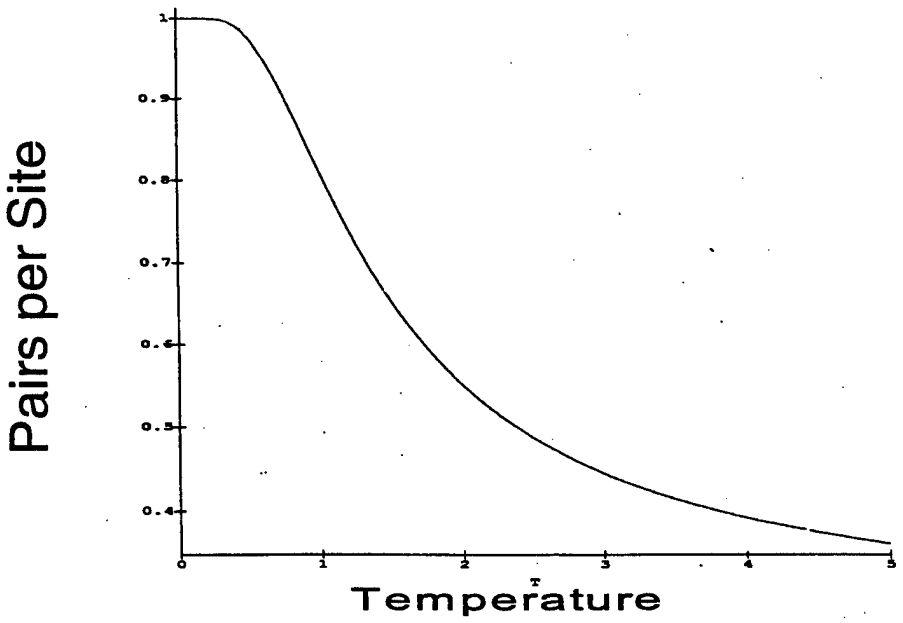

FIGURE 5. Number of pairs $\langle \hat{r} \rangle$ at a site as a function of temperature.

In our investigation, the ratio between |U| and $k_B T_c$ is to lie approximately between 3 and 5 for a transition relevant to superconductivity to occur. Furthermore, there is no upper limit to this T_c.

4. CONCLUSIONS

The present analysis demonstrates that the same Hamiltonian has the ability, depending on the choice of parameters, to produce at least two different sorts of phase transitions, one relevant to magnetoresistance (colossal or otherwise), and the other arguably relevant to superconductivity. One behavior may be made to merge smoothly into the other merely by varying continuously the concomitant parameters. The latter acquires particular signficance in light of the fact that **both behaviors are exhibited by the same class of materials**. Doping may well be the experimental technique of choice to "push" the materials either into the magnetoresistive or the superconductor-like behavior.

ACKNOWLEDGMENT

The authors are pleased to acknowledge the guidance and many fruitful discussions with Dr. M. Ciftan. They are particularly thankful to the U.S. army and research office and Batelle for a grant no. TCN9046-DO 1871-USARO. One of us, FBM is also pleased to acknowledge a travel grant no. DAAH04-96-1-0184 from the U.S. army research office and the warm hospitality of the local organizing committee of the XX International Workshop on Condensed Matter Theories.

REFERENCES

[1] For a recent survey, see e.g., "Recent Developments in High Temperature Superconductivity," eds. J. Klamut et al. (Springer Verlag 1996).

[2] E. E. Fullerton, M. J. Conover, J. E. Mattson, C. H. Sowers, and S. O. Bader, Appl. Phys. Lett. **63**, 1699 (1993).

[3] S. Jin, T. H. Tiefel, M. McCormack, R. A. Fastnacht, R. Ramesh, and L. H. Chen, Science **264**, 413 (1994).

[4] L. H. Chen, S. Jin, T. H. Tiefel, and R. Ramesh, Appl. Phys. Lett. **64**, 1039 (1994).

[5] M. McCormack, S. Jin, T. H. Tiefel, R. M. Fleming, J. M. Phillips, and R. Ramesh, Appl. Phys. Lett. **64**, 3045 (1994).

[6] S. Jin, T. H. Tiefel, M. McCormack, H. M. O'Bryan, L. H. Chen, R. Ramesh, and D. Schurig, Appl. Phys. Lett. **67**, 557 (1995).

[7] J. Fontcuberta, B. Martinez, A. Seffar, S. Piñol, J. L. Garcia-Muñoz, and X. Obradors, Phys. Rev. Lett. **76**, 1122 (1996).

[8] This Hamiltonian has been introduced by S. Picozzi and F. B. Malik, in: "Thermodynamic transition from an anti-aligned to an aligned spin state relevant to colossal mangnetoresistance," submitted for publication to Phys. Rev. Lett. (1996).

However, see also: J. Aliaga, A. N. Proto and V. Zunino, Condensed Matter Theories, **7**, 335 (1992), in which a slightly less general Hamiltonian is derived from Hubbard's.

[9] A. N. Proto, Condensed Matter Theories, **5**, 355 (1990), and refs. therein.

[10] The literature on the subject is indeed immense. The original articles by E. T. Jaynes,however, still constitute a valid introduction: E. T. Jaynes, Phys. Rev. **106**, 620 (1957); Ibid. **108**, 171 (1957).

[11] For a somewhat more extended outline of the procedure utilized herein, see: S. Picozzi, A. N. Proto and F. B. Malik: "On the formation of fermion pairs as a function of temperature," to be submitted for publication to Phys. Rev. B (1997).

BOSE CONDENSATION IN ^{4}He AND NEUTRON SCATTERING

Richard N. Silver

MS B262 Theoretical Division
Theoretical Division
Los Alamos, NM 87505, USA
e-mail: rns@loke.lanl.gov

The discovery of superfluidity in liquid ^4He below $T_\lambda = 2.17^oK$, and its phenomenological characterization since then, has been one of the great success stories of condensed matter physics. The relation of superfluidity to the behavior of atoms was conjectured by F. London in 1938. Superfluidity is a manifestation of the Bose condensation of helium atoms, the extensive occupation of the zero momentum state. Ever since ^4He has been the paradigm in the search for Bose condensates in other systems. At the Pune meeting we have heard exciting new evidence for Bose condensates of laser cooled alkali atoms in magnetic traps [1], of excitons in Cu_2O [2], and possibly pre-formed Cooper pairs of electrons in the high T_c perovskite superconductors [3]. There remains the holy-grail of forming a Bose condensate in spin-polarized hydrogen [4].

Laser cooled alkali atoms in magnetic traps [1] are much closer to ideal Bose condensation than superfluid ^4He. The densities are low, interaction effects are small, and they can be approximated as a weakly interacting dilute Bose gas. The fraction of atoms n_o condensed in the zero momentum state proceeds from zero at a critical temperature $T = T_c$ to nearly one at $T = 0^oK$. The momentum distribution $n(p)$ has a δ-function spike at $p = 0$ with an integrated intensity of n_o. The momentum distribution can be measured by experiments in which the magnetic trap is released, allowing the velocities of the escaping atoms to be observed by time-of-flight. The results conform to expectations within small corrections. Very recent experiments have discovered quantum coherent phenomena such as the atomic equivalent of lasing and quantum interference between two traps.

In contrast, liquid ^4He is a strongly interacting Bose system. That complicates the experimental verification of F. London's prediction that the superfluid transition should be associated with an $n_o\delta(p)$ spike in $n(p)$. The strong interactions dramatically alter $n(p)$ from an ideal Bose gas. Sophisticated many-body calculational methods, such as Greens Function Monte Carlo [8] (GFMC) for zero temperature and

Path Integral Monte Carlo [9] (PIMC) methods for non-zero temperatures, have been developed for such problems. They predict an n_o of only about 0.10 at $T = 0^oK$. This small value contrasts with alkali Bose condensates where n_o is near one. The 90% non-condensate ^4He atoms undergo quantum zero-point motion with momenta spread over a width of about $1\mathring{A}^{-1}$.

In the current excitement for new types of Bose condensates, and new phenomena such as atom lasers, it may be useful to recall the older story of the experimental verification of a relation between superfluidity and Bose condensation in ^4He. This topic has been investigated over many years by neutron scattering experiments and quantum many-body theory. My goal is to illustrate the difficulties of establishing the existence of a Bose condensate in a strongly interacting system, even though its macroscopic effects are manifest. I assume readers have access to a review by Silver and Sokol [5] which emphasizes the neutron scattering theory through 1990 and a review by Snow and Sokol [6] of the *deep inelastic neutron scattering* (DINS) (or *neutron Compton scattering*) experiments through 1995. Another good source is the 1989 book *Momentum Distributions* which addresses related Compton scattering experiments throughout physics. These reviews present the details, equations and data. I focus here on the key concepts, the current status and some recent developments. The insight gained may also be useful for other momentum distribution studies.

Direct experimental observation of $n(p)$ in ^4He has proved elusive. It can not be measured by kinetic experiments on escaping atoms, because ^4He is self bound. Hohenberg and Platzman [10] suggested in 1966 that the best hope for measuring $n(p)$ is DINS. This is the neutron analogue of X-ray Compton scattering measurements of electron momentum distributions in solids and molecules. But after decades of effort and hundreds of research papers, the conclusion reached is that the strong interactions among ^4He atoms invalidate a simple *impulse approximation* (IA) interpretation of DINS experiments. The Bose condensate δ-function predicted in the dynamical structure function by the IA is irretrievably broadened. Only circumstantial evidence remains for a correlation between superfluidity and Bose condensation in ^4He. It consists of excellent quantitative agreement between experiment and *ab-initio* many-body theories, which predict a Bose condensate. But this requires a more sophisticated theory for what DINS measures than the IA.

More generically, *deep inelastic scattering* refers to experiments in which a high energy probe particle scatters at sufficient energy $\hbar\omega$ and momentum $\hbar Q$ transfers that the incoherent dynamical structure function for single particle scattering dominates the coherent structure function for interference scattering between particles. For this concept to be applicable to neutron scattering from ^4He, Q and ω must be much larger than the scales set by the phonon-roton spectrum or the static structure function, $S(Q)$, related by Fourier transform to the radial distribution function $g(r)$. This scale is approximately $Q \geq 5\mathring{A}^{-1}$. The *impulse approximation* (IA) to deep inelastic scattering further assumes that a target particle recoiling from a scattering event has high kinetic energy compared with potential energies with neighboring particles. This is an excellent assumption for x-ray Compton scattering studies of electronic momentum distributions in solids, and for electron scattering studies of subtructure of nucleons in high energy physics. The IA incoherent structure function $S(Q,\omega)$ has a simple integral relation to single-particle momentum distribution $n(p)$. The Compton profile $J(Y,Q) \equiv QS(Q,\omega)$ is a universal function of a scaling variable

$Y \equiv (\omega - \hbar Q^2/2M)/Q$ and independent of Q [11]. For DINS from liquid ^4He, a condensate would produce a $n_o\delta(Y)$ peak in the Compton profile, corresponding to a peak in $S(Q,\omega)$ at the recoil energy $\omega = \hbar Q^2/2M$ with integrated intensity proportional to n_o. This prediction provides motivation to use DINS experiments to study the relation of Bose condensation and superfluidity in ^4He.

Unfortunately, this IA ideal can not be reached for liquid ^4He at any feasible Q due to *final state effects* (FSE). Even though experimental Q's can now reach deep into the DINS range, interactions of the recoiling helium atom with neighboring atoms broaden the Compton profile. This broadening may be represented as a convolution of $J_{IA}(Y)$ in Y with a FSE broadening function $R(Y,Q)$. The combination of a FSE theory and quantum many-body calculations of $n(p)$ yields quantitative predictions for neutron Compton profiles. The remarkable story of Monte Carlo and quantum many-body calculations of $n(p)$ has been told elsewhere [8,9]. In these proceedings, I emphasize developments in the theory of FSE, and the comparison of recent DINS experiments to theory.

The first physical picture of FSE was presented by Hohenberg and Platzman [10] in 1966. A helium atom recoiling from a neutron scattering event has a collision lifetime with neighboring atoms, $1/\tau = \hbar Q\rho\sigma(Q)/M$. Here ρ is density, $\sigma(Q)$ is the He-He cross section and M is mass. $R(Y,Q)$ would be a Lorentzian in Y of width $\Delta Y = \rho\sigma(Q)$. If the ^4He-^4He potential had a hard core, such that $\sigma(Q)$ went to a constant at high Q, the Compton profile would obey Y-scaling without satisfying the IA. The IA would not be valid no matter how high the Q. The actual $\sigma(Q)$ has been measured and found to decrease slowly with increasing Q (approximately logarithmically), modulated by 'glory' oscillations resulting from quantum interference between identical particles. The corresponding potential is steeply repulsive at short distances. The IA would be approached equally slowly with increasing Q, while the required instrumental energy resolution would scale as $\Delta\hbar\omega \propto Q^{-1}$. The corresponding required neutron intensity increases approximately as Q^3 for most spectrometers providing an intensity limit to the achievable Q.

However, this Lorentzian broadening FSE theory disagrees with experiment even for the normal fluid where the PIMC prediction for $J_{IA}(Y)$ is approximately Gaussian except as it tails off at large $|Y|$. Normal fluid experiments are within a few % of the PIMC-IA prediction. The Lorentzian FSE theory predicts too much broadening as well as Lorentzian tails decreasing as $O(Y^{-2})$ at large $|Y|$ that are not observed. A Lorentzian $R(Y,Q)$ would also violate the kinetic energy sum rule which requires the second moment of the Compton profile to have the IA value. Thus, the sum rule requires the second moment of $R(Y,Q)$ in Y to be zero.

Another approach to FSE has been to develop additive corrections to the IA as a truncated power series in inverse powers of Q [12,13]. The first term in this expansion is the IA. The next term decreases as Q^{-1} and involves the semi-diagonal two-body density matrix $\rho_2(r,r";r',r")$. It is natural (although, we shall learn later, incorrect) to assume that only the first few terms in this series are important at high Q, and therefore that FSE fall off as $O(Q^{-1})$. No such additive corrections to the IA can cancel a Y-scaling Bose condensate δ-function.

The empirical failure of the Lorentzian broadening theories in the normal fluid and the additive correction FSE theories decreasing as $O(Q^{-1})$ encouraged investigation of $n(p)$ by DINS at increasingly large Q [14]. Early reactor neutron experiments

with their thermal neutron spectrum could not practically exceed $Q = 12\mathring{A}^{-1}$. But the advent of pulsed spallation neutron sources in the 1980's with their high flux of epithermal neutrons enabled practical experiments at Q's up to $30\mathring{A}^{-1}$, well into the DINS range.

Unfortunately, as we shall see, Nature frustrates any hope that FSE could be ignored at any feasible momentum transfers Q. The correct qualitative physics of FSE was first identified by Gersch and Rodriguez [15] (GR) in 1973. The positions of atoms in the ground state of liquid ^4He are correlated as described by their radial distribution function $g(r)$. They stay away from the repulsive core of neighboring atoms in order to minimize their energy. A high kinetic energy ^4He atom recoiling from a neutron collision must travel a distance on the order of the first peak ($\approx 3\mathring{A}^{-1}$) in the radial distribution function before it begins to scatter at the rate $1/\tau$ of the Hohenberg-Platzman theory. This significantly reduces FSE, but it does not eliminate them. FSE still scale like the cross section $\sigma(Q)$. The GR quantitative calculation of FSE used an eikonal approximation for the scattering, a novel cumulant expansion of $S(Q,\omega)$ involving again the semi-diagonal two-body density matrix ρ_2, and an approximation to ρ_2 in terms of the one-body density matrix $\rho_1(r,r')$ and the radial distribution function $g(r)$. The resulting FSE broadening function $R(Y,Q)$ is non-Lorentzian with a central peak for small $|Y|$, rapidly damped oscillations at large $|Y|$, and a zero second moment in Y as required by the kinetic energy sum rule.

Actually, the above description is a paraphrase in modern language of what GR accomplished. Their work was perhaps 15 years ahead of its time, phrased in different language, and largely ignored. One can speculate about the reasons. It was published prior to the realization of the general character of Y-scaling in all Compton scattering (or deep inelastic scattering) experiments throughout physics [11]. It appeared at a time when the only experiments had been performed at the low Q's of reactor sources, and Monte Carlo and variational calculations of $n(p)$ were not accurate. Their quantitative predictions were buried in an experimental paper which claimed to measure $n_o \simeq 0.02$, in disagreement with both many-body theory and all subsequent experiments. Their step function approximation to the radial distribution function is unrealistic. The approach did not make contact with the more familiar methods of diagrammatic perturbation theory. In retrospect, their quantitative theory underestimated the FSE broadening.

In 1987-89 the author [16] (S) developed a new approach to FSE using a Liouville projection superoperator expansion of $S(Q,\omega)$ about the ground state wave function. The superoperator projected all single particle excitations of momentum transfer $\hbar Q$ above the ground state. The expansion was truncated at the level of ρ_2, which again is approximated in terms of the $g(r)$ and ρ_1 in a somewhat different manner than GR. Although the expansion generates many terms, all terms which did not Y-scale in the asymptotically high Q limit for hard core potentials are dropped. The theory has a perturbative representation as a Dyson equation in which FSE are vertex corrections involving additional single particle excitations. The two-body t-matrix is approximated by semiclassical methods which are accurate at high Q. The small parameter is a product of the t-matrix and ρ_2 which is well behaved. The Dyson equation corresponds to an infinite order partial resummation of the additive FSE correction series. This resummation has an entirely different asymptotic Q dependence than the first correction to the IA in the additive series.

The result is, like the GR theory, a convolution broadening $R(Y,Q)$ of the IA Compton profile $J_{IA}(Y)$. Moreover, it may be described by a simple physical picture. The scaling variable Y is canonically conjugate to the distance traveled by a recoiling ^4He atom. The FSE broadening function $R(Y,Q)$ is the Fourier transform of the classical scattering probability of no collisions as a function of this distance. This probability depends on real space correlations in the ground state wave function through the radial distribution function. The inputs required to calculate FSE are all known from experiment, so the theory has no adjustable parameters. The central peak of $R(Y,Q)$ is about twice as wide in Y as the GR calculation. FSE effects on the normal fluid Compton profile are very small in agreement with experiment, because the IA profile is almost Gaussian and FSE do not alter the second moment of the Compton profile. But for the superfluid where the IA Compton profile is very non-Gaussian, the FSE broadening is sufficient to eliminate the distinct Bose condensate δ-function peak predicted by the IA. The Q dependence follows $\sigma(Q)$, so that FSE decrease very slowly with increasing Q.

My theory appeared a year or two before the high Q experiments from the new generation of pulsed spallation neutron sources. These beautiful experiments are best described in the aforementioned review by Snow and Sokol [6] to which we refer readers. After correcting the data for instrumental effects such as resolution and backgrounds, there is almost perfect agreement within statistical error between experiment at $Q = 23\mathring{A}^{-1}$ and ab initio predictions for $J(Y,Q)$ obtained by combining GFMC and PIMC $n(p)$ with the author's theory for FSE [16]. This is true even though the shape of the Compton profile varies significantly with temperature, becoming more sharply peaked and less Gaussian as lower temperatures. As $g(r)$ changes little in this range, the same $R(Y,Q)$ can be used at all temperatures to a good approximation apart from a simple linear scaling of the Y variable with density. Thus the experimental data are consistent with calculations that predict a Bose condensate fraction $n_o \approx 10\%$. The forward prediction of experiment by S-PIMC and S-GFMC theory is quite good at high Q [17].

Detailed comparisons with other FSE theories can be made assuming the $n(p)$ calculations are correct [18]. There is dramatic disagreement with the IA theory at superfluid temperatures especially in the region near $Y = 0$ where the condensate would contribute. There is similar disagreement with additive FSE corrections that allow a condensate δ-function to persist. The broadening predicted by GR is about a factor two too small.

Not everything is perfect, however. One unexplained discrepancy is a slight asymmetry in which the $Y \ll 0$ ($Y \gg 0$) side of the Compton profile is slightly lower (higher) than experiment [6]. The agreement is not so good at smaller Q [19], as should be expected from the approximations employed. These discrepancies point to the need for further development of the DINS theory.

The inverse problem of extracting $n(p)$ and $R(Y)$ from experiment in the presence of noise, instrumental broadening, and backgrounds is ill-posed and more difficult. One approach is to assume the FSE theory to be correct, and to fit a model form for $n(p)$ that includes a Bose condensate with n_o as a parameter along with other known singular structures induced by the condensate. Using this model fitting approach, Snow and Sokol [6] report broad trends in the extracted values for n_o and the kinetic energy as functions of temperature and density that are in reasonable

agreement with expectations. However, the error bars on n_o are approximately $\pm 2\%$ which are not small compared to n_o itself. With those errors it is impossible to say with precision that there is evidence for a sharp transition from zero to non-zero n_o as the temperature is lowered past T_λ. Indeed, the data below T_λ may also be adequately fit by $n(p)$ that is a sum of narrow and wide Gaussians that have no δ-function. Attempts to extract $R(Y,Q)$ assume, conversely, that the GFMC and PIMC calculations of $n(p)$ are correct. The result is reasonably close to my theory at high Q, although there are differences in the damped oscillatory wings at large $|Y|$. There is no estimate of the statistical significance of those differences.

The most serious theoretical criticism of the my approach to FSE has addressed the approximation to the semi-diagonal two-particle density matrix ρ_2. Ristig and Clark [20] in 1989 pointed out that the my approximation, while satisfying the $p-$ and $q-$ sum rules on ρ_2, does not satisfy other known properties such as symmetry and sequential relations. The different approximations of GR and by Rinat [21] also satisfy these properties to a limited extent. Ristig and Clark suggest a general structure for ρ_2 based on hypernetted chain theory which satisfies all the known constraints including sum rules, symmetry and sequential relations. Unfortunately, this form has not yet been quantitatively used in my theory.

Carraro and Koonin (CK) in 1990 [22] presented a calculation of FSE that did not depend on approximations to ρ_2. They solved the scattering problem of a high Q recoiling atom moving in the instantaneous potential of a Jastrow approximation to the many-body wave function, the assumption being that neighboring atoms provide a static field. Their resulting $R(Y,Q)$ has approximately the same width central peak as I predicted at high Q, and so they also agree well with experiment. There are some differences between the two predictions in the damped oscillatory wings at large $|Y|$, but the available experiments are insensitive. They also predict a more severe Q dependence, but the discrepancies between of both CK and S theories with experiment increase at small Q and are comparable in magnitude.

In 1996 Mazzanti et al. [23] reexamined the GR theory using an HNC estimate for the semi-diagonal two-body density matrix ρ_2 based on the earlier work of Ristig and Clark. They claim essential agreement between the GR, CK and S predictions for the width of the central peak of $R(Y,Q)$ provided that a proper ρ_2 is used in GR theory. Experiments are insensitive to somewhat larger differences between theories in the damped oscillatory wings at large $|Y|$. In the original GR paper, their ρ_2 relied on a step function approximation to $g(r)$ at $r_o = 2.5\mathring{A}$ which gave too little FSE broadening. Mazzanti et al. note that a choice of $r_o = 2.1\mathring{A}$ in the original theory would also yield good agreement with experiment and the CK and S theories for $R(Y,Q)$. However, examination of the measured $g(r)$ reveals that there is almost no probability for collisions at $r = 2.1\mathring{A}$.

Thus, today there are three different theoretical approaches that are in quantitative agreement about the magnitude and character of FSE at high Q. What remains to be tested is whether use of a better ρ_2 in my theory would significantly alter its prediction.

A focus of recent experimental work has been systematic studies as a function of Q [19,24]. Andersen et al. [24] in 1994 measured the FWHM (full-width-half-maximum) and peak position of $S(Q,\omega)$ in the range $3 \leq Q \leq 12\mathring{A}^{-1}$. They observe at least four oscillations in the FWHM and peak position in both the normal fluid and

the superfluid that appear to track the aforementioned glory oscillations of the He-He cross section. Their interpretation is that it provides model-independent evidence that final state effects are present in the data which vary like $\sigma(Q)$. However, the Q's are not large enough to ignore coherent scattering. The shift in peak position also suggests there are real part of the self-energy corrections to the IA in addition to the vertex corrections associated, in my theory, with FSE broadening.

The most significant attempt to use Q-dependent data has been by Glyde and coworkers [25]. They fit the dynamic structure function to a cumulant expansion in the Fourier transform of Y (to paraphrase) using up to sixth order cumulants. They claim to separate the contributions from the IA and FSE by their differing Q dependencies. For example, we know that the second cumulant (moment) of the Compton profile is independent of FSE. But in the fourth moment the IA contributions are independent of Q varying as the fourth cumulant of $n(p)$, while the FSE contribution varies as Q^{-2} with a coeffecient. proportional to the force-force correlation function. They claim to observe just such Q dependencies in the data. Such fits are used to simultaneously infer $n(p)$ and $R(Y,Q)$.

Two comments on this approach may be offered. First, if ^4He had a hard core potential, there would be no way to separate the IA and FSE contributions using differing Q-dependences as they would both Y-scale. The cumulant expansion would not converge, e.g. in the fourth moment the force-force correlation function would be infinite as it would be the expectation of products of two δ-functions. Although the real He-He potential may not be hard core, it is steeply repulsive such that this cumulant expansion should converge slowly at high Q. It seems unlikely that only a few terms in the expansion provide an adequate description. This discussion is obviously related to the earlier controversy regarding additive vs. convolution theories of FSE. Second, prior work by Sokol and collaborators has found statistical evidence for the adequacy of a two Gaussian description of $n(p)$. The data analyzed by Glyde et al. are not dramatically better, so the claim to determine many more parameters seems inconsistent.

"Where there's smoke, there's fire." This old adage is good enough for me. I am sure about the correlation between Bose condensation and superfluidity. The empirical manifestations are overwhelming. We have achieved excellent quantitative agreement between *ab initio* theory and high precision DINS experiments. Further efforts to understand the 'smoke' should tell us more about the 'fire'. But for those who insist on "Seeing is believing!", a new approach other than DINS will be needed to directly observe a Bose condensate δ-function in the momentum distribution of superfluid ^4He.

ACKNOWLEDGMENTS

This research was funded by the U. S. Dept. of Energy. We acknowledge the Army Research Office for financial assistance to attend the Workshop on Condensed Matter Theories XX and the U. S. / India Joint Seminar on Bose Einstein Condensation and Pairing Phenomena in Pune, India where this paper was presented in December, 1996.

REFERENCES

[1] E. Cornell, these proceedings.

[2] G. Mysyrowicz, these proceedings.

[3] M. Randeria, these proceedings.

[4] I. Silvera, these proceedings.

[5] R. N. Silver, P. E. Sokol, in *Recent Progress in Many-Body Theories,* **2** Y. Avishai, ed., Plenum Press, New York (1990), p. 221-250.

[6] W. M. Snow, P. E. Sokol, J. Low Temperature Physics **101**, 881-928 (1995).

[7] R. N. Silver, P. E. Sokol, eds., *Momentum Distributions*, Plenum Press, New York (1989).

[8] P. Whitlock, R. M. Panoff, Can. J. Phys. **65**, 1409 (1987).

[9] D. M. Ceperley, E. L. Pollock, Can. J. Phys. **65**, 1416 (1987).

[10] P. C. Hohenberg, P. M. Platzman, Phys. Rev. **152**, 198 (1966).

[11] G. B. West, Physics Reports **18C**, 263 (1975).

[12] V. F. Sears, Phys. Rev. B**30**, 44 (1984).

[13] H. A. Gersch, L. J. Rodriguez, P. N. Smith, Phys. Rev. A**5**, 1547 (1972).

[14] H. R. Glyde, E. C. Svensson, in *Methods of Experimental Physics* **23B**, D. L. Price, K. Skold, eds., Academic Press (1987), p. 303; E. C. Svensson, V. F. Sears, Physica **137B**, 126 (1986).

[15] H. A. Gersch, L. J. Rodriguez, Phys. Rev. A**8**, 905 (1973); H. A. Gersch, L. J. Rodriguez, H. A. Mook, Phys. Rev. A**9**, 2085 (1974).

[16] R. N. Silver, in *Condensed Matter Theories* **3**, J. S. Arponen, R. F. Bishop, M. Manninen, eds., Plenum Press, New York (1988), p. 131; R. N. Silver, Phys. Rev. B**37**, 3794 (1988); Phys. Rev. B**38**, 2283 (1988); Phys. Rev. B**39**, 4022 (1989).

[17] T. R. Sosnick, W. M. Snow, P. E. Sokol, R. N. Silver, Europhysics Letters **9**, 707 (1989).

[18] T. R. Sosnick, W. M. Snow, P. E. Sokol, R. N. Silver, Phys. Rev. B**43**, 216 (1991).

[19] K. W. Herwig, P. E. Sokol, W. M. Snow, R. C. Blaisdell, Phys. Rev. B**44**, 308 (1991).

[20] M. L. Ristig, J. W. Clark, Phys. Rev. B**40**, 4355 (1989).

[21] A. S. Rinat, Phys. Rev. B**40**, 6625 (1989); **42**, 9944 (1990).

[22] C. Carraro, S. E. Koonin, Phys. Rev. Lett. **65**, 2792 (1990); Phys. Rev. B**41**, 6741 (1990).

[23] F. Mazzanti, J. Boronat, A. Polls, Phys. Rev. B**53**, 5661 (1996).

[24] K. H. Andersen, et al., Physica B**197**, 198 (1994).

[25] H. R. Glyde, Phys. Rev. B**50**, 6726 (1994).

EXPERIMENTS DESIGNED TO ACHIEVE BEC IN SPIN-POLARIZED HYDROGEN

Isaac F. Silvera, Ismardo J. Bonalde, Thilo M. Brill
Konstantin Penanen, and Latha Venkataraman

Lyman Laboratory of Physics
Harvard University, Cambridge, MA 02138 USA

1. INTRODUCTION

A program to produce a weakly interacting atomic gas of identical bosons in spin-polarized hydrogen (SPH) was started in the early 1970's with the objective of studying Bose-Einstein condensation (BEC). Although great progress has been made in the study of atomic hydrogen it has not yet been Bose condensed. By contrast, experimental efforts to Bose condense alkali gases began in the late 1980's and a gas of rubidium was Bose condensed for the first time in 1995. Dramatic evidence was provided by the observation of the growth of the condensate density in the center of an inhomogeneous magnetic trap when conditions for BEC were met. In this paper we shall review the progress on spin-polarized hydrogen and compare this system to the alkalis.

2. EARLY STUDIES OF SPH

Under ordinary conditions found in nature, hydrogen is a very reactive atom and is found strongly bonded to other atoms. In particular the H_2 molecule is very stable and requires 4.6 eV (52,000 K) of energy to be dissociated into two free atoms. In the hydrogen molecule the electron spins are in a singlet spin state. By contrast two H atoms in the triplet state (spin-polarized) interact weakly, with a potential minimum of about 0.55 meV (6.4 K), as shown in Fig. 1. The triplet hydrogen potential ($^3\Sigma$) does not support a bound state; it has an effective repulsive interaction with an s-wave scattering length of 0.72 Å. In spite of this, a gas of unpolarized hydrogen rapidly decays in density by 3-body recombination to form H_2 molecules. Silvera and Walraven [1] devised a method to stabilize atomic hydrogen by producing a very low density gas of H in a room temperature discharge and fluxing it into a low temperature cell in a high magnetic field, B.

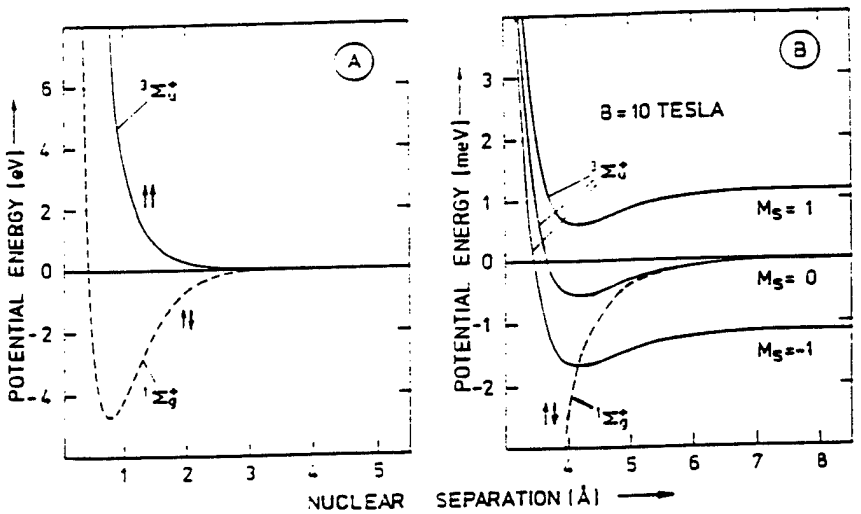

Figure 1. (a) The singlet and triplet interatomic potentials of hydrogen according to calculations of Kolos and Wolniewicz [2]. (b) The hydrogen potentials on a magnified scale and in a magnetic field.

Since the ratio of electron spin-down atoms to spin-up atoms is $\exp(\mu_B B/k_B T)$, where μ_B is the Bohr magneton, k_B the Boltzmann constant, and T the temperature, for large B/T ratio the equilibrium state of the gas will be spin-down, or the gas will be spin-polarized. The walls of the cell were covered with a film of liquid helium to inhibit condensation on the walls where recombination can be more rapid. Since the H-He adsorption potential is very weak, only at very low temperatures, of order 200 mK, does H begin to adsorb on the helium surface at densities such that 3-body surface recombination becomes important.

When spin-polarized hydrogen was first stabilized, the achieved density was about 10^{14} cm^{-3} at temperatures of a few hundred millikelvin. This was far from the conditions necessary for BEC given by

$$T_c = 3.31 \frac{\hbar}{m k_B} n^{2/3} \quad . \tag{1}$$

For hydrogen with mass $m = 1$ amu at a temperature of 100 mK, the critical density n is 1.57×10^{19} cm^{-3}. Intense efforts were started by several groups to achieve BEC. The progress is reviewed in detail by Silvera and Walraven [3] and we shall sketch the results here. Densities of order 5×10^{18} cm^{-3} were achieved by compressing a gas of SPH, but in this density range 3-body recombination becomes an important loss mechanism. Two problems arose. First, it was difficult to increase the density further due to the increased loss rate; more important, the large amount of energy released by recombination heated the sample to several hundred millikelvin.

A second approach was to achieve BEC at low densities and low temperatures. With ^{3}He on the surface, due to the lower adsorption energy, a gas of SPH could

be cooled below 100 mK by thermalization with the walls. Thermalization is due to adsorption-evaporation of H atoms from the helium walls. However, at around 50 mK the gas loses thermal contact with the walls. Atoms which stick to the walls reside for long periods of time; the surface density builds up and recombination on the surface heats the cell, again preventing the attainment of conditions for BEC.

It was also realized that hydrogen atoms on the He surface form an almost ideal 2-D gas as they are weakly bound to the He surface. This was recognized as a candidate for a new superfluid with a Kosterlitz-Thouless (KT) transition [4]. The critical temperature for a KT transition is given by

$$T_c^{KT} = \pi\hbar^2\sigma_s/2k_B m \quad . \tag{2}$$

where σ_s is the superfluid surface coverage. The low-density relationship between the surface coverage σ and the bulk density n is

$$\sigma = n\lambda_{th} exp(\epsilon a/k_B T) \tag{3}$$

where $\lambda_{th} = (2\pi\hbar^2/mk_B T)^{1/2}$ is the thermal de Broglie wavelength and ε_a is the adsorption energy of H on He. Thus, by simply filling a cell with a density n, in thermal equilibrium, a 2-D gas of known surface density is also present. In the initial efforts to study this 2-D gas, high surface coverages were not achievable as the increased recombination heated the cell. A number of schemes were proposed to overcome the severe problems which were encountered and observe BEC at high densities $[5-6]$. However, the most important idea was from Hess [7] who proposed to build a magnetic trap and use magnetic forces to isolate SPH from the cell walls and thereby eliminate wall recombination.

A static magnetic field does not have a spatial field maximum and therefore SPH atoms in the ground state cannot be trapped by such a field, but must be contained by the normal walls of a cell. In this configuration, wall recombination sets a limit to the achievable density and temperature. However, Maxwell's equations do allow a static field minimum and in principle isolation of the atoms from the walls. To further understand the trapping scheme we refer to the hyperfine diagram in Fig. 2. In the high field limit, the states labeled a and b are predominantly electron spin-down and are attracted to high fields where their energy is lowest. These high-field seekers were the states studied in the first experiments on SPH. States c and d are low field seekers and will be attracted to a field minimum. Thus, an experimental configuration with a field minimum can trap states c and d and isolate them from the walls of a cell. Hess et al. [8] built a trap with an Ioffe configuration: a radial field minimum due to superconducting race track magnets, with an axial minimum due to two solenoidal "pinch" magnets is shown in Fig. 3.

Although both c and d-state atoms are initially trapped, the c-state atoms are depleted due to rapid spin exchange-scattering, leaving a gas of pure spin-up polarized atoms in the d-state. The density of the gas was in the $10^{13} - 10^{14}$ cm^{-3} range and the temperature of order 50 mK. The gas was then cooled by evaporative cooling. In this technique the field of one of the pinch magnets is reduced, which lowers the trap depth. Energetic atoms can escape over the magnetic barrier, while the remaining atoms thermalize to lower temperatures by elastic collisions. The field barrier can be continually reduced in height to achieve extremely low temperatures. The optimum

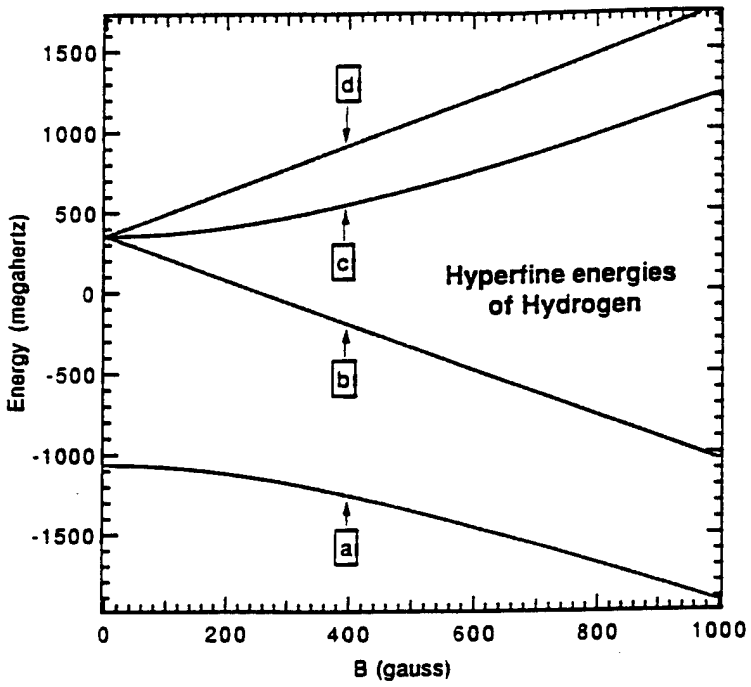

Figure 2. The hyperfine energy levels of atomic hydrogen in a magnetic field.

rate of lowering of the field is determined by the collision rate $\sigma_e n\bar{\nu}$, where σ_e is the elastic scattering cross section and $\bar{\nu}$ is the collision velocity.

Evaporative cooling is limited by inelastic spin-flip processes which become important at higher density as the spin-flip rate is second order in n. As the gas cools the total number of atoms decreases but the central density increases. Spin-flipped atoms, mainly low energy atoms at the bottom of the trap, are ejected. However, if atoms are in the bottom of the trap where the density is high and the energy is lower than average, the gas heats subsequent to the loss of these colder atoms. This process sets a limit to the density and temperature in a trap.

The closest approach to BEC of hydrogen in a trap was by Doyle et al. [9] who evaporatively cooled to $\sim 100\mu$K, but were about a factor of 3 too high in temperature for BEC. This experiment stopped at this point due to detection sensitivity limits or inability to detect atoms when the total number of atoms in the trap was down to about 10^{10}.

3. COMPARISON TO THE ALKALIS

In the mid 1980's techniques were developed to laser cool atoms to microkelvin temperatures. By the late 1980's atomic physicists became interested in using this tool to attain BEC. It soon became clear that laser cooling alone would be insufficient, as the minimum attainable temperatures and densities were inadequate for BEC. A double cooling approach was taken. Atoms were pre-cooled by means of lasers and then further cooled in a magnetic trap by rf evaporative cooling. In this technique evaporative cooling is due to an rf field which induces spin-flip transitions, selectively

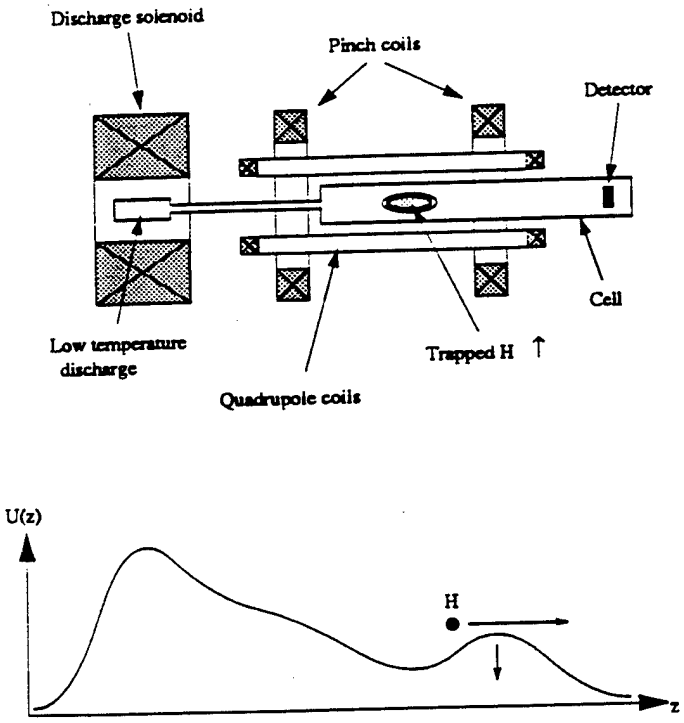

Figure 3. A magnetic trap for hydrogen showing the axial magnetic potential.

tuned to remove the most energetic atoms in the trap. BEC was observed in rubidium in 1995 by Anderson et al. [10] with about 10^4 atoms in the trap. Subsequently BEC was reported in Na [11] and Li [12].

There are two important reasons why the alkalis have enjoyed a successful path to BEC, compared to SPH. First, the alkalis have a much larger elastic scattering cross section than triplet hydrogen. The alkalis have s-wave scattering lengths of order 25 - 50 Å, whereas SPH has $a_s = 0.72$ Å. A figure of merit for the effectiveness of evaporative cooling is the ratio of cooling rate to the loss rate. Since the loss rate is mainly due to spin relaxation, which is roughly the same for the alkalis and hydrogen, the ratio of the figure of merits is proportional to the ratio of elastic cross sections

$$\frac{\sigma_e^{alkali}}{\sigma_e^{hydrogen}} = \left(\frac{a_s^{alkali}}{a_s^{hydrogen}} \right)^2 \sim 10^3 \ . \tag{4}$$

The second advantage of the alkalis is detector sensitivity. Alkalis in a trap are observed by illuminating the gas with a resonant laser beam and shadowing the gas onto a CCD detector. The sensitivity is 10's of atoms and in the first observation of BEC, of order 10^4 atoms were detected with a high signal-to-noise ratio. By contrast this technique is not easily applicable to hydrogen which has its first optical transition in the far UV, not the visible. In the experiment of Doyle et al. [9] a bolometer detector was used with a minimum number of detectable particles (MNDP) of 10^{10}

atoms. Thus, the alkalis have an experimental advantage for achieving and studying BEC.

4. CURRENT EXPERIMENTS ON HYDROGEN

In this section we shall discuss current or planned experiments on SPH at Harvard. There are two categories of experiments: 3-D traps and a 2-D KT-BEC experiment. There are two types of traps, a static trap and a microwave trap. Originally the static trap was to be part of a hybrid static-microwave trap, with the static trap used to pre cool atoms so that they could be loaded into the shallow microwave trap. With the recent development of more sensitive detectors it appears that BEC might be achieved directly in the static trap. The 2-D experiment is designed with an inhomogeneous magnetic field, which in principle should enable BEC to be observed in two-dimensions.

5. THE STATIC TRAP

The static trap is a flexible trap consisting of 11 superconducting magnet coils used for both the static and microwave trap. The cell, made of plastic (G10), is connected to the mixing chamber of a high cooling power Leiden Cryogenics dilution refrigerator; hydrogen is filled from a pulsed rf discharge. Helium which covers the walls of the cell and is important for the loading step, can be removed with a "film pump" after the gas is trapped and isolated from the walls. This improves the performance of the detectors, two bolometers located at either end of the cell. These bolometers, described elsewhere [13], are calculated to have an MNDP of between $10^3 - 10^4$ and atoms, or several orders of magnitude smaller than previously used bolometers in a trap. This large improvement is achieved by using state-of-the-art transmutation doped germanium thermometers to measure the heat released when hydrogen atoms recombine, and using geometric structures which capture a large percentage of the available recombination energy. We believe that these detectors will have sufficient sensitivity to detect crossing the critical $n-T$ boundary for BEC. The density-temperature range in these experiments is expected to be 10^{14} cm^{-3} - microkelvin, as limited by dipolar spin relaxation.

6. THE MICROWAVE TRAP

The microwave (MW) trap utilizes the fact that a time varying magnetic field can have a field maximum. It is operated at frequencies in the vicinity of the Larmor frequency of the electron spins where the trap potential is deepest. By operating at a frequency below resonance, states which are predominantly spin-down (a or b-states) can be trapped and thereby suppress the spin relaxation losses by a Boltzmann factor.

The MW trap is most easily analyzed using the dressed state formalism. Atoms in the presence of an electromagnetic field characterized by a photon mode occupation at frequency ω near the transition frequency ω_0 between states, say $|c\rangle$ and $|b\rangle$ are in

dressed states

$$|1\rangle = \cos\theta|c\rangle \otimes |N-1\rangle + \sin\theta|b\rangle \otimes |N\rangle \ ,$$
$$|2\rangle = -\sin\theta|c\rangle \otimes |N-1\rangle + \cos\theta|b\rangle \otimes |N\rangle \ . \qquad (5)$$

Here $|2\rangle$ is a trapped state and $|1\rangle$ is an anti-trapped state. The depth of the trap on resonance is given by

$$U = \hbar\mu_{cb}B_{mw}/2 \ . \qquad (6)$$

where B_{mw} is the microwave field amplitude and μ_{cb} is a dipole matrix element between bare states c and b. On resonance the states $|1\rangle$ and $|2\rangle$ are equal admixtures of states b and c. As the detuning, $\delta = \omega - \omega_o$, is increased or decreased from zero, the depth decreases as shown in Fig. 4, however, the admixture becomes dominated by one bare state or the other.

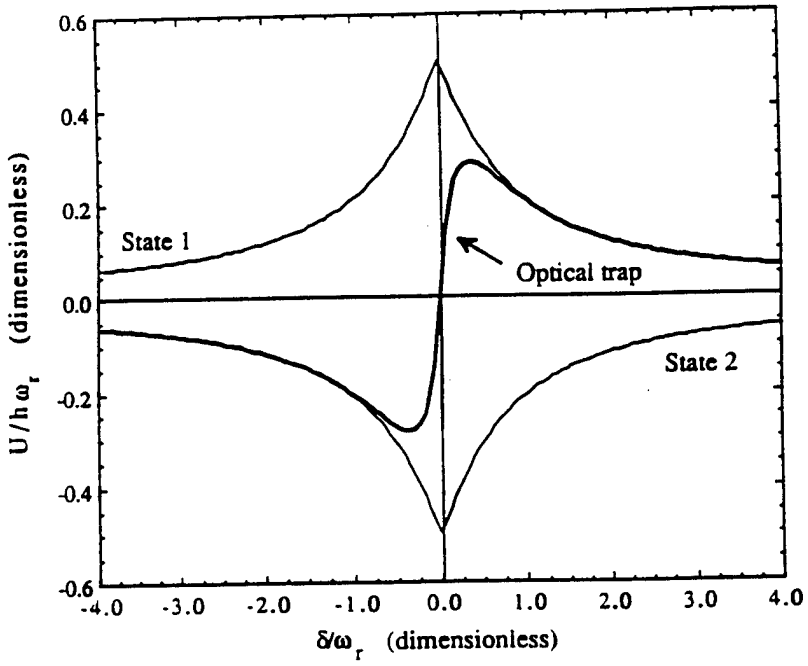

Figure 4. The microwave trap potential for hydrogen atoms as a function of detuning scaled to the Rabi frequency ω_r. The potential for a trap at optical frequencies is also shown for comparison.

It is straightforward to show that negative detuning results in trapping of the high field seeking b-state, as discussed earlier. The MW trap has been experimentally demonstrated on cesium [14]. One of the difficulties of the MW trap for hydrogen is that microwave field amplitudes that can be achieved are of order 10^2 Gauss so that the well depth U/k_B is shallow, of order a few millikelvin. In order to fill a trap, the temperature of the gas should be $T \leq U/k_B$, however a gas of hydrogen can only be cooled to $50 - 100$ mK. To overcome this limitation the atoms are first cooled to a

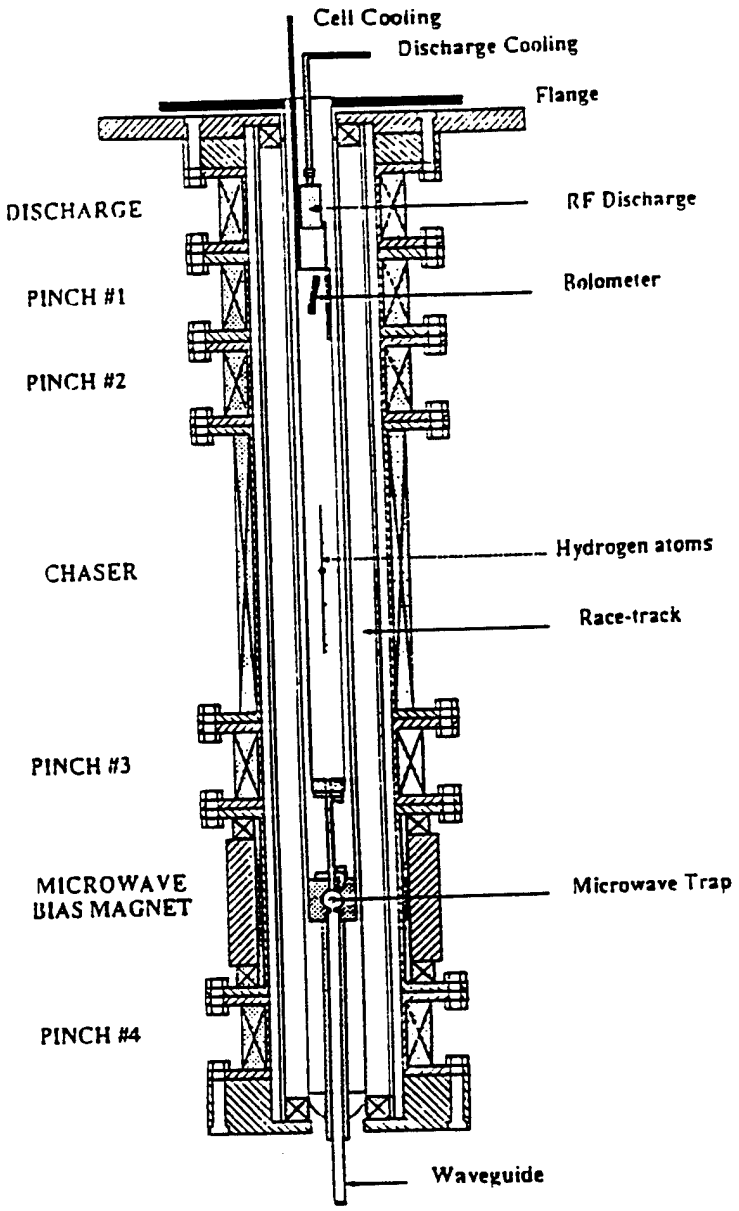

Figure 5. The hybrid trap–a microwave trap in a static trap, showing the microwave cavity.

few hundred microkelvin in a static trap and then transferred into the MW trap, as shown in Fig. 5.

The detuning is adiabatically changed from positive to negative so that the spin-relaxation rate is suppressed. The gas can be further cooled to BEC by evaporative cooling. It is expected that densities of order 10^{18} cm^{-3}, where 3-body recombination losses become important, can be achieved.

7. TWO-DIMENSIONAL GAS OF SPH

A well-known theorem due to Hohenberg [15] states that in a homogeneous 2-D system, BEC does not exist; however the KT transition to superfluidity does [16]. It has been shown that an inhomogeneous potential in 2-D alters the situation so that BEC will take place [17 – 18]. We shall describe an experiment designed to overcome the earlier mentioned heating problem and to observe 2-D BEC.

In earlier studies of SPH as a 2-D gas on helium, typically the 2-D surface area was a few square centimeters and all of the recombination energy was eventually dissipated into the surface. At coverages of order $10^{12} - 10^{13}$ cm^{-2} the total power due to recombination severely warms the cell. Meyer et al. [19] studied the kinetics of the recombination process and found that less than 4% of the available energy was deposited at the point where recombination was initiated. When two atoms recombine they do so into a vibrational-rotational state of H_2 near the continuum so that only of order 10^{-3} of the total recombination energy is released. The energetic excited molecule flies off and cascades down the ro-vibrational levels by wall collisions until it finally reaches the ground state. Our 2-D cell shown in Fig. 6 takes advantage of the non-local dissipation of recombination energy.

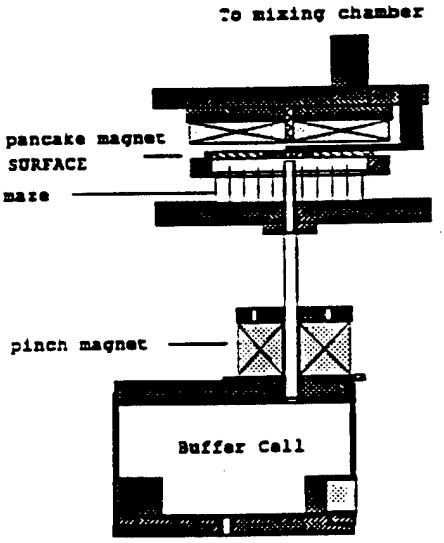

Figure 6. A cell for the study of SPH in a 2-D configuration. The 2-D surface is under the pancake magnet which creates a field gradient. Atoms are loaded into the buffer cell; their flow to the 2-D surface is controlled with a pinch magnet which creates a variable height potential barrier

Atoms from a storage volume flow onto the 2-D surface. The recombined atoms are trapped in a maze opposing the 2-D surface; a simulation has shown that $\sim$ 90% of the recombination energy is released in the maze [20]. In this way the heating of the 2-D surface is reduced. A further reduction is realized by turning on a "pancake" magnet, situated above the 2-D surface. This magnet creates a large magnetic field

gradient, with a maximum at the center of the surface, so that the effective area of coverage is reduced by a few orders of magnitude. In order to determine the surface density the heat flow from the surface is measured by thermometric methods. Since recombination will be a 3-body process, the coverage decreases as

$$\frac{d\sigma}{dt} = -K_s^{(3)}\sigma^3 \quad , \tag{7}$$

where $K_s^{(3)}$ is the surface recombination rate constant. Then the heating per unit area

$$\dot{Q}_s = c\frac{d\sigma}{dt} \quad , \tag{8}$$

where c is the fraction of energy deposited in the surface. Thus, the measured quantity $\dot{Q}_s$ is proportional to $K_s^{(3)}\sigma^3$. The transition will actually have a special signature. For condensate atoms $K_s^{(3)}$ is at least a factor of 6 smaller than for normal atoms [21]. In addition, the surface coverage σ should increase by at least a factor of 2 [22] as elastic pair interactions between condensate atoms are reduced by 2. This experiment should be capable of detecting the 2-D BEC transition and mapping its dependence on the field gradient.

In the preceding sections we have discussed three experiments which are designed to reveal the quantum degenerate nature of SPH. Hopefully, success will be realized in the near future.

8. ACKNOWLEDGMENTS

We thank the Army Office of Research for a travel grant and the Department of Energy grant DE-FG02-85ER45190 for support of this research.

REFERENCES

[1] I. F. Silvera and J. T. M. Walraven, Phys. Rev. Lett. **44**, 164 (1980).
[2] W. Kolos and L. Wolniewicz, J. Chem. Phys. **43**, 2429 (1965).
[3] I. F. Silvera and J. T. M. Walraven, Progress in Low Temp. Physics, edited by D. F. Brewer (Elsevier Science Publ., 1986), p. 139.
[4] D. O. Edwards and I. B. Mantz, J. Phys. (France) **41**, C7 (1980).
[5] Y. Kagan and G. V. Shlyapnikov, Phys. Lett. A **130**, 483 (1988).
[6] I. F. Silvera, J. D. Gillaspy, and J. G. Brisson, To BE(C) or Not to BE(C): The Possibility of Bose-Einstein Condensation of Hydrogen at High Densities in High Magnetic Fields. Spin Polarized Quantum Systems, edited by S. Stringari (Singapore: World Scientific, 1989).
[7] H. F. Hess, Phys. Rev. B **34**, 3476 (1986).
[8] H. F. Hess, G. P. Kochanski, J. M. Doyle, N. Masuhara, D. Kleppner, and T. J. Greytak, Phys. Rev. Lett. **59**, 672 (1987).
[9] J. M. Doyle, J. C. Sandberg, I. A. Yu, C. L. Lesar, D. Kleppner, and T. J. Greytak, Phys. Rev. Lett. **67**, 603 (1991).

[10] M. H. Anderson, J. R. Ensher, M. R. Matthews, C. E. Wieman, and E. A. Cornell, Science **269**, 198 (1995).
[11] K. B. Davis, M.-O. Mewes, M. R. Andrews, N. J. van Druten, D. S. Durfee, D. M. Kurn, and W. Ketterle, Phys. Rev. Lett. **75**, 3969 (1995).
[12] C. C. Bradley, C. A. Sackett, J. J. Tollett, and R. G. Hulet, Phys. Rev. Lett. **75**, 9 (1995).
[13] I. J. Bonalde, T. M. Brill, M. Nahum, and I. F. Silvera, J. Low Temp. Phys. **101**, 555 (1995).
[14] R. J. C. Spreeuw, C. Gerz, L. S. Goldner, W. D. Phillips, S. L. Rolston, C. I. Westbrook, M. W. Reynolds, and I. F. Silvera, Phys. Rev. Lett. **72**, 3162 (1994).
[15] P. C. Hohenberg, Phys. Rev. **158**, 383 (1967).
[16] J. M. Kosterlitz and D. J. Thouless, Physica B **109-110**, 1181 (1973).
[17] V. Bagnato and D. Kleppner, Phys Rev. A **44**, 7439 (1991).
[18] S. I. Shevchenko, Sov. Phys. JETP **73**, 1009 (1991).
[19] E. S. Meyer, Z. Zhao, J. C. Mester, and I. F. Silvera, Phys. Rev. B **50**, 9339 (1993).
[20] M. F. Chang, L. Venkataraman, and I. F. Silvera, Journal of Low Temperature Physics **101**, 739 (1995).
[21] Y. Kagan, B. V. Svistunov and G. V. Shlyapnikov, Sov. Phys.-JETP **66**, 314 (1987).
[22] B. V. Svistunov, T. W. Hijmans, B. V. Shlyapnikov, and J. T. M. Walraven, Phys. Rev. B **43**, 13412 (1991).

SUPERFLUIDITY AND CRITICALITY IN BOSE SYSTEMS

Peter B. Weichman

Department of Physics
California Institute of Technology 114-36, Pasadena, CA 91125 USA

1. HELIUM IN POROUS MEDIA

The physics of bosons has found a fascinating rebirth in recent years, sometimes in systems far removed from superfluid helium. In this article I will review some of the theoretical advances and indicate some of the experiments that motivated them.

I will begin with superfluid ^{4}He since this boson system is the most familiar. The transition to superfluidity in bulk ^{4}He at temperatures of a few Kelvins (the exact temperature depending on the external pressure) is probably the most accurately studied phenomenon in condensed matter physics. Theoretically the transition is understood to be in the universality class of a three dimensional XY-model, exemplified by a lattice of two-component, unit-length classical spins, $\vec{s}_i$, interacting via a nearest neighbor coupling, $-J\vec{s}_i \cdot \vec{s}_j$, with ferromagnetic exchange $J > 0$ (how this comes about should become clearer below). Indeed, calculations based on this identification, especially using renormalization group methods, yield an amazingly accurate description of experiments close to the critical point [1].

Although the basic physics of the *bulk* superfluid transition has been understood for several decades, it is only comparatively recently that we have begun to understand the superfluid transition under more exotic circumstances. Motivated to some extent by experiments on the Kosterlitz-Thouless transition in two-dimensional thin *films* [2], experimentalists began to explore the behavior of ^{4}He adsorbed in various porous media, especially Vycor glass [3]. One interest was in very *low* coverages of helium, with the expectation that the resulting thermodynamic behavior might appear two-dimensional. If such a regime were achievable, the advantage of porous systems over the conventional rolled Mylar [2] would be the enormous surface area-to-volume ratio (over one-hundred square meters in a cubic centimeter sample of Vycor, as opposed to only a few tenths of a square meter in a Mylar roll of similar size).

The great surprise was that observations showed nothing of the kind! Thus over a wide range of coverages of helium in Vycor, from full pores down to fractions of a monolayer of surface adsorption, superfluid density data demonstrated clear bulk three-dimensional behavior—ρ_s vanishing with the characteristic three-dimensional

2/3-power law near the transition temperature T_λ [3], *not* the discontinuous jump characteristic of two-dimensional Kosterlitz-Thouless behavior [2]. Even more surprising was the behavior at ultra-low coverages [3], where the effective density, $\bar{\rho}$, of mobile helium is on the order of a few atoms per pore, i.e., interatomic separations, d_s, of order 50-100Å, 20-30 times the helium effective hard-core diameter, a. Note that there is always a localized/frozen "inert" monolayer or so—which will later be important, but at this stage is assumed to play no role—and we define $\bar{\rho}$ as the total density minus the density of this inert layer. In this regime the superfluid density profiles increasingly resemble those of an *ideal* Bose gas, vanishing nearly *linearly* as $T_\lambda(\bar{\rho})$ is approached. The interpretation, then, is that although the helium atoms are believed to reside on the pore surfaces, so that the film is *locally* two-dimensional, the pores are fully interconnected in three dimensions, and the atoms are in fact moving throughout a three-dimensional volume. Hence the three-dimensional nature of the phase transition. Furthermore, the characteristic size of an atomic wavepacket is set by the thermal de Broglie wavelength $\Lambda_T = h/(2\pi m k_B T)^{1/2}$, where m is the mass of a helium atom. The superfluid transition takes place when $d_s \sim \Lambda_T$, hence $T_\lambda(\bar{\rho}) \sim \bar{\rho}^{2/3}$. At the ultra-low coverages, T_λ is therefore strongly suppressed, and Λ_T becomes of order the pore size. One might imagine, then, that such a wavepacket sees the porous medium only in an *average* sense, with details below the scale Λ_T washed out. It is not a great leap of imagination to go from this observation to the picture of a dilute Bose gas in which the only role of the porous medium is to yield an effective mass m_{eff}, and some effective interatomic scattering potential. This last assumption is crucial since in pure bulk helium the atomic potential has a long-ranged attractive tail which causes it to condense into a dense strongly interacting fluid. A key effect of the porous medium must then be to screen out this attractive tail, leaving only the repulsive core. This allows the density to be continuously tuned without the usual first-order liquid-vapor transition intervening.

The above picture is intuitively appealing, but does it stand up to close theoretical scrutiny? The answer is both yes and no. On the one hand a detailed analysis [4], based entirely on the above effective medium picture, of the *crossover* from strongly interacting to dilute weakly interacting Bose gas behavior as the density, $\bar{\rho}$, is reduced matches the experiments [3] remarkably well (the appropriate small parameter describing the strength of interactions is the ratio a/Λ_T). I will have no more to say about the details of this agreement, but refer the reader to the literature [4]. I will focus rather on the *no* part of the answer, which leads to even more interesting physics.

The problem with the above effective medium picture is that it does not account for the *disorder* or *randomness* inherent in porous media. The effects of disorder near a critical point can be very serious, sometimes completely changing the universality class of the transition. There is a simple criterion, called the Harris criterion [5], which determines when this happens: If the specific heat exponent, α, of the pure nonrandom transition is positive (i.e., the specific heat actually *diverges* at the transition) then disorder is a *relevant* perturbation and will give rise to new critical behavior. If α is negative, disorder is irrelevant and the critical behavior should be unchanged. Now, the value of α for bulk ^{4}He is $\alpha \approx -.02 \pm .02$, very likely negative. This is consistent with the observation of bulk critical exponents for not too low coverages of helium in Vycor. However, as the coverage is reduced the critical be-

havior crosses over to that of an ideal Bose gas with specific heat exponent $\alpha = 1/2$, a strongly positive value. Thus we expect disorder to have an increasingly stronger effect at low coverages. This calls into question the validity of calculations based on the effective medium picture, despite their good agreement with the experimental data.

A partial way out is provided by understanding the detailed properties of Vycor glass [6]. It transpires that the method by which Vycor is made effectively ensures that the disorder on long length scales is *extremely weak*. It is therefore required that $\bar{\rho}$ be *extremely low*, probably below present experimental resolution, before the observed nearly ideal behavior is strongly perturbed [6]. Although this observation leaves one more comfortable with the effective medium theory, it merely sidesteps the really interesting question of what the behavior would be if the disorder was much stronger, or equivalently, if the experiments were to probe much lower coverages of helium in Vycor. Answering this question leads us into the realm of *localization effects* and *quantum phase transitions* in interacting boson systems.

2. BOSON LOCALIZATION AT ZERO TEMPERATURE

Quantum phase transitions are those that occur at zero temperature, where fluctuations are entirely due to the Heisenberg uncertainty principle: The fact that certain observables may not commute with the Hamiltonian. As observed previously, the superfluid transition temperature decreases with coverage, and *vanishes* at some critical coverage, ρ_c (the "inert" layer), below which superfluidity ceases to exist even at $T = 0$. Changing our perspective slightly, if we sit *at* $T = 0$ and consider the total density, ρ, as the independent variable (recall that $\bar{\rho} = \rho - \rho_c$), we see that the system passes from an insulating *localized* phase with superfluid density $\rho_s = 0$ for $\rho < \rho_c$ to a *superfluid* phase with $\rho_s > 0$ for $\rho > \rho_c$. This is precisely a quantum phase transition.

One may define critical exponents associated with this transition. For example we may ask how $\rho_s(T = 0)$ increases with $\bar{\rho} > 0$. We expect $\rho_s(0) \sim \bar{\rho}^{\zeta}$ for some exponent ζ. If, as in the effective medium picture, one views ρ_c as a totally inert substrate on which the excess density "skates", then we expect $\rho_s(0) \propto \bar{\rho}$, i.e., $\zeta = 1$. Indeed for a continuum dilute Bose gas with repulsive interactions one finds precisely $\rho_c = 0$ and $\rho_s(0) = \bar{\rho} = \rho$. In general we do not expect the precise equality $\rho_s(0) = \bar{\rho}$, even in cases where $\zeta = 1$ (for example in the case of regular *periodic* porous media), since it is a result of Galilean invariance, which will be broken by any residual interactions with the porous medium. As we have seen from the Harris criterion argument, the effective medium picture is incorrect in disordered systems when ρ is very close to ρ_c, and $\zeta \neq 1$ would not be unexpected. We can gain some intuition about the physics by thinking about Anderson localization in noninteracting Fermi systems. There, for a given external random potential, which may be thought of as a porous medium for our purposes, it is believed that one has low energy *localized* states separated from higher energy *extended* states by a *mobility edge*. Therefore if free fermions are added to such a system at $T = 0$, two per state, one first fills up the localized levels until a critical density ρ_c is reached, at which point all states below the mobility edge are filled; then any excess density $\bar{\rho} = \rho - \rho_c$ goes into the extended states and is therefore free to move about the entire system. This Anderson

metal-insulator type transition is another example of a quantum phase transition. Furthermore it *violates* the effective medium picture. For example, although the analogue of ρ_s is absent, one may define a correlation length: The localization length $\xi_L \sim |\bar{\rho}|^{-\nu}$ for $\bar{\rho} < 0$, which measures the diverging linear extent of the localized states as the mobility edge is approached. The exponent ν, which turns out to take the value $\frac{1}{2}$ in the effective medium picture, is highly nontrivial, and its exact value is still controversial.

Building upon the above picture, we now consider bosons instead of fermions. It is immediately apparent that repulsive interactions are crucial: Without them the ground state would consist of all particles occupying the single lowest energy localized state. Clearly the particle density in the region of space occupied by this state would be infinite. Any kind of short ranged repulsion would therefore immediately preclude behavior of this type. A more accurate picture of what happens is the following: As particles are added to the system they more-or-less fill up the low-lying localized states until the particles' hard cores preclude further density increase. Further additions then have no choice but to occupy higher-lying localized states. In effect, the single particle states seen by the added particles are renormalized by interactions with the particles already present. Eventually, just as in the free fermion case, a critical density ρ_c is reached beyond which, in some self consistent sense to be discussed further below, subsequent added particles go into extended states. Since the particles are bosons, any occupying these states will Bose condense, forming a superfluid. This picture, then, provides the framework for a microscopic, quantum mechanical description of the formation of the frozen "inert" layer in Vycor, and an intuitive argument for the existence of a critical density ρ_c.

One can make this picture much more precise [7]. It is convenient to begin from a simple lattice boson model with nearest neighbor hopping and an on-site repulsion $U > 0$. Disorder is included via random site energies ϵ_i. Thus we consider the second-quantized Hamiltonian, sometimes called the boson Hubbard model,

$$H = J \sum_{<ij>} (a_i^\dagger a_j + h.c.) + \frac{1}{2} U \sum_i \hat{n}_i^2 + \sum_i (\epsilon_i - \mu) \hat{n}_i \qquad (1)$$

where $\hat{n}_i = a_i^\dagger a_i$ is the site number operator and μ the overall chemical potential. The indices i are assumed to label the sites of a d-dimensional hypercubic lattice and $< ij >$ denotes nearest neighbor pairs. One may think of the lattice sites as idealized "pores", and the random ϵ_i as embodying the varying size, surface curvature, etc. of the pores. Clearly J and U ought also to have random components, but it turns out that all the important physics may be elucidated keeping only the ϵ_i.

As pointed out above, the random ideal Bose gas, represented by the first and last terms in (1), is the wrong starting point for the problem. Rather, one should begin in the *opposite* limit, where one throws out the *first* term in (1) by setting the hopping $J = 0$. In this limit there is no communication between different lattice sites and the Hamiltonian is diagonal in the basis of eigenstates of the $\hat{n}_j$: The ground state consists of an exact number, n_i, of bosons on each site, i, obtained by minimizing the single site energy

$$E_i = \frac{1}{2} U n_i^2 + (\epsilon_i - \mu) n_i, \quad n_i \geq 0 \; . \qquad (2)$$

The solution is

$$n_i = \begin{cases} n_0 \geq 0 & \text{for } n_0 - \frac{1}{2} < \frac{\mu - \epsilon_i}{U} < n_0 + \frac{1}{2} \\ 0 & \text{for } \frac{\mu - \epsilon_i}{U} < \frac{1}{2} \, . \end{cases} \tag{3}$$

Thus as μ/U is increased by unity, one more particle is added to each site (except for those sites which remain empty). Note that if the ϵ_i are bounded such that $-\Delta \leq \frac{\epsilon_i}{U} \leq \Delta$, with $\Delta < \frac{1}{2}$ (by redefining the origin of μ if necessary, we assume the ϵ_i/U cover the symmetric interval $[-\Delta, \Delta]$), there are a discrete set of intervals $I_{n_0} = (n_0 - \frac{1}{2} + \Delta, n_0 + \frac{1}{2} - \Delta)$, for each $n_0 \geq 0$, such that when $\frac{\mu}{U} \in I_{n_0}$ all sites have precisely n_0 particles. We call these intervals *Mott insulating phases*, identified by the fact that the compressibility $\kappa = \partial n / \partial \mu$, where $n = \frac{1}{N} \sum_i n_i$ is the average number of particles per site, *vanishes* within each interval. For μ outside these intervals n varies continuously and $\kappa > 0$. We shall call these latter intervals *Bose glass* phases. Clearly both types of phase are insulating because $J = 0$. If $\Delta \geq \frac{1}{2}$ all Mott phases disappear, and only the Bose glass remains. Conversely, if $\Delta = 0$ (*no* disorder) the phase diagram consists entirely of Mott phases, pair-wise degenerate at half-integer values of μ/U. One may, of course, generate much richer phase diagrams with charge-density-wave-type Mott ground states (rational values of n) by allowing off-site interactions $\frac{1}{2} \sum_{i,j} U_{ij} n_i n_j$, or by making the ϵ_i *periodic* (with, perhaps, a small random component added). None of this changes the nature of the superfluid transition so long as U_{ij} is short-ranged (see below), so we consider only the simplest case, $U_{ij} = U \delta_{ij}$.

Let us now introduce the possibility of superfluidity by adding back the hopping J. This adds a new dimension to our (so far) one-dimensional phase diagram. We begin by considering J as a perturbation, first on the Mott phases. One may construct the ground state perturbatively in J/U. It will consist primarily of the $J = 0$ ground state with precisely n_0 particles per site, however there will also be small admixtures of the excited states in which one, or more, of the sites have one or more extra particles, with corresponding depleted sites with one or more "holes" (note that the hopping term conserves overall particle number, so the number of particles equals the number of holes). However, each new particle-hole pair costs an extra energy of order U (the random potential, if present, will modulate this energy cost in the range $[U(1-\Delta), U(1+\Delta)]$, but this does not change the physics of the argument) and yields a component of the ground state with amplitude down by a factor J/U. Similarly, each time a particle is hopped one site further from the hole from which it originated, the amplitude goes down by a factor J/U. Roughly speaking, then, the probability that a particle will hop r steps varies as $(J/U)^r \sim e^{-r/\xi}$, where $\xi \sim 1/\ln(U/J)$ is a correlation length. From here it is not hard to argue that so long as ξ is finite one remains in the incompressible Mott phase. Thus, although there is a certain amount of local fluctuation in the particle number over regions of size ξ, the overall density remains precisely n_0. Correspondingly, there will remain an interval, $\mu_-(n_0, J) \leq \mu \leq \mu_+(n_0, J)$ on which $\kappa \equiv 0$, although the width $W(n_0, J) \equiv \mu_+(n_0, J) - \mu_-(n_0, J)$ will generally be less than the $J = 0$ value $W(n_0, 0) = U(1 - 2\Delta)$. The function $W(n_0, J)$ represents the effective energy required to create a particle-hole pair, and for positive J it will be reduced because the energy cost U is effectively shared among ξ^d particles through a net gain in kinetic (delocalization) energy. As J increases, there will come a point $J_c(n_0)$ at which $W(n_0, J_c(n_0))$ *vanishes*, i.e., it costs no energy to create

particle-hole pairs. At this same point the correlation length ξ will diverge. In the absence of disorder, $\Delta \equiv 0$, this would signal the onset of superfluidity: Particles and holes are now free to hop throughout the system and will Bose condense. The phase diagram therefore consists of an infinite set of Mott *lobes*, one for each value of n_0, which meet pairwise only at $J = 0$ and μ/U half-integer. Everything outside the lobes is superfluid. Clearly the superfluid phase penetrates right to $J = 0$ at these half-integer points.

Consider now the transition to superfluidity for $J < J_c(n_0)$. For μ just above $\mu_+(n_0, j)$, so that n is slightly larger than n_0, it may be verified in detail by explicit calculation [7] that the system behaves like a dilute gas of bosons floating on top of the essentially inert Mott layer. Similarly, for μ just beneath $\mu_-(n_0, J)$ one has a dilute gas of holes. The transition from Mott to superfluid phase at fixed J is in every way identical to the bulk transition from an empty system to a dilute superfluid when μ increases through zero, and is described theoretically by the Bogoliubov model [8] (the same transition also occurs, of course, in the lattice system for $n_0 = 0$).

The point $J = J_c(n_0)$ is special. This is the point one goes through when the transition occurs at *fixed density* $n = n_0$, and is *particle-hole symmetric*. Since the density is precisely n_0 one can never view the system as a dilute addition to an otherwise inert background. It turns out [7] that this extra symmetry puts the transition in a different universality class: That of the $(d+1)$-dimensional XY-model. This is the same transition as occurs in helium at finite temperature, but in one higher dimension.

Let us now consider the effects of disorder. We expect, for bounded disorder ($\Delta < \frac{1}{2}$), that the phase diagram will consist of *three* phases in the $\mu - J$ plane, namely the superfluid phase in addition to the Mott and Bose glass insulating phases which exist at $J = 0$. We first discuss the perturbative effects of J on the $J = 0$ Bose glass phase. The fact that $n(\mu)$ is continuous follows simply from the fact that, due to the random nature of the ϵ_i, *somewhere* in the system there will be sites arbitrarily close in energy to a degenerate point $\frac{\mu - \epsilon_i}{U}$ = half integer. A slight increase in μ will then add a particle to these sites. Equivalently, there is no energy barrier to the creation of particle-hole pairs: Pick two sites, one with energy just below a degenerate point, the other with energy just above. At arbitrarily small cost in energy, $\Delta\epsilon$, one may then transfer a particle from the second site to the first. Why, then is the phase not superfluid? The argument that it is not is precisely along the lines of the original Anderson localization argument for free fermions [7,9]. Two sites with very small $\Delta\epsilon$ will generally be very far apart as $\Delta\epsilon \to 0$. But then the amplitude for hopping a particle from one site to the other will be of order $(J/U)^r$, where r is the distance between the two sites. For small J this factor will dominate and kill the net amplitude for the formation of such a particle-hole excitation. Thus for small J each individual Bose particle is localized in a self consistent way by a *combination* of interactions with other particles, and the residual hopping versus near-degeneracy effects described above.

Consider now the transitions between the three phases. Suppose one sits very close to the edge of a Mott lobe so that the average density, n, differs only slightly from n_0. One again expects the residual particles (or holes) to behave very much like a dilute fluid of density $\delta n = |n - n_0|$. However, in the presence of disorder this dilute fluid will still see a residual random potential due to the ϵ_i. For sufficiently

small δn we therefore expect all particles to be localized [see the discussion above eq. (1)]. The conclusion is that at any fixed $J < J_c(n_0)$, the transition out of the Mott lobe must be into the Bose glass phase. This still leaves open the question of what happens at the special symmetric point $J = J_c(n_0)$, $n = n_0$. The argument is more shaky, but in essence we expect the system, for J slightly larger than $J_c(n_0)$, to look like a dilute "binary" fluid of particles and holes. Thus barring some exotic collective effect, we expect the residual random potential to localize both components of the fluid, and hence the Bose glass phase should completely surround the Mott lobes. Note that in any case, for strong randomness, $\Delta \geq \frac{1}{2}$, as certainly holds for all porous systems studied experimentally so far, the Mott lobes disappear entirely and Bose glass phase will exist for *all* values of μ, and sufficiently small values of J. For given μ we expect the onset of superfluidity to occur at some critical value $J = J_c(\mu)$.

3. THE BOSE GLASS TO SUPERFLUID TRANSITION

It is very likely, then, that the transition to superfluidity takes place *only* from the Bose glass phase [7], and it is the physics of this transition which will concern us from now on. This is the transition which ought to describe the zero temperature insulator to superfluid transition in porous media.

It turns out that there are a number of conclusions one can draw about this transition simply on the basis of the expected *scaling* behavior of the thermodynamic functions. Central to scaling is the existence of a divergent correlation length, in this case the effective many body localization length, ξ. In quantum critical phenomena all fluctuations are driven by the quantum dynamics of the ground state wavefunction. This introduces, in addition to ξ, a correlation *time*, ξ_τ, into the equilibrium thermodynamics, with a corresponding frequency or energy scale $\Omega = 1/\xi_\tau$. Near the transition both ξ and ξ_τ diverge, and one defines a dynamical exponent, z, via $\xi_\tau \sim \xi^z \sim \delta^{-z\nu}$, where δ is any convenient measure of the deviation from the critical point, e.g., $\delta = \mu - \mu_c$, $J - J_c$, or $\rho - \rho_c$. The scaling hypothesis states that near the critical point all lengths scale with ξ and all times scale with ξ_τ. In addition the hypothesis of *hyperuniversality* states that the critical part of the free energy scales as $f_s \approx A\xi^{-d}(\hbar/\xi_\tau)$, where A is a universal constant. (This form is motivated by dimensional analysis – f_s is an energy per unit volume – and may be derived, with certain assumptions, from renormalization group theory [10]). With the definition $f_s \sim |\delta|^{2-\alpha}$, where α is the $T = 0$ analogue of the specific heat exponent, this yields the generalized hyperscaling relation $2 - \alpha = (d + z)\nu$.

The superfluid density is derived by imposing a long wavelength *twist* with wavevector $k_0 \to 0$ on the superfluid order parameter [11], then computing the derivative $\rho_s = \frac{m^2}{\hbar^2}(\partial^2 f/\partial k_0^2)_{k_0=0}$. Since k_0^{-1} is a length it must scale in the combination $k_0\xi$. We therefore have immediately [7] $\rho_s \sim |\delta|^\zeta$, with $\zeta = 2 - \alpha - 2\nu = (d + z - 2)\nu$. Using the Josephson relation between the time rate of change of the superfluid order parameter phase and the chemical potential, $\dot{\phi} = -\mu/\hbar$, one may write the total compressibility, $\kappa = -\frac{\partial^2 f}{\partial \mu^2}$, in the superfluid phase as a response to a slow twist in *time*, i.e. $\kappa = \hbar^{-2}\partial^2 f/\partial\omega_0^2$, where $\omega_0 \to 0$ is the frequency of the twist. We expect ω_0 to scale in the combination $\omega_0\xi_\tau$, therefore $\kappa \sim \xi_\tau\xi^{-d} \sim \delta^{(d-z)\nu}$ (note that in

general the *total* compressibility κ includes, but is distinct from, the *singular* part of the compressibility $\kappa_s = -\partial^2 f_s/\partial\mu^2 \sim \delta^{-\alpha}$). We now come to the key observation: Since both the Bose glass and superfluid phases have a positive, non-zero compressibility (the argument fails for the Mott to superfluid transition in the pure case) we expect κ to be *finite* through the critical point. This clearly requires $\alpha < 0$, since κ includes κ_s, and immediately implies the equality $z = d$.

A further constraint on the exponents follows from a recent theorem [12] which states that in a random system one has the inequality $\nu \geq 2/d$. Using $z = d$ and $\alpha = 2 - (d + z)\nu$ this implies $\alpha < -2$, consistent with the finiteness of κ at $\delta = 0$. From the formula for ζ we also have $\zeta > 4(d-1)/d = 8/3$ for $d = 3$. This implies that ρ_s turns on very *slowly* as ρ passes through ρ_c, making it an extremely difficult exponent to measure.

One may define certain exponents which depend only on z and d, and which therefore may be evaluated explicitly. For example, for $\delta > 0$ there is a finite temperature transition with a T_c that should scale as some power, $T_c(\delta) \sim \delta^\theta$. What is θ? The quantity $\hbar/k_B T$ is a time scale, so T_c must scale with ξ_τ, implying $\theta = z\nu$. But $\rho_s(T = 0) \sim \delta^{(d+z-2)\nu}$, so we may eliminate ν by writing $T_c \sim \rho_s(0)^x$ with $x = z/(d+z-2) = 3/4$ for $d = 3$. This should be compared to $x = 2/d (= 2/3, d = 3)$ for the Mott to superfluid transition in the pure case.

Though we have come remarkably far using scaling ideas alone, we have yet to address the problem of calculating quantities, such as the exponent ν, explicitly. For the classical magnetic transitions, the primary analytic technique used for such calculations is the epsilon expansion about four dimensions [13]. This expansion relies upon the existence of a classical field theoretical representation for the problem—the φ^4 model in the classical magnetic case [13]. Such classical field theories can indeed be found for the dirty boson problem, but they are more complicated than their classical magnetic counterparts [7,14]. The crucial difference is the existence of the time scale ξ_τ: The quantum dynamics must be included in the effective classical theory, leading to complex fields $\varphi(\mathbf{x}, \tau)$ depending on both space *and* time. Furthermore space and time are not equivalent, so the effective field theory is anisotropic in time. The addition of disorder adds yet another complication: It couples $\varphi(\mathbf{x}, \tau)$ with an external *static* random potential $w(\mathbf{x})$. The fact that $w(\mathbf{x})$ does not depend on τ implies, in effect, that the disorder, instead of being interpreted as a set of bounded point-like impurities, must be interpreted, rather, as a set of one-dimensional rigid *rods*. This makes the problem even *more* anisotropic. To be more explicit, the effective classical Lagrangian is given by

$$\mathcal{L} = \int d^d x \int_0^\beta d\tau \left\{ \varphi^*(\mathbf{x},\tau)\left(\frac{\partial}{\partial\tau} - J\nabla^2 - \mu\right)\varphi(\mathbf{x},\tau) + w(\mathbf{x})|\varphi(\mathbf{x},\tau)|^2 + u|\varphi(\mathbf{x},\tau)|^4 \right\}, \tag{4}$$

with $\beta = (k_B T)^{-1}$ and thermodynamics obtained from the partition function $\mathcal{Z} = tr^\varphi[e^{-\mathcal{L}}]$ in the usual way. If all τ-dependence is suppressed, the form reverts precisely to the classical φ^4-model for a random XY-magnet. Note that only for $T \to 0$ does the time dimension become infinite in extent. In this formulation, then, positive temperature represents a kind of finite size effect. As is standard in critical phenomena, any dimension of a system that is finite may be ignored when deciding the universality class of a transition. From this follows the irrelevance of quantum mechanics at $T > 0$: The behavior near $T_c(\delta)$ will be asymptotically governed by the

classical φ^4-model in which all τ-dependence is suppressed.

Although the field theory defined by (4) is very complicated, there still exists an epsilon expansion type formalism within which one may derive renormalization group recursion relations [14]. The temporal anisotropy of the model, unfortunately, forces one to introduce a *second* expansion parameter, ϵ_d, the dimension of *time*, which along with $\epsilon = 4 - D$ (here $D = d + \epsilon_d$) must be presumed small in order to obtain a well defined expansion. Physically one has, of course, $\epsilon_d = 1$ and, for $d = 3$, $\epsilon = 0$. The argument leading to the exact exponent relation $z = d$ was very special to $\epsilon_d = 1$, and fails for general ϵ_d: One finds $z = 2 + a_1\epsilon + a_2\epsilon_d + \theta(\epsilon^2, \epsilon\epsilon_d, \epsilon_d^2)$ with nontrivial coefficients a_1, a_2 [14]. The inequality $\nu > 2/d$ must still be obeyed, however, and the expansion for ν is consistent with this requirement [14]. This inequality also leads to very stringent requirements on how mean field theory becomes exact for $d > 4$ ($\epsilon + \epsilon_d < 0$), forcing the exponents to jump discontinuously as d increases through 4. Amazingly enough the ϵ, ϵ_d-expansion provides an explicit mechanism for this, whereby the nontrivial and mean field fixed points exchange stability without coalescing [14].

This completes our general description of the dirty boson problem. We finally turn to applications outside helium, in particular to two-dimensional granular and amorphous superconductors, and, very briefly, to magnetic flux phases of high T_c compounds.

4. BOSONS AND SUPERCONDUCTIVITY

The starting point for comparisons between superconductivity and superfluidity is the Josephson junction array Hamiltonian [15]

$$H_J = -\tilde{J} \sum_{<ij>} \cos(\hat{\phi}_i - \hat{\phi}_j) + \sum_i (\tilde{\epsilon}_i - \tilde{\mu}) + \frac{1}{2}\tilde{U} \sum_i \tilde{n}_i^2, \tag{5}$$

where $\hat{\phi}_i$ is the *phase* operator on grain i, and $\tilde{n}_i$ is the conjugate number operator which measures the deviation of the number of Cooper pairs on grain i from some reference value N_0. The $\tilde{U}$ term is the so-called *charging energy* which disfavors large fluctuations in the $\tilde{n}_i$. The random site energies $\tilde{\epsilon}_i$ are precisely analogous to those in (1), and the chemical potential $\tilde{\mu}$ controls the average density. Note that if one were to accurately model the coulomb interactions between Cooper pairs the charging term should be replaced by $\frac{1}{2}\sum_{i,j} U_{ij}\tilde{n}_i\tilde{n}_j$, with $U_{ij} \propto e^2|\mathbf{r}_i - \mathbf{r}_j|^{-1}$. Quantum mechanics is completely defined by the commutation relations $[\hat{\phi}_i, \tilde{n}_j] = i\delta_{ij}$, all others vanishing. It is then easy to check that the eigenvalues of $\tilde{n}_i$ are integers (both positive and negative), and that if $\tilde{n}_i|n_i> = n_i|n_i>$, then $e^{i\hat{\phi}_i}|n_i> = |n_i + 1>$ and $e^{-i\hat{\phi}_i}|n_i> = |n_i - 1>$. Furthermore, the operators $a_i^\dagger = (N_0 + \tilde{n}_i)^{\frac{1}{2}} e^{i\hat{\phi}_i}$ and $a_i = e^{-i\hat{\phi}_i}(N_0 + \tilde{n}_i)^{\frac{1}{2}}$ obey *Bose* commutation relations, and $\hat{n}_i = a_i^\dagger a_i = N_0 + \tilde{n}_i$. Substituting these relations into (1) we find that the hopping term takes the form $J \sum_{<ij>} [(N_0 + \tilde{n}_i)^{\frac{1}{2}} e^{i(\hat{\phi}_i - \hat{\phi}_j)} (N_0 + \tilde{n}_j)^{\frac{1}{2}} + h.c.]$, which reduces precisely to the Josephson coupling term in (5) if the fluctuations $\tilde{n}_i$ are neglected relative to N_0, and if we

identify $\tilde{J} = 2JN_0$. Modulo an N_0-dependent additive constant, the rest of the terms in (1) and (5) match exactly. We conclude that if N_0 is large (1) and (5) are quantitatively the same. For small N_0 the detailed physics of the two will differ, but will still possess precisely the same critical behavior. The general structure of the phase diagram, with Mott, Bose glass, and superfluid phases may be verified [7] in a straightforward way. Superfluidity and superconductivity, of course, correspond to long range or, perhaps, power law order in the phases $\hat{\phi}_i$, which for intuitive purposes may be thought of as classical angles in the interval $[0, 2\pi]$. The Josephson coupling is then precisely analogous to the usual XY-coupling between phases. For $T > 0$ this intuition is precisely correct, in some renormalized sense. All of quantum mechanics is buried in the operator character of the $\hat{\phi}_i$, and only at $T = 0$ does the classical intuition break down and more complicated behavior result.

The essence of the equivalence between granular superconductors and superfluids is the assumption of the existence of well defined Cooper pairs well *before* actual superconductivity occurs. Thus the operators $\hat{\phi}_i, \tilde{n}_i$ are well defined even above the critical temperature. In granular systems this assumption is valid because individual grains are usually sufficiently large that they behave like small pieces of bulk superconductor, and order at the bulk transition temperature, T_c^0. Ordering *between* grains, mediated by the Josephson coupling $\tilde{J}$, occurs at a much lower temperature $T_c(\tilde{J}) \ll T_c^0$. Thus well defined Cooper pairs exist within each grain and may be treated to good approximation as bosons. To the extent that all excitations of a fermionic character, such as pair breaking and residual interactions with normal electrons [16], are separated from the bosonic excitations, embodied in (5), by a finite energy scale $\Delta E \gg T_c(\tilde{J})$ this treatment should be *exact* near the critical point.

For amorphous systems, without well defined grains, the validity of the boson model is less clear. However, one can argue [17] that in dirty systems, which are of main interest here, the role of grains is played by localized states in which it is favorable to put *pairs* of electrons. Nearby localized states are then assumed to interact via some effective Josephson coupling, eventually leading to bulk superconductivity. An experimental signal of this would again be the existence of a well defined energy gap between hopping of localized Cooper pairs and single electron-type excitations.

The experiments I wish to address are the two-dimensional thin film analogues of the zero temperature Bose glass to superfluid transition, or, more appropriately for electron systems, the Cooper-pair glass to superconducting transition. The transition can be accessed in various ways: For example, by changing the degree of disorder in the film; by varying the thickness of the film [18]; or by adjusting an external magnetic field [19]. The most interesting observation, which led to much of the interest in these systems, is that of *universal critical conductances.* Thus it was observed that the conductance $\sigma(T, \delta)$, where again δ is any of the above parameters which moves the system through the $T = 0$ transition located at $\delta = 0$, *diverges* at some $T_c(\delta)$ for $\delta > 0$, and *vanishes* as $T \to 0$ for $\delta < 0$, but approaches a *constant* of order unity (in units of $4e^2/h$, the inverse quantum of resistance) as $T \to 0$ for $\delta \equiv 0$. This constant, $\sigma^* \equiv \frac{h}{4e^2} \lim_{T \to 0} \sigma(T, 0)$, was seen to be remarkably close to unity, and a number of theories were proposed suggesting that $\sigma^* \equiv 1$ [20]. Unfortunately, although σ^* is in fact a universal number [21] (see below) it is only unity for a very special set of *self-dual* [22] models, which unfortunately do not correspond to physical reality. One concludes then that the experiments which see $\sigma^* \approx 1$ are probably not

yet in the asymptotic zero temperature limit.

The proof [21] that σ^* is universal follows from hyperuniversality (see Sec. 3) and the Kubo formula which relates the conductivity to the superfluid density

$$\sigma(T,\delta,\omega) = \frac{4e^2\hbar}{m^2}\rho_s(-i\omega)/(-i\hbar\omega) \tag{6}$$

where m is the boson (i.e., Cooper pair) mass, and ω is the frequency. This formula holds only if the physics is described by the boson model. The detailed definition of the frequency dependent ρ_s is not important, only that it scales as $B\xi_\tau^{-1}\xi^{2-d}$, with a universal coefficient, B (this is equivalent to the hyperuniversality assumption for the free energy). Since ω and T scale with ξ_τ we have, as $\delta \to 0$, $\frac{h}{4e^2}\sigma \approx \xi^{2-d}R_\sigma(\omega\xi_\tau, T\xi_\tau)$. Once one sets the units of ω, τ, and σ, the function $R_\sigma(x,y)$ is *universal* [21]. In particular, for $d = 2$ the ξ^{2-d} prefactor drops out, and in the limit $T \to 0$ with $\omega = \delta \equiv 0$ we see that $\sigma^* = R_\sigma(0,\infty)$ is indeed a universal number. Note that this result does not depend on the values of the exponents z or ν. Thus it should hold even in the presence of long ranged Coulomb interactions, or applied magnetic fields, where the universality class of the transition will in general be different.

There are a number of other universal combinations one can define not involving the conductance [21]. For example, again in $d = 2$, the combination $\lim_{\delta\to 0}\rho_s(T = 0,\delta)/T_c(\delta)$ yields a universal number, which could in principle be measured in helium experiments. A wide-open problem is the actual calculation of some of these numbers for realistic models.

As a final example of boson physics in electronic systems, we mention the exotic magnetic flux phases of high temperature superconductors [23,24]. Using the well-known Feynman path-integral formulation of boson statistical mechanics [25], one may view the flux lines in the mixed phase of high T_c compounds as boson *world lines*, with time progressing parallel to the applied field. The sample thickness then represents the effective *inverse temperature* of a two-dimensional system of interacting bosons. The proposed transitions between flux phases in bulk three-dimensional samples then correspond to zero temperature transitions between crystalline, superfluid, etc. phases of $2-d$ bosons. A major complication, however, arises when one considers *disordered* materials. Physically the disorder comes from impurities spread randomly through the bulk sample. Thus the effective bosons will see a *time-varying* as well as spatially-varying random potential. This is very different from the "random-rod" problem discussed earlier for the conventional Bose glass. One has instead a "vortex glass" which is expected to display many novel properties similar to those of a spin glass [24]. Experiments now confirm quite unambiguously the existence of this transition [26], but do not as yet give any reasonable estimates for the critical exponents, or any detailed properties of the glass phase. Much of the theory is of a phenomenological nature [24], but detailed calculations on reasonable models are also beginning to appear [27].

ACKNOWLEDGMENTS

This research was funded in part by the U. S. National Science Foundation under Grant No. DMR-9308205. Travel funding from the U. S. Army Research Office for my participation in the CMT-XX Workshop in Pune, India is gratefully acknowledged.

REFERENCES

[1] For a relatively recent review of the state of the art see V. Dohm, J. Low Temp. Phys. **69**, 51 (1987).

[2] D.J. Bishop and J.D. Reppy, Phys. Rev. B**22**, 5171 (1980).

[3] See J.D. Reppy, Physica B**126**, 335 (1984) and references therein.

[4] P.B. Weichman, M. Rasolt, M.E. Fisher and M.J. Stephen, Phys. Rev. B**33**, 4632 (1986); M. Rasolt, M.J. Stephen, M.E. Fisher and P.B. Weichman, Phys. Rev. Lett. **53**, 798 (1984). See also P.B. Weichman, Phys. Rev. B**38**, 8739 (1988).

[5] A.B. Harris, J. Phys. C **7**, 1671 (1974).

[6] P.B. Weichman and M.E. Fisher, Phys. Rev. B**34**, 7652 (1986).

[7] M.P.A. Fisher, P.B. Weichman, G. Grinstein and D.S. Fisher, Phys. Rev. B **40**, 546 (1989). Recent Quantum Monte Carlo work has confirmed the basic structure of the phase diagram presented here. See G.G. Batrouni, R.T. Scalettar and G.T. Zimanyi, Phys. Rev. Lett. **65**, 1765 (1990); **66**, 3144 (1991).

[8] See P.B. Weichman, Phys. Rev. B**38**, 8739 (1988) for a modern view of this transition.

[9] P.W. Anderson, Phys. Rev. **109**, 1492 (1958).

[10] K. Kim and P.B. Weichman, Phys. Rev. B**43**, 13583 (1991).

[11] M.E. Fisher, M.N. Barber and D. Jasnow, Phys. Rev. A**8**, 1111 (1973).

[12] J.T. Chayes, L. Chayes, D.S. Fisher and T. Spencer, Phys. Rev. Lett. **57**, 2999 (1986).

[13] See, e.g., K.G. Wilson and J. Kogut, Physics Reports **12C**, 75 (1974).

[14] P.B. Weichman and K. Kim. Phys. Rev. B**40**, 813 (1989).

[15] S. Doniach, Phys. Rev. B**24**, 5063 (1981).

[16] Such interactions are often treated by coupling harmonic oscillator baths to the superconducting grains: A.O. Caldeira and A.J. Leggett, Ann. Phys. (N.Y.) **149**, 374 (1983).

[17] M. Ma, B.I. Halperin and P.A. Lee, Phys. Rev. B**34**, 3136 (1986).

[18] D.B. Haviland, Y. Liu and A.M. Goldman, Phys. Rev. Lett. **62**, 2180 (1989); A.E. White, R.C. Dynes and J.P. Garno, Phys. Rev. B**33**, 3549 (1986).

[19] A.F. Hebard and M.A. Paalanen, Phys. Rev. Lett. **65**, 927 (1990).

[20] See, e.g., M.P.A. Fisher, Phys. Rev. Lett. **57**, 885 (1986); T. Pang, Phys. Rev. Lett. **62**, 2176 (1989).

[21] K. Kim and P.B. Weichman, Phys. Rev. B**43**, 13583 (1991). Universality of σ^* was first proposed by M.P.A. Fisher, G. Grinstein and S.M. Girvin, Phys. Rev. Lett. **64**, 587 (1990), but the derivation given is incomplete.

[22] See M.P.A. Fisher, *et al.*, Ref. 21.

[23] D.R. Nelson and H.S. Seung, Phys. Rev. B**39**, 9153 (1989).

[24] D.S. Fisher, M.P.A. Fisher and D.A. Huse, Phys. Rev. B**43**, 130 (1991).

[25] R.P. Feynman and A.R. Hibbs, *Quantum Mechanics and Path Integrals* (McGraw Hill, 1965), Chap. 10.

[26] See, e.g., P.L. Gammel, L.F. Schneemeyer and D.J. Bishop, Phys. Rev. Lett. **66**, 953 (1991).

[27] See, e.g., D.R. Nelson and P. Le Doussal, Phys. Rev. B**42**, 10113 (1990); J.D. Reger, T.A. Tokuyasu, A.P. Young and M.P.A. Fisher, Phys. Rev. B **44**, 7147 (1991)

A MODEL FOR COLOSSAL MAGNETORESISTANCE BASED ON THE MAXIMUM ENTROPY PRINCIPLE

Sergio Picozzi and F. Bary Malik

Department of Physics, Southern Illinois University, Carbondale, IL 62901-4401 USA

ABSTRACT

The resistance R of a sample depends, in general, on the magnitude H of the magnetic field to which the sample is exposed. The magneto-resistive ratio $\Delta R/R$ defined in (1) is a measure of the intensity of the magneto-resistive effect. Recently, certain manganese oxides of perovskite structure have exhibited values of $\Delta R/R$ well above 100,000%, orders of magnitude greater than observed in magnetic layered materials. We present a theoretical model to calculate $\Delta R/R$. The site-dependent distribution function of carriers is determined by means of the Maximum Entropy Principle (MEP). In the spirit of Landauer's approach to resistance calculations, the difference in chemical potentials at neighboring sites is interpreted as the local voltage V, while the local current density J is calculated by an analogue of Fick's first law of diffusion with a site-dependent diffusivity. The input to the latter is furnished by the difference in particle number at neighboring sites derived via the MEP. The resistance then is proportional to V/J, and $\Delta R/R$ promptly ensues at the distribution function is explicitly dependent on the magnetic field H. Our results will be contrasted with relevant experimental data.

1. INTRODUCTION

Magnetoresistance is the study of the change in electrical resistance in a material as a function of temperature in the presence of an externally applied magnetic field. Quantitatively, the effect is often expressed in terms of the magnetoresistance ratio, $\Delta R/R(H)$, defined as

$$\Delta R/R(H) \equiv [(R(H) - R(0))/R(H)]\, X\, 100 \qquad (1)$$

where R(H) and R(0) denote, respectively, the measured resistance at a given temperature in the presence of an externally applied field H and in the absence of such an applied field. In normal metals, this ratio changes very slowly, only about a few percent, with temperature [1-2]. In the 1980s, it is found that this ratio, in certain ferromagnetic multi-layered films, exhibits a sudden negative change of 5 to 150% at temperatures of few Kelvins [3,4]. This phenomenon is usually referred to as Giant Magnetoresistance or GMR. More recently, measurements of the magnetoresistance ratios well in excess of 100,000% have been reported in certain perovskites, particularly those having manganese as a constituent, under various doping conditions [5,6].

This phenomenon, termed as Colossal Magnetoresistance or CMR, like GMR, exhibits a negative ratio but distinguishes itself in many other aspects. Besides the sheer difference in magnitude between GMR and CMR and between the usual magnetoresistance and CMR, CMR is observed while subjecting perovskites to a broad range of environmental conditions. While, the usual magnetoresistance is always associated with metallic compounds at very low temperature, CMR is observed at temperatures well into the domain of room temperatures in ceramic materials which belong, intriguingly, to the same class of materials exhibiting high temperature superconductivity. The critical temperature associated with CMR increases with the increasing strength of the applied field and the latter could be as high as several Teslas. Clearly, the phenomenon involves the thermodynamical evolution of a system characterized by a given Hamiltonian in the presence of an applied field. In this paper we, therefore, consider a system characterized by a simple Hamiltonian containing a mean field, interaction terms involving spin-alignment and spin-anti-alignment, a background or a bath, and interaction with that bath. The investigation then centers around studying the temperature evolution of such a system using the Maximum Entropy Principle or MEP [7-9] and to see whether magnetoresistance associated with such a system could exhibit CMR like behavior for a typical set of parameters characteristic of ceramic materials.

2. THE MODEL

The Hamiltonian describing the carriers in materials exhibiting CMR is taken to be the same one that under different circumstances could exhibit physical properties relevant to high temperature superconductivity [10,11], namely

$$\hat{H} = \sum_i E(i)\hat{n}_i + (B\Delta(i) + M)\hat{n}_{di} + U(i)\hat{r}_i + t\Delta^2(i)\hat{I} \equiv \sum_i \hat{h}(i) \qquad (2)$$

where

$$\hat{n}_i = \hat{n}_{i\uparrow} + \hat{n}_{i\downarrow}\ ;\ n_{di} = \hat{n}_{i\uparrow} - \hat{n}_{i\downarrow}\ ,\ \textit{and}\ \hat{r}_i = \hat{n}_{i\uparrow}\hat{n}_{i\downarrow}\ ,$$

and $\hat{n}_{i\uparrow}$ and $\hat{n}_{i\downarrow}$ are related to Fermion creation and annihilation operators $a_i^\dagger$ and a_i obeying canonical anti-commutation rules by

$$\hat{n}_{i\uparrow} = a_{i\uparrow}^\dagger a_{i\uparrow} \ \textit{and}\ \hat{n}_{i\downarrow} = a_{i\downarrow}^\dagger a_{i\downarrow}.$$

The index i runs over all sites, either in coordinate or momentum space, depending on whether one is envisioning a system of localized or itinerant components. As explained subsequently, the model's parameters E, B, M U, t chosen for our investigation are typical for materials exhibiting CMR. Δ, a dimensionless parameter, is determined from the minimization of the Helmholtz Free Energy of the system at each temperature. Although, in principle, the parameters may be made to vary at different sites, in the present work no such variation is being included.

To study the thermodynamic evolution of the system characterized by this Hamiltonian, we adopt the Maximum Entropy Principle enunciated for similar Hamiltonians [7-11]. In this method the entropy (κ =Boltzmann constant)

$$S = -\kappa Tr(\hat{\rho}\ln\hat{\rho})$$

is extremized with respect to Lagrange multipliers associated with the auxiliary conditions that the same density matrix yields the expectation values of a set of chosen relevant operators. For our purpose, these relevant operators are (i) $\hat{h}(i)$, the energy at a site i, (ii) $\hat{n}(i)$, the number of particles at a site i, (iii) $\hat{r}(i)$, the number of pair at a site i, and (iv) the number of anti-pairs at a site. The thermodynamic averages of these relevant operators are given by [10,11].

$$<\hat{n}> = 2\,\frac{e^{-\beta[U+2E]} + e^{-\beta E}\cosh[\beta(B\Delta+M)]}{1 + e^{-\beta[U+2E]} + 2e^{-\beta E}\cosh[\beta(B\Delta+M)]} \tag{3}$$

$$<\hat{r}> = \frac{e^{-\beta(U+2E)}}{1 + e^{-\beta(U+2E)} + 2e^{-\beta E}\cosh[\beta(B\Delta+M)]} \tag{4}$$

$$<\hat{n}_d> = -2\,\frac{\sinh[\beta(B\Delta+M)]e^{-\beta E}}{1 + e^{-\beta(U+2E)} + 2e^{-\beta E}\cosh[\beta(B\Delta+M)]} \tag{5}$$

$$<\hat{h}> = E<\hat{n}> + (B\Delta + M)<\hat{n}_d> + U<\hat{r}> + t\Delta^2 \tag{6}$$

In the above β may be identified as the reciprocal of the temperature, T, in the units obtained by setting Boltzmann constant to one. $<\hat{n}>$ represents the total number of spins, up and down, at a single site; $<\hat{r}>$ is the number of pairs at a site, with the spins of a pair's constituents pointing in opposite directions; $<\hat{n}_d>$ is the number of spins up minus spins down at a site, and is, thus, proportional to the local magnetic moment; $<\hat{h}>$ is the total energy at a site. All of the above are extensive thermodynamic quantities and, as such, are additive. The expression for the free energy F reads:

$$F = \frac{\beta t\Delta^2 - \ln[1 + e^{-\beta(U+2E)} + 2e^{-\beta E}\cosh(\beta(B\Delta+M))]}{\beta} \tag{7}$$

The condition for thermodynamic equilibrium is that the latter, as a function of Δ, be a minimum. Differentiating (7) and equating the result to zero yields the following self-consistent transcendental equation for Δ

$$2t\Delta - \frac{2B \sinh[\beta(B\Delta + M)]\, e^{-\beta E}}{1 + e^{-\beta(U+2E)} + 2e^{-\beta E}\cosh[\beta(B\Delta + M)]} = 0 \qquad (8)$$

which, in light of (5), may be rewritten as

$$\Delta = -\frac{B}{2t}\langle \hat{n}_d \rangle \qquad (9)$$

When Δ is interpreted as being proportional to the local mean field responsible for ferromagnetic alignment [10], (9) represents the result that such a mean field is proportional to the local magnetization, obtained here simply as a consequence of thermodynamic equilibrium, while in the conventional Weiss mean-field theory it is postulated a priori [1,12].

In materials exhibiting CMR, conductance is believed to occur via the process of site-to-site hopping. In practice, carriers are still attracted towards stationary ions, except that the number of attraction sites exceeds that of mobile carriers, with the result that no single configuration is stable and the system fluctuates continually between available configurations. In the absence of a bias, such a process is randomized and no net current results. An applied voltage provides the necessary bias for a net current to arise, corresponding to the fact that hopping becomes more likely in one particular direction than in any other. However, when a voltage is applied at the opposite ends of a sample, the field "seen" by a carrier situated deep within the sample (i.e., at least a few interatomic distances away from one end) cannot in general be assumed to coincide with the field that the charge would see if it were isolated in empty space. Rather, as electric currents flow through the sample, fields build up into configurations compatible with the current [13].

In principle, such a picture allows one to calculate the electrical resistance through a self-consistent scheme. In the case of hopping, electric transport may be modeled as a diffusive process, to which we can apply Fick's first law of diffusion [14]

$$J(x) = -D(x)\frac{\partial w(x)}{\partial x} \qquad (10)$$

where J(x) is the local probability current, w(x) the local probability density and D(x) is the diffusivity. Hopping is triggered by a charge density gradient and Fick's Law simply reflects the assumption that current and density gradient be proportional to each other. Since we are considering hopping between sites distributed over a discrete lattice, we adopt a discrete version

of (10) in the form

$$eJ_{AB} = -D_{AB}\frac{(\langle\hat{n}_A\rangle - \langle\hat{n}_B\rangle)}{d_{AB}} \tag{11}$$

where eJ_{AB} is the electric current density, $e\langle\hat{n}_A\rangle$ and $e\langle\hat{n}_B\rangle$ are the charge densities at site A and B, respectively, and d_{AB} is the intersite distance.

The occupation number $\langle\hat{n}\rangle$ at a site is given by

$$\langle\hat{n}\rangle = 2\left\{\frac{e^{-\beta[U+2(E-\mu)]} + e^{-\beta(E-\mu)}\cosh[\beta(B\Delta+M)]}{1 + e^{-\beta[U+2(E-\mu)]} + e^{-\beta(E-\mu)}\cosh[\beta(B\Delta+M)]}\right\} \tag{12}$$

(12) indicates that all other conditions being equal (i.e., temperature, magnetic field and coupling parameters), a difference in $\langle\hat{n}\rangle$ between two sites can only be due to a difference in their respective electrochemical potentials, μ_A and μ_B. The magnitude of the resulting gradient $(\mu_A - \mu_B)/ed_{AB}$ will be interpreted physically as the average electric field perceived by a carrier hopping between sites A and B. It should be made clear that in this picture it is completely immaterial whether one considers the difference in electrochemical potentials (and thus the field) as the cause and the ensuing difference in $\langle\hat{n}\rangle$, proportional to the current, as the effect, or the other way around. Such a duality of perspectives is inherent in Landauer's approach to electric transport calculations, which we are adopting here [13,15]. Defining the electrical resistance R_{AB} as the ratio between voltage and current, we obtain the expression

$$R_{AB} \equiv \frac{V_{AB}}{I_{AB}} = \frac{\mu_A - \mu_B}{Ae^2J_{AB}} = \frac{\mu_A - \mu_B}{Ae^2[-D_{AB}(\langle\hat{n}_A\rangle - \langle\hat{n}_B\rangle)/d_{AB}]} \tag{13}$$

in which A is the sample's cross sectional area in a direction perpendicular to the current's. (13) is sufficiently general as to allow for local variations of resistance due to, for example, impurities or defects. However, here we assume that the sample be reasonably homogeneous and thus, omit the subscript AB. Under the present assumptions, the resistance as measured between the ends of the sample would simple be proportional to R_{AB}, the proportionality factor being the number N of ionic layers constituting the sample in a direction parallel to the current's. Combining (12) and (13), the magnetoresistance ratio can be written as

$$\frac{\Delta R}{R}(T) = \frac{R(T,H) - R(T,0)}{R(T,H)} x\ 100 = \left[1 - \left(\frac{\langle\hat{n}_A\rangle(H) - \langle\hat{n}_B\rangle(H)}{\langle\hat{n}_A\rangle(0) - \langle\hat{n}_B\rangle(0)}\right)x\ 100\right] \tag{14}$$

In (12) the dependence of $\langle\hat{n}\rangle$ upon temperature T and applied magnetic field H arises from the equalities $\beta = 1/T$ and $M = (g\mu_B/2)\,H$, in which μ_B denotes Bohr's magneton and g is the carriers' gyromagnetic ratio.

3. RESULTS AND DISCUSSION

In our calculations, we have chosen the following values for the parameters: (a) E = 0.9 eV. E essentially represents the carriers' effective kinetic energy, possibly incorporating a contribution from the Coulomb mean field. The chosen value is typical in the class of materials under consideration. (b) U = -1.84 eV. U represents the energy related to the formation of fermion pairs. In conventional as well as high-temperature superconductors such energy is generally a few times the fermions' kinetic energy near the transition temperature [10,11]. We have assumed that pairing energies are related in a similar fashion to kinetic energies in CMR materials as well. (c) $B = 1.84 \times 10^{-2}$ eV; $t = 9.0 \times 10^{-5}$ eV; in ferromagnetic materials the estimated Weiss field typically reaches magnitudes of the order $\sim 10^4$ Telsa, and hence, the quantity $B^2/2t$ corresponding to the maximal field is chosen as to attain the same order of magnitude, (d) Finally, $M = 4.05 \times 10^{-4}$ eV; this corresponds to a field of 7.0 Tesla, a magnitude utilized in CMR experiments [5,6].

In actual calculations the preceding parameters have been inserted in dimensionless form, in which their values are, respectively: E = 200; U = -410; B = 4.1; t = 0.02; M = 0.09. In [11] it is demonstrated how the Hamiltonian (2), for certain values of the intervening parameters, can describe a succession of magnetic phases relevant to CMR. In the absence of an external magnetic field (M = 0), it is found that the system is fully aligned ($|\langle \hat{n}_d \rangle| = 1$; $\langle \hat{r} \rangle = 0$) below a certain temperature T_c, suddenly becoming anti-aligned ($|\langle \hat{n}_d \rangle| = 0$; $\langle \hat{r} \rangle = 1$) at T_c and tending gradually towards a random alignment at higher and higher temperatures (Fig. 1). The application of a sufficiently intense magnetic fields ($M \neq 0$) does not alter the latter succession of phases, but it causes an upward shift of the transition temperature $T_c(H)$, to a higher value i.e., $T_c(H) > T_C$. Hence, in the "window" between T_c and $T_c(H)$ a system that is normally anti-aligned, or antiferromagnetic, suddenly turns aligned, or ferromagnetic, when a magnetic field is switched on. Such a field would have otherwise little influence outside of the window. The situation we have just described, is illustrated in Fig. 1.

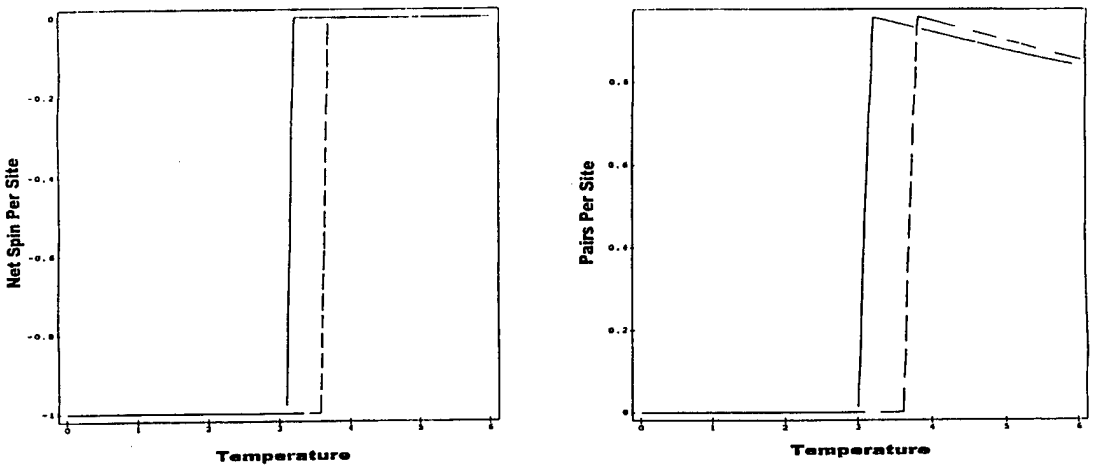

Figure 1. Net spin (left insert) and net pair (right insert) per site as a function of temperature. Solid and dashed line in each insert refer, respectively, to the absence of an applied magnetic field and 7T applied field.

In the left insert of that figure, the net spin per site has been plotted both in the absence of an applied field i.e., for M = 0, and in the presence of an applied field of 7 Tesla. Clearly, the transition temperature from alignment to anti-alignment increases with the applied field. Similarly, as shown in the right insert, the transition from the absence of pairs to substantial pairing per site occurs at a higher temperature in the presence of an applied field.

In Table 1, we present our calculated R(0), R(H) and $\Delta R/R$ for three temperatures and note that (a) as observed experimentally [16], $\Delta R/R(H) = 0$ outside a given temperature zone i.e., there is a temperature window for such an effect to occur; (b) the effect starts around 150° K and ends around 230° K which is in accord with the observation; (c) the relative change in resistivity is, indeed, negative as observed; and (d) the magnitude of $\Delta R/R$ could, indeed, be very large. For our choice of parameters, the maximum is about 3700%.

Table 1

In the table, T, R(0), R(H) and $\Delta R/R(H)$ are, respectively, temperature in Kelvin, resistance in the absence of an applied field, resistance in the presence of the applied field, and the magnetoresistance ratio as defined in (1). The resistances are in the units of $d/(Ae^2D)$.

T	R(0)	R(H)	$\Delta R/R(H)$
146.2	0.52	0.52	0%
177.5	14.59	0.54	-3658%
234.9	13.93	13.93	0%

One can, conclude, that our model makes correct qualitative predictions of the magnetic phases. On the other hand, our calculations have shown an extreme sensitivity of the transition temperature to the parameters being used, and, thus, we believe that allowing for appropriate variations, even of modest magnitude, of the parameters from site to site can enable us to obtain good quantitative results as well. In particular, the discrepancy between the sharpness of our calculated transition temperature and the smoother experimental ones would be explained if we keep in mind that, in actuality, one is measuring bulk properties of a sample, i.e. an average over many sites, while our calculations refer to an idealized case, in which the physical parameters are taken to be equal at all sites. Calculations with site-dependent parameters are planned in the continuation of our program.

4. CONCLUSION

Although calculations presented here are limited in scope and further investigations are needed and continuing, the model does account for the broad features of the CMR effect. In particular, it provides (a) a connection between magnetoresistive effects and the observed magnetic phases, (b) an understanding of how the magnetoresistive effect could manifest itself in a particular temperature zone, and (c) quantitative results for CMR.

ACKNOWLEDGMENTS

The authors are pleased to acknowledge the Grant No. TCN96046-DO#1871-USARO from the U.S. Army Research Office for sponsoring this research and another travel grant from the said office for attending the XXI Workshop.

REFERENCES

1. C. Kittel, *Introduction to Solid State Physics* (John Wiley, New York 1986).
2. Ashcroft-Mermin, *Solid State Physics* (Sanders College, PA 1976).
3. M. N. Baibich, J. M. Broto, A. Fert, F. N. V. Dau, F. Petroff, P. Etienne, G. Creutzt, A. Friederich and J. Chazelas, Phys. Rev. Lett. **61**, 2472 (1988).
4. J. Wecker, R. von Helmott, L. Schutte and K. Samwer, Appl. Phys. Lett. **62**, 1985 (1993).
5. S. Jin et al., Science **264**, 413 (1994).
6. M. McCormack, Appl. Phys. Lett. **64**, 3045 (1994); S. Jin, Appli. Phys. Lett. **67**, 557 (1995); J. Fontcuberta et al., Phys. Rev. Lett. **76**, 1122 (1996).
7. J. Aliaga, D. Otero, A. Plastino and A. N. Proto, Phys. Rev. A **38**, 918 (1988).
8. J. Aliaga, A. N. Proto and V. Zunino, Condensed Matter Theories **7**, 335 (1992).
9. R. Balian, *From Statistical Physics to Statistical Inference and Back* eds. P. Grassberger and J. P. Nadal (Kluwer Academic Publishers 1994) p. 11.
10. S. Picozzi, Doctoral dissertation, Southern Illinois Univesity at Carbondale (1997).
11. S. Picozzi, A. N. Proto, and F. B. Malik, Condensed Matter Theories **12**, 319 (1997).
12. D. C. Mattis, *Theory of Magnetism*, (Springer Verlag, Heildelberg, 1981).
13. R. Landauer, Z. Physik B **68**, 217 (1987) and references therein.
14. R. Collins, S. R. Carson and A. D. Mathew, Am. J. Phys. **65**, 230 (1997).
15. M. Büttiker, Phys. Rev. B. **31**, 6207 (1985).
16. T. Kimura, Y. Tomioka, H. Kuwahara, A. Asamitsu, M. Tamura and Y. Tokura, Science **274**, 1698 (1996) and Preprint, 1997.